2007

Finite element analysis and field observation of a residential roof subjected to hurricane winds

Matz David Jungmann
Iowa State University

Finite element analysis and field observation of a residential roof subjected to hurricane winds

by

Matz David Jungmann

A thesis submitted to the graduate faculty

in partial fulfillment of the requirements for the degree of

MASTER OF SCIENCE

Major: Civil Engineering (Structural Engineering)

Program of Study Committee:

Fouad Fanous, Co-major Professor
Sivalingam Sritharan, Co-major Professor
Terry Wipf
Partha Sarkar

Iowa State University

Ames, Iowa

2007

DEDICATION

To my wife Jennifer

TABLE OF CONTENTS

LIST OF FIGURES

LIST OF TABLES

ABSTRACT

Every year, natural disasters take a great toll on the economy and infrastructure of the United States. When specifically considering the insured property losses of U.S. natural disasters, seven out of ten highest natural disasters are caused by a hurricane event. Hurricane seasons have increased in activity over the past few years, with the 2005 Atlantic storm season seeing 14 hurricanes, 7 of which were major hurricanes. This thesis focuses on an analysis performed under the winds of Hurricane Katrina on an instrumented roof structure of a house built in Pensacola, Florida. The data recorded is compared to results obtained from a theoretical finite element (FE) model as well as those stipulated from a design standard.

The instrumented test structure was a low-rise residential house with 76 pressure cells attached to the hip roof sheathing and 68 load cells placed between the rafters/trusses and the top of the wall. A wind anemometer was located near the test structure to record the wind's angle of attack and speeds during a hurricane event. Although Hurricane Katrina data is the focus of this report, the test structure, which was built in 2002, has experienced several other hurricanes. Data recorded during Hurricane Katrina data was chosen to be analyzed and compared against the FE analysis results as this storm event produced one of the highest peak wind speed of 56.2 mph.

The results from the FE model was compared to Hurricane Katrina field data by performing a gravity analysis, analyzing equivalent loads from three wind speeds, and comparing the field data to the requirements of *ASCE 7-02 Standard*. The gravity analysis was important to verify that the assumptions used in the FE model were satisfactory and

produce the load distribution similar to that observed for gravity loads determined from the field data at very low wind speeds during Hurricane Katrina.

The three static wind pressures were applied to the FE model to determine if the FE model was comparable to the wind loading at the particular times during Hurricane Katrina. The model showed that the FE model was significantly higher in wind loading than the field data because all sheathing elements in the FE model had wind pressures applied normal to the test roof. Also, the linear interpolation used for the applied wind pressures to the FE model could have been different from what was measured in the field over the test roof.

Thirdly, the *ASCE 7-02 Standard* wind loads were analyzed for both applied pressures and total wind loading on the test roof for a comparative analysis to the field data. This was done to investigate the adequate representation of wind loads in the *ASCE 7-02 Standard*. The results showed that the components and cladding (C&C) wind pressures were much greater than the main wind force-resistance system (MWFRS) since C&C accounts for the localized effect that could occur. The conservativeness of the *ASCE 7-02 Standard* could not be addressed for the MWFRS applied pressures at the peak wind speed of 56.2 mph during Hurricane Katrina because the averaged load cell reactions of the field data fluctuated greatly in adjacent load cells. However the S*tandard* wasn't conservative when comparing the C&C design pressures to the field data.

Overall the loads induced by wind effects on the test roof during Hurricane Katrina were small in comparison to gravity effects, if the peak wind speed of a hurricane event been greater, then the field data may provide a better comparison to FE analysis results. This leaves many areas of future studies for finite element analysis such as dynamic loads, fatigue, or cyclic loading. A field test of the test roof is greatly needed to get a satisfactory feel for

correct gravity loading to be established for the future studies of the test structure. Also, the precipitation during the hurricane event should be studied as this is suspected to have influenced the load cell data.

CHAPTER 1. INTRODUCTION

1.1 Hurricane Damage to Residential Structures

On August 29, 2005, Hurricane Katrina slammed into the United States Gulf Coast as one of the most deadly hurricanes in United States history. Hurricane Katrina was the costliest hurricane ever to strike the United States, and two others in that same season (Wilma and Rita) made the top 10 costliest hurricanes (Infoplease, 2006). The estimated value of damage caused by Hurricane Katrina was approximately $80 billion (Infoplease, 2006).

The 2005 Atlantic hurricane season included 27 named storms, 14 of which developed into hurricanes and was the most active in the 154 year history, for which weather records have been tracked by the United States government (Infoplease, 2006). Of these hurricanes, three storms were classified as category 5 storms, or those with the greatest potential to cause severe damage. Seven of the 27 storms occurring in 2005 were classified as major hurricanes (category 3 or higher), while only four of the seven storms actually impacted the United States. An average season based on the past 40 years would have had eleven named storms and six hurricanes, including two major hurricanes. This information reveals the severity of the Atlantic hurricane season experienced in 2005.

Each year natural disasters take a huge toll on the United States. This toll is commonly measured in deaths, injuries, property damage, and economic losses. Property damage and economic losses from hurricanes have increased with population growth in coastal areas. The likelihood of property damage seemed minimal for those along the East

and Gulf coasts of the U.S. throughout the significant period of residential and commercial development in the 1970s and 1980s. At that time, these coastal areas were not as active during tropical storm seasons, with many homeowners never experiencing severe hurricanes. In Florida, a major hurricane had not hit land for 30 years since Hurricane Betsey in 1965, putting a false sense of security in the minds of homeowners (Ayscue, 1996). Although storm activity has increased since the 1980s, today's structural designs provide safer dwellings by ensuring some protection against hurricane damages due to the hurricane activity and subsequent design improvements made in the past 20 years.

Table 1.1 illustrates the top 10 insured property losses incurred in the history of the United States due to natural or man-made hazards. These losses were adjusted for 2005 United States dollars (Insurance Information Institute, 2006).

Table 1.1. Top ten insured property losses in United States (in billions $) (Insurance Information Institute, 2006)

			Insured Loss ($ Billions)	
Rank	Date	Disaster	Dollars When occurred	In 2005 Dollars (2)
1	Aug. 2005	Hurricane Katrina	40.6	40.6
2	Aug. 1992	Hurricane Andrew	15.5	21.576
3	Sept. 2001	World Trade Center & Pentagon Terrorist Attacks	18.8	20.732
4	Jan. 2004	Northridge, CA Earthquake	12.5	16.473
5	Oct. 2005	Hurricane Wilma	10.3	10.3
6	Aug. 2004	Hurricane Charley	7.475	7.728
7	Aug. 2004	Hurricane Ivan	7.11	7.351
8	Sept. 1989	Hurricane Hugo	4.195	6.607
9	Sept. 2005	Hurricane Rita	5	5
10	Aug. 2004	Hurricane Frances	4.595	4.751

Source Insurance Service Office, Insurance Information Institute

(1) Property coverage only
(2) Adjusted to 2005 dollars by the Insurance Information Institute

1.2 Brief Hurricane History

Hurricanes are tropical cyclones, which are low pressure systems that generally form over large expanses of water. Tropical cyclones become a hurricane when the intense tropical weather system produces strong thunderstorms with a well-defined surface circulation and maximum sustained winds of 74 mph or higher. A sustained wind is classified by having a 1-minute average wind, measured at about 33 ft. (10 m) above the surface (National Hurricane Preparedness, 2006). Hurricanes are classified according to the strength of their wind. There are five classifications for hurricanes and are represented by the Saffir – Simpson Hurricane Scale. Table 1.2 describes this scale in detail.

Table 1.2. Saffir – Simpson Hurricane Scale (FEMA, 2006)

Category	Definition	Effects
One	Winds 74-95 mph	No real damage to building structures. Damage primarily to unanchored mobile homes, shrubbery, and trees. Also, some coastal road flooding and minor pier damage
Two	Winds 96-110 mph	Some roofing material, door, and window damage to buildings. Considerable damage to vegetation, mobile homes, and piers. Coastal and low-lying escape routes flood 2-4 hours before arrival of center. Small craft in unprotected anchorages break moorings.
Three	Winds 111-130 mph	Some structural damage to small residences and utility buildings with a minor amount of curtainwall failures. Mobile homes are destroyed. Flooding near the coast destroys smaller structures with larger structures damaged by floating debris. Terrain continuously lower than 5 feet ASL may be flooded inland 8 miles or more.
Four	Winds 131-155 mph	More extensive curtainwall failures with some complete roof structure failure on small residences. Major erosion of beach. Major damage to lower floors of structures near the shore. Terrain continuously lower than 10 feet ASL may be flooded requiring massive evacuation of residential areas inland as far as 6 miles.
Five	Winds greater than 155 mph	Complete roof failure on many residences and industrial buildings. Some complete building failures with small utility buildings blown over or away. Major damage to lower floors of all structures located less than 15 feet ASL and within 500 yards of the shoreline.Massive evacuation of residential areas on low ground within 5 to 10 miles of the shoreline may be required.

1.3 Analysis of Housing for Hurricane Prone Regions

According to Ayscue (1996), residential structures are especially vulnerable to damage during hurricanes because less engineering oversight is applied to design and construction. "As opposed to hospitals and public buildings, which are considered "fully engineered," and office and light industrial buildings, which are considered "marginally engineered," residential construction is categorized as "non-engineered."(Ayscue, 1996)." Therefore, much needed attention must be paid to residential construction because, historically, the bulk of wind damage in the United States has occurred to residential construction.

The following figure illustrates that most catastrophes are caused by severe winds such as hurricanes and tornadoes. These catastrophes are all events causing direct insured losses to property of $25 million, in 2004 dollars, and are adjusted to 2005 dollars. One should note that these catastrophes exclude snow and flood damage.

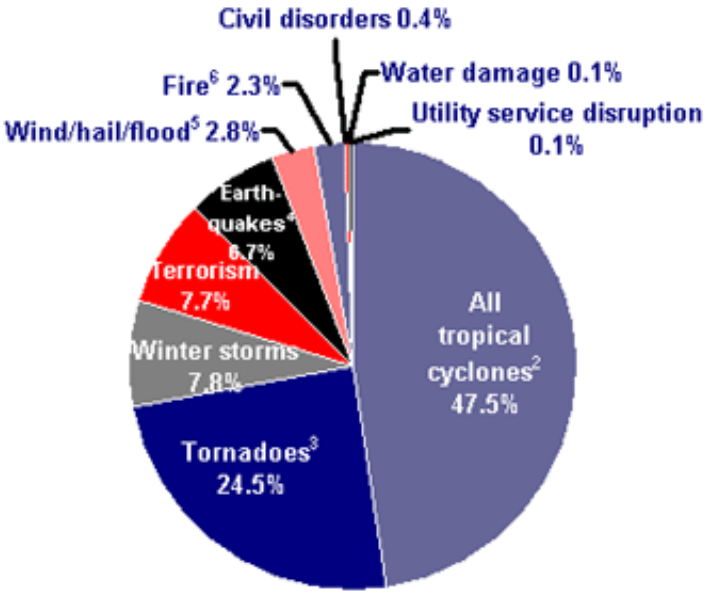

Figure 1.1. Inflation-adjusted U.S. catastrophe losses by cause of loss, 1986-2005 (Insurance Information Institute, 2006)

Most residential structures are timber frame systems and are commonly referred to as light frame buildings (LFBs). Light frame buildings consist of many elements including the roof, floor, walls, and intercomponent connections. When LFBs are exposed to hurricane forces, roofs are most susceptible to damage, followed by walls in particular those with openings, and then foundations (Ayscue, 1996). Research by Cook, (1991) estimated that roof failures accounted for 80% of structural losses.

There are a limited number of analytical models for residential construction that can be used for analysis under severe loads. When modeling and analyzing LFBs, many simplifications and assumptions are made. On the other hand, finite element (FE) modeling can be used as a tool that can analytically model the structural response when subjected to severe loading conditions, such as hurricanes.

1.4 Scope of Research

The purpose of the work presented here in was to develop an analytical model for a hip roof of a residential timber house that was constructed with extensive instrumentation to investigate its response during a hurricane event. The theoretical model was developed using the ANSYS finite element program. That structure was a 15 ft. tall residential house constructed by the Forest Products Laboratory (FPL) group based in Madison, Wisconsin. Located in Pensacola, Florida, the test structure survived the 2005 storm season, most notably Hurricane Katrina. The test structure was instrumented to measure wind pressures at various locations on the roof and load cell reactions underneath the roof between the bottom chord of the truss members and the wall support. The model was analyzed using the finite element program for the following cases:

- A gravity load analysis was performed and the results were compared to the load cell reactions obtained from the field data at the beginning and end of Hurricane Katrina;
- The data from various pressure cells at various time intervals from Hurricane Katrina were used to analyze the wind effect on the test roof and the results were compared to the measured load cell data from the field; and
- The *ASCE 7-02 Standard* for minimum design wind loads were utilized to calculate the pressure distributions that a designer may utilize and their effects with comparable data from the field.

CHAPTER 2. LITERATURE REVIEW

This chapter of the report will focus on the studies that have been previously done for finite element (FE) modeling of residential structures, and particularly, a wood truss roof system for a light framed building. A hurricane wind analysis on lightly framed residential structures was also analyzed in this study both in the field and for an analytical FE model. This chapter will incorporate FE modeling approaches for an entire residential structure (see Section 2.2), a roof system (see Section 2.3), and a single truss (see Section 2.3). Finally, this chapter will address hurricane loading on residential structures (see Section 2.1) and applications of applying the hurricane wind forces to the FE model (see Section 2.4).

2.1 Field Evaluation of Residential Houses under Hurricane Loads

Pinelli et al. (2004) estimated the expected annual damage induced by hurricane winds to residential structures in Florida. The damage was modeled as a stepwise process. For example, as damage to openings in structures occurred, this gave rise to increased internal pressure, and resulted in a sudden collapse of the roof. This ultimately resulted in immediate damage to the structure's walls. The five significant damage modes investigated by Pinelli et al. (2004) were as follows: 1) breakage of openings, 2) loss of shingles, 3) loss of roof or gable end sheathing, 4) roof to wall connection damage, and 5) masonry wall damage. This model was further subdivided into subdamage modes according to the degree of damage: no damage, light, moderate, or heavy damage. Pinelli's research produced a series of Venn diagrams to represent the many different damage modes that could be

produced for residential structures (457 total damage state events). Actual probabilistic input must be based on laboratory studies, post damage surveys, insurance claims data, engineering analyses and judgment, or Monte Carlo simulation methods. The component-based model produced by Pinelli et al. (2004) could be used in conjunction with historical loss data, to which the final damage estimation can be determined.

Jones and Porterfield (1999) instrumented a residential two-story house in Southern Shores, North Carolina, to gauge the impact of winds up to and including hurricane force winds. The aim of this research was to develop changes in construction methods and materials to reduce property loss in future storms. This was accomplished by using various materials in the test house, such as the steel rods used to anchor the roof to the building's foundation. The tested two-story house is shown in Figure 2.1. The equipment used in the study consisted of 13 pressure gauges on the walls and roof, 20 strain gauges on the studs and rafters, an ultrasonic anemometer to measure wind speed in three directions and rooftop equipment to measure rainfall, temperature, and barometric pressure. From this instrumentation pattern, the researchers were able to measure the weather conditions, wind pressure on the building, and movement of the structure itself. The system was activated in October 1997 and since then, has collected more than 2,000 data sets; one of which was Hurricane Bonnie in August 1998. Hurricane Bonnie produced nearly 60 mph wind speeds. From this specific data collected, the researchers looked at the current design codes to determine whether or not they were conservative. From this study, the researchers have concluded: the anemometer showed some significant vertical wind speeds, pressure cells showed high levels of pressure pulling away from the roof and eaves (suctions), pressure sensors reported strong values at different times and in localized areas, and the strain gages

connected to the wall studs and rafters showed little structural movement of the test house and therefore, could not say these were wind-induced movements. It is worthy to note the results of this data were not found to see how well this research was in comparison to current design codes.

Figure 2.1. Two-story test house located in Southern Shores, N.C., used by Jones and Porterfield (1999)

Texas Tech Hurricane Intercept Team (TTUHIT) researchers set up many WEMITE/SBCCOM towers in hurricane paths for data collection (Castellon, 2005). The primary good of this research is to use the data to gain a better understanding of how hurricanes affect structures. To deploy their instrumentation devices, the researchers haul several trailers that have their own power source. The towers are strategically set up along the shoreline at the first hint of the hurricane landfall. The team of researchers also uses two mobile Doppler radars used in collaboration with the University of Oklahoma, Texas A&M University, and the National Severe Storms Laboratory in Norman, Oklahoma. The research towers used collected data from Hurricane Katrina, although this data is yet to be published. There have been 22 storms since the start of the program. Data that the team of researchers

collects is distributed in the form of publications and journal articles that contribute to global awareness of the nature of hurricanes and their effect on the world's environment.

University of Florida researchers and Clemson University researchers are currently involved in a joint project to measure field data from hurricanes along the Florida coastline (ASCE newsletter, 2001). Portable instruments specifically built for high winds capture wind velocity data from various hurricanes. This project is sponsored by The Florida Department and Community Affairs and is called the Florida Coastal Monitoring Program (FCMP). The group of researchers are currently measuring the wind pressures on the exterior of residential low-rise structures. Currently, the researchers have ten houses wired for obtaining hurricane data in south Florida. The ultimate goal of this research is to set up houses along every vulnerable stretch of Florida shoreline and use the wind velocity and pressure data to calibrate wind tunnel studies and develop computational models of wind loads on low-rise structures. This will provide the baseline information needed to develop cost efficient solutions to mitigate severe wind damage.

2.2 FE Analysis of Lightly Framed Residential Houses

Past research in modeling of lightly-framed buildings (LFB) structures has primarily focused on individual subassemblies and joints. Although the behavior of the subassemblies is an important factor, it is generally not sufficient for understanding the overall behavior of an entire building as discussed in the previous section. Modeling the entire structure is important because much of the response and performance of a LFB is dictated by the structure's diaphragms (e.g. floor, walls, and roof) and intercomponent connections such as nails or metal plates for wall-to-wall, ceiling-to-wall, floor-to-wall, and roof-to-wall

connections (Collins et al. 2005). Much of the previous research has focused on the analysis and testing of these diaphragms, especially shear walls.

A detailed, 3D finite element model for a LFB that was tested by Phillips (1990) was analyzed by Kasal et al. (1994). Kasal et al. (1994) research focused on taking individual substructures and components of Phillips' (1990) experimental structure and incorporated them into a full-structure FE model, which was the first time this had ever been done. The test house developed by Phillips (1990) was a one-story, wood-frame building, which was examined under quasi-static loads. In their analysis, Kasal et al. (1994) used linear superelements for the roof and floor diaphragms. The roof and floor were modeled using shell elements that accounted for membrane and bending stiffness to satisfactorily capture the diaphragm action. The shear walls and intercomponent connections were also modeled in the full-scale FE model. For more modeling details, the reader is referred to Kasal et al. (1994) research. Experimental results of Phillips (1990) and analytical results of Kasal et al.'s (1994) research agreed closely. The FE model results predicted reaction forces and deformations at the boundaries better than at the walls distant from the acting force. Kasal et al. (1994) felt that the disagreements between the experimental and analytical results could have been due to the assumption of many properties values were taken from several substructures of analytical models.

Collins et al. (2005) analyzed the same structure using a model based on FE model formulation of Kasal et al. (1994). Collins' et al. (2005) research used the FE model to investigate various aspects of LFB behavior under both static and dynamic loading when subjected to severe loading conditions. Collins' research did not include interior finishes and some other elements that are typically considered non-structural, which would have increased

the complexity of the finite element model. Collins recommended that, to fully quantify this effect of non-structural finishes, both short-term and long-term performance for a LFB would need to be evaluated and analyzed. These effects may warrant the incorporation of additional features and capabilities into available analytical and design tools (Collins et al., 2005). The accuracy of the analysis results was evaluated by comparing them to the test data using global response criteria and energy dissipation parameters describing the hysteretic elements used for the FE model (e.g. spring elements used as intercomponent connections). Global response criteria referred to the response of a LFB in 3-dimensions for forces, displacements, and accelerations. Figure 2.2 shows the finite element model of the experimental house created by Collins et al. (2005). Collins' research found that the experimental test and finite element model test showed good comparison for the energy dissipation, hysteretic response, load sharing between the walls, and contribution of torsional response. The results of the FE model predicted the higher order response parameters (such as energy dissipation) more accurately than the load or displacement prediction.

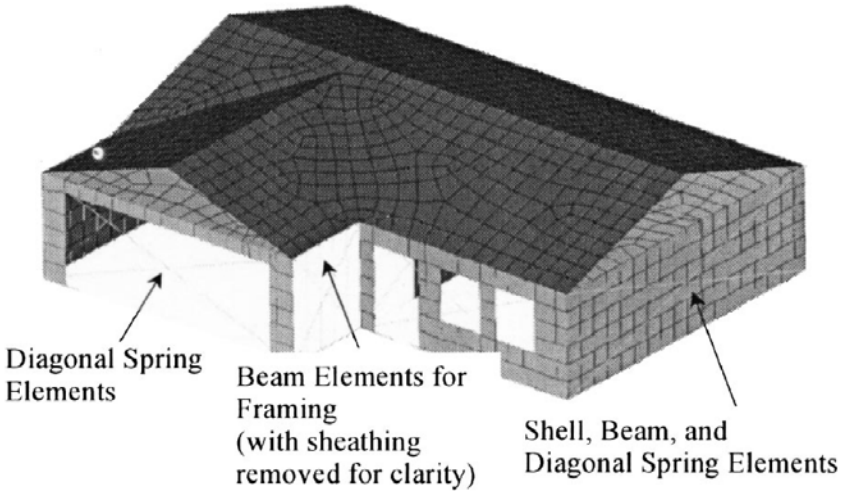

Figure 2.2. Finite Element model of a light frame building (Collins et al., 2005)

All the elements shown in Figure 2.2 were shown using finite element software from ANSYS (Swanson Analysis Systems, 2000). The beam elements are 3D with six degrees of freedom (DOF) per node and two nodes per element. The DOF are translations and rotations about mutually perpendicular axes. The mass was given as mass per unit length. For more information on the beam elements, please see Section 5.1.1.1. The shell elements in Figure 2.2 were linear elastic with orthotropic or isotropic material properties with four nodes and six DOF per node. Shell elements may have either membrane and bending action or one of membrane only or bending only actions. The mass of the shell element was specified as a mass per unit of area for a given thickness. For more information on the shell element, please see Sections 5.1.1.3 and 5.2.1. The spring elements were the last element type used in Figure 2.2. Two types of hysteresis were used for the nonlinear springs. Both spring types had either a finite or zero length value, depending on the number of DOF. The first spring type was the standard, nonlinear spring from ANSYS (Swanson Analysis Systems, 2000), possessing the following characteristics: nonlinear with piecewise linear segments, asymmetric or symmetric behavior, rotational or translational spring, large deflection capability, and nodal loads may be either forces or displacements. The other type of hysteresis spring was a customized element incorporated into the ANSYS FE package (Swanson Analysis Systems, 2000) by Collins et al. (2005). One key feature of this spring type was the incorporation of the hysteretic response of wooden structures and connections, such as history dependence, energy dissipation, strength and stiffness degradation, and pinching.

2.3 Roof Systems

Wood truss systems, both for roofs and floors, offer one of the best ways to resist vertical loads in many structures, and have a long history of good performance. Recently, configurations of roof truss assemblies have become increasing complex (Gupta, 2005), increasing the importance of studying the system behavior of these complex truss assemblies. Such studies may bring better understanding of how the loads are resisted, transferred, and distributed in order to design them safely and economically.

In general, the roof is considered to be the most engineered part of the light-framed-building (LFB) (Kasal, 1992). Most wood trusses are pre-engineered components fabricated from dimension lumber and connected with metal connector plates (Gupta, 2005). To construct a light frame wood truss assembly, the trusses are erected and spaced typically 0.61 m on center (Gupta, 2005). The sheathing is then nailed to the truss top chord members. Not only is the sheathing used to cover a particular facility and carry imposed loads, but it also serves as a load-distributing element among trusses in the assembly. Moreover, there are other structural components, such as purlins and bracing, connecting the trusses together. These construction characteristics make the truss assembly act as a system. This roof system of the test house uses metal-plate-connected trusses, which have been widely used by the housing industry over the past 30 years. Besides transmitting vertical forces into walls, the roof and ceiling act together as a horizontal diaphragm.

2.3.1 Full-Scale Testing of Roof Systems in Residential Houses

A vast amount of literature was reviewed on single trusses and metal-plate connected joints, while only a few researchers studied the system behavior of wood truss assemblies.

These investigators, which studied the structural behavior of wood truss assemblies, did so using both experimental testing and computer modeling. Experimental testing of complex truss assemblies is expensive, leading researchers to test only simple truss assemblies. Such tests do provide convincing results, but these results are mostly applicable to the system tested (Gupta, 2005).

Full-scale testing of wood truss assemblies has mainly been studied for load sharing among various components of an assembly. Wolfe and McCarthy (1989) and Wolfe and LaBissoniere (1991) tested four full-scale, nine-truss roof systems to improve design methods for light frame roof systems. Their goals were to incorporate the results of their tests into the development and evaluation of analytical models capable of predicting roof system stiffness and load capacity. In both studies, all of the nine-truss assemblies had nine identical and symmetric trusses, and no gable end trusses. Therefore, the results of both studies showed that the experimental tests of nine-truss assemblies were not directly applicable to other or more complex truss assemblies.

Percival and Comus (1980) investigated the load distribution in a full-scale hip-roof system. The load tests showed that the hip girder in a terminal hip system carried much lower loads than generally assumed in the design of the girders. The folded plate action of the sheathing and three-dimensional interaction of the framing members were the primary reasons for the reduced loads. More recently, Waltz (2002) described a series of three-dimensional finite element models used to define load paths and behavior of a hip roof under uniform vertical loads. The model results were confirmed using test data from full-scale hip roof assembly tests. This showed that 'many of the load paths utilized members and connections that were not always considered to share the burden.' It was further concluded

that 'much of the disparity between historical performance and a component-based, two-dimensional analysis can be attributed to the three-dimensional behavior of the roof that is not considered in the simplifying assumptions' (Waltz, 2002).

2.3.2 FE Analysis of Roof Systems in Residential Houses

As detailed in Sections 1.3 and 3.2, the research presented in this report focuses on a test structure that included a heavily instrumented residential hip roof. Since reconciliation of the data from the field can largely be realized using a finite element model, this section discusses previous finite element modeling schemes used to produce a theoretical representation of the roof systems.

Li et al. (1998) developed a finite element model for metal-plate-connected Fink trusses (see Figure 2.3) and truss systems (see Figure 2.4) comprised of nine Fink trusses. The semi-rigid truss and nine-truss roof system finite element models were verified by comparing the predicted vertical deflection, truss member internal forces, truss strength, and load-sharing of four nine-truss roof systems with the experimental results. Li et al. (1998) used the modulus of elasticity determined by Gerhards (1983) to determine truss strength. Also, the load-sharing was found by dividing the sum of the vertical reactions for each truss by the total applied load.

In Li et al.'s (1998) finite element model, beam elements were used to represent the wood trusses and sheathing members, while spring elements modeled the heel joints and bottom-chord-tension-splice joints. The spring elements had no physical dimensions and were used to represent semi-rigid behavior at the ends of wood truss members connected by

metal plates, which were modeled by rigid links. Figure 2.3 shows the semi-rigid model for a metal-plate-connected, Fink roof truss with a 3:12 slope.

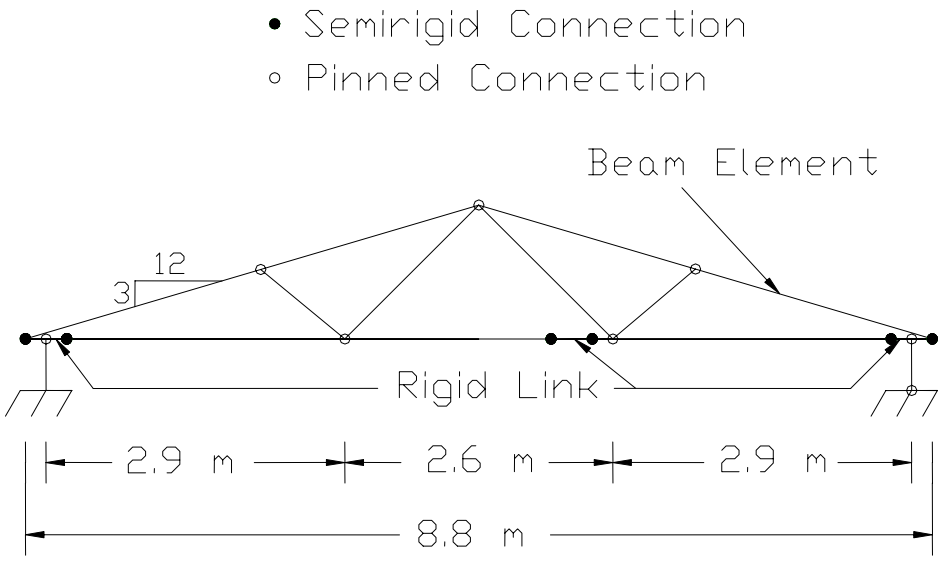

Figure 2.3. Semi-rigid model used for a Fink truss by Li et al. (1998)

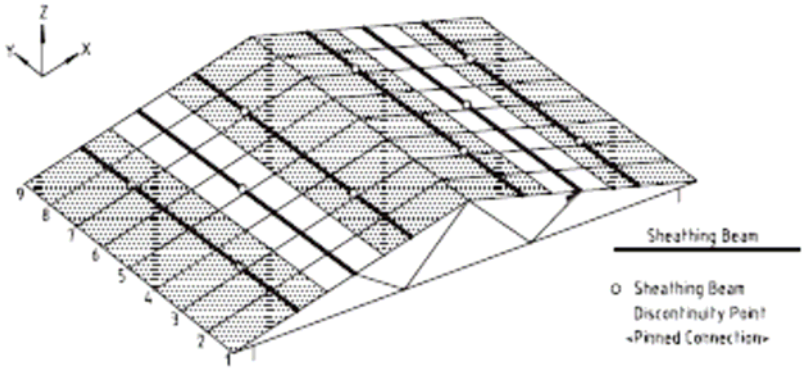

Figure 2.4. Nine-truss roof system finite element model by Li et al. (1998)

The nine-truss roof system is shown in Figure 2.4. Li et al. (1998) accounted for the partial composite action between the plywood sheathing and top chord members by increasing the bending stiffness of the truss top chord members. Kuenzi and Wilkinson (1971) developed an equation relating the deflections of a partially composite beam with that of a completely composite beam. From here, Li et al. (1998) rewrote Kuenzi and Wilkinson's (1971) equation to determine an effective stiffness for the truss top chord members. The plywood sheathing shown in Figure 2.4 was modeled using beam elements connected to the top chord member of each truss in the assembly. Not only does the plywood sheathing contribute to an increase in the stiffness of truss top chord members due to partial composite action, but it also functions as a distributor beam to transfer the load from loaded or stiffer trusses to unloaded or more limber trusses. The gaps in the plywood sheathing were taken into account by discontinuing (using a pin joint) those sheathing beams at the trusses that approximately corresponded to the gap locations.

When more than two truss members are connected through a metal-plate-connection at a truss joint, the centerlines of the members usually do not intersect at one point. This joint eccentricity, which occurred in the heel joints, was included in the model proposed by Li et al. (1998) by offsetting the intersection point between the top chord and bottom chord members by an appropriate distance along the bottom chord from the intersection point between the centerline of the truss bearing plate and truss bottom chord. This was accomplished by adopting one node for each intersection point at the heel connection (see Figure 2.3). Joint eccentricities were ignored when the nodes for the beam elements met at a common node. Joint eccentricities occurred at web joints and ridge joints in the pitched Fink trusses, but they were not modeled to maintain simplicity in the model. The supports beneath

each truss were modeled as a pinned connection at one end and a roller connection at the other end.

Cramer and Wolfe (1989) developed a 3D frame analysis program (ROOFSYS) to model a roof system of trusses connected by plywood sheathing. The plywood sheathing on each side of a pitched roof system was represented by a single continuous beam having bending stiffness about two axes to account for the wood's anisotropic properties. Nail slip between the sheathing beam and the truss top chords was assumed to have a negligible effect on system performance, and was consequently ignored. The T-beam effect of the attached sheathing or composite action was accounted for by using the bending stiffness equation developed for the deflection of a simply supported, partially composite T-beam by Kuenzi and Wilkinson (1971). Results from Cramer and Wolfe (1989) showed that a loaded truss carried approximately 50% of the load directly applied to it, which indicates significant distribution of load occurring in the roof system.

The most comprehensive analytical model of load sharing and composite action is referred to as NARSYS (nonlinear analysis of roof systems), and was developed by Cramer et al. (1993) and Mtenga et al. (1995). The study's results showed that the conventional design procedure (CDP) of repetitive-use members in a roof assembly was conservative. CDP refers to a truss assembly analyzed and designed on a single-truss basis, which assumes that each truss in the assembly carries loads based on its tributary area. The study also indicated that the roof slope and other truss characteristics could cause significant changes in the system effects.

Since trusses have been traditionally analyzed and designed on a single-truss basis, which assumes that each truss in the assembly carries loads based on its tributary area, the

approach does not take into account all system effects encountered in realistic assemblies. This conventional design procedure, in fact, may or may not be conservative in actual truss assemblies (Gupta, 2005). Although finite element modeling of the whole structure behavior can provide a more accurate estimation of the structural response, over the full duration of the defined loading scenario, models can be insufficient at predicting localized behaviors such as plate buckling on truss displacement being localized near the buckled plate, connection failure due to the need to refine the element type and mesh density to adequately identify localized behaviors (Bailey, 2006 and Stahl et al., 1996). For details of the finite element model formulation used in this report, the reader is referred to Chapter 5: *Finite Element Modeling of the Roof Structure*.

2.4 Representation of Hurricane Wind Loads Used in Design

Hurricane wind speeds have been measured and historically compared using many different methods through the years of design by engineers. One of the most common approaches to estimating wind loads due to hurricanes on residential structures is given by the *ASCE 7 Standard*. However, this *Standard* is only a guide for the minimum design winds loads on a particular structure with 50- and 100-year return period peak gust wind speeds for hurricane wind speeds along the coast (*ASCE 7*, 2003). This means that this *Standard* is shown for wind speeds that should statistically peak once at these design wind speeds for every 50 or 100 years, which depends on the area being designed and are similar to Vickery and Twisdale (1995) and Georgiou (1985) design methodology for hurricane wind speeds. Revisions are made to this *Standard* once every three years to account for advancements made through recent research. For more details about the *ASCE 7 Standard*, the reader is

referred to Chapter 4: *Distribution of Wind Pressure on the Hip Roof in Accordance with the ASCE 7-02 Standard* .

Kasal et al. (2004) produced a FE model of the LFB using Paevere et al. (2003) test house. The lateral load distribution on the structure was the main focus of this study, using eight different methods to predict the best distribution of design wind forces to the walls of the house for a moderately hurricane prone environment. The wind load was calculated assuming a 120-mph zone with an exposure *B*, which is equivalent to a suburban exposure condition based on *ASCE 7-98* (*ASCE 7*, 1999). The eight methods for analysis are the tributary area method, continuous and simple beam methods, total shear method, relative stiffness method (with and without torsion), rigid beam on elastic foundation method, rigid beam on inelastic foundation method, plate method, and a three-dimensional finite element model. Figure 2.5 depicts the eight methods used for calculating the reaction forces due to the lateral wind force distributions. In Kasal et al.'s (2004) research, the first seven methods aforementioned were described and compared to the three-dimensional finite element model and with the results of experiments on a full-scale L-shaped woodframe test house by Paevere et al. (2003). The results showed that the variation among the calculated reaction forces using the different methods was quite large, which was determined to be understandable due to the methods covering a range of complexity and the fact that the methods were each based on different assumptions about the behavior of the tested house. The plate model produced the most accurate results to the finite element model. However, the eight methods assumed a more rigid diaphragm and allowed for better control of the degree of flexibility of the structure. Paevere et al. (2003) used the same assumption to find

a similar conclusion to Kasal et al. (2004). This indicated that the roof and ceiling diaphragm for the house had some degree of flexibility, but was effectively rigid compared to the walls.

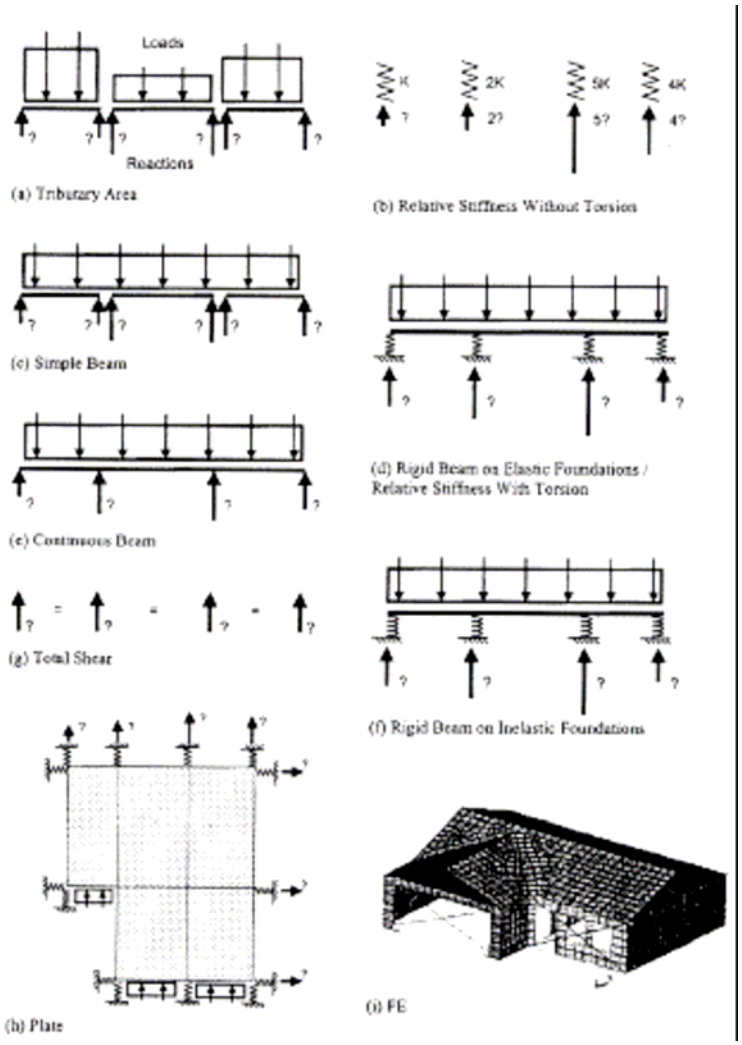

Figure 2.5. Description of different load distribution methods [(a) to (h) in plan view] by Kasal et al. (2004)

Although Kasal et al.'s (2004) analytical methods were useful for evaluating lateral loads on a particular structure, the FE model produced for the roof system (see Chapter 5) was used for distributing the lateral wind forces induced by Hurricane Katrina in this research. The wind distribution used for this study was calculated using the *ASCE 7-02*

Standard. The *Standard* was used as it is used readily by design engineers, and is utilized in many design codes today (see Chapter 4).

After reviewing the literature, there is a need for evaluating a test structure under a severe loading such as a hurricane event using finite element methods because not many finite element models were studied for wind loading effects. Also, as Section 2.1 pointed out, there is a need for studying much higher wind loading on a residential structure's performance because the peak wind speed from Hurricane Bonnie was only 60 mph in Jones and Porterfield's (1999) research.

CHAPTER 3. DETAILS OF THE TEST STRUCTURE AND INSTRUMENTATION SCHEME

3.1 Test Structure

As previously noted, a one-story timber house was constructed in 2001 by researchers from the Forest Products Laboratory (FPL) to evaluate the house's performance under real hurricane loads. In addition this structure functions as an office building with an all-wood safe room, as referred to in FEMA Publication 320 (1998). This test house is visited daily by the National Park Service (FPL News Release, 2006). The location for this structure was chosen to be Pensacola, Florida, because this location along with Miami, Florida, were recognized as two locations that have historically experienced most frequent hurricane activities. Pensacola is a city off the southwestern coast of Florida in Escambia County, and the global positioning system (GPS) coordinates at the east end wall of the test house are N30^{o} 21' 59.13'' latitude and W87^{o} 8' 15.80'' longitude. Figure 3.1 shows the location of the test house.

The test house did not have any topographic features around it that may have caused a discrepancy in the wind data collected for this field investigation (see Figure 3.11). Certain topographic features of concern in wind design may include, but are not limited to: canyons, hills, valleys, escarpments, high-rise buildings, and other large structures nearby. Also, the FPL group reported that test house was in a live oak reservation, and the forest was trimmed extensively by Hurricanes Ivan and Dennis (FPL, 2006). Figure 3.1 shows the location of the test house.

Figure 3.1. Test house location in Pensacola, Florida (FPL, 2006)

The test structure, which has a floor area of 48 ft x 32 ft, includes a hip roof as shown in Figure 3.2. The wall studs, which are 2x6's, are 10 feet high spaced at 2 ft. on center. The dimension 2x6 represents the cross sectional area of the lumber used in the construction of the test structure. Worthy to note that the 2x6 is not actually a 2-in. x 6-in. wood member, but is a 1 ½-in. x 5 ½-in. member. A 2x6 is common sizing for lumber with a ½-in. shorter linear dimension for both width and depth. This report will refer to lumber with common sizing.

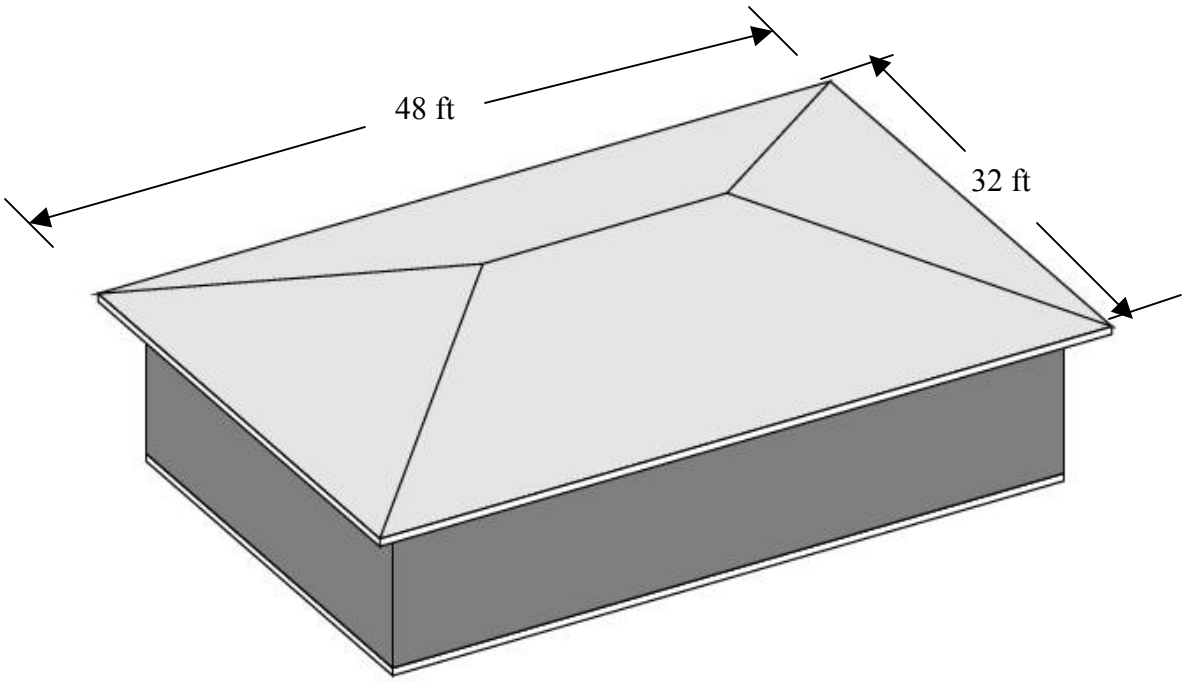

Figure 3.2. Test structure with hip roof (FPL, 2006)

The perimeter walls of the house are secured to the foundation using 5/8-in. diameter threaded rods that run from the top of the wall to the foundation beneath the walls. These rods are shown in the plan view of Figure 3.3. As seen in Figure 3.3, the threaded rods are located approximately every 4 ft between the wall studs in the exterior walls. These threaded rods replace the metal hurricane straps or clips that are usually utilized in construction located in hurricane prone regions. The common practice of toenailing the trusses or rafters to the wall is often not sufficient to hold a roof in place under high winds (Flager Emergency, 2006). Because the threaded rods do not pass up into the hip roof, the hip roof has the potential to lift off the frame of the test structure when subjected to high wind loads. Motivated by the frequent observation of hurricane damage to roofs in residential structures as reported by Ayscue (1996), these construction details were deliberately chosen such that

the field evaluation could be concentrated to the hip roof of the test structure while minimizing the deformation and damage to the perimeter walls.

Since the threaded rods are connected to the foundation of the test structure, the combined wall foundation unit of the test structure represents a rigid system. Also, since there are no hurricane straps or clips, nor were the trusses toenailed to remain in place, the connection from the roof to the walls represents a flexible connection. Therefore, the test structure is classified as a semi-rigid structure.

Recall that the primary objective of the study presented herein was to analyze the test structure, particularly the hip roof under the recorded wind condition. Particular attention was given to the hip roof portion and how its elements were connected together. Figure 3.4 shows a schematic for the test structure without the hip roof sheathing. The roofing elements, which are the rafters and trusses, indicate the orientation of the rafter/truss system. It is noted that the voids of the wood rafter/truss system were not taken out in Figure 3.4, whereas the trusses of the roof in the test structure has voids as subsequently shown. Also, for simplicity, the openings such as doors and windows are omitted in Figure 3.4.

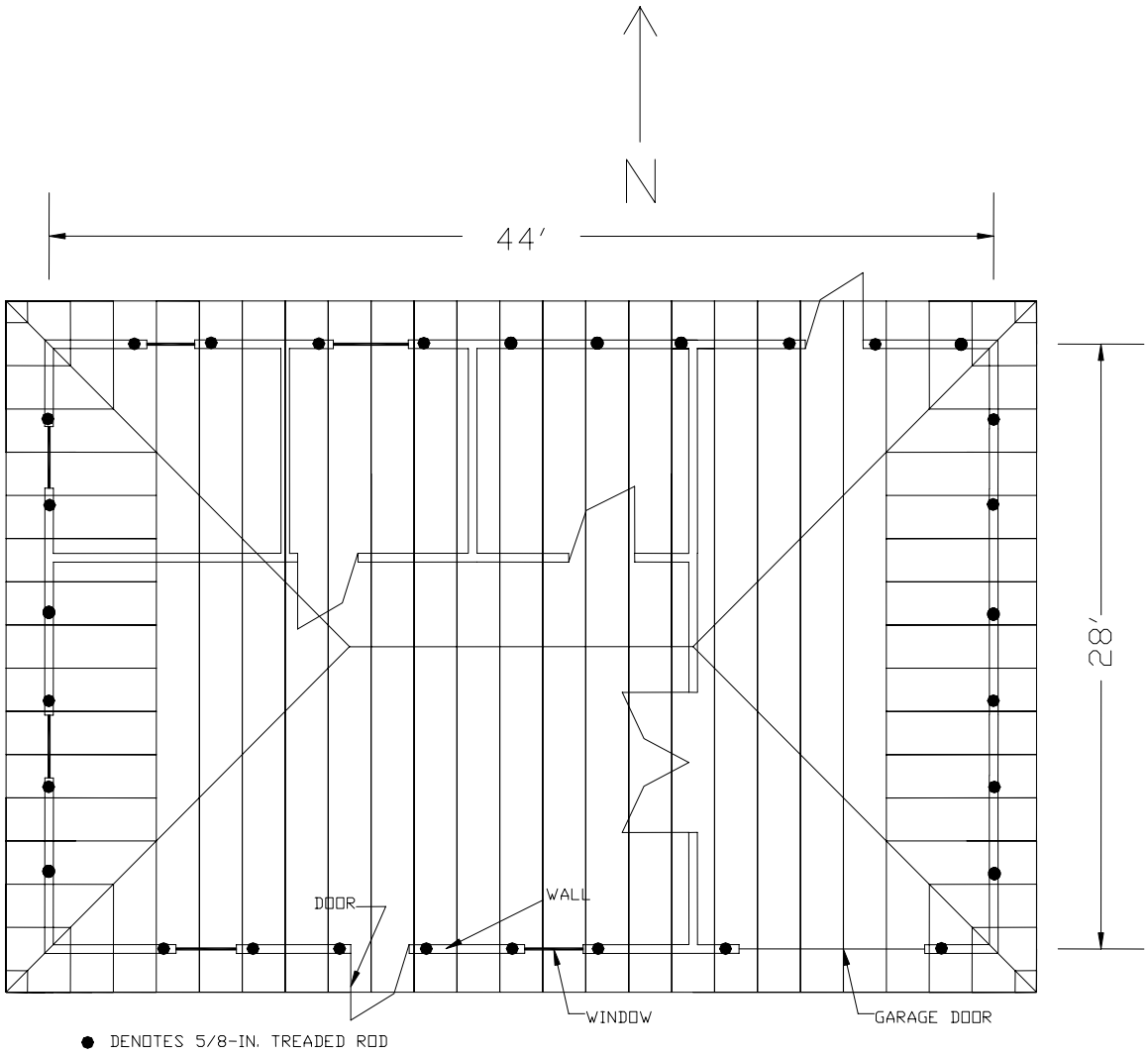

Figure 3.3. Plan view of test structure with treaded rods (FPL, 2006)

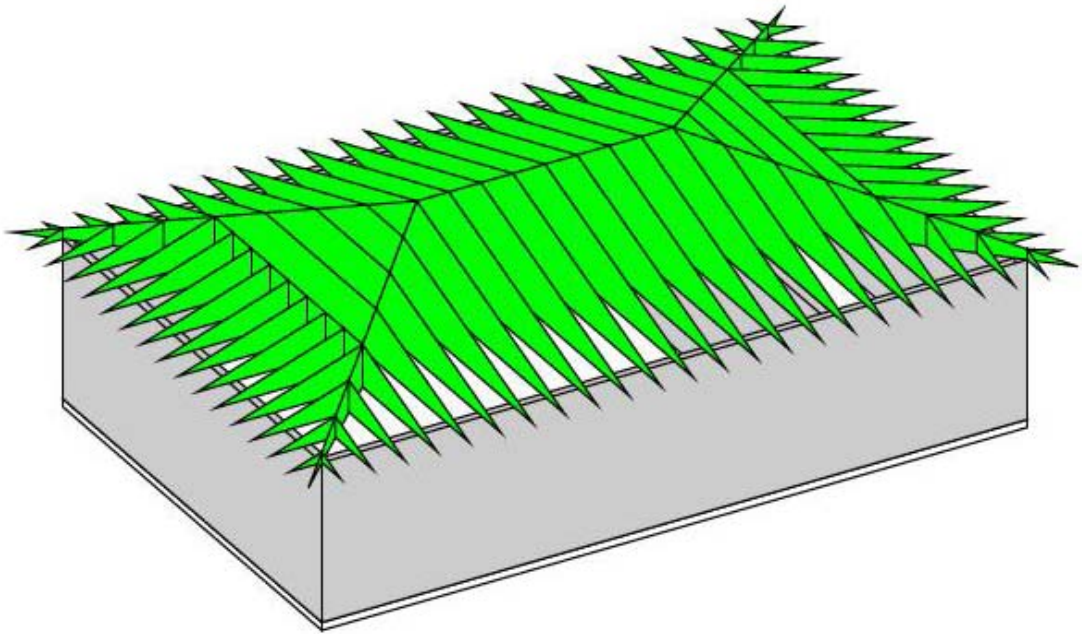

Figure 3.4. Test structure without hip roof sheathing (FPL, 2006)

3.2 Test Roof

Figure 3.5 depicts a plan view of the hip roof with ridgelines shown. The wall line is indicated by the double line and is located 2 ft. in from the hip roof edge. The overall dimensions of the hip roof, which has 1:4 pitch on every side, measures 32 ft. x 48 ft., with a 2 ft. overhang from the wall edge. The wood trusses and rafters are placed on the wall at two-foot intervals with the first one located at one foot away from the corners.

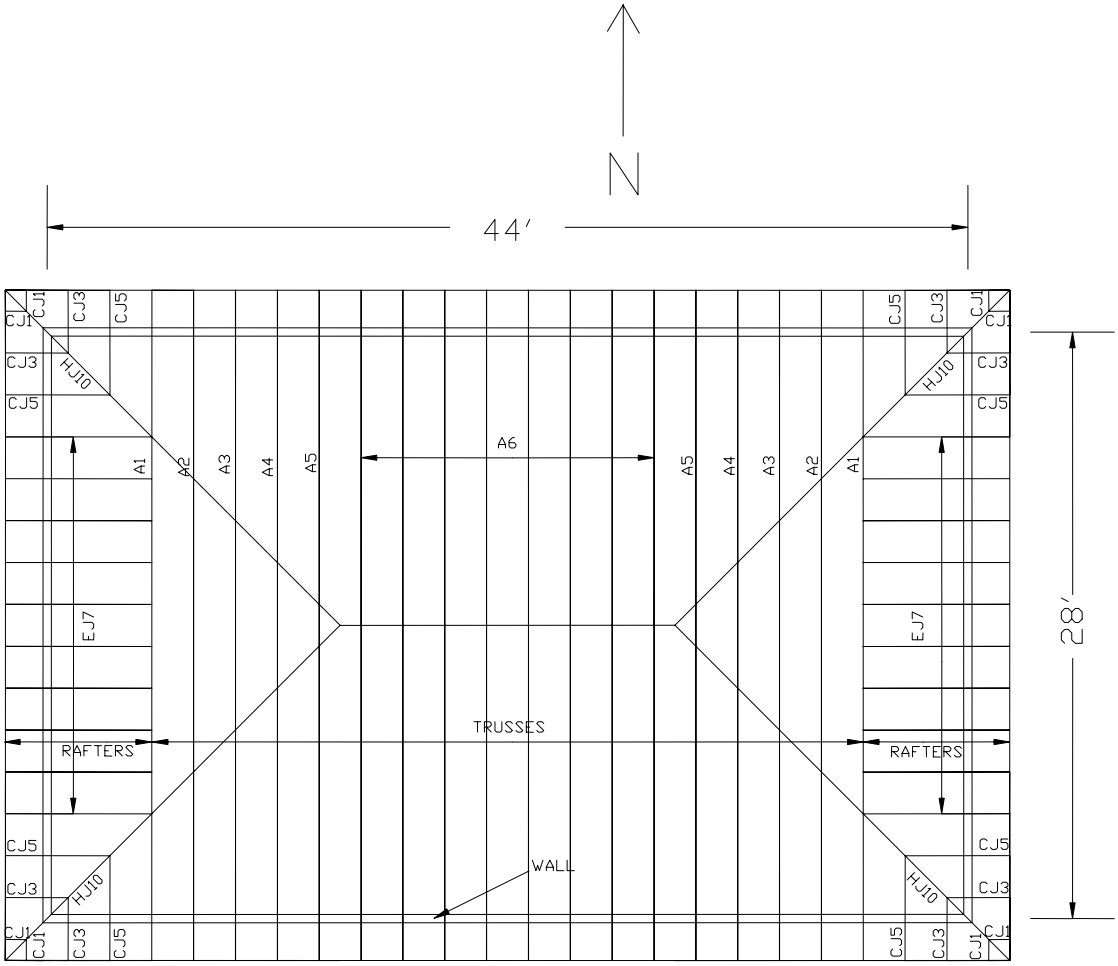

Figure 3.5. Plan view of hip roof (J. M. Harold Construction, 2006)

As identified in Figure 3.5, all wood trusses are designated as *A1*, *A2*, *A3*, *A4*, *A5*, or *A6*. The trusses have an overall span of 32 ft. and run in the north/south direction. Wood truss *A1* is a two-ply wood truss, meaning that two identical wood trusses were nailed back-to-back to form truss *A1*. The nailing schedule is included in Appendix A. Wood trusses *A2, A3, A4, A5,* and *A6* are one-ply wood trusses. These trusses were made with 2-in. x 4-in. wood members except for the stiffeners in each truss, which were 2-in. x 6-in. lumber. These stiffeners were used primarily to better distribute the load from the top chord down to

supports on top of the walls. Figure 3.6 shows the designations of the truss members and the stiffeners for truss *A1*. The roof system was designed for 30-psf live load and 7-psf dead load applied to the top chord, and 10-psf dead load applied to the bottom chord (J.M. Harold Construction, 2006). These loads were chosen by the truss manufacturer given the materials utilized in the test roof. For more details of the wood trusses used in the roof, refer to Appendix A. In the following paragraphs, a summary of how the elements of the roof structure were connected together to ensure satisfactory load transfer is provided.

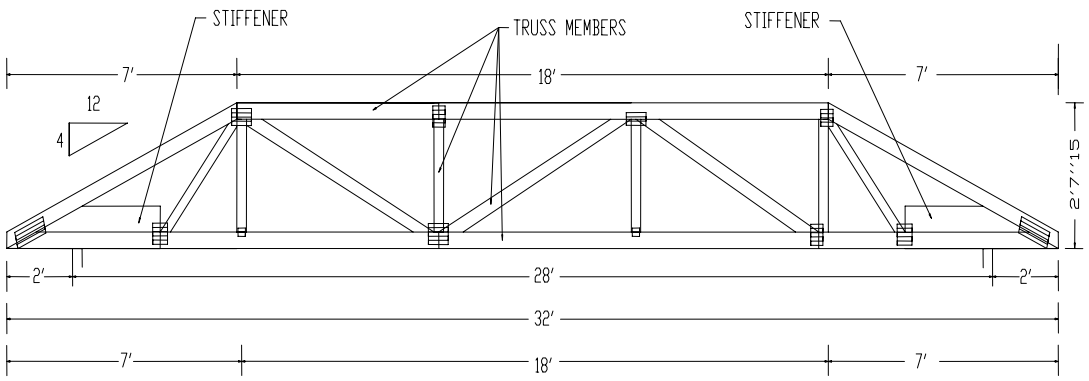

Figure 3.6. Member designations for truss *A1* (not to scale)

The rafters are designated as *CJ1*, *CJ3*, *CJ5*, *EJ7*, or *HJ10*. The designation *CJ* represents the corner jack while the attached number defines the length of the bottom chord. The designation *EJ* represents the end jack, and the attached number again defines the bottom chord length. This number also indicates the distance of the end jack from a hip roof corner. For example, the *EJ7*'s refers to an end jack with a bottom chord length of 7 ft. that is located 7 ft. in from a hip roof corner. The *HJ* represents the hip jacks. These elements span in the diagonal direction and frame into truss *A1* (see Figure 3.5). Rafters *CJ1, CJ3, CJ5,* and the first *EJ7* are framed into the *HJ10*'s. Worthy to mention that *CJ1* rafter is not

included in Appendix A because the details were not included by the manufacturer, J.M. Harold Construction. This investigative report assumed rafter *CJ1* to have similar properties to the other rafters in the truss system. The wood rafters are all one-ply rafters. The rafters are made with 2-in. x 4-in. wood members except for the stiffeners in each rafter end, which were constructed with 2-in. x 6-in. lumber. For more detailed sketches of the rafters, the reader is referred to Appendix A. Unfortunately, no nailing schedule for the rafters was available.

The roofing components in the test structure consist of asphaltic shingles, roofing felt, plywood, rafters/trusses, and gypsum board (see Figure 3.7). The roof sheathing is comprised of asphaltic shingles, roofing felt, and plywood. Furthermore, a ½-in. thick gypsum board is used as ceiling, which is attached by gypsum nails to the bottom chord of the wood trusses and rafters.

Member properties of the trusses/rafters are typically that of southern pine #2 grade and are included in Appendix A. The properties of asphaltic shingles, roofing felt, plywood, and gypsum board properties are assumed using the *ASCE 7-02 Standard* (2003). These properties are further discussed in Chapter 5: *Finite Element Modeling of the Roof Structure.*

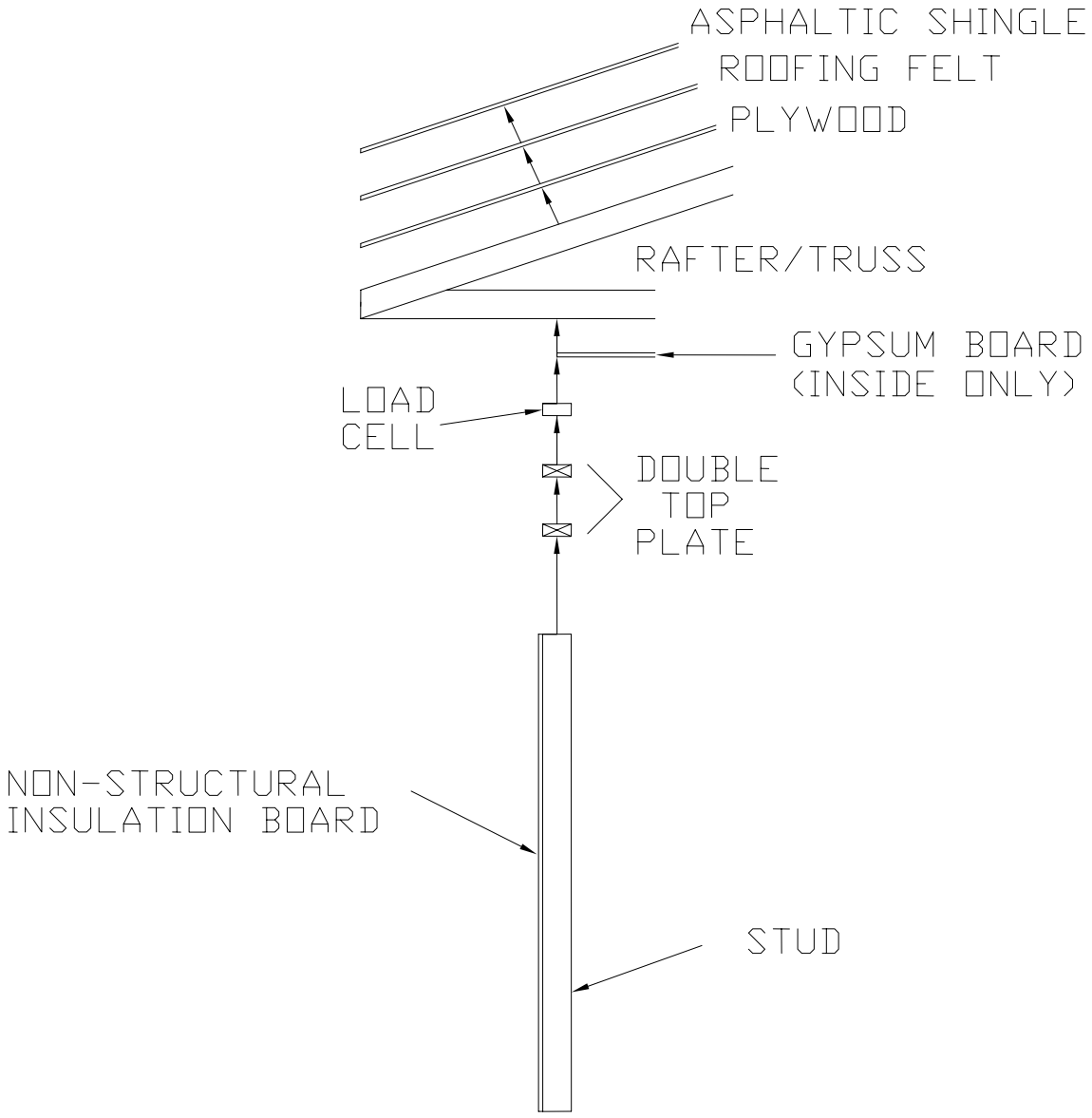

Figure 3.7. Roofing components and load cell location

3.3 Instrumentation

The measurement devices for recording the wind load effects on the roof of the test structure are load and pressure cells. Figure 3.8 shows a schematic of the load cell distributions, which are represented by the lightly colored circles, along the roof/wall line, represented as hidden line. The load cells were listed by the direction, followed by the

number of the load cell and an *L* representing the load cell. For example, the 11th north load cell is represented by *N11L*. There were 68 load cells instrumented to measure the vertical reactions at the wall/roof line at a given wind speed and time. The only place a load cell wasn't located is underneath all *CJ3* rafters, which are positioned 3 ft. in from the hip roof corner (see Figure 3.5). There is no load cell at this location as there should not be a reaction measured at this location due to the fact that the rafter does not sit on the wall support. As mentioned earlier, a wooden block is removed at this location.

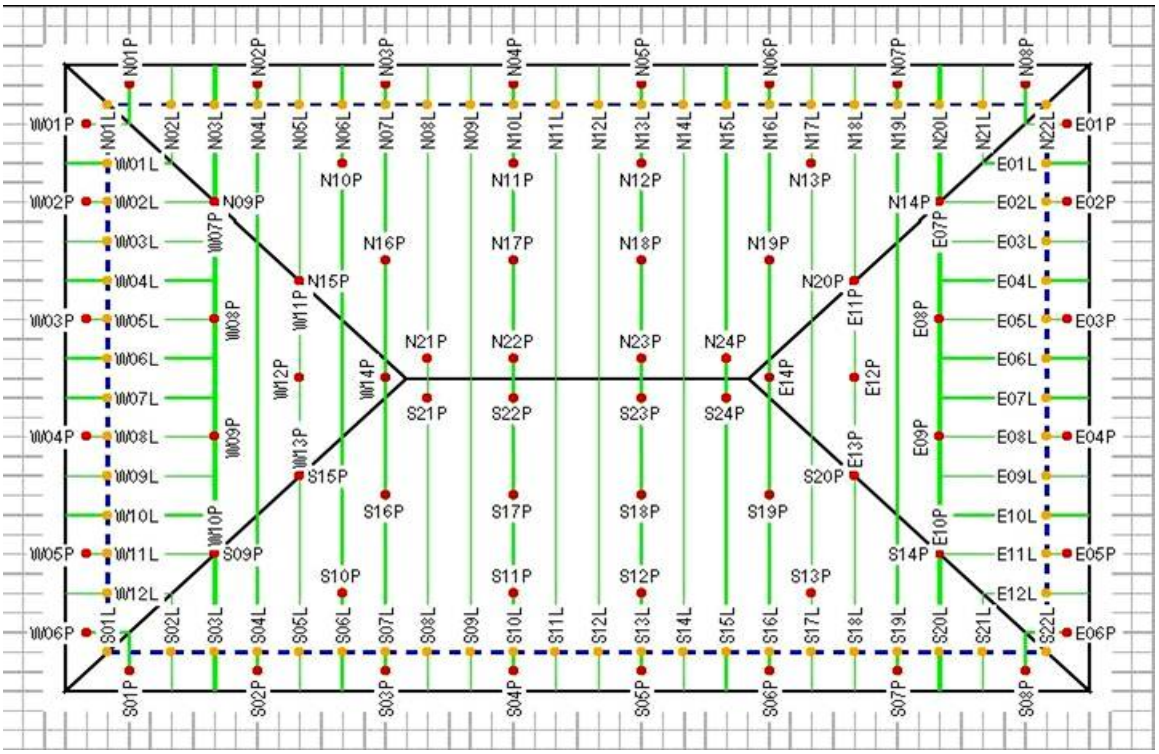

Figure 3.8. Plan view of hip roof showing the locations of load cells and pressure cells (FPL, 2006)

The load cells are located on the top of the walls below the rafter and the truss bottom chord as shown in Figures 3.9 and 3.10. By completely separating the roof from the walls, the load cells record the vertical loads transmitted from the roof to the walls. It is worthy to

mention here that the load cells are anchored to the roof system by an inverted L-brackets on both sides of the double top plates to take the horizontal wind forces. The slots in the L-brackets allow for the vertical movement of the roof system. Figure 3.9 shows mockup of the positioning of the load cells between the roof and the wall used to measure the reactions under each rafter/truss.

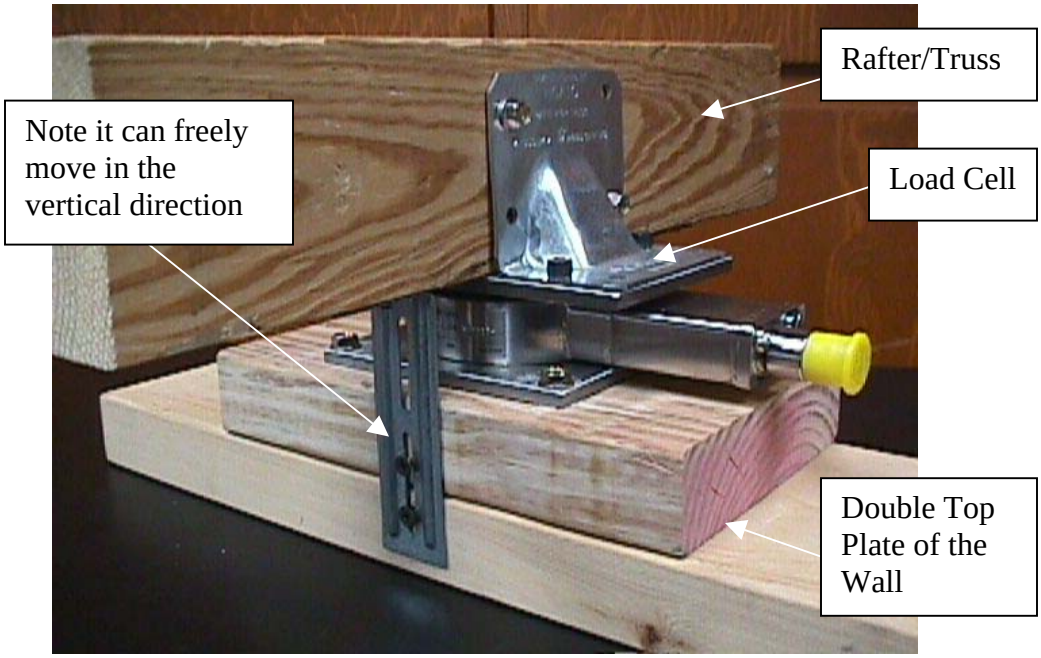

Figure 3.9. Illustration of load cells placed between the roof and wall under each rafter/truss [FPL, 2006]

The load cells were placed in the test structure by first zeroing out each load cell. The test roof was then jacked up at each wall support. Upon removing a temporary small wood block under the rafter/truss, each individual load cell was engaged in the test structure. The load cells were Sensotec ™ load cells and had the capacity to measure up to 3,000 lbs. in compression underneath truss *A1* and the rest of the load cells had the capacity to measure up to 2,000 lbs. in compression (FPL, 2006).

Figure 3.8 also shows the pressure cells located on the outside of the roof. These pressure cells are represented with darker colored circles, and are listed as the coordinate direction followed by the number of the pressure cell, followed by a *P* representing the pressure cell. For example the 11th north pressure cell is represented by *N11P*. There are 76 pressure cells to measure the pressure at a given wind speed and time.

The pressure cells were distributed on the top surface of the roof to measure the wind pressure in psf (lbs/ft^2) in a direction normal to the surface of the hip roof. Figure 3.10 shows a photo of the pressure ports on the hip roof. The pressure cells are located directly underneath the pressure ports. These recording devices are further discussed in the following section. Also, refer to Figure 3.8 for the actual locations of load cells and pressure cells on the test structure.

Figure 3.10. A view showing the pressure ports on the hip roof (FPL, 2006)

The pressure cells were Sentra ™ differential pressure transducers and were attached to the inside of the roof by 1¼-in. diameter holes drilled through the roof sheathing and shingles. Dishwasher air gaps were fitted and sealed in the roof holes. The outside tube or port was attached to the pressure transducers with the reference to the inside of the roof. The transducers were ± 5-in. H_2O column (FPL, 2006). These pressure cells measured the relative pressure on the test roof, which was the outside pressure minus the inside pressure.

Figures 3.11 and 3.12 below show the anemometer to capture the wind speed and direction of the hurricane wind forces during Hurricane Katrina data collection. The wind monitor was a R.M. Young model 05103VP ™ with a propeller/vane unit (FPL, 2006), and was placed 25 ft. above the ground.

Figure 3.11. A close view of anemometer (FPL, 2006)

Figure 3.12. Proximity of anemometer with respect to the test structure (FPL, 2006)

3.4 Wind Speed Data

The instrumented test house collected various data sets from the following hurricanes: Ivan (September 16, 2004), Arlene (June 13, 2005), Dennis (July 10, 2005), Katrina (August 29, 2005), and Wilma (October 19, 2005) (FPL, 2006). However, the study presented herein primarily considered only the recorded data from Hurricane Katrina because of the extensive wind speed information available for this event.

Data from the test structure including the anemometer data was collected from the FPL group for the test house located in Pensacola, Florida. The collected data for Hurricane Katrina was recorded for every second over nearly a 24-hour duration starting from 4:40:43 PM on August 28, 2005 to 3:53:57 PM on August 29, 2005. The peak wind speed of 56.2 mph occurred at 1:14:6.43 PM on August 29, 2005. The wind speed data included the time at wind speed in hundredths of a second since midnight, wind speed in miles per hour, relative humidity, degree of wind attacking house, and coordinate direction of wind attacking house.

3.5 Sample of Recorded Wind Speed Data

Table 3.1 shows a sample of the recorded wind speed data that included minimum wind speed, maximum wind speed, and the average wind speed for each coordinate direction measured. In this study, three different arithmetic averaged wind speeds were determined. In each case, the arithmetic average over the specified time intervals was found. The average wind speed for the full 24-hour duration was found by adding the arithmetic average of the first 12-hours plus the average of the second 12-hours and dividing by two. As listed in Table 3.1, 16 coordinate directions used to identify the dominant wind direction.

Table 3.1. Wind speed data arranged by coordinate directions

		Average Wind Speeds (MPH)			Wind Speeds (MPH)	
Wind Direction	Degree (measured)	4:00 PM on August 28, 2005 to 4:00 AM on August 29, 2005	4:00 PM on August 29, 2005 to 4:00 PM on August 29, 2005	4:00PM on August 28, 2005 to 4:00 PM on August 29, 2005	Minimum	Maximum
N	5-11	4.4555	4.7667	4.6111	1.33	7.40
NNE	12-34	6.2891	5.1976	5.7433	0.33	14.73
NE	34-56	8.5783	7.4007	7.9895	0.20	24.00
ENE	56-78	10.9889	10.0855	10.5372	0.27	29.47
E	79-101	13.8179	12.3104	13.0641	0.27	40.33
ESE	101-123	17.0705	14.5827	15.8266	0.40	56.20
SE	124-146	18.8058	20.8887	19.8473	0.33	51.73
SSE	147-168	16.0765	23.2204	19.6485	0.13	56.00
S	170-190	10.0561	22.5573	16.3067	1.07	54.27
SSW	191-213	5.5594	16.3293	10.9443	0.33	40.27
SW	214-234	3.6343	8.2513	5.9447	0.4	20.87
WSW	239-258	2.1333	4.4583	3.2959	1.00	14.80
W	261-278	2.9111	2.25	2.5805	0.47	6.13
WNW	286-298	3.3333	3.0667	3.2	1.33	4.80
NW	311-326	2.9667	3.1333	3.05	1.40	4.20
NNW	327-345	0.0000	2.4067	2.4067	0.60	4.00

* Standard time shown above was converted from hundredths of seconds since midnight in the data set (e.g., 7,560,016 hsec converts to 9:00:16 PM)

To demonstrate the strong wind direction on the test structure, two wind-rose diagrams were created using the data from Table 3.1. Figures 3.13 and 3.14 show the maximum wind speed and the average wind speed over a 24-hour duration for each coordinate direction, respectively. The tick marks on each axis represent a unit of 10 mph. A wind-rose diagram was not created for the minimum wind speed since low wind speeds in all directions were within 2 mph of each other.

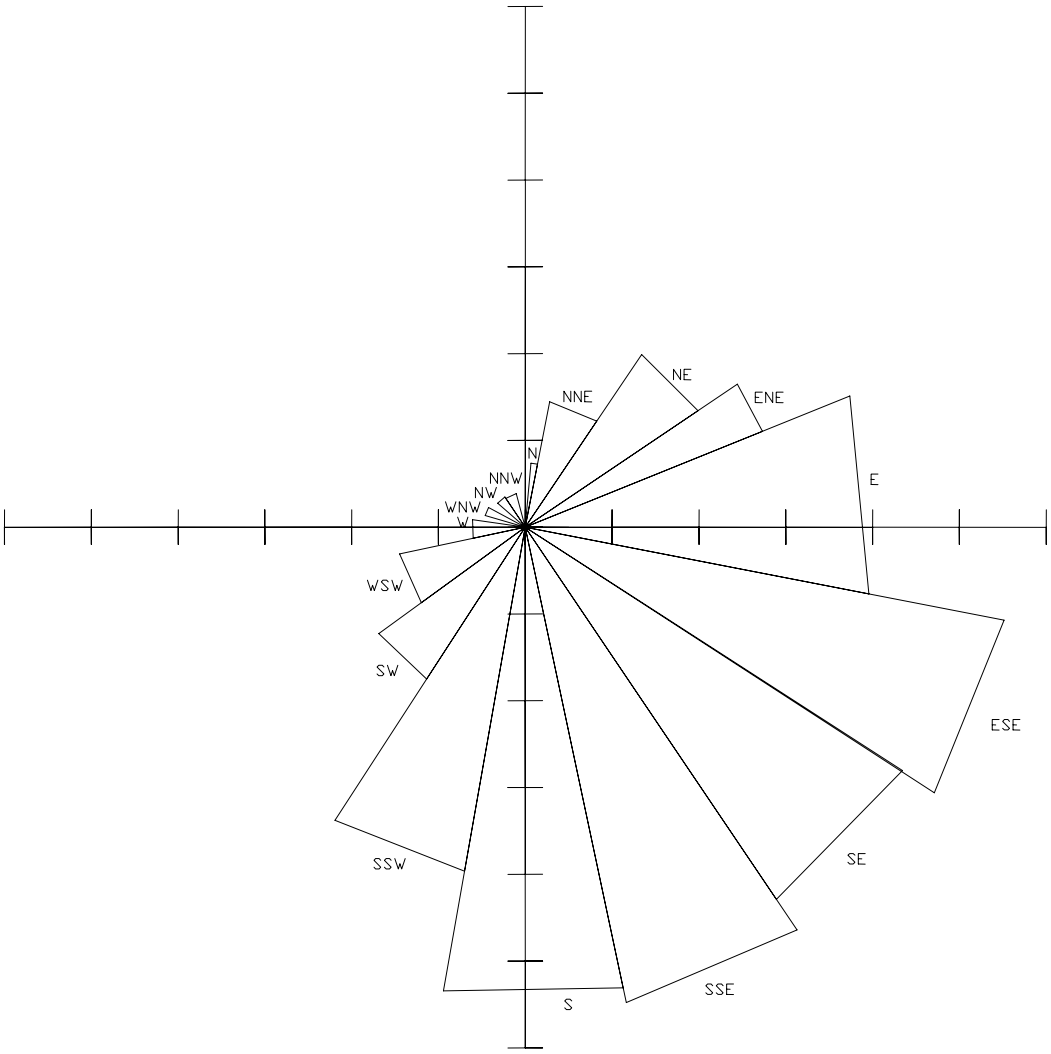

Figure 3.13. Wind-Rose diagram for maximum wind speed data collected during 24-hour duration of Hurricane Katrina

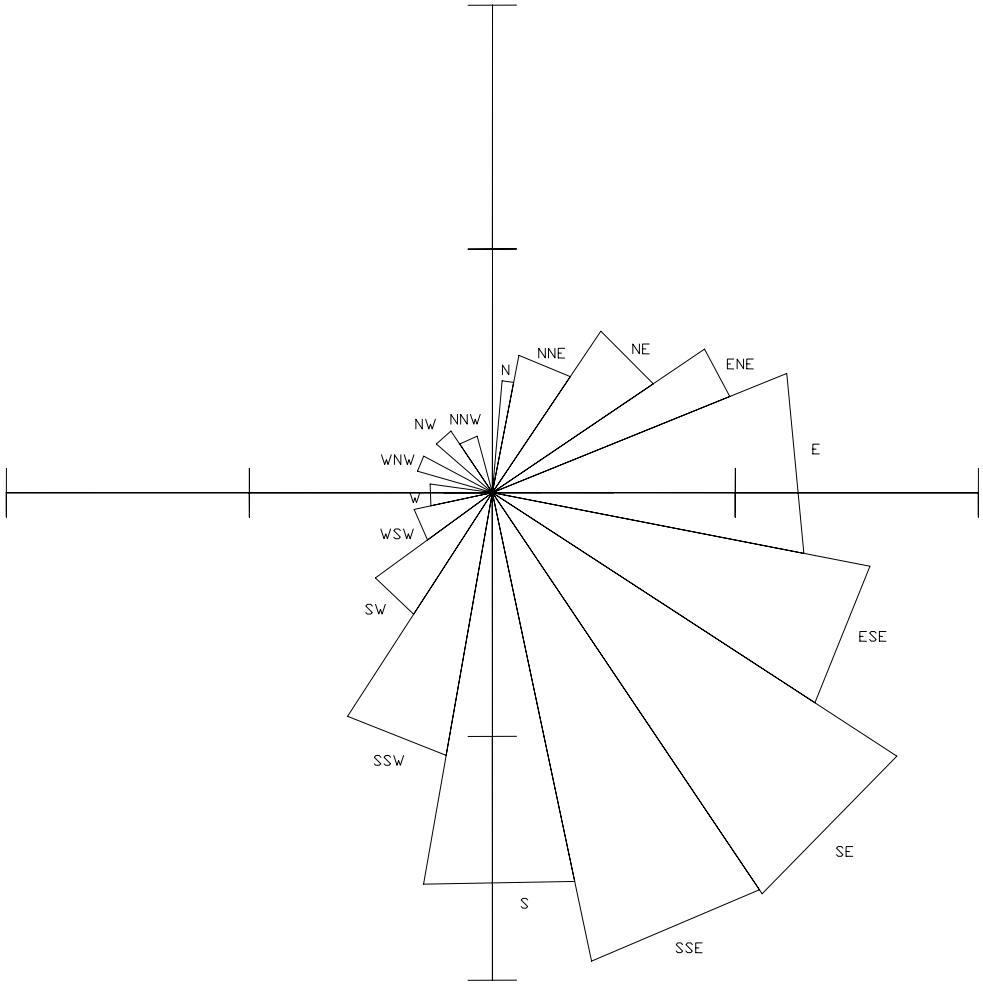

Figure 3.14. Wind-Rose diagram for average wind speed data collected during 24-hour duration of Hurricane Katrina

From Table 3.1 and Figures 3.13 and 3.14, the results indicate that the east-southeastern (ESE) direction had the maximum wind speed of approximately 56.2 mph. A peak wind speed of 50 knots, which is 57.5 mph, was recorded by WEAR-TV in Pensacola, Florida (NWS Forecast Office, 2006) on August 29, 2005. The peak wind speeds recorded by both the FPL data and the NWS Forecast Office corresponded well to one another with a 2.33% error. The south-southeastern (SSE) direction had the minimum wind speed of 0.13 mph. Therefore, the east-southeastern direction was chosen as the major direction for

investigating the response of the roof structure. In addition, the maximum wind speed was useful in that it provided a comparison to the *ASCE 7-02 Standard* approach for the observed wind speed. The recorded data associated with the minimum wind speed was utilized to verify gravity load analysis of the roof structure. Additional information obtained using the minimum wind speed data is the extra weight of the roof resulting from the build-up of moisture during a hurricane event. This was investigated in Section 6.1 of the report.

Figure 3.15 shows the path of the eye of Hurricane Katrina as it made landfall in the southeastern United States. Even though the eye of Hurricane Katrina did not come close to Pensacola, Florida, wind forces were still measured.

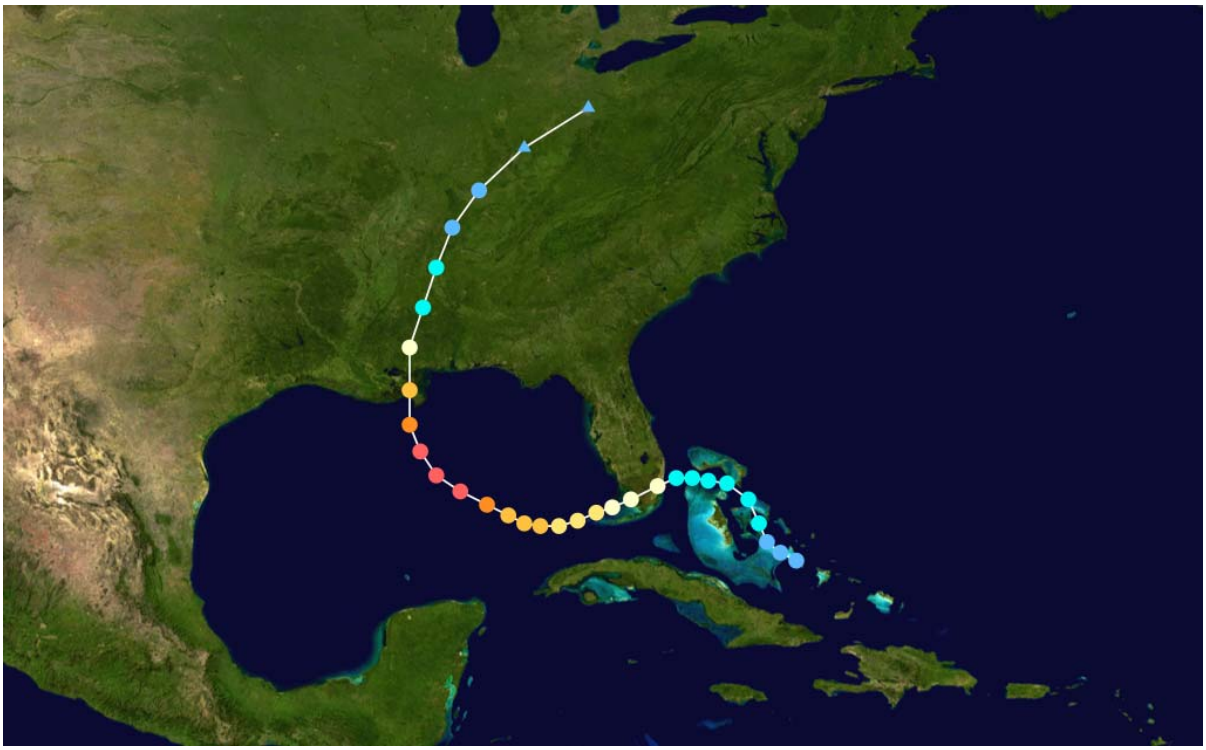

Figure 3.15. Path of eye of Hurricane Katrina beginning in the Atlantic Ocean and ending in the eastern United States (Hurricane Katrina Storm Path, 2006)

For more in depth analysis of the field results, the reader is referred to Chapter 6: *Finite Element Analysis Results and Modeling Comparisons with Field Data and Load Specified in Design Codes.* The intention of this chapter was to introduce the test structure, instrumentation, and gather a sample of the wind speeds and direction associated with the hurricane winds produced during Hurricane Katrina data collection.

CHAPTER 4. DISTRIBUTION OF WIND PRESSURE ON THE HIP ROOF IN ACCORDANCE WITH THE *ASCE 7-02 STANDARD*

A widely used approach for wind design in current practice is that established by the *ASCE 7 Standard* (*ASCE 7*, 2003), which defines various minimum design loads for buildings and other structures for the particular structures location. For a given structure, the minimum positive and negative wind pressures needed for determining wind loads can be found using this *Standard* and are represented by pressures and suctions, respectively. This chapter provides the basis for, and determination of the minimum design wind loads for the entire test structure as well as the components and cladding using the *ASCE 7-02 Standard*.

The newest building codes such as the International Building Code (IBC), National Fire Protection Association (NFPA), and Florida Building Code reference the wind provisions of the *ASCE 7 Standard – Minimum Design Loads for Buildings and Other Structures* (*ASCE*, 2006). The *ASCE 7 Standard* calculates the wind effect that a particular structure experiences given its location in the continental United States. Although the *ASCE 7 Standard* is designated for a 50-year or 100-year return period, the wind loading on the structure in this study, as per the *ASCE 7-02 Standard,* was also found given the peak wind speed measured during Hurricane Katrina. This chapter will discuss how the wind pressures were determined for this test structure and its components. In addition, the *ASCE 7-02 Standard* wind pressure distributions will be compared in this report with the field data and the FE model in Section 6.4.

4.1 Minimum Design Wind Loading Conditions

The two minimum design wind loading conditions used by the *ASCE 7-02 Standard* are the Main Wind Force-Resisting System (MWFRS) and the Components and Cladding (C&C). The minimum design wind loading for the entire test structure was calculated using the MWFRS, and the minimum design wind loading for certain components of the test roof was calculated using the C&C.

The MWFRS is an assemblage of structural elements assigned to provide support and stability for the overall structure, and to transfer wind loads to the ground. Structural elements such as shear walls, roof trusses, and roof diaphragms are all part of the MWFRS when they assist in transferring overall wind loads. Components and cladding refers to elements of the building envelope that do not qualify as part of the main wind force-resisting system. Components receive wind loads directly or from cladding, and transfer the load to the MWFRS. The cladding receives the wind loads directly. Examples of components include: fasteners, purlins, girts, studs, roof decking, and roof trusses. Components may be part of the MWFRS when they act as shear walls or roof diaphragms, but they may also be loaded individually.

A direct comparison will be given between the design wind pressures found using the *ASCE 7-02 Standard* MWFRS and C&C design for the test roof (see Section 6.3.1). The design wind loads for the entire test structure using the MWFRS approach were applied to the FE model produced (see Chapter 5) and compared with the reactions and pressures measured in the field (see Section 6.3.2). Also, the design wind loads were applied to the FE model at the pressures produced during the peak wind speed of 50.33 mph (as established in Section 4.3.1) and the wind speed for the location of the test structure of 120.34 mph (as

established in Section 4.3.1) (see Section 6.3.3). The design wind loads for the studs in the walls and the rafters/trusses in the hip roof were determined using the C&C approach. The design wind pressures found using the C&C provided for a direct comparison to the field data to determine if the pressures recorded in the field correlated well with the *ASCE 7-02 Standard* pressures calculated (see Section 6.3.4). The design wind pressures found using the C&C approach, in theory, should produce a more accurate representation of the design wind pressures and reactions measured in the field because the field data measured wind pressures instaneously during Hurricane Katrina. However, these design wind pressures were not applied to the FE model because localized pressures occurred at different times and locations on the test structure. Other components, such as the plywood sheathing for the roof and walls were not analyzed for wind pressure distributions because the member properties and material properties weren't known.

4.2 Wind Load Methods for Both MWFRS and C&C

There are three methods available in *ASCE 7-02 Standard* for computing wind loads on structures: Method 1 (simplified procedure), Method 2 (analytical procedure), and Method 3 (wind-tunnel procedure). Method 1 is used when the designer can select wind pressures directly from a chart without any calculation, and when the building meets all the requirements for application. There are nine requirements in accordance with the *ASCE 7-02 Standard* for Method 1 application for the MWFRS, which include:

- The building is simple diaphragm building,
- The building is a low-rise building,
- The building is enclosed and conforms to the wind-borne debris provisions,

- The building is a regular shaped building or structure,
- The building is not classified as a flexible building,
- The building does not have response characteristics making it subject to across-wind loading, vortex shedding, instability due to galloping or flutter; and does not have a site location for which channeling effects or buffeting in the wake of upwind obstructions warrant special consideration,
- The building has no expansion joints or separations,
- The building is not subjected to topographic effects, and
- The building has an approximately symmetrical cross section in each direction with either a flat roof, or a gable or hip roof with $\theta \leq 45$ degrees.

This structure meets all of the above qualifications for the MWFRS to be used for wind design, but was not be used because Method 2 was seen to be more accurate due to the various pressure coefficients and interpolation used in the design charts. However, Method 1 will was plotted for case 1 in Figure 4.11.

There are six requirements for Method 1 to be used for Components and Cladding, which include:

- The mean roof height is $h \leq$ 60 ft.,
- The building is enclosed and conforms to the wind-borne debris provisions,
- The building is a regular shaped building or structure,
- The building does not have response characteristics making it subject to across-wind loading, vortex shedding, instability due to galloping or flutter; and does not have a

site location for which channeling effects or buffeting in the wake of upwind obstructions warrant special consideration,

- The building is not subject to the topographic effects, and
- The building has either a flat roof, or a gable roof with $\theta \leq 45$ degrees, or a hip roof with $\theta \leq 27$ degrees.

Once again, this structure meets all of the above qualifications for the C&C to be used for wind design, but was not be used because Method 2 was seen to be more accurate due to the various pressure coefficients and interpolation used in the design charts. However, Method 1 was plotted to show the difference in the wind pressure distributions from Method 2 for the studs in the walls in Figures 4.16 and 4.17 and the rafters/trusses in the test roof in Figures 4.22 and 4.23.

Method 2 and Method 3 are relatively more complex procedures that are expected to lead to a more accurate representation of the wind loads because this method accounts for all heights and flexibilities in a particular structure. To be considered for design this method must meet the following two conditions as per the *ASCE 7-02 Standard*: 1) the building or other structure is a regular shaped building or structure, and 2) the building or other structure does not have response characteristics making it subject to across-wind loading, vortex shedding, instability due to galloping or flutter; or does not have a site location for which channeling effects or buffeting in the wake of upwind obstructions warrant special consideration.

Method 2 is referred to as the *Analytical Procedure* in the *ASCE 7-02 Standard.* This procedure involves the determination of wind directionality and a velocity pressure, the selection or determination of an appropriate gust effect factor, the selection of appropriate

pressure or force coefficients, the required level of structural reliability, the effects of differing wind exposures, the speed-up effects of certain topographic features such as hills and escarpments, and the size and geometry of the building or other structure under consideration. It also requires identifying the structure as rigid or flexible, and produces results that generally envelope the most critical load conditions for the design of main wind force-resisting systems as well as components and cladding.

Method 3 is referred to as the *Wind-Tunnel Procedure.* This method is used to determine wind loads more accurately because it can reduce the conservatism due to enveloping of the wind loads in Method 1 and Method 2. Method 3 is only used when the structure satisfies one or more of the following conditions: 1) it has a shape which differs significantly from the uniform rectangular prism, 2) it is flexible with natural frequencies normally below 1 Hz, 3) it is subject to buffeting by the wake of upwind buildings or other structures, and 4) it is subject to accelerated flow caused by channeling or local topographic features.

Given that the test structure is of uniform, rectangular shape and is located in a hurricane prone region, Method 2 was used to calculate the minimum design wind loads on the entire test structure as well as individual studs in the walls and individual rafters/trusses in the hip roof. Since the test structure was estimated to be a semi-rigid structure (see Section 3.1), it was assumed to be a rigid structure for the *ASCE 7-02 Standard* wind design. Also, the test structure was shown to have no topographic effects near or at the test structure location (see Section 3.1).

4.3 Wind Load for Entire Test Structure Using Method 2

It was necessary to study the wind effect on the entire test structure to help understand the critical sections for wind loading. The wind load for the entire test structure provided the minimum design pressures that the test structure is expected to see based on its return period (see Section 2.4). However, it is important to note that these design pressures are representative of average values for the entire test structure, and that actual wind pressures at localized areas would be higher. In accordance with the *ASCE 7-02 Standard*, the wind load for the entire test structure was distributed normal to the walls, roof sheathing, and roof overhang. Therefore, no internal loading would attack the structure, but would factor into the wind load design as per the *ASCE 7-02 Standard* wind design (see Eq. 4.3).

As previously mentioned, the MWFRS was used for the wind load on the entire test structure including the roof. The MWFRS procedure involves the determination of wind directionality and a velocity pressure, the selection of an appropriate gust effect factor, and the selection of appropriate pressure or force coefficients. This procedure accounts for the required level of structural reliability, the effects of differing wind exposures, the speed-up effects of certain topographic features, and the size and geometry of the building under consideration. As there were no topographic features present around the test structure (see Section 3.1), the terrain was considered to be homogeneous, open terrain.

4.3.1 Basic Wind Speed

The basic wind speed (V) was used in the determination of the design wind speed on the test structure. This variable factors in the design wind speed equation utilized in Method 2 (see Eq. 4.2). In accordance with the *ASCE 7-02 Standard*, this variable was selected from

a graph of the United States by county where the test structure is located. The basic wind speed corresponded to a 3-second gust speed at 33 ft above ground for Exposure Category C, which is an open terrain condition as per *ASCE 7-02 Standard*.

The basic wind speed for the test structure located in Pensacola, Florida, was 140 mph. However, this basic wind speed utilized in the *ASCE 7-02 Standard* map of the United States acted at 33 ft. above the ground surface and was consequently changed to the test structure's mean roof height of 12.5 ft. This was the average height at which the wind attacked the test structure. Using the Log Law (Simiu and Scanlan, 1996) as defined by Eq. 4.1 below, the wind speed was converted from 33 ft. above ground to 12.5 ft. above ground:

$$\frac{U(z_1)}{U(z_2)} = \frac{\ln z_1 - \ln z_0}{\ln z_2 - \ln z_0} \qquad (4.1)$$

where z_1 was 12.5 ft. above ground, z_2 was 33 ft. above ground, and z_0 was 0.0328 ft. above ground. It is worthy to note that z_0 corresponds to the open terrain condition (Simiu and Scanlan, 1996). The resultant wind speed for the basic wind speed at 140 mph converted to 12.5 ft. above ground was calculated as V = 120.34 mph. This wind speed was used for design wind pressures on the given test structure at the location of the test structure. Eq. 4.1 is often used to convert wind speeds from different heights as well as different terrain conditions.

Since this design report also analyzes the peak wind speed for Hurricane Katrina data, the peak wind speed was reduced to the wind speed at the mean roof height of the test structure. The resultant wind speed for the peak wind at 56.2 mph at 25 ft above ground for

the anemometer height (see Section 3.3 and Figure 3.12), converted to 12.5 ft. above ground for the mean roof height was calculated as V = 50.33 mph. This resultant wind speed was used in both the MWFRS and C&C wind design because Chapter 6 of this design report will use these wind pressure distributions for comparison to the field data of Hurricane Katrina.

4.3.2 Building Exposure and Surface Roughness Category

The test structure was located in Pensacola, Florida (Escambia County), for which surface roughness category C was used for all wind directions. Surface roughness category C was used for open terrain with scattered obstructions having heights generally less than 30 ft (see Section 3.1). This category includes flat open country and all water surfaces in hurricane-prone regions. Exposure category C was used in conjunction with surface roughness category C as per *ASCE 7-02 Standard*.

4.3.3 Building Classification

The classification for the test structure was rated by the nature of its occupancy. The test structure was a single-story house, located on the Florida coastline. The test structure served as an office building during research site visits and as a safe house during hurricanes because of the all-wood safe room in the test structure (see Section 3.1). In light of these facts, the test structure was classified as a category I building as per the *ASCE 7-02 Standard*. Category I buildings refer to buildings that represent a low hazard to human life in the event of failure, which includes minor storage facilities.

4.3.4 Velocity Pressure

The velocity pressure, q_z, was the horizontal pressure that attacked the test structure, and was to be evaluated at height *z* above the ground. As per the *ASCE 7-02 Standard*, the velocity pressure was determined by the following equation:

$$q_z = 0.00256 k_z k_{zt} k_d V^2 I \quad \text{(psf)} \qquad (4.2)$$

where q_z was the velocity pressure exposure coefficient, k_{zt} was the topographic factor, k_d was the wind directionality factor, V was the velocity pressure, and I was the importance factor. The numerical coefficient 0.00256 is used unless sufficient climatic data are available to justify a different value.

4.3.5 Design Wind Pressures

Design wind pressures were determined for the building at all heights. As per the *ASCE 7-02 Standard*, the wind pressure was given by the following equation:

$$p = qGC_p - q_i (GC_{pi}) \quad \text{(psf)} \qquad (4.3)$$

where $q = q_z$ for windward walls at height *z* above the ground, $q = q_h$ for leeward walls, side walls, and roof at height *h*, $q_i = q_h$ for windward walls, side walls, leeward walls, and roof of enclosed buildings, G was the gust effect factor, C_p was the external pressure coefficient, and (GC_{pi}) was the internal pressure coefficient. One should note that this structure was

considered to be an enclosed building due to the small number of openings along each wall (see Figure 3.3).

Finding values for the factors used in Eq. 4.3 from the *ASCE 7-02 Standard* was relatively straight forward, with the exception of the external pressure coefficients (C_p) for the hip roof. The external pressure coefficients for the hip roof had to be linearly interpolated using the data table to obtain the correct values. The variables used in this process were: 1) values of the angle the roof makes with the horizontal (θ), 2) building height divided by wall length parallel with the wind direction (h/L), and 3) wall length parallel with the wind direction divided by the wall length perpendicular to the wind direction (L/B). Linear interpolation should be carried out only between values of the same sign. When two C_p values are listed in the data table, this indicated that the windward roof slope was subjected to either positive or negative pressures. In this case, the hip roof shall be designed for both conditions.

The low-rise building pressure equation, which is similar to Eq. 4.3, in the *ASCE 7-02 Standard* could also have been applied to the test structure. However, this was an alternative design and was not used for wind load design.

4.3.5.1 MWFRS Design Upwind Exposure Quadrants

According to the *ASCE 7-02 Standard*, the test structure must be designed for wind load in eight quadrants. Figure 4.1 identifies these eight quadrants in a plan view of the test structure.

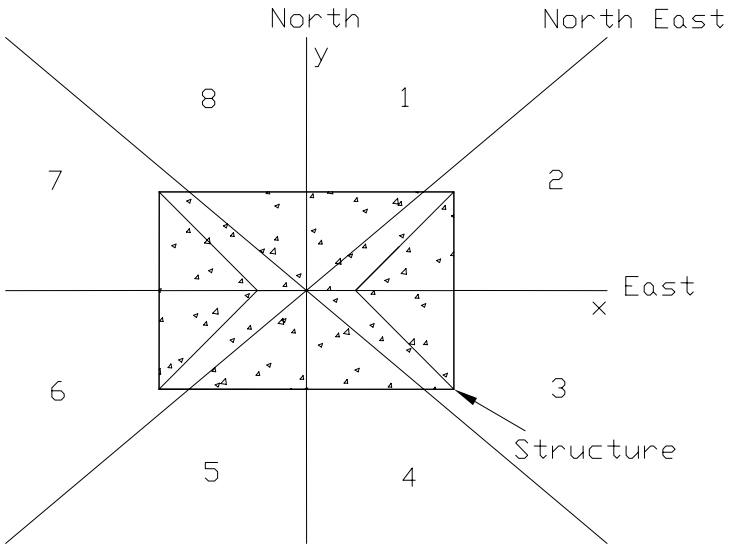

Figure 4.1. Wind loading quadrants used for MWFRS design (*ASCE 7*, 2003)

The wind loading quadrants above show how the determination of wind loads from different directions could have influenced the test structure. For each of the eight directions, upwind exposure was determined for each of two 45° sectors, with one on each side of the wind direction axis.

According to the *ASCE 7-02 Standard*, the sector with the exposure giving the highest loads was used to define wind loads for that direction. For example, for winds from the east, the highest exposure from sector two or three was used. Also, for wind coming from southeast, the most exposed of sectors three or four was used to determine full x and y loading individually. Then, 75% of these loads were applied in each direction at the same time.

Since the upwind exposure was assumed to be equal for all eight wind loading quadrants, the test structure was not evaluated differently for each quadrant. For the basic

wind speed of V = 120.34 mph, the test structure was evaluated from wind from all eight quadrants shown in Figure 4.1. The maximum of the eight wind loading quadrants gave the wind design that the test structure could expect to experience within a 50-year or 100-year return period.

Since this report focuses on a comparative analysis to the field data, only wind from the east and southeast direction was evaluated, since the test structure recorded the highest wind speed at 56.2 mph (50.33 mph when adjusted using Eq. 4.1) in the east-southeastern direction. The maximum of the two wind loading quadrants gave the wind design for the test structure when compared to the field data for Hurricane Katrina (see Section 6.4.2).

4.3.5.2 MWFRS Design Wind Load Cases

Four design wind load cases were used for the MWFRS for Method 2. These design wind load cases gave different wind pressure distributions across the entire test structure. Since the maximum wind speed recorded from Hurricane Katrina was in the east-southeastern direction, no other wind loading directions were considered for design, as the test structure must be designed for the worst case scenario. The four wind load design cases implemented are shown in Figure 4.2. It is worthy to note that in designing the test structure under a basic wind speed of V = 120.34 mph given the test structure's location, wind must be evaluated for all eight wind directions.

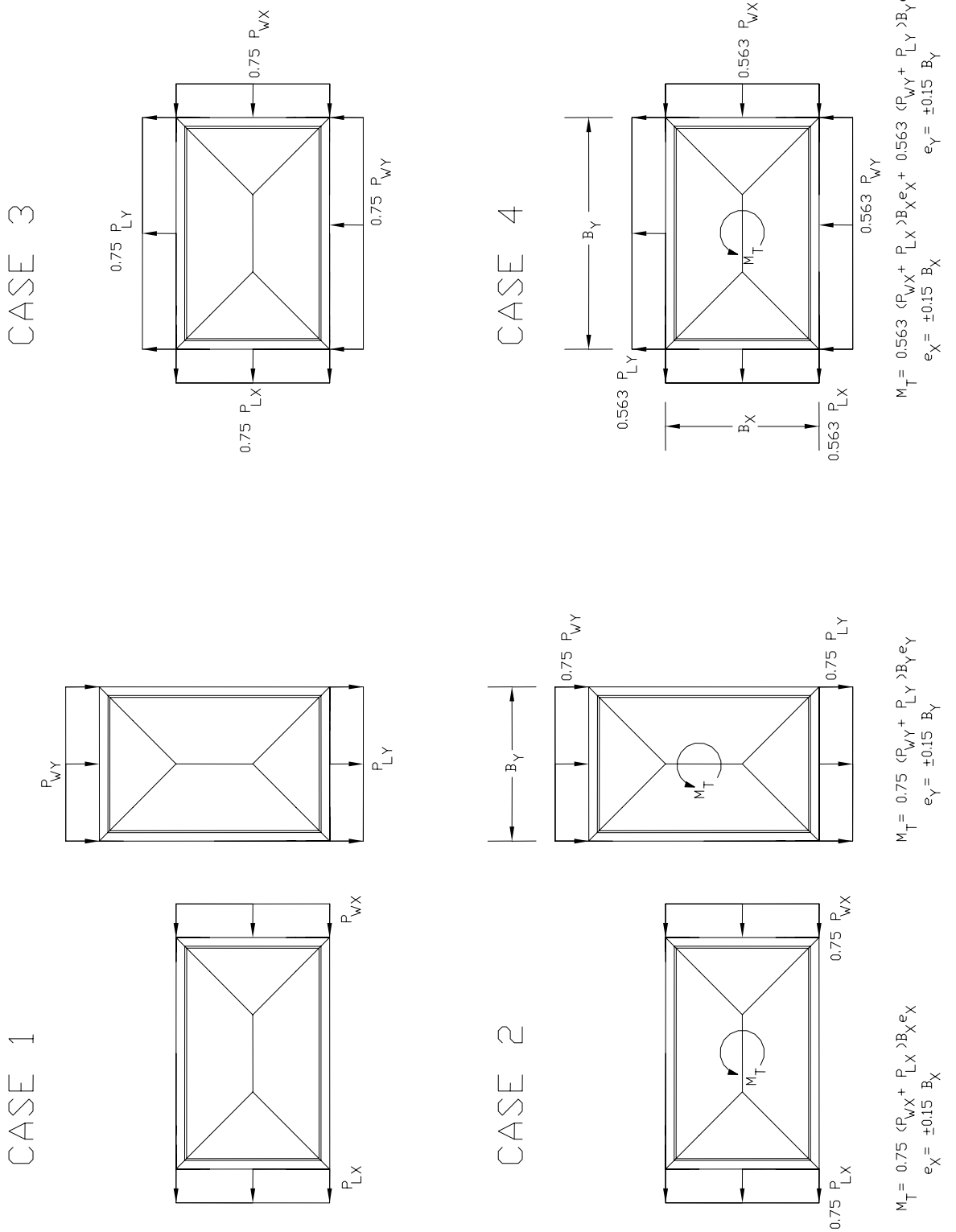

Figure 4.2. Design wind load cases for MWFRS (*ASCE 7*, 2003)

- Wind load case 1 was for the full design wind pressure acting normal to the projected surface. This design wind pressure gave the wind pressure distribution for winds from the east direction without torsional effects.
- Wind load Case 2 was for three quarters of the design wind pressure acting normal to the projected surface. This design wind pressure corresponded to the wind pressure distribution for the winds from the east direction with torsional effects. The torsional effects were represented by moment per unit height about the vertical axis of the building.
- Wind load Case 3 was for wind loading as defined in wind load Case 1, but was considered to act simultaneously at 75% of the specified value. This design wind pressure gave the wind pressure distribution for the winds from the southeast direction without torsional effects.
- Wind load Case 4 was for wind loading as defined in wind load Case 2, but was considered to act simultaneously at 75% of the specified value. This design wind pressure determined the wind pressure distribution for the winds from the southeast direction with torsional effects.

Figures 4.3 through 4.10 represent the design wind pressures calculated for 50.33 mph wind speeds from the east and southeast direction, which was the same direction to be evaluated as the peak wind speeds recorded from Hurricane Katrina. These figures represent the wind pressures for wind load Case 1 with pressure and suction, respectively; wind pressures for wind load Case 2 with pressure and suction, respectively; wind pressures for wind load Case 3 with pressure and suction, respectively; and wind pressures for wind load Case 4 with pressure and suction, respectively. All wind pressures were applied externally to

the test structure. There are two figures presented for each wind load case to delineate the positive and negative internal pressures separately (see Eq. 4.3). The directional arrows included in the figures show the direction of the wind normal to the surface in contact. Wind pressures outward signify suction and wind pressures inward signify pressure. Also, the torsional component (M_T) in wind load Cases 2 and 4 was applied per unit height along the building. Therefore, at the mean roof height the torsional component was multiplied by 12.5-ft.

To show the comparison of the wind pressure distribution on the test structure at its given location with V = 120.34 mph wind speeds, the pressures and suctions in Figures 4.3 through 4.10 would need to be multiplied by 5.72. In addition to winds from the east and southeast as shown in Figures 4.3 through 4.10, the design wind pressures would need to be calculated for winds from the north, northeast, south, southwest, west, and northwest. This is due to wind attacking the test structure from all eight wind loading quadrants (see Figure 4.1).

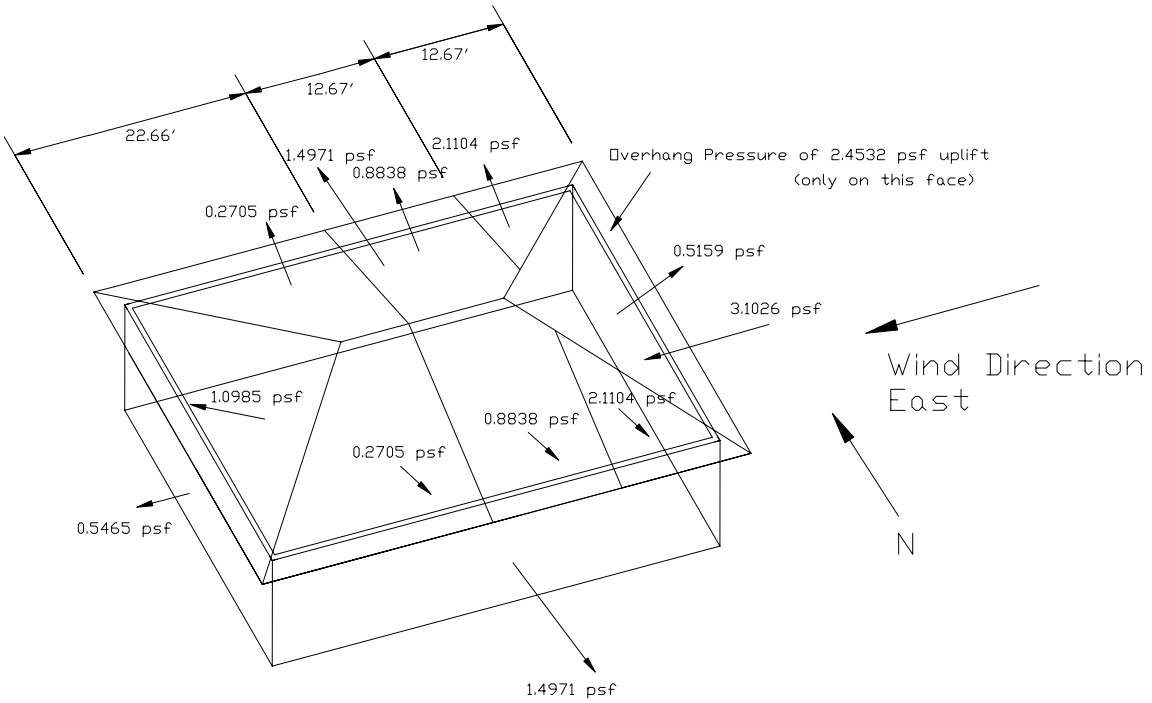

Figure 4.3. Method 2: MWFRS Case 1 for wind direction east at 50.33 mph wind speed with internal pressure 0.6494 psf

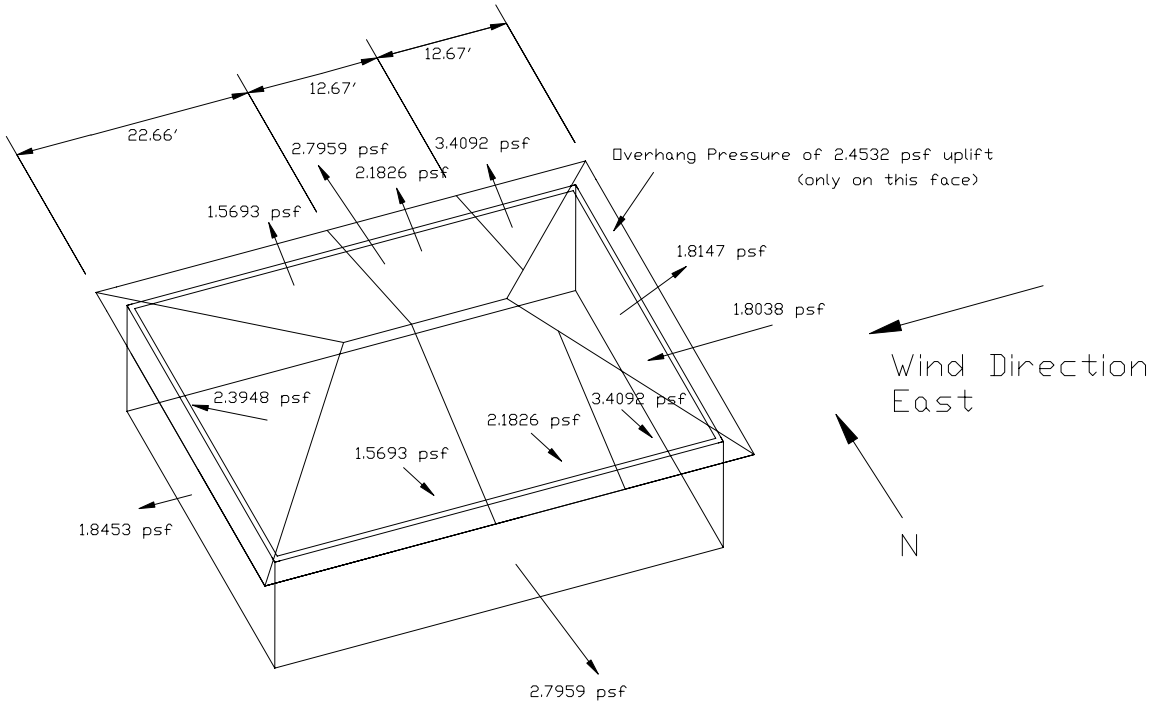

Figure 4.4. Method 2: MWFRS Case 1 for wind direction east at 50.33 mph wind speed with internal suction of –0.6494 psf

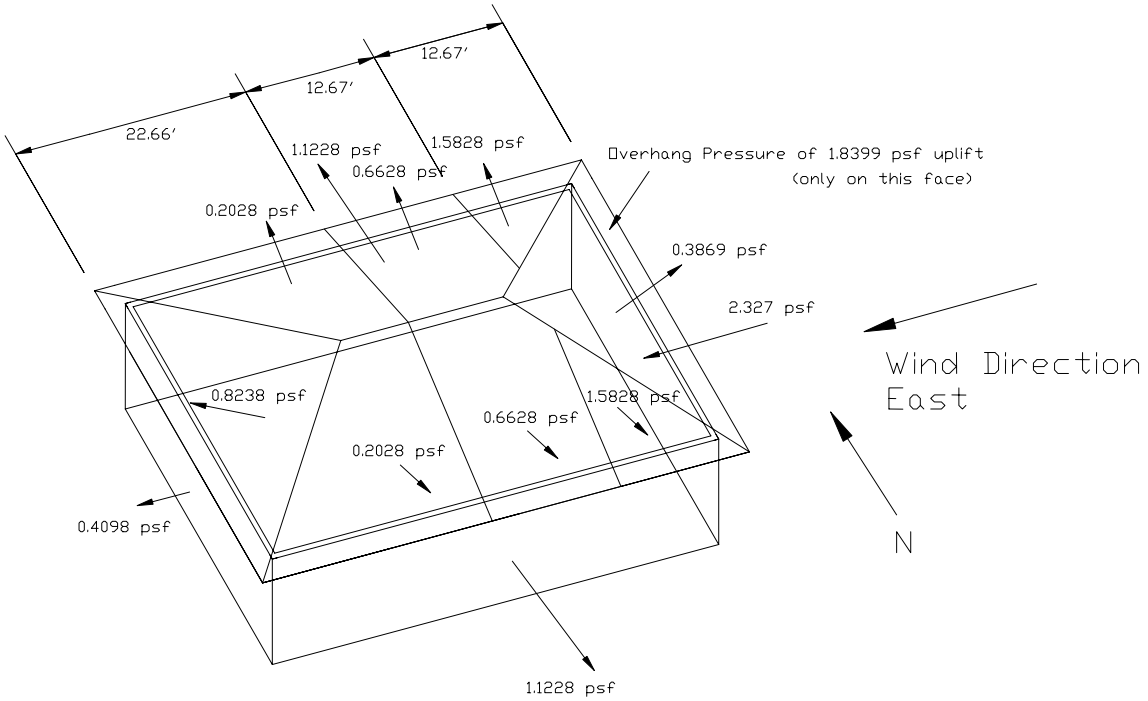

Note: Torsion is ±225.45 lb per unit height about the center of resistance of the building

Figure 4.5. Method 2: MWFRS Case 2 for wind direction east at 50.33 mph wind speed with internal pressure of 0.4871 psf

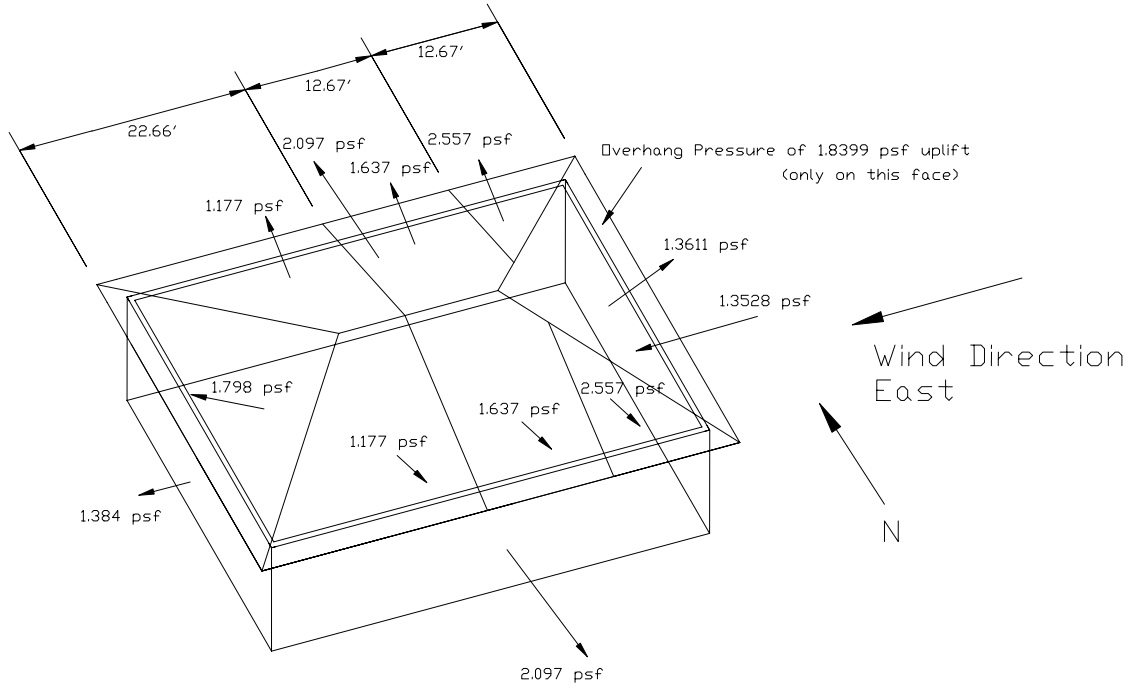

Note: Torsion is ±225.45 lb per unit height about the center of resistance of the building

Figure 4.6. Method 2: MWFRS Case 2 for wind direction east at 50.33 mph wind speed with internal suction of –0.4871 psf

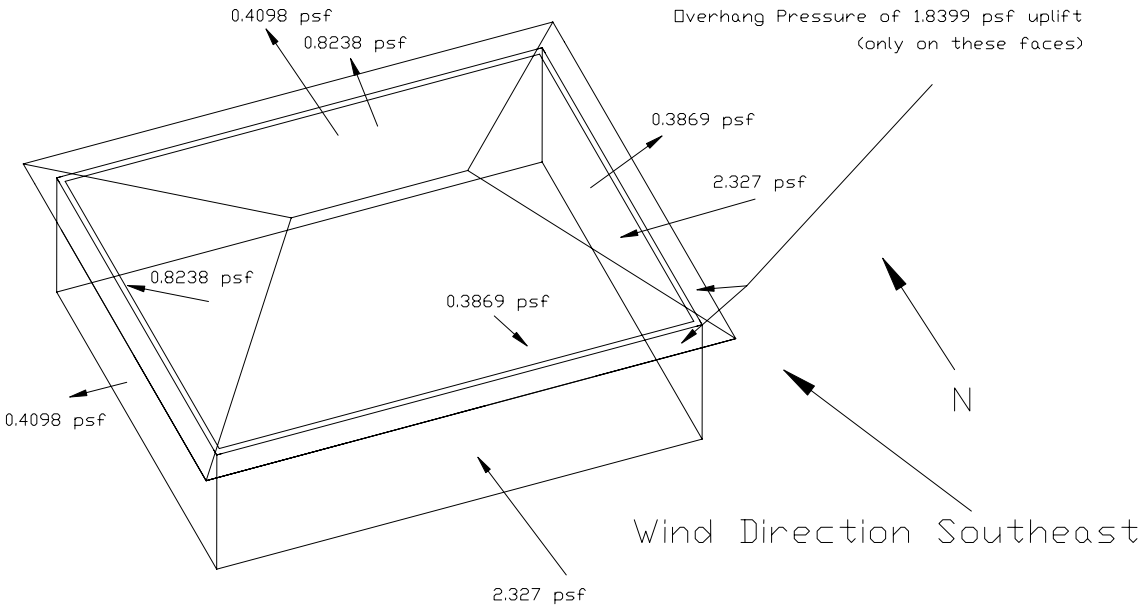

Figure 4.7. Method 2: MWFRS Case 3 for wind direction southeast at 50.33 mph wind speed with internal pressure of 0.4871 psf

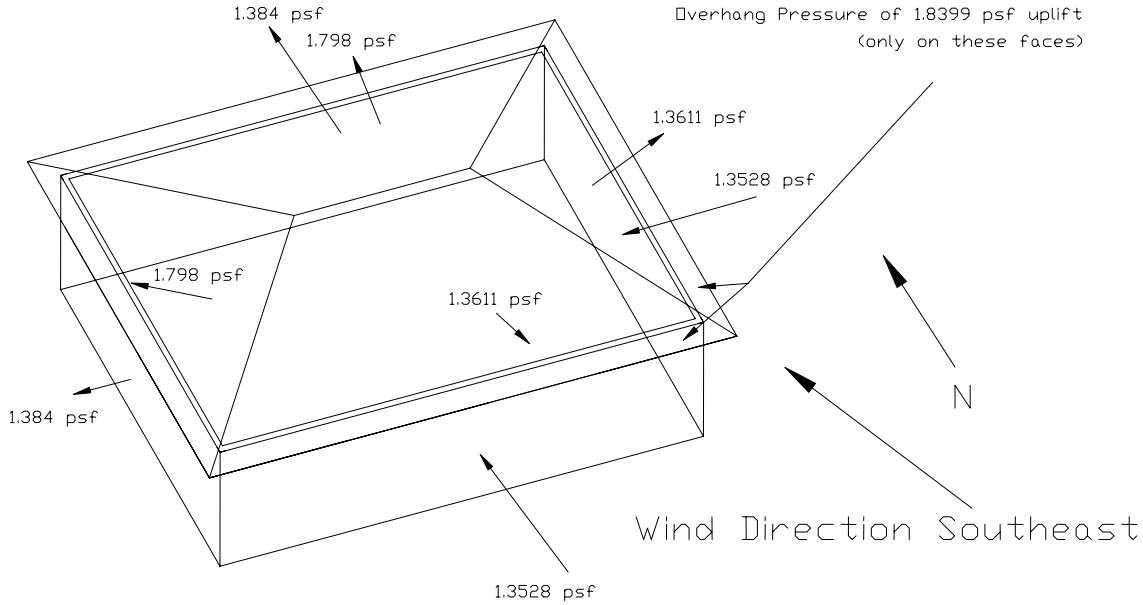

Figure 4.8. Method 2: MWFRS Case 3 for wind direction southeast at 50.33 mph wind speed with internal suction of –0.4871 psf

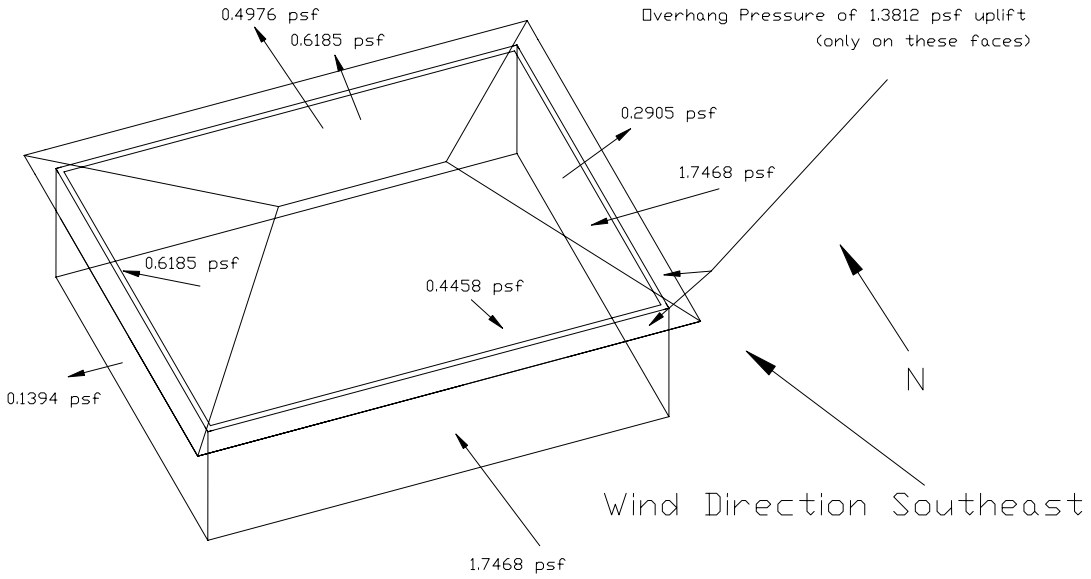

Note: Torsion is ±532.06 lb per unit height about the center of resistance of the building

Figure 4.9. Method 2: MWFRS Case 4 for wind direction southeast at 50.33 mph wind speed with internal pressure of 0.3656 psf

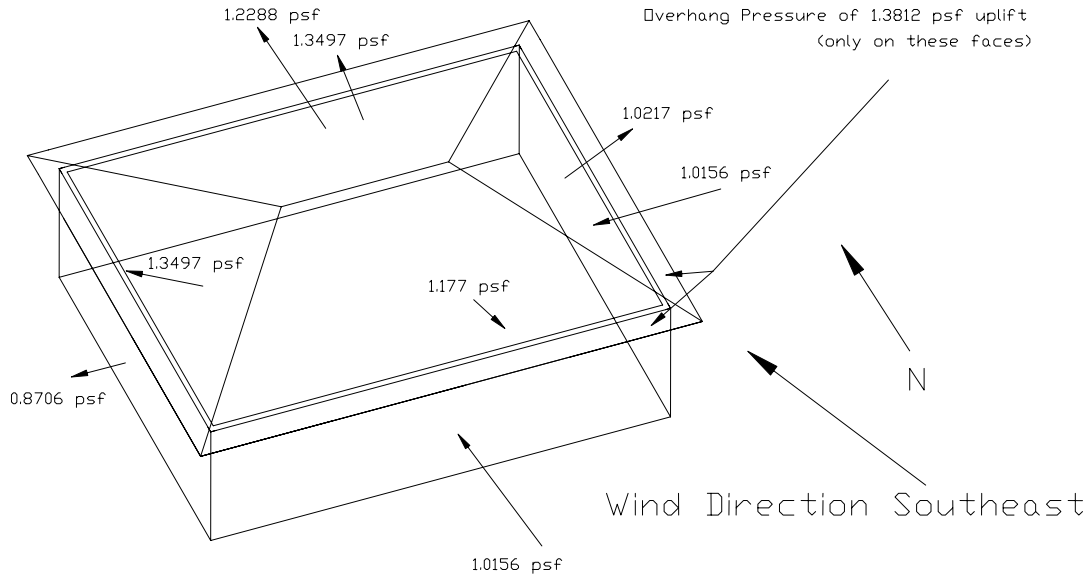

Note: Torsion is ±532.06 lb per unit height about the center of resistance of the building

Figure 4.10. Method 2: MWFRS Case 4 for wind direction southeast at 50.33 mph wind speed with internal suction of –0.3656 psf

As previously mentioned, the worst wind load case controlled the design for the wind pressures. Since the maximum wind speed recorded from Hurricane Katrina was measured in the east-southeast direction, only the easterly and southeast wind directions were considered. Therefore, all eight figures listed above must be plotted in the finite element model to give the worst wind load case for each individual rafter/truss in the hip roof. These design wind pressures controlled the hip roof design at wind speeds of 50.33 mph, which was the maximum recorded (as established in Section 4.3.1) wind speed during Hurricane Katrina data collection. It should be noted that the eight figures listed above were not adjusted for the basic wind speed of V = 120.34 mph wind speeds and found for winds from the other six wind directions. Figures 4.3 through 4.10 wind pressures would need to be multiplied by 5.72 to obtain the wind pressure distributions at V = 120.34 mph.

4.3.5.3 Method 1 Wind Pressure Distributions

As mentioned in Section 4.2, Method 1 design wind pressures were also plotted to compare to Method 2. However, these design wind pressures could not be adjusted to the maximum wind speed of 56.2 mph, or 50.33 mph after adjusting for height (see Section 4.3.1), because the design charts for Method 1 did not read any less than 85 mph. Also, the design charts for Method 1 wind design are for exposure B at h = 30 ft. Adjustment was done for exposure C at h = 15 ft, which was the smallest height, using the adjustment factor λ.

Figure 4.11 shows the horizontal and vertical projections for the wind pressure distributions at the basic wind speed of V = 120.34 mph. Since the wind speeds are only shown for winds from the east with the southeast corner of the structure seeing the critical

loads, there are seven other loading conditions for the basic wind speed of V = 120.34 mph that need to be evaluated for design. Positive pressures represent pressures into the test structure and negative pressures represent suctions on the test structure. It is worthy to note that there the test structure is only evaluated by load case 1 because the slope of the hip roof, θ, is only 18.435^{o}.

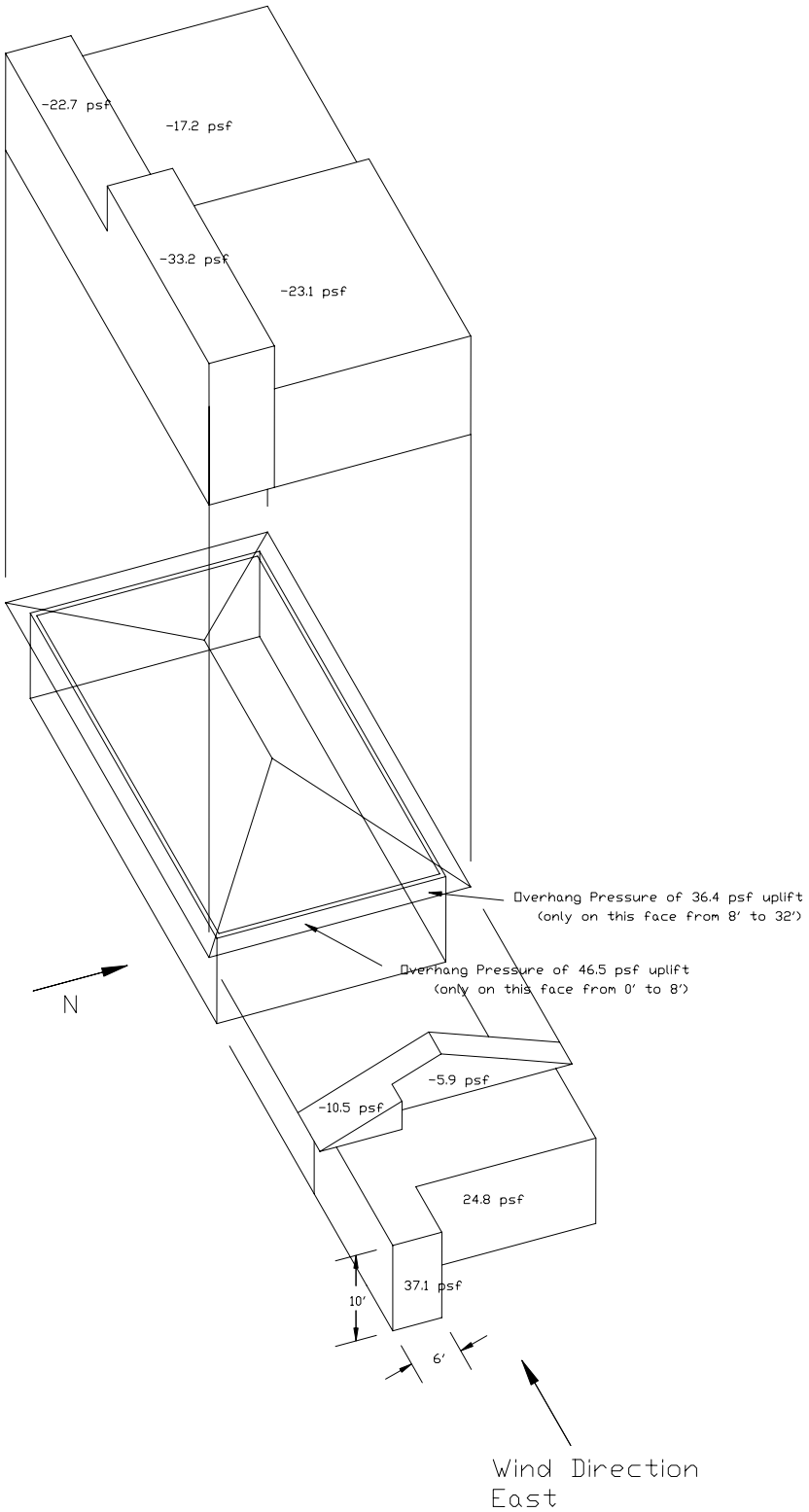

Figure 4.11. Method 1: MWFRS Case 1 for wind from the east at 120.34 mph wind speed

4.4 Wind Load for Components and Cladding (C&C) for Method 2

Once the wind load for the entire test structure was determined, more detailed attention was given to the components and cladding (C&C) for the test structure. A wind design was done for the components and cladding, which were designed for the studs in the walls and the wood rafters/trusses in the hip roof. These were the only two components evaluated since both the member properties and the material properties were known.

The wind design for components and cladding was done similar to the entire test structure, with the exception of the critical dimension of the component and cladding under wind load and the effective area in contact. The effective area in contact depended on the selected component. The critical dimension was represented by *a,* which was the lesser of 10% of the least horizontal dimension, or 40% of the building height, but not less than either 4% of least horizontal dimension or 3 ft (*ASCE 7*, 2003). As per the *ASCE 7-02 Standard*, the distance *a* defined the critical zones for components and cladding. The effective area in contact depended on the studs in the walls and the rafters/trusses for the hip roof, which were the components selected for analysis. The effective area in contact was the larger of the tributary area for the component being selected or the component length squared divided by three (*ASCE 7*, 2003). The effective area in contact limits the external pressure coefficient, GC_p.

The wind pressures were found by the following equation:

$$p = q_h[(GC_p) - (GC_{pi})] \text{ (psf)} \qquad (4.4)$$

where q_h was the velocity pressure evaluated at the mean roof height *h*, (GC_p) was the external pressure coefficients, and (GC_{pi}) was the internal pressure coefficients. One should note that both the external pressure coefficients and the internal pressure coefficients were taken from a different table than the MWFRS for the entire test structure. Eq. 4.4 can only be used for low-rise buildings of height less than or equal to 60 ft.

4.4.1 Wind Loads for Studs in the Walls for Method 2

The critical dimension, *a*, of the studs in the walls was 3 ft for the test structure. The effective area was based on the wall studs, which were 10 ft. tall and 2 ft. apart. Figures 4.12 and 4.13 represent the applied wind pressures acting normal to the walls at 120.34 mph (as established in Section 4.3.1) basic wind speed. All wind pressures were external on the test structure. The pressures are for both negative and positive pressures, suction and pressure, respectively. Figures 4.14 and 4.15 represent the applied wind pressures acting normal to the walls at 50.33 mph (as established in Section 4.3.1), which was the maximum recorded wind speed from Hurricane Katrina. The above listed figures indicate what wind pressure a given stud should be designed for. Therefore, a corner stud would have a different design wind load than a central stud in the wall. These design pressures on the wall studs could be used later for future research.

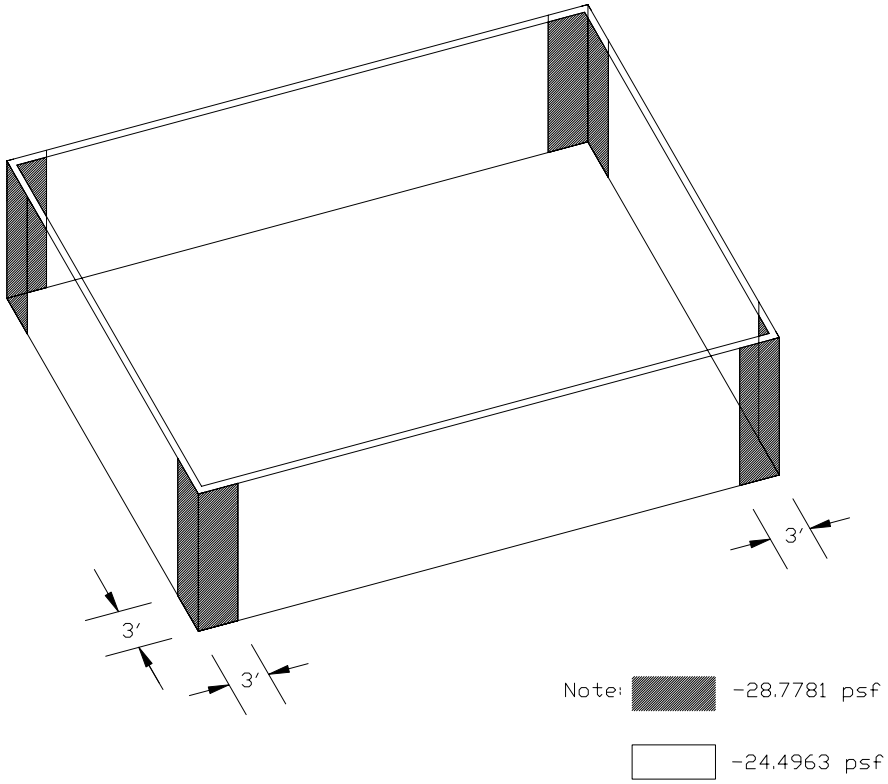

Figure 4.12. Method 2: C&C studs in the walls at 120.34 mph wind speed with suction

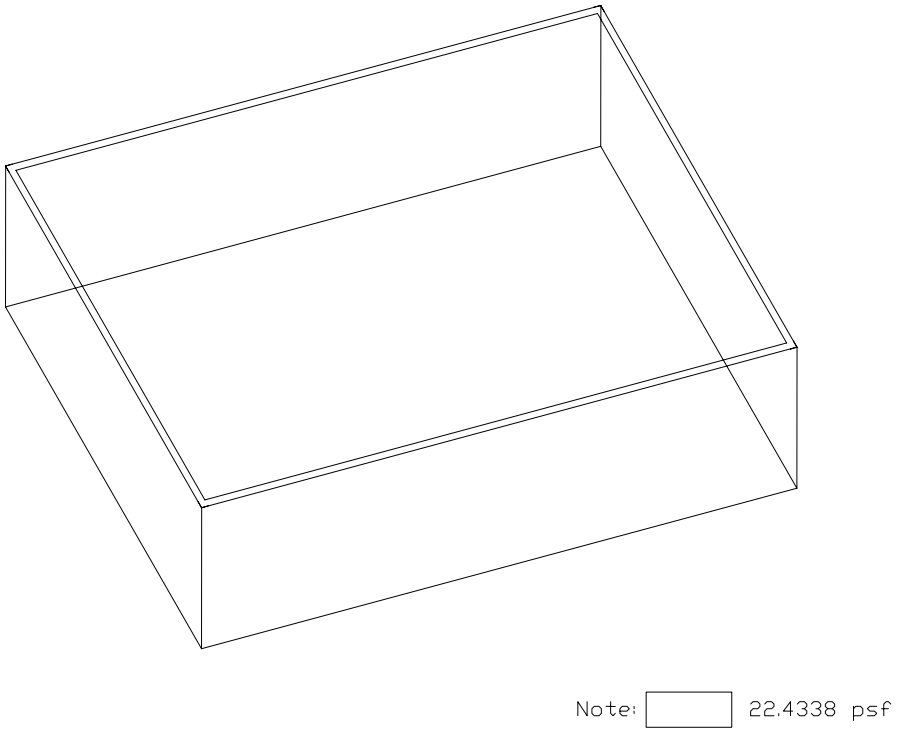

Figure 4.13. Method 2: C&C studs in the walls at 120.34 mph wind speed with pressure

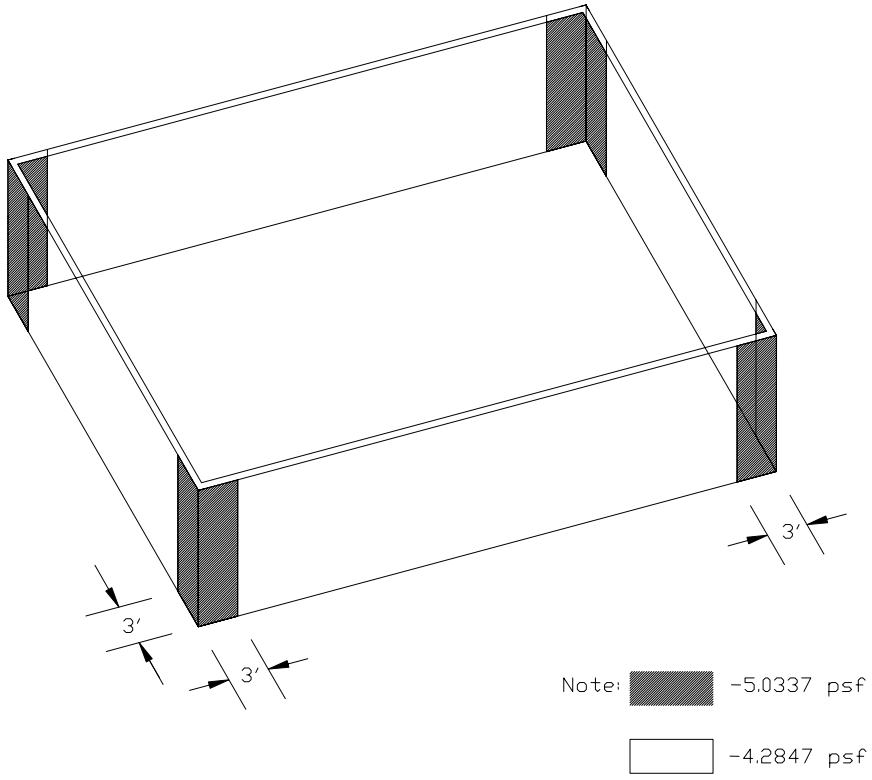

Figure 4.14. Method 2: C&C studs in the walls at 50.33 mph wind speed with suction

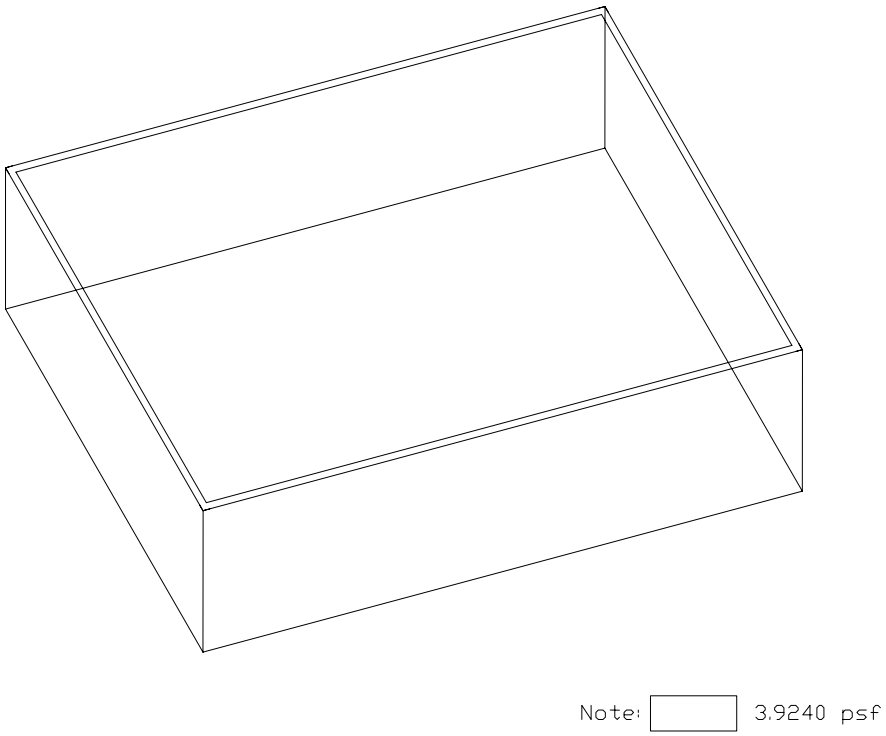

Figure 4.15. Method 2: C&C studs in the walls at 50.33 mph wind speed with pressure

4.4.2 Wind Loads for Studs in the Walls for Method 1

As mentioned in Section 4.2, Method 1 design wind pressures were also calculated. However, these design wind pressures could not be adjusted to the maximum wind speed of 56.2 mph, or 50.33 mph after adjusting for height (see Eq. 4.1), because the design charts for Method 1 did not read any less than 85 mph. Also, the design charts for Method 1 wind design are for exposure B at h = 30 ft. Adjustment was done for exposure C at h = 15 ft, which was the smallest height, using the adjustment factor λ. Also, adjustment for the effective wind area was linearly interpolated in the design charts.

Figures 4.16 and 4.17 show the applied normal wind pressure distributions at the basic wind speed of V = 120.34 mph. Positive pressures represent pressures into the test structure and negative pressures represent suctions on the test structure.

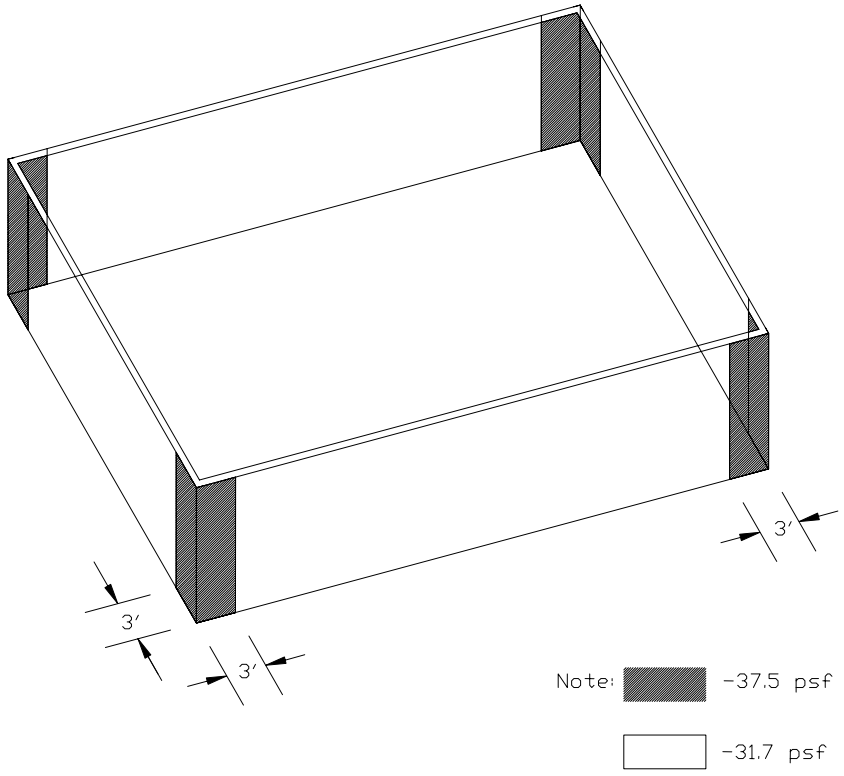

Figure 4.16. Method 1: C&C studs in the walls at 120.34 mph wind speed with suction

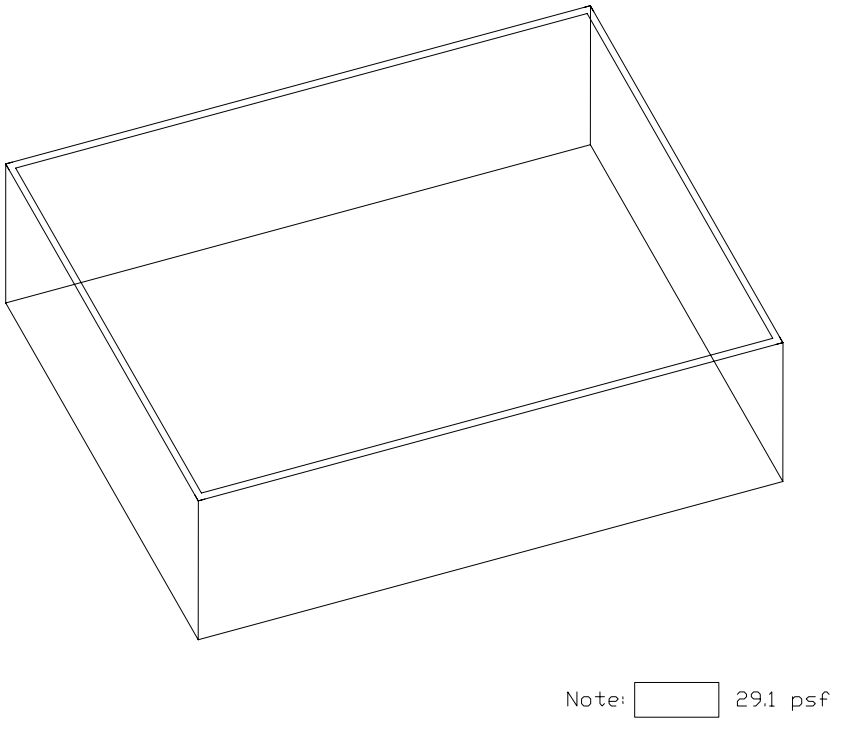

Figure 4.17. Method 1: C&C studs in the walls at 120.34 mph wind speed with pressure

4.4.3 Wind Loads for Rafters/Trusses in the Hip Roof for Method 2

The critical dimension, *a*, of the wood rafters/trusses in the hip roof was 3 ft for the test structure. The effective area was based on the roof trusses, which were 32 ft. long and spaced 2 ft. apart. Figures 4.18 and 4.19 represent the applied wind pressures which acted normal to the hip roof at the basic wind speed of 120.34 mph (as established in Section 4.3.1). All wind pressures were external on the test structure. Figures 4.20 and 4.21 represent the applied wind pressures acting normal to the hip roof at 50.33 mph (as established in Section 4.3.1), which was the maximum recorded wind speed from Hurricane Katrina. The above listed figures indicate which pressure a given rafter/truss in the hip roof should be designed for. Therefore, a particular rafter/truss would have a variety of design wind loads along its length. Since the pressures recorded from the test structure were given at specific locations (see Figure 3.8), this pressure distribution was compared directly to the field data recorded from Hurricane Katrina (see Section 6.4.3).

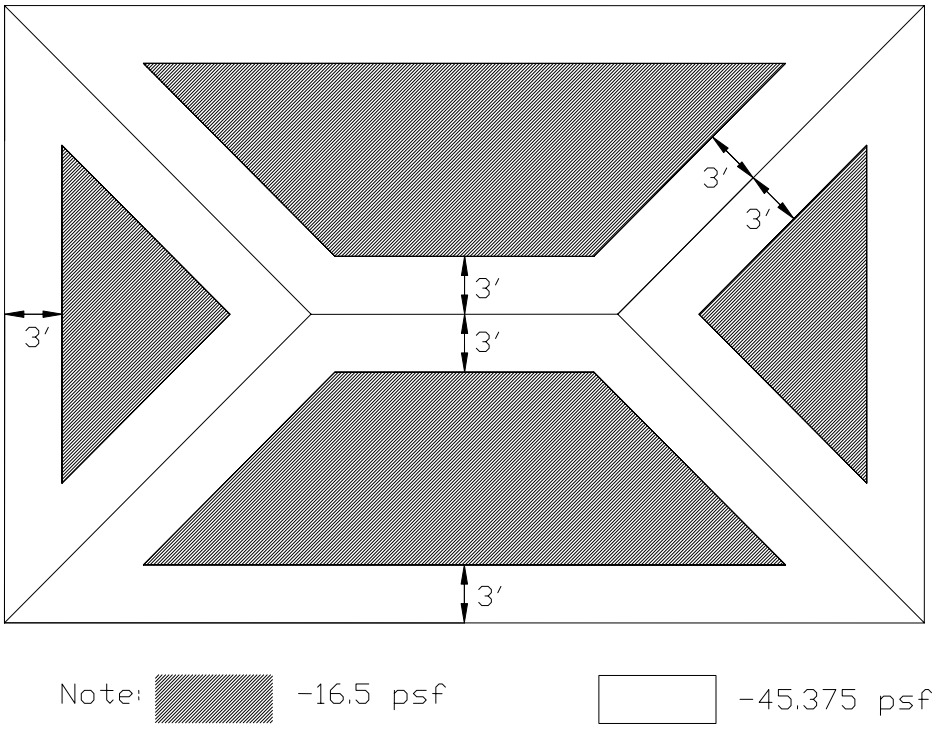

Figure 4.18. Method 2: C&C rafters/trusses at 120.34 mph wind speed with suction

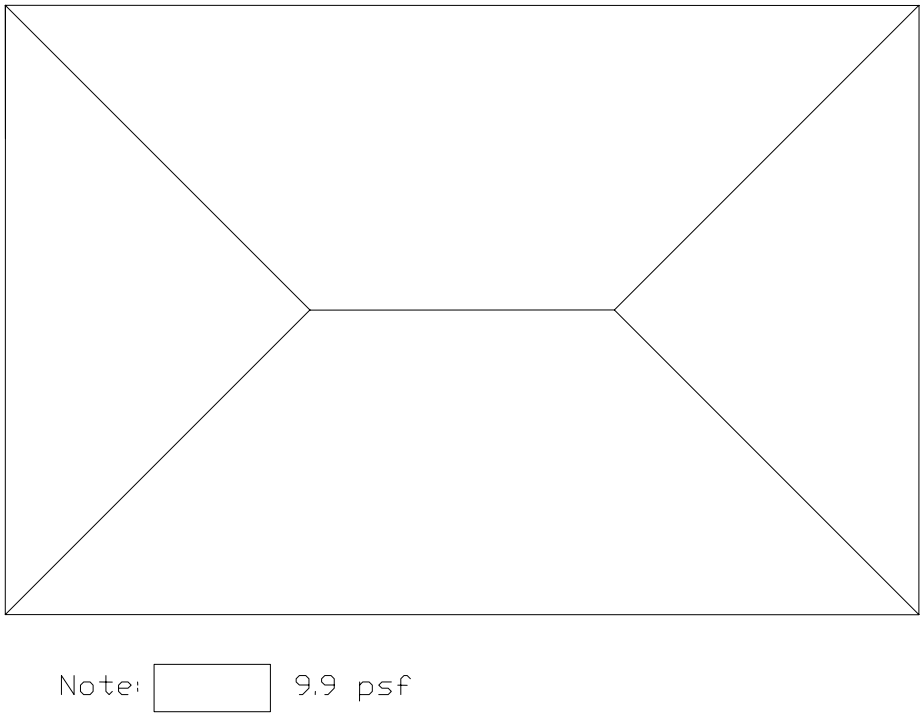

Figure 4.19. Method 2: C&C rafters/trusses at 120.34 mph wind speed with pressure

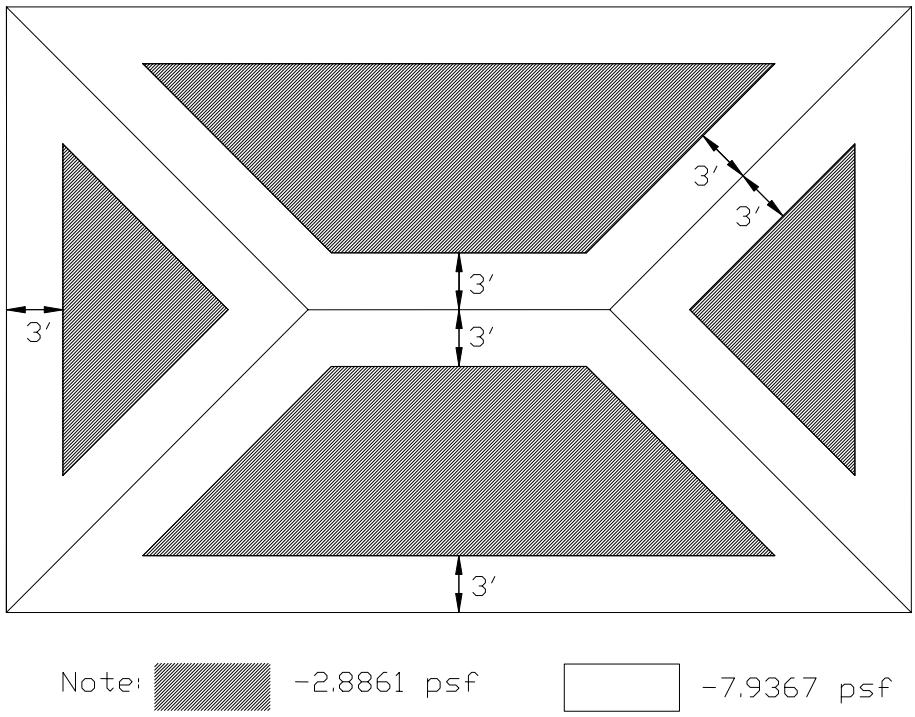

Figure 4.20. Method 2: C&C rafters/trusses at 50.33 mph wind speed with suction

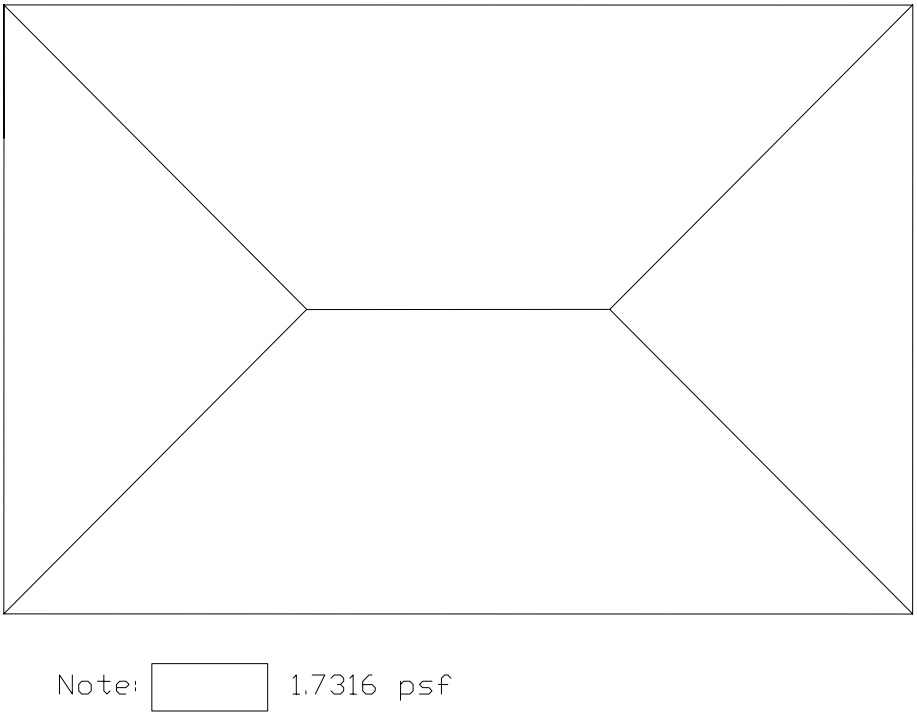

Figure 4.21. Method 2: C&C Rafters/Trusses at 50.33 mph wind speed with pressure

4.4.4 Wind Loads for Rafters/Trusses in the Hip Roof for Method 1

As mentioned in Section 4.2, Method 1 design wind pressures were also calculated. However, these design wind pressures could not be adjusted to the maximum wind speed of 56.2 mph, or 50.33 mph after adjusting for height (see Eq. 4.1), because the design charts for Method 1 did not read any less than 85 mph. Also, the design charts for Method 1 wind design are for exposure B at h = 30 ft. Adjustment was done for exposure C at h = 15 ft, which was the smallest height, using the adjustment factor λ. Also, adjustment for the effective wind area was interpolated in the design charts.

Figures 4.23 and 4.24 show the applied normal wind pressure distributions at the basic wind speed of V = 120.34 mph. Positive pressures represent pressures into the test structure and negative pressures represent suctions on the test structure.

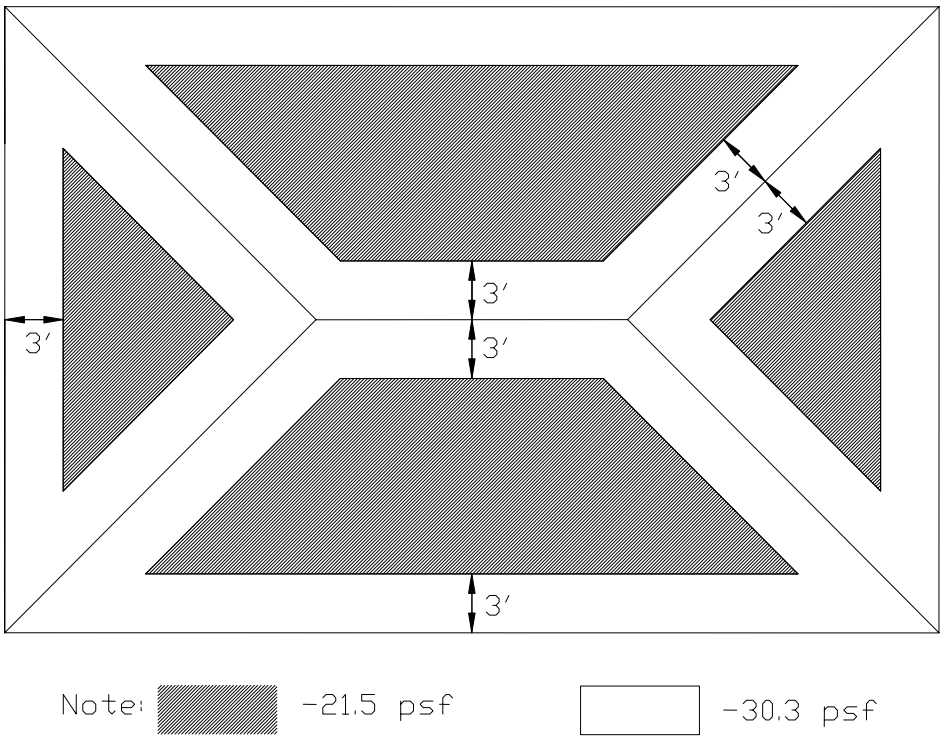

Figure 4.22. Method 1: C&C rafters/trusses at 120.34 mph wind speed with suction

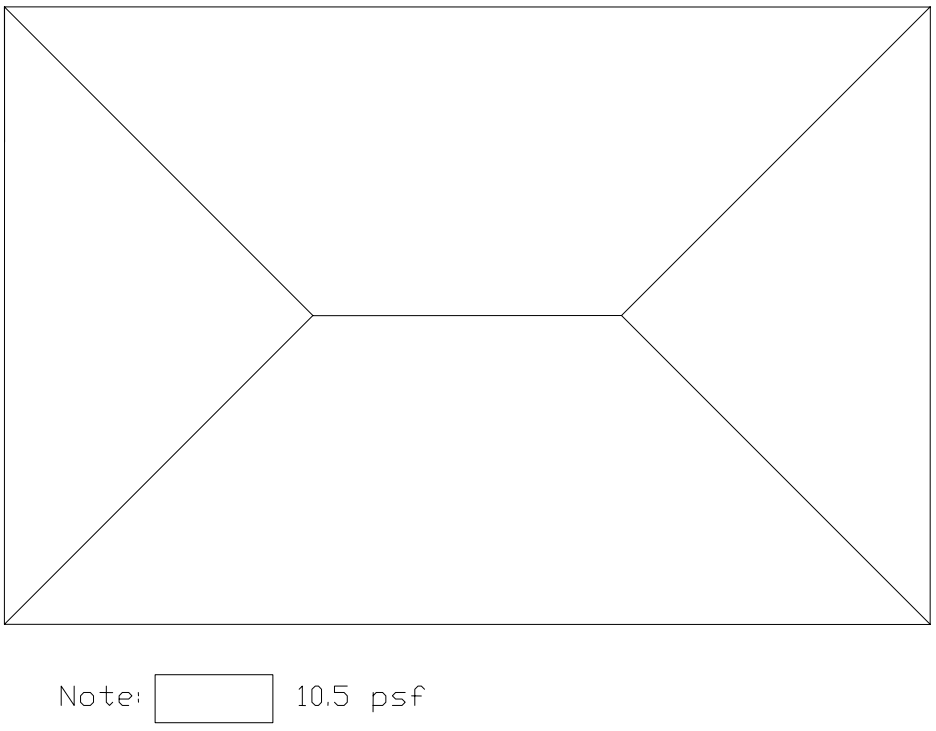

Figure 4.23. Method 1: C&C rafters/trusses at 120.34 mph wind speed with pressure

CHAPTER 5. FINITE ELEMENT MODELING OF THE ROOF STRUCTURE

The roof structure of the test house was analyzed using finite element computer software ANSYS 9.0 (Swanson Analysis Systems, 2006) and the results were compared to the available test data. The analytical investigation was limited only to the roof structure because this component of the house was isolated from the rest of the house and the field data were obtained only for the hip roof (see details in Section 3.1). Detailed modeling of the different roof components are presented in this chapter while the analysis results as well as comparisons between the analysis and experimental results are given in Chapter 6.

5.1 Rafter/Truss System

The finite element model of the rafter/truss system is shown in Figure 5.1. The type of elements used and the idealization process of these trusses and rafters are summarized in the following sub-sections.

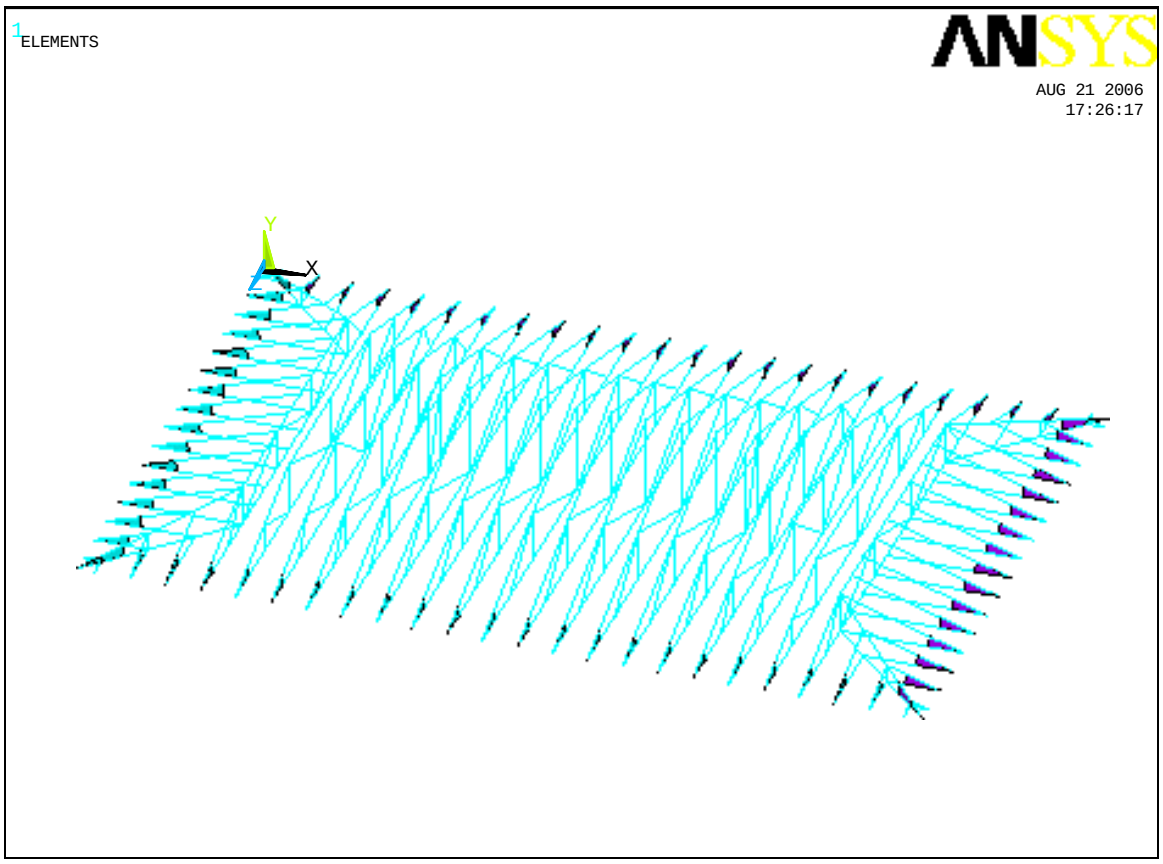

Figure 5.1. Finite element model used for the rafter/truss system

5.1.1 Element Types Used

Various structural elements available in the ANSYS element library were used to produce the finite element (FE) model of the rafter/truss system. Beam elements (beam4 as referred to in the ANSYS element library) were used to model the top and bottom chords of all trusses. Truss elements (link8 in the ANSYS element library) were used to model the cross braces, or webs, in all the trusses and *HJ10* rafters. To account for the additional stiffness provided by the plates at the corners of the rafters (see Figure 3.6, Figure 5.2, and Appendix A), plate elements (shell63 in the ANSYS element library) were employed. Figure 5.2 shows a typical idealization for one of the truss structures. More details on the three

different element types used for the rafter/truss system and the reasons for selecting these specific elements are presented below.

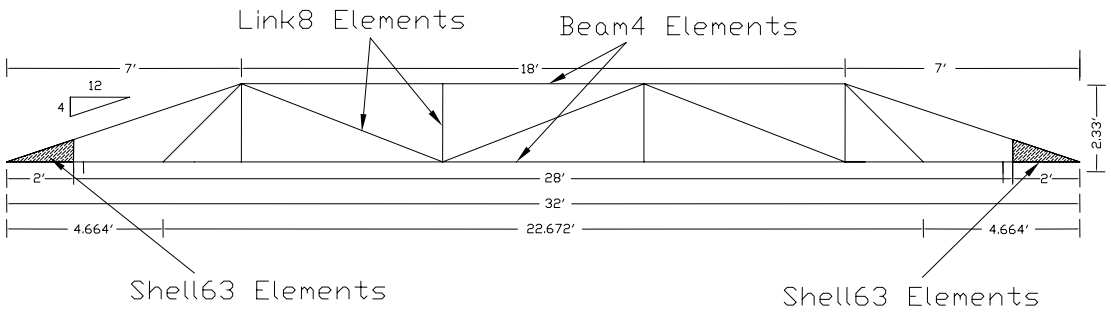

Figure 5.2. Different elements used establishing a FE model for truss *A1*

Figure 5.2 describes the modeling technique utilized in the finite element model by all rafter/truss members of the roof system, except the rafter *CJ1*. Since this rafter was shown to be a part of the roof system, but was not provided by J.M. Harold Construction (2006) documents, the elements that comprised this rafter were assumed similar to that modeled in all other rafters. For the location of rafter *CJ1* refer to Figure 3.5. Figure 5.3 depicts the elements utilized in rafter *CJ1*.

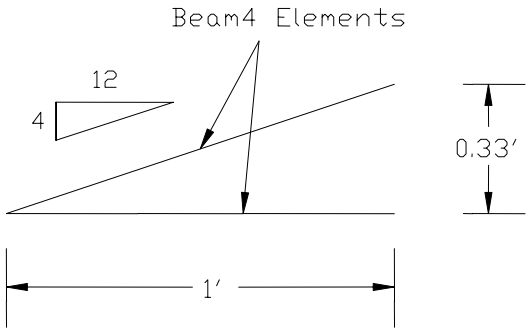

Figure 5.3. Assumed elements used for establishing a FE model for rafter *CJ1*

5.1.1.1 Beam4 Elements

Beam4 elements are three-dimensional elements with 6-degrees of freedom per node with tension, compression, torsion, and bending capabilities. This idealization was necessary since direct loads from the roof sheathing and ceiling were transferred to the top and bottom chords of the trusses, respectively.

The orientation of the local axes of the element cross section was accomplished by defining each element with respect to three nodes. The nodes are entered as I, J, and K. The first two nodes defined the element while the third node (K) ensures the proper orientation of the element in the 3-D space. Figure 5.4 shows the orientation of the members using the three-node option. The member properties for all beam4 elements, except wood truss *A1*, are listed in Table 5.1. Wood truss *A1* has different member properties since it is a two-ply truss (see details in Section 3.2), which were two trusses nailed back-to-back. The member properties for wood truss *A1* are listed in Table 5.2.

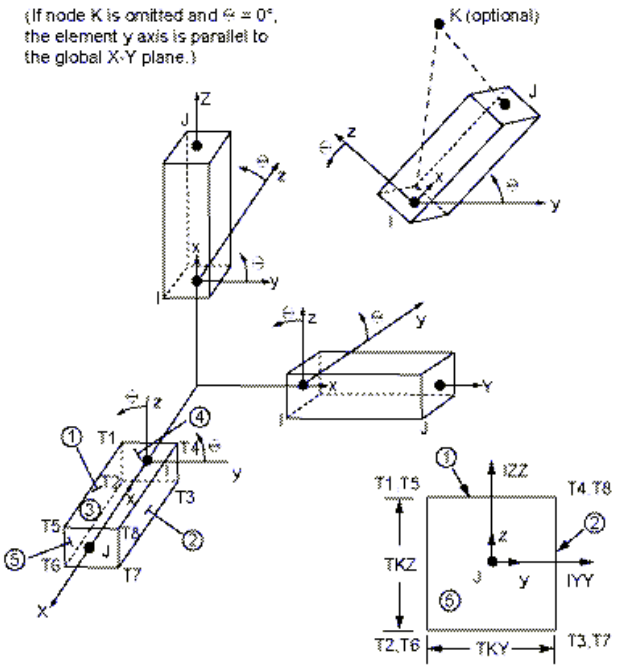

Figure 5.4. Defining orientation of a beam4 element using three-node option (Swanson Analysis Systems, 2006)

Table 5.1. Geometric properties of Beam4 elements used for trusses, except truss *A1*

Variable and Units Used	Value
Cross-sectional area, A (in^2)	5.25
Area moment of inertia, IZZ (in^4)	0.984
Area moment of inertia, IYY (in^4)	5.359
Thickness, TKZ (in)	3.5
Thickness, TKY (in)	1.5
Torsional moment of inertia, IXX (in^4)	6.344

Note: Remaining member properties were assumed a value of zero

Torsional moment of inertia was given as the polar moment of inertia by IZZ + IYY

Table 5.2. Geometric properties of Beam4 element used for truss *A1*

Variable and Units Used	Value
Cross-sectional area, A (in^2)	10.5
Area moment of inertia, IZZ (in^4)	7.875
Area moment of inertia, IYY (in^4)	10.719
Thickness, TKY (in)	3.5
Thickness, TKZ (in)	3
Torsional moment of inertia, IXX (in^4)	18.594

Note: Remaining member properties were assumed a value of zero

Torsional moment of inertia was given as the polar moment of inertia by IZZ + IYY

5.1.1.2 Link8 Elements

Three dimensional truss members were used to model the diagonal and vertical members of the rafter/truss system. Link8 elements are three-dimensional, uniaxial tension-compression elements with three DOFs at each node. The member properties for the link8 elements are given in Table 5.3 below.

Table 5.3. Geometric properties of link8 elements used for the diagonal and vertical members of the rafter/truss system

Variable and Units Used	Value
Cross-sectional area, A (in^2)	5.25
Initial strain	0

5.1.1.3 Shell63 Elements

Shell63 elements were used to model the stiffener plates in the ends of all the rafters/trusses, except for the *CJ1* rafters (see Section 5.1.1). This element has six DOF at each node. The six DOF are translations in the nodal x-, y-, and z-directions and rotations in

the nodal x-, y-, and z-directions. The stiffener plates are the 2x6-in. members that run along the bottom chord of the rafters/trusses. Although they are referred to as 2x6-in. members by manufacturers, the actual cross-section of these members is 1.5-in. x 5.5-in., which is used to define the properties of the shell element. Shell63 elements were only used from the outermost corners, which is the overhang, to the wall support that is 2 ft. from the hip roof overhang (see Figures 5.1 and 5.2). The stiffener plates in some cases extend beyond the wall supports; however, for simplicity they were not included in the model.

Shell63 elements have both membrane and bending capabilities, which allow the element to move in- and out-of-plane, respectively. After a preliminary analysis, membrane action was determined to be more important for the FE model. Furthermore, out-of-plane action was completely neglected for the stiffener plates.

The geometric properties for the shell63 elements utilized in the stiffener plates are given in Table 5.4 below.

Table 5.4. Geometric properties of shell63 elements used for the stiffener plates of the rafter/truss system

Variable and Units Used	Value
Shell thickness at node I (in)	1.5
Shell thickness at node J (in)	1.5
Shell thickness at node K (in)	1.5
Shell thickness at node L (in)	1.5

Note: Remaining member properties were assumed a value of zero

5.1.2 Material Properties

The material properties for all element types of the rafter/truss system were assumed to be the same because the majority of the members were Southern Pine #2 grade lumber (see Appendix A). The density for this lumber grade was established using a wood design guide (National Design Specification Supplement, 2001). Accordingly, the density was determined from Eq. 5.1.

$$Density = 62.4\left[\frac{G}{1+G(0.009)(MC)}\right]\left[1+\frac{MC}{100}\right] \qquad (5.1)$$

Eq. 5.1, where G is the specific gravity and MC is the moisture content, was based on the southern pine #2 grade lumber and an assumed moisture content of 15%, which is a common industry standard. Also, it was assumed that 5% of the rafter/truss material density be used for the nailing and connections. The density input into ANSYS 9.0 is not a weight density, but mass density. Mass density was obtained by dividing the weight density by the acceleration of gravity (32.2 ft/s^2). Including mass density in ANSYS analyses accounts for effects of self weight. Table 5.5 summarizes the material properties utilized in the FE model of the roof structure and more details can be found in Appendix A. These properties, including the mass density, modulus of elasticity (EX) in the nodal x-direction and poisson's ratio (ν), were assumed isotropic material properties in the FE model. This assumption was considered adequate for the scope of the work presented in this report.

Table 5.5. Material properties used for rafter/truss system

Variable and Units Used	Value
Specific gravity, G	0.55
Modulus of elasticity, EX (psi)	1,600,000
Poisson's ratio, v	0
Weight density (rafters/trusses), D (lb/ft^3)	36.7402
Weight density (nailing/connections), D (lb/ft^3)	1.837
Mass density, D ($lb\text{-}s/ft^4$)	1.1981

The total weight of the rafter/truss system was 3,867.4 lbs., using the above table for material properties. The weight of the roof sheathing is further evaluated in Section 5.2.2. The weight of the structure, including the sheathing weight is further evaluated in Section 6.1.

5.2 Roof Sheathing

Roof sheathing of the test house consists of asphaltic shingles, roofing felt, plywood, and gypsum board. Figure 5.5 shows the FE model of the hip roof sheathing. The element size used for sheathing in conjunction with the model of the rafter/truss system was 2-ft. x 2-ft. over the entire hip roof. However, since this was a hip roof and the truss webs intersected the sheathing differently along every truss, the sheathing could not retain this rectangular grid across the entire structure. This is evident along the ridgelines, corners, and a few areas of the north and south roof surfaces (see Figure 5.5). The selection of the size of sheathing elements was of importance since it was necessary to interpolate the recorded field pressure data to represent the distribution of the pressure over the entire roof. More information on the sheathing elements is presented below while details on how the interpolation of the

measured pressures were carried out to represent them as external loads on sheathing elements is given in Section 6.2.2.

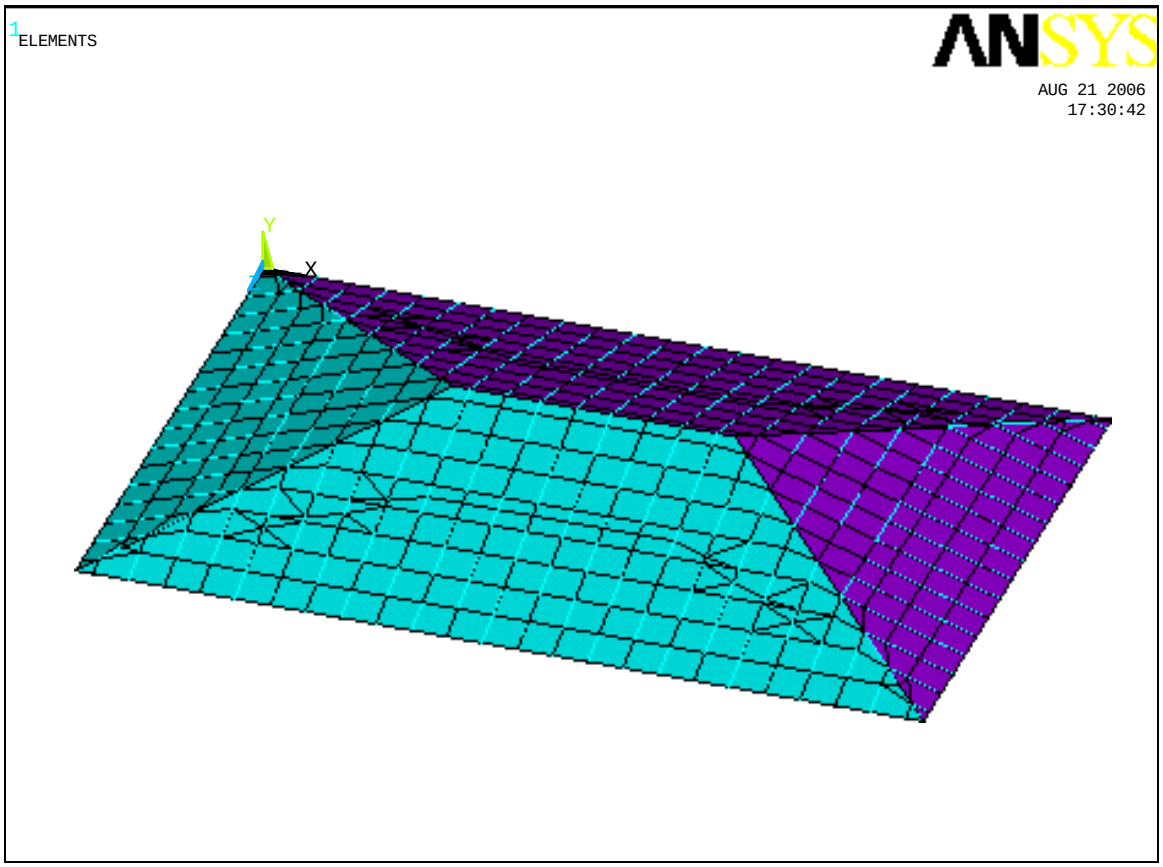

Figure 5.5. FE model of sheathing used for the hip roof

5.2.1 Shell63 Element

Shell63 element available in ANSYS 9.0 was used to model the roof sheathing and description of this element can be found in Section 5.1.3. However, two noticeable changes were adopted when using the shell63 element as roof sheathing. First, the element is modeled to have membrane and bending capabilities to simulate realistic behavior of the sheathing, allowing the element to move in- and out-of-plane, respectively. Second, the orientation of the element is important because the wind load needs to be applied normal to

the surface of the sheathing. Figure 5.6 shows the member orientation of a shell63 element along with its face numbers. All shell63 elements were represented in the FE model such that they represent static wind pressures acting on face surface number 1 or 2, whichever is the exterior face surface modeled (see Figure 5.5).

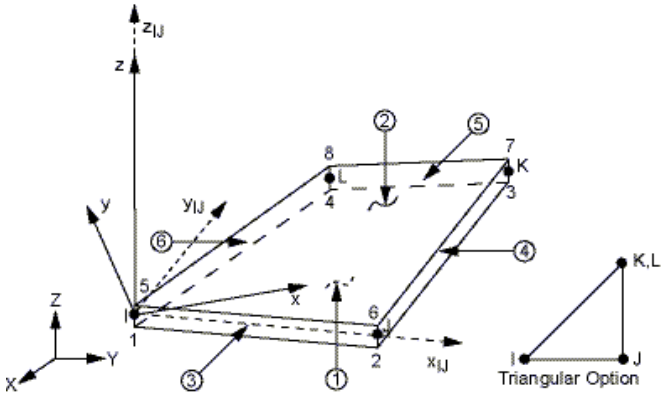

Figure 5.6. Member orientation of shell63 element (Swanson Analysis Systems, 2006)

5.2.2 Material Properties

The material properties for the hip roof sheathing were established as additive of those of all the layered elements. The self weights of the asphaltic shingles, roofing felt, plywood, and gypsum board were taken as those specified in *ASCE 7-02 Standard* because more accurate estimates of material used in the test house were not available. In addition, a 5% of weight of the plywood and gypsum board used to model the weight of nailing and connections to the hip roof.

The plywood sheathing was the material used for calculation of the modulus of elasticity in the x-direction (EX) and poisson's ratio (ν) because the plywood sheathing was

the thickest element used for the layered roof sheathing. Although wood utilizes anisotropic material properties due the wood grain's direction, the plywood sheathing was assumed with isotropic properties to keep the FE model as a simple, linear model. Changing the roof sheathing to anisotropic is yet another area of future research.

The sheathing properties entered in the FE model were the mass density established from the estimation of the self weight and other isotropic material properties. The additional isotropic material properties included the modulus of elasticity in the nodal x-direction (EX) in units of lb/in^2 (psi) and poisson's ratio (ν). Table 5.6 lists the material properties used for the hip roof sheathing in the FE model. Although the member properties given by the *ASCE 7-02 Standard* are listed as lb/ft^2, they were adjusted to obtain the equivalent mass density from Eq. 5.2, where the thickness refers to the ½-in. thickness of the shell63 element.

$$MassDensity = \frac{Load(psf)}{thickness * accelerationofgravity} \tag{5.2}$$

Table 5.6. Material properties used for the hip roof sheathing

Variable and Units Used	Value
Unit weight of asphalt shingles (psf)	2
Unit weight of single ply sheet (roofing felt) (psf)	0.7
Unit weight of 1/2-in. plywood (psf)	1.6
Unit weight of 1/2-in. plywood (nailing/connections), (psf)	0.08
Unit weight of gypsum sheathing (psf)	2
Unit weight of gypsum sheathing (nailing/connections) (psf)	0.1
Total weight (psf)	6.48
Modulus of elasticity, EX (psi)	1,600,000
Poisson's ratio, v	0
Mass density, D (lb-s/ft^4)	4.8298

The total weight of the hip roof sheathing was 10,492 lbs., using the above table for material properties. The weight of the structure, including the sheathing weight is further evaluated in Section 6.1.

5.3 Boundary Conditions

The boundary conditions used in the FE model formulation consisted of coupling of nodes and constraints at various nodes including the support locations. Nodes connecting the sheathing to the truss were coupled in the x-, y-, and z-directions. All nodes were modeled as rollers at all wall/rafter/truss supports, except underneath the *CJ3* rafters, to ensure a realistic model. Nodes connecting the sheathing to the truss were coupled in the x-, y-, and z-directions.

5.3.1 Coupled Nodes

Coupling of nodes enables forcing of one node to undergo identical deformation of another node in the selected degrees of freedom. A set of coupled DOFs contains a *prime* DOF (master node), and one or more slave DOFs. The master node with the DOF to be retained and the slave nodes represent those DOF to be condensed in the stiffness matrix.

Translational degrees of freedom for the rafters *CJ1*, *CJ3*, and *CJ5* were coupled in all three directions, except to the top chord of rafter *HJ10*, to the nodes of rafter HJ10 (see Figure 5.9). Translational degrees of freedom for the rafters *EJ7* and *HJ10* were coupled in all three directions, except to the top chord of rafter *HJ10*, to the nodes on the *A1* trusses (see Figure 5.9). This will simulate a pinned connection at these locations. The top chord of rafter *HJ10* was only coupled in the vertical, or y-direction, degree of freedom due to the large shear thrust force that develops along this diagonal rafter. After preliminary analysis, this coupling in only the vertical direction was determined to be a better fit for the FE model comparison to the field data in Chapter 6 (see Section 6.1). In this case, the master nodes were the nodes for rafter *HJ10* and the other rafter nodes were treated as the slave nodes. For the wood rafters that frame into the truss *A1* (e.g. *EJ7* and *HJ10*), the master node will be the node for truss *A1* and the slave nodes will be the rafter nodes. Figure 5.7 illustrates how wood rafter *EJ7* was connected to the *A1* truss to establish pin connections at the top and bottom chords of rafter *EJ7*. Figure 5.8 illustrates how wood rafter *CJ5* was connected to rafter *HJ10*. Rafters *CJ1* and *CJ3* were similarly connected to rafter *HJ10*.

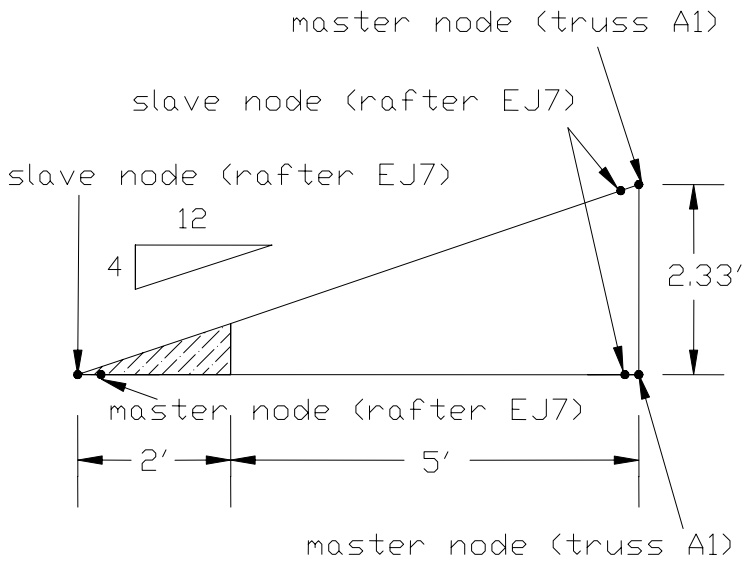

Figure 5.7. Coupling of nodes of rafter *EJ7* to nodes of truss *A1*

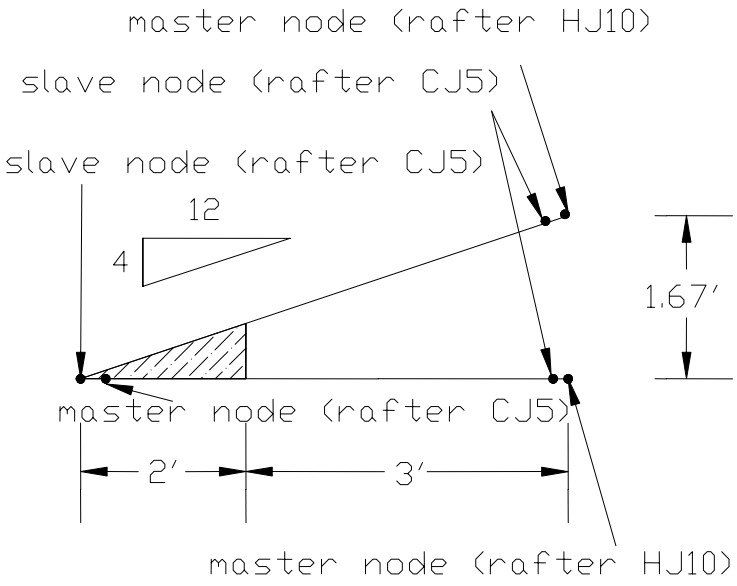

Figure 5.8. Coupling of nodes of rafter *CJ5* to nodes of rafter *HJ10*

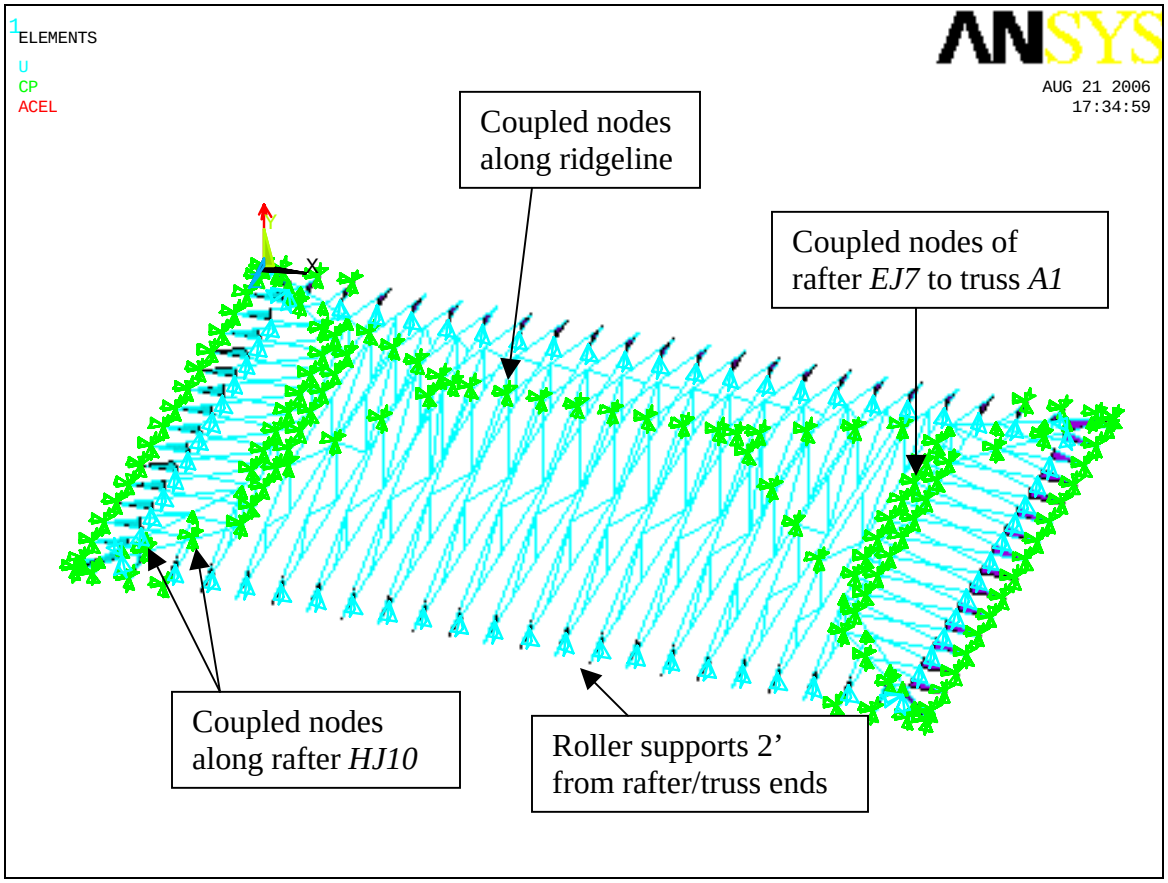

Figure 5.9. Coupling of nodes between rafters and truss *A1*, coupling of nodes along ridgeline, and support conditions shown

The translations of the nodes representing the sheathing elements were also coupled to the rafters and trusses (see Figure 5.9). In other words, the ridgelines of the sheathing were coupled together for the nodal displacements in the x-, y-, and z-directions. This was necessary to simulate the discontinuity of the plywood used as the roof sheathing along the ridgelines.

5.3.2 Support Conditions

The support conditions for the hip roof trusses are rollers at the wall/rafter/truss support, which are 2-ft. in from the hip roof overhang (see Figure 5.9 and details in Section

3.2). The rollers were chosen to allow the trusses to move along the lengths of their bottom chords enabling the rafter/truss system to move in-plane and out-of-plane. Although the out-of-plane movement was relatively small in comparison to the in-plane movement, the FE model was assumed to allow the rafter/truss system to move in both directions. Only where the test structure had load cells was there a roller support (see Figures 3.7 and 3.8). However, for stability purposes one node must be restrained in the nodal x-, y-, and z-directions. This was accomplished in the FE model by rotating the nodal coordinates of the node at the corner wall/rafter underneath rafter *HJ10* as shown in Figure 5.10.

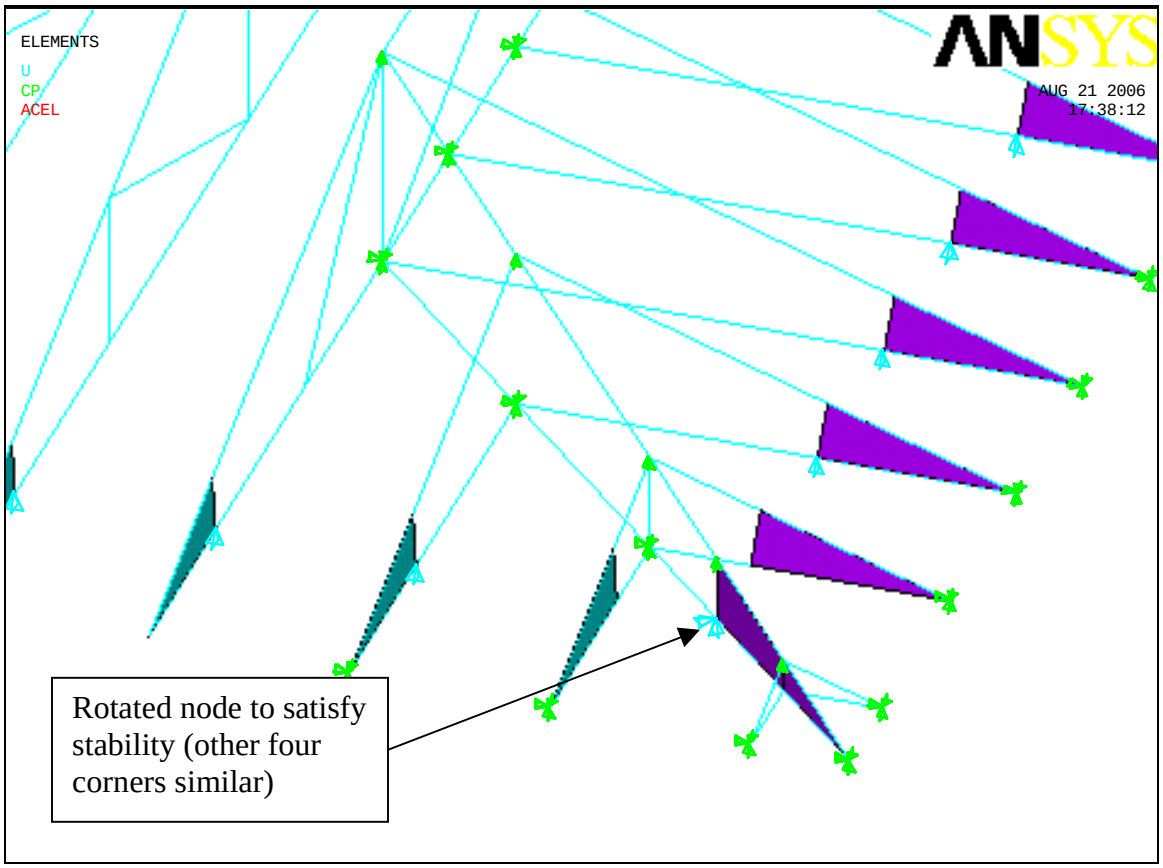

Figure 5.10. Rotation of nodal coordinates to satisfy support condition

CHAPTER 6. FINITE ELEMENT ANALYSIS RESULTS AND COMPARISONS WITH FIELD DATA AND LOAD SPECIFIED IN DESIGN CODES

A finite element model for the roof of the test structure was presented in Chapter 5. In this chapter, the analysis results obtained using the finite element model are presented and the results are compared to the field data where appropriate. As detailed in Chapter 3, the test structure was instrumented to measure both the load carried by each wood truss in the roof system and the pressure induced at discrete locations on the roof during a hurricane event (see Figure 3.8). First, a model validation is carried out considering only the gravity loads of the roof system. Next, various pressure distributions from Hurricane Katrina at specified times are applied to the FE model as static loads and the results were compared with the results obtained from the field data for Hurricane Katrina. Finally, the *ASCE 7-02 Standard* wind pressure distributions of the MWFRS at the peak wind speed of 56.2 mph from Hurricane Katrina were applied to the FE model and are compared to the field data of Hurricane Katrina. The MWFRS wind pressure distributions for the wind speed of the location of the test roof, which was Pensacola, Florida, was then compared to the peak wind speed. Also, the *ASCE 7-02 Standard* wind pressure distributions of the C&C was utilized and compared to the field measurements during Hurricane Katrina.

6.1 Analysis of the Tested Structure under Gravity Loads

As previously stated, the roof of the test structure was analyzed under its own weight and the results were compared to field data to examine the validity of the FE model and evaluate the accuracy of the estimated gravity loads. Unfortunately, field data was not recorded under calm wind conditions. Therefore, the test data representing the gravity effects alone was chosen from the data collected during Hurricane Katrina at the beginning and towards the end of the event at very low wind speeds. For this purpose, four sets of data were identified and the corresponding wind speeds and time occurrences were: 0.13 mph at 8:38:1.23 PM on August 28, 2005, 1.87 mph at 12:50:26.55 AM on August 29, 2005, 0.2 mph at 3:21:47.94 AM on August 29, 2005, and 2:01:43.66 PM on August 29, 2005. One should note that the peak wind speed of 56.2 mph was registered at 1:14:6.43 PM on August 29, 2005. Table 6.1 lists the recorded total weight of the roof at the selected times along with other field data.

Table 6.1. Recorded weight of test structure at given times

Load Case Number	Wind Speed (mph)	Time *	Date	Total Weight (lbs)
1	0.13	8:38:1.23 PM	August 28, 2005	13,087
2	1.87	12:50:26.55 AM	August 29, 2005	13,133
3	0.2	3:21:47.94 AM	August 29, 2005	13,348
4	0.47	2:01:43.66 PM	August 29, 2005	13,452

* Standard time shown above was converted from hundredths of seconds since midnight in the data set. (e.g., 7,560,016 hsec converts to 9:00:16 PM)

Examining the table above illustrates that there is insignificant differences between the total roof weight estimated for the four load cases. Even though Load Case 4

corresponded to a time well beyond the peak wind activity that could have increased the roof weight possibly due to increased moisture, there was essentially no change to the total weight of the roof before and after the peak hurricane activity. At the beginning of the research, the FPL researchers notified that a set of data was collected on from the structure when it was first instrumented in March 15, 2002, which essentially captured the effects of the gravity load. Accordingly, the total weight of the roof at that time was estimated to be 16,149 lbs. There was no obvious explanation for the noticeably large discrepancy between the data sets listed in Table 6.1 and the initial estimate of the roof weight. After consultation with the FPL personnel, it was decided not to use the initial data set in the gravity load analysis of the roof system. However, it is recommended that this issue be resolved in the future by taking periodic gravity load measurements during wet and dry seasons.

Referring to Sections 5.1.2 and 5.2.2 where the material densities were estimated, the finite element analysis of the tested structure yielded a total dead weight of 14,359 lbs. This value is about 10% larger than the average weight of 13,255 lbs estimated from Table 6.1. This discrepancy between the measured and analytical values could have resulted from the differences between the actual material mass density and these listed in Sections 5.1.2 and 5.2.2. To simplify the load distribution comparison between the measured and FE results and validate the analysis model, the mass density was proportionally reduced to match a total weight of 13,087 lbs, which is used in the subsequent finite element analyses.

Figures 6.1 through 6.4 show the measured loads corresponding to the different load cells and results obtained from the theoretical analyses for Load Cases 1, 2, 3 and 4 identified in Table 6.1 (see Section 3.3 for location of the load cells).

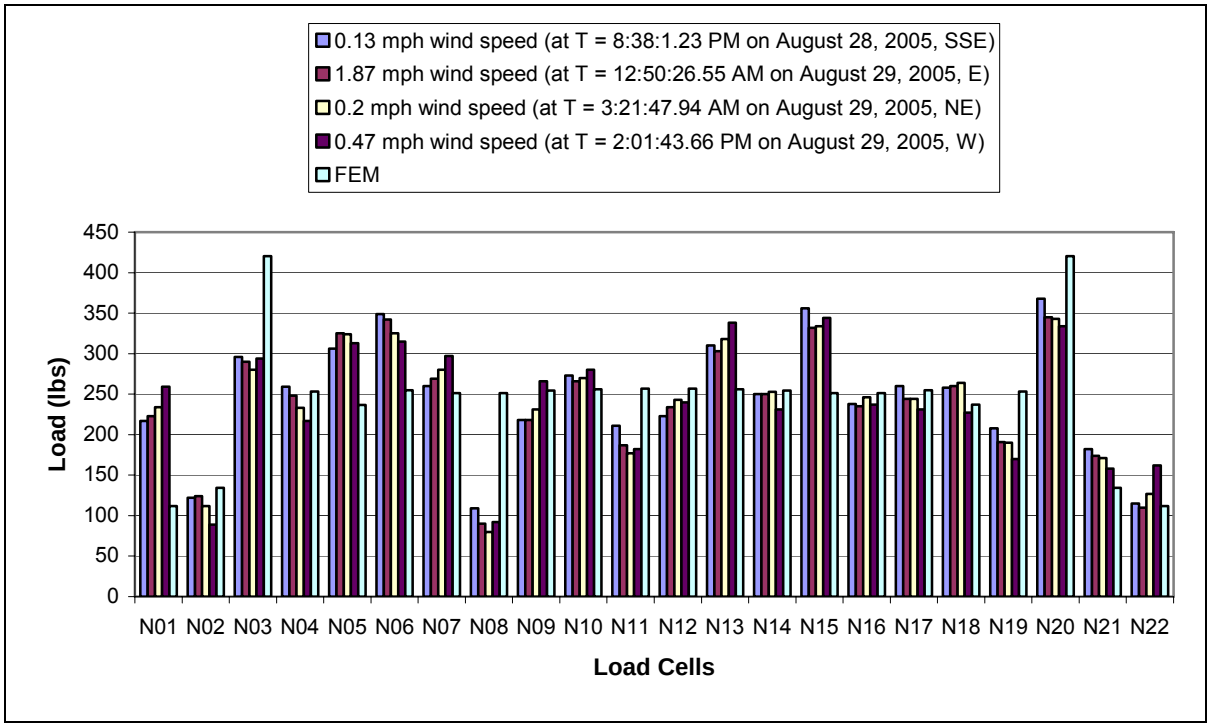

Figure 6.1. Comparison of measured data from load cells along the north wall under gravity loads

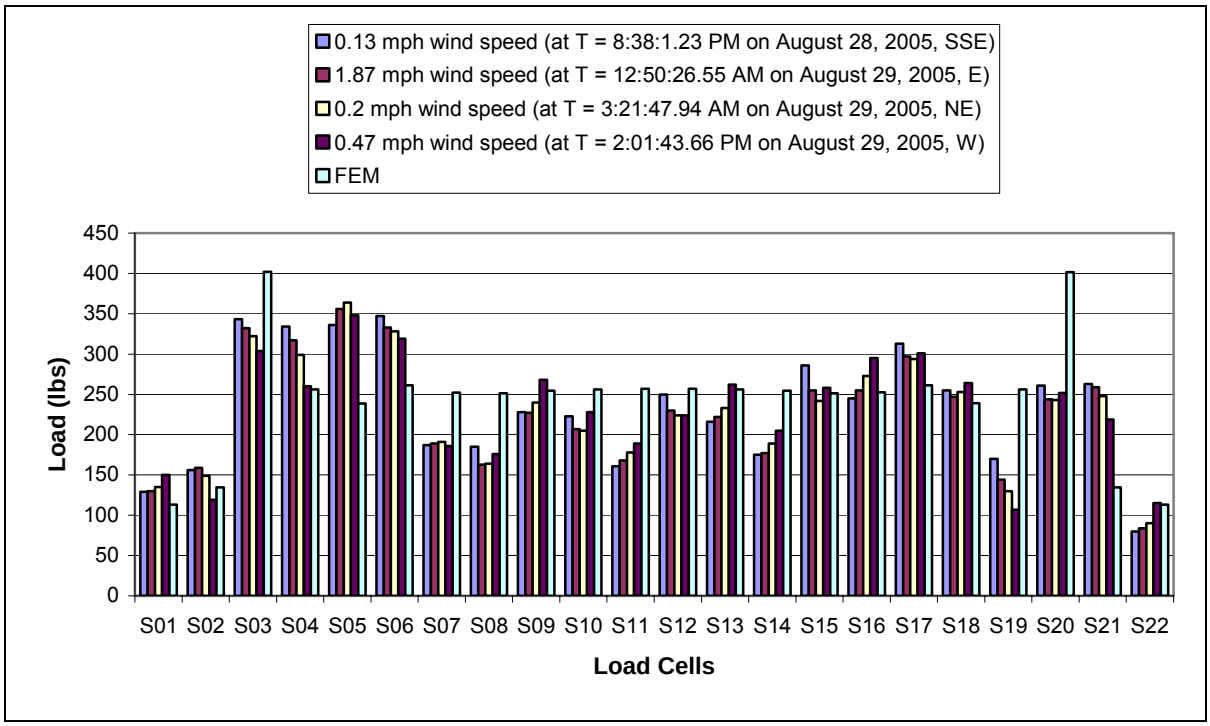

Figure 6.2. Comparison of measured data from load cells along the south wall under gravity loads

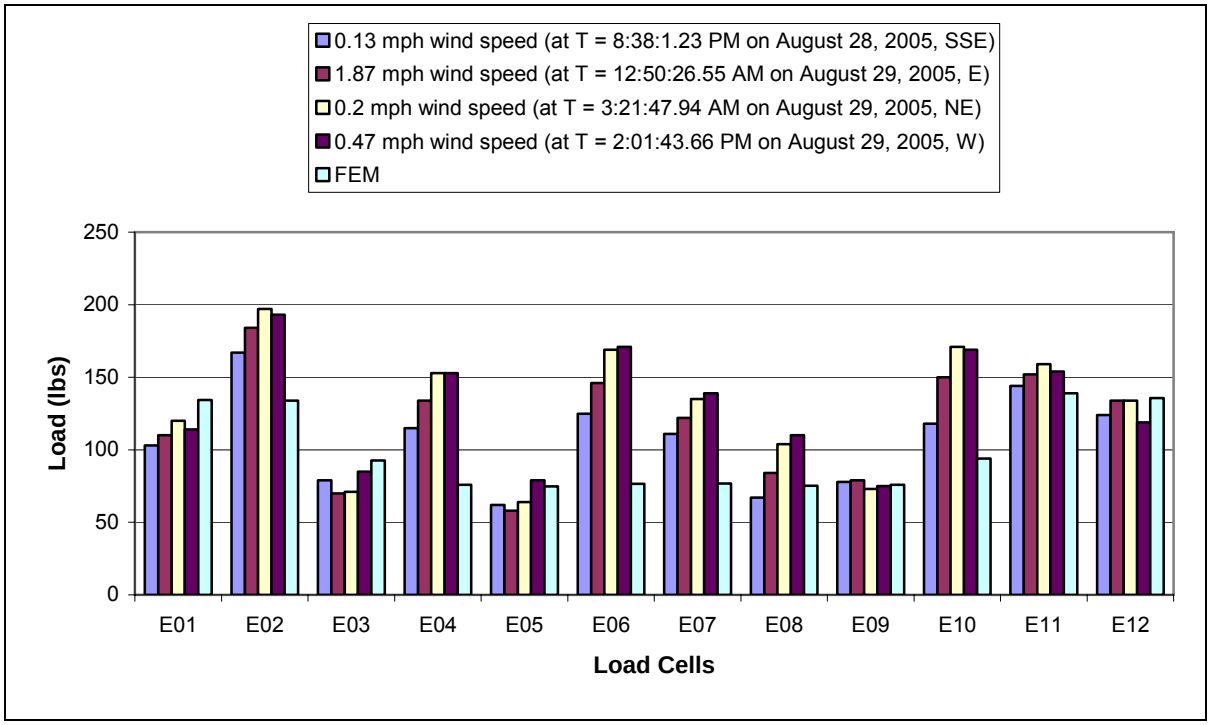

Figure 6.3. Comparison of measured data from load cells along the east wall under gravity loads

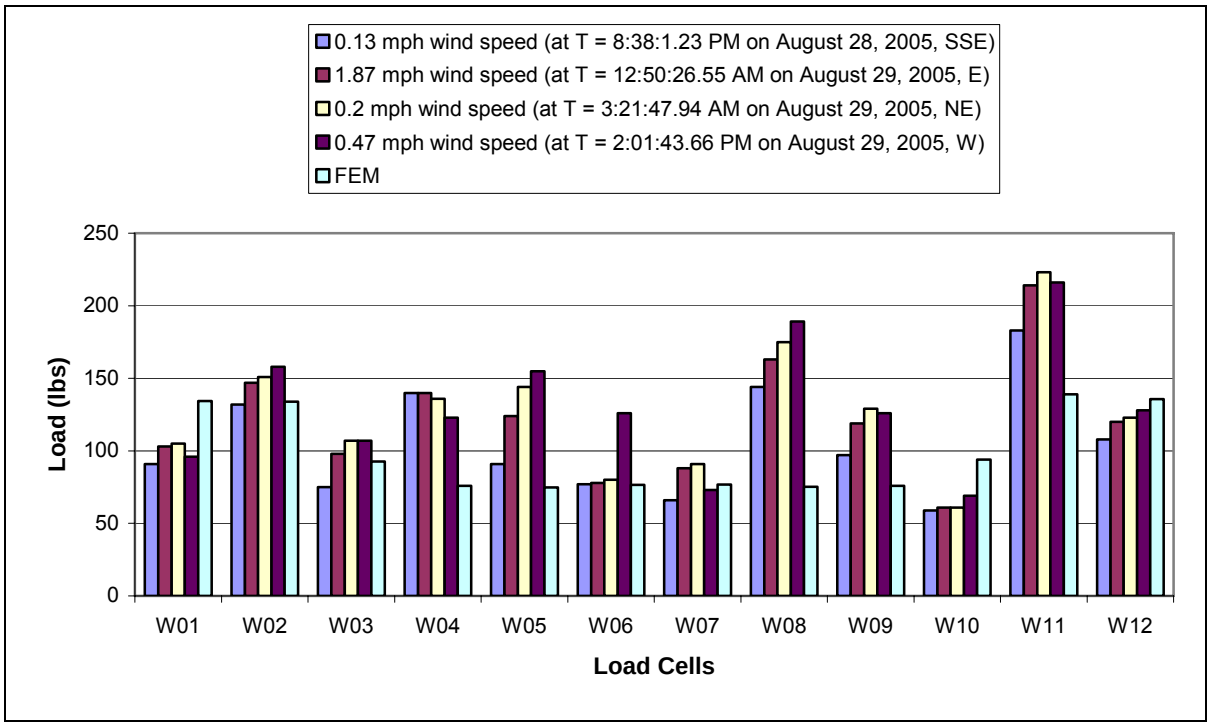

Figure 6.4. Comparison of measured data from load cells along the west wall under gravity loads

As can be seen in Figures 6.1 to 6.4, the measured and the analytical results for the four load cases are in satisfactory agreement. The differences between the measured and analytical results could have been due to the idealization used in the finite element approach to model the connections between the different elements of the roof system. In addition, it is observed that the distribution of the experimental data is affected by localized variations in the actual structure because the measured loads do not reflect the symmetry of the roof structure. For example, load cells *N8* through *N15* should record identical reactions since all the members supported by these load cells are *A6* trusses and the hip roof is symmetric. To alleviate this problem, the measured loads at similar load cell locations were averaged. For example, reactions from all *HJ10* rafters were averaged to obtain a common experimental value.

Figures 6.5 to 6.8 compare the average experimental load cell reactions obtained at 0.13 mph wind speed (i.e., Load Case 3) with the analytical results reported above in Figures 6.1 to 6.4. It is seen that the comparison between the experimental and analytical reactions at the load cell locations has noticeably improved. The analytical results are within ±10% of the experimental values along the north and south walls, and the analytical results are within ±25% of the experimental values along the east and west walls. However, larger discrepancies are seen at the north and south walls at the following locations: *N03, N05, N06, N17, N18, N20, S03, S05, S06, S17, S18* and *S20* (see Figures 6.5 and 6.6). Possible factor that may attribute to the difference in loads may be due to the realistic support conditions at these particular locations may not be modeled correctly and not modeling the load conditions or support path that the gravity load takes. For more conclusions to the gravity analysis refer to Section 7.1.

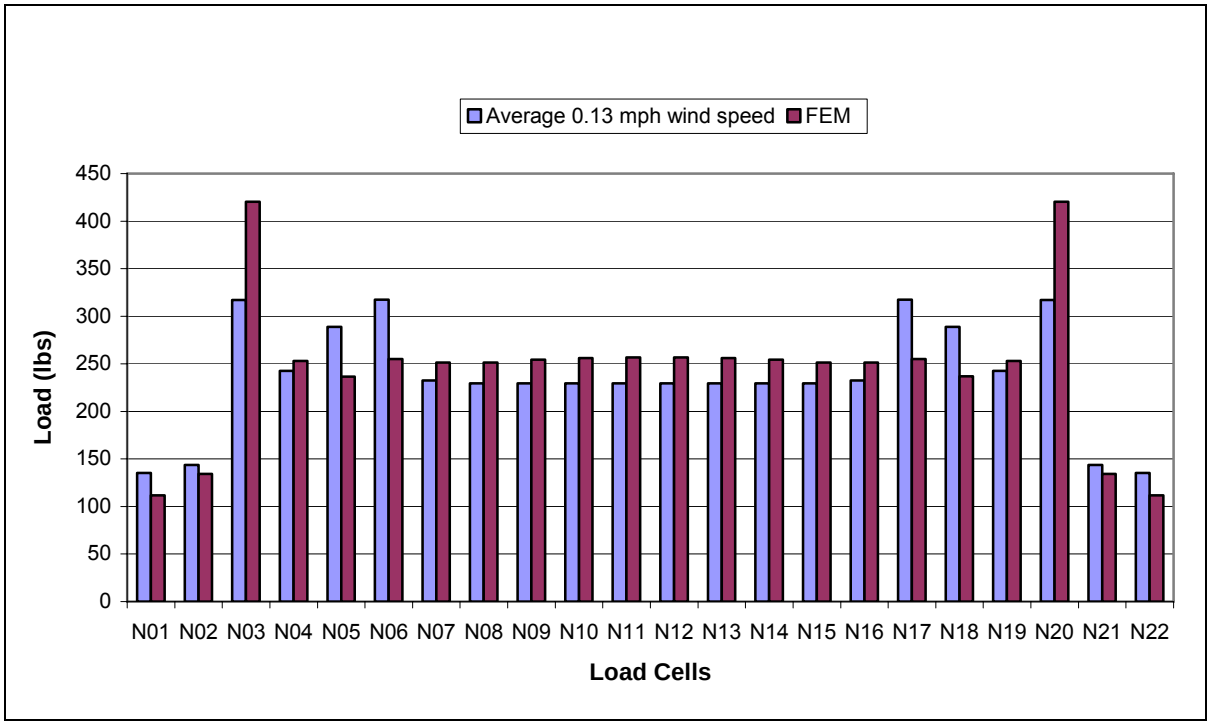

Figure 6.5. Comparison of averaged data from load cells along north wall under gravity loads

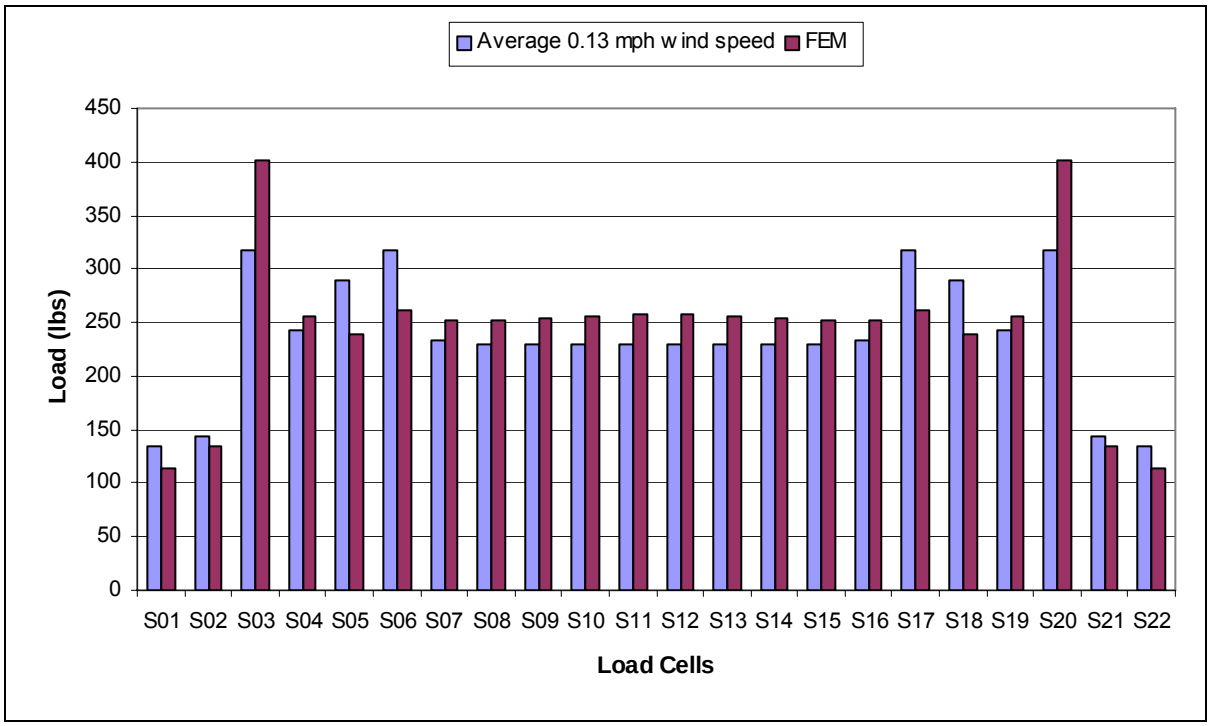

Figure 6.6. Comparison of averaged data from load cells along south wall under gravity loads

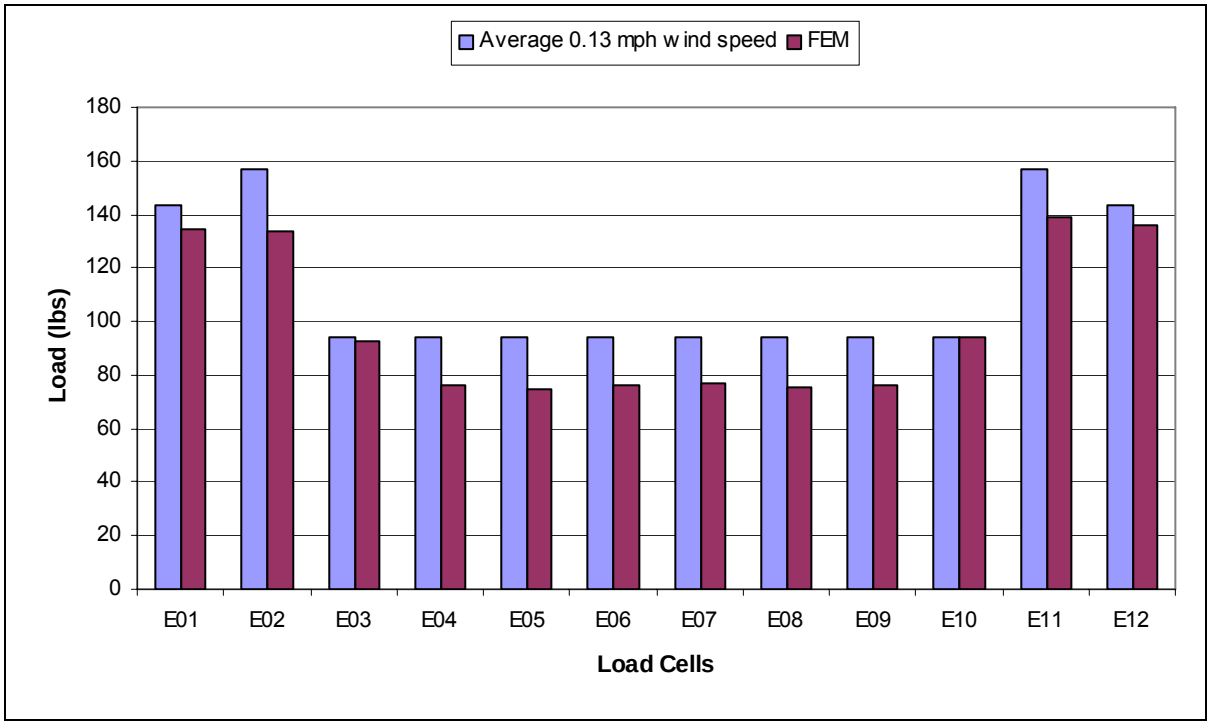

Figure 6.7. Comparison of averaged data from load cells along east wall under gravity loads

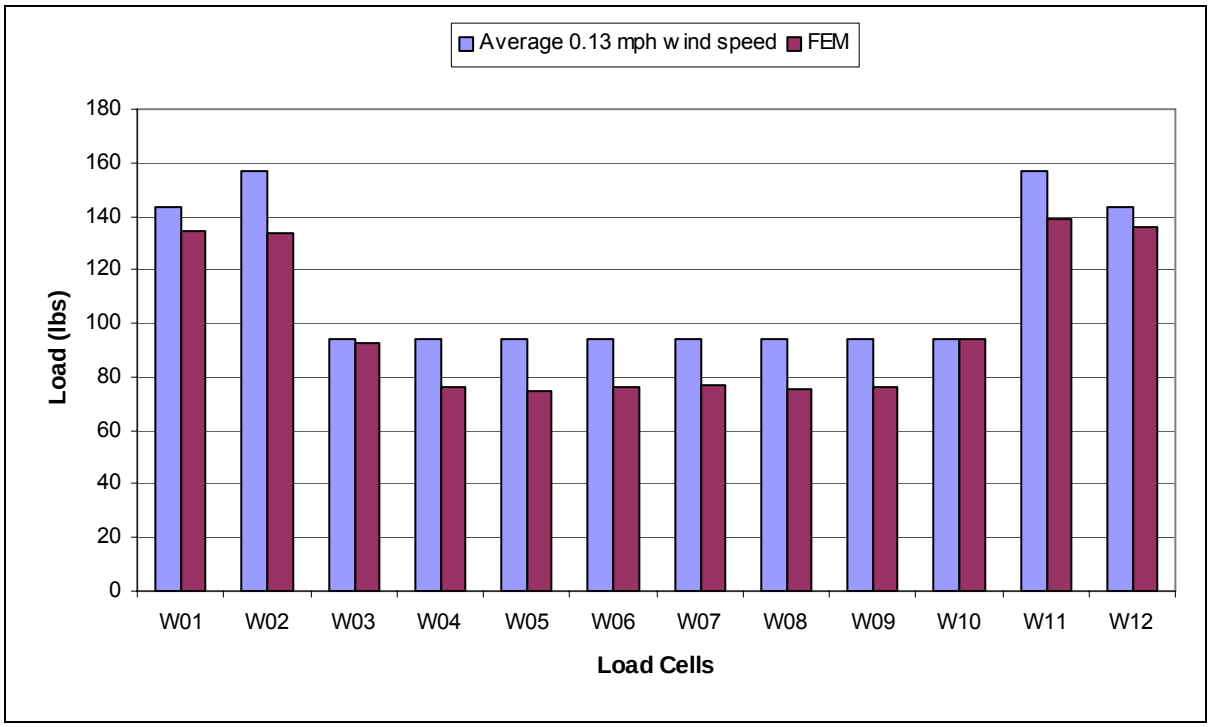

Figure 6.8. Comparison of averaged data from load cells along west wall under gravity loads

6.1.1 Other Results from the Finite Element Analysis

Figure 6.9 summarizes the deflection of the roof system. Areas of interest in the deflected shape were along the east and west hip surfaces of the roof system, which were the short hips. These hip surfaces show that small regions experience uplift outside of the wall support due to self weight of the roof system. The maximum deflection occurs at the center of the hip roof along the north hip surface. It should be noted that the maximum deflection occurs along the hip roof sheathing and top chord of one of the middle *A1* trusses.

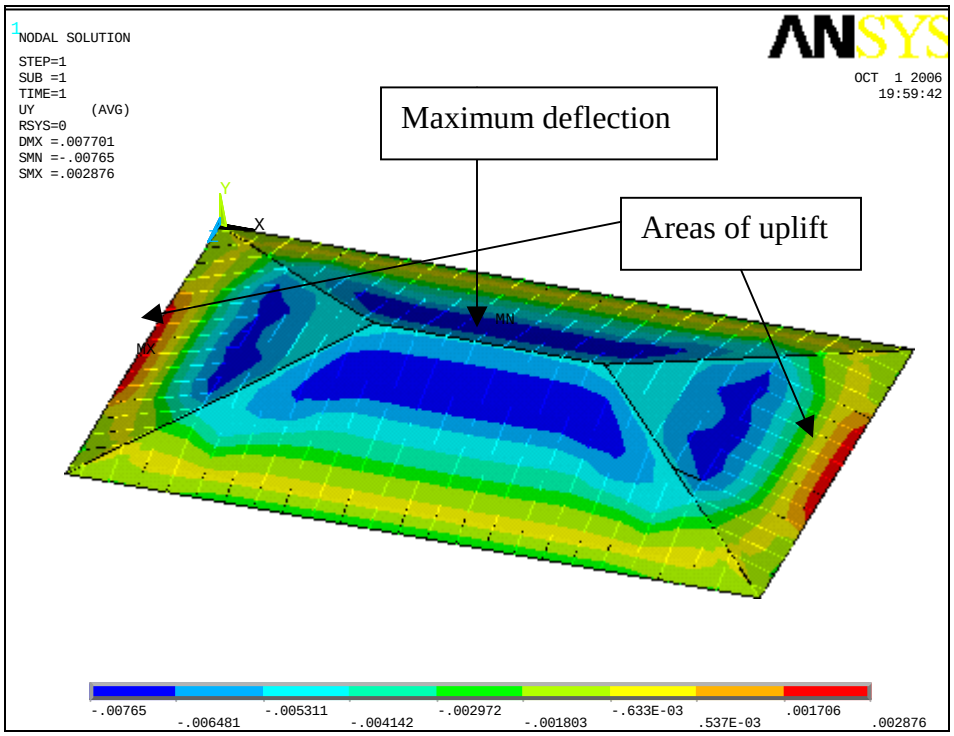

Figure 6.9. Vertical component of displacement for hip roof sheathing in units of ft.

Figure 6.10 shows the 1st principal stress for the test roof under gravity loading. The figure further validates the FE results because most of the stress on the test roof is negative, which indicate compressive stresses. Only on the outside edges of the test roof is there a

positive stress, or tension stress, induced on the hip roof. This is due to the uplift at the wall overhang.

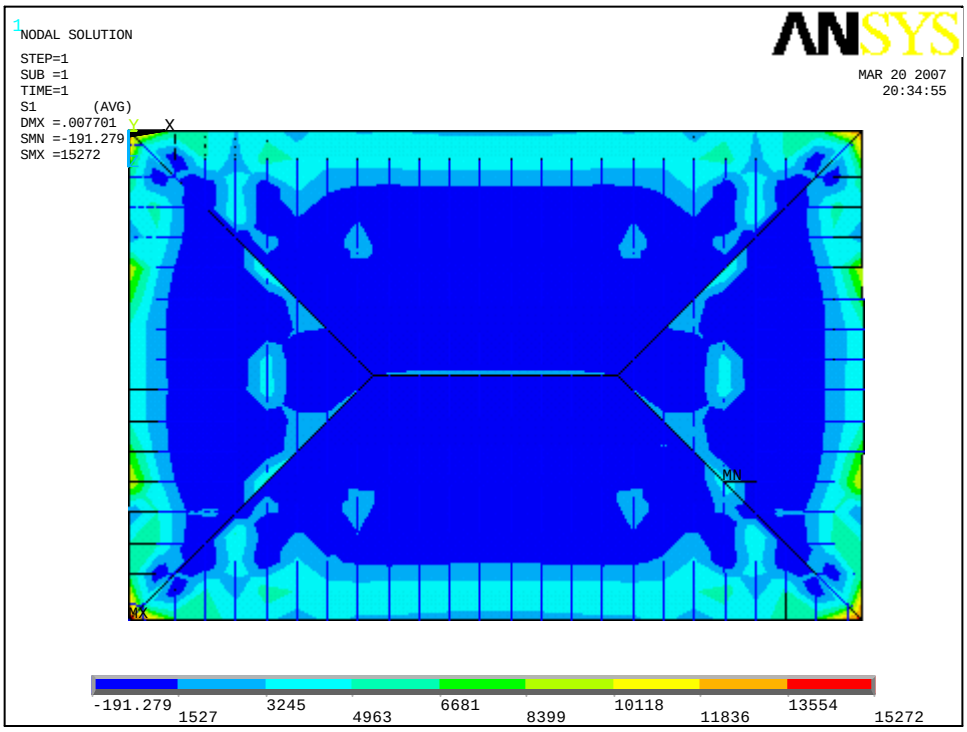

Figure 6.10. 1st principal stress for hip roof sheathing in units of psf

Figure 6.11 shows a vector plot of the principal stress scaled in magnitude with their proper direction of where the load is being transferred through the roof system. From Figure 6.11 it is obvious that much of the load is toward the corners of the roof system. Also, the ridgeline of the roof caused a change in direction of the load path.

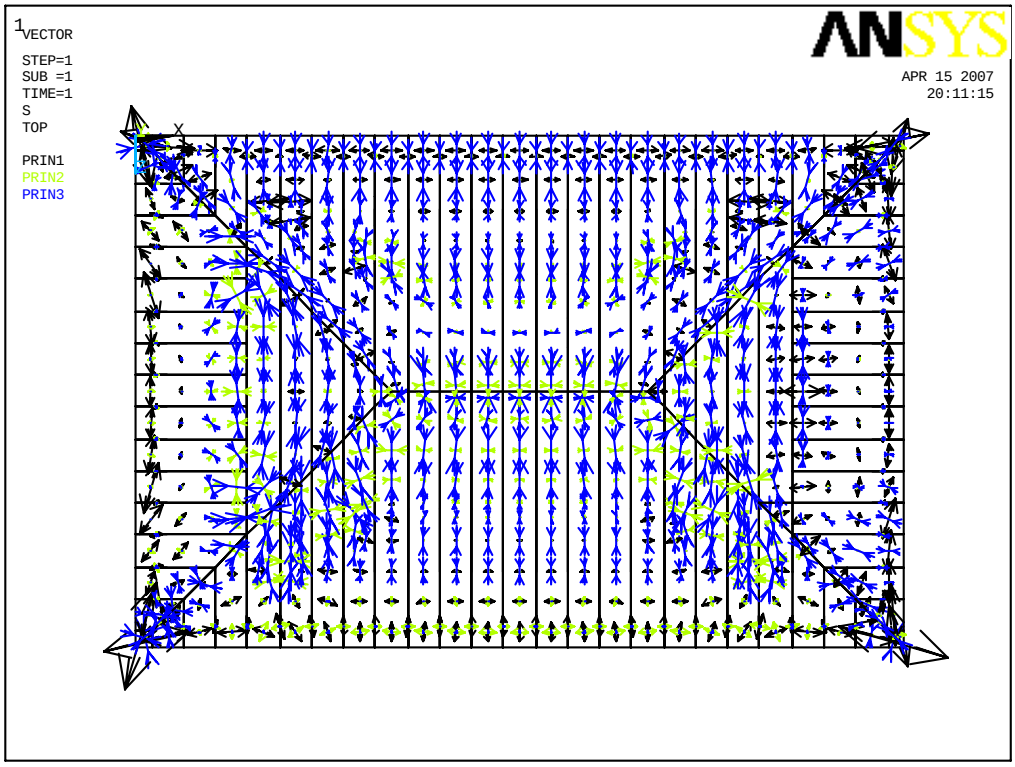

Figure 6.11. Vector plot of roof system using centroid of each sheathing element

6.2 Analysis of the Tested Structure under Wind Loads

A hurricane wind speed is defined as a sustained wind, which is an average one-minute wind gust, at 74 mph or greater measured at 10 ft above ground (National Hurricane Preparedness, 2006). Even though the Katrina was a hurricane event, the speed of the wind near the location of the test house cannot be classified as a hurricane wind, but is more of a basic wind speed condition. This is not surprising due to the fact that the eye of the Hurricane Katrina traveled about 200 miles west of Pensacola, Florida. A one-minute average wind speed for the field data obtained at the location of the test house was only 27.1 mph when the peak wind speed of 56.2 mph was used as the median wind speed.

Representing an action induced by wind from the field as equivalent loads on a structure posses several challenges. The reasons behind these challenges include: continuous change in wind speed, continuous change in wind direction, change in angle of attack on a structure, wind vortices are shed across a structure surface, added influence of precipitation, and change in climatic data such as humidity. There is also a possibility that the wind may attack the test structure in a circular pattern during a hurricane event and dissipate over land, which is almost impossible to account for based on the collected data. Despite these uncertainties this report assumes that the wind that attacked the test house during Hurricane Katrina was a straight wind causing pressures only in the direction normal to the surface and quantify its effects on the roof of the test structure. This exercise is expected to shed light on how well the FE results compared to the field data to further validate the theoretical model produced in this investigation.

According to the National Weather Service (NWS) Forecast Office (2006), Hurricane Katrina caused sustained winds of up to 140 mph during landfall, which classified it as a

strong category 4 hurricane. The impact of the storm's landfall was measured near Grand Isle, Louisiana (NWS Forecast Office, 2006). Since the field data received in this study was measured in Pensacola, Florida, the data used in this report had to be verified against wind data reported by NWS (see Section 3.5). A peak wind speed of 50 knots, or 57.5 mph, was recorded by WEAR-TV in Pensacola, Florida (NWS Forecast Office, 2006) on August 29, 2005. The peak wind speed measured in the field was 56.2 mph at 1:14:6.43 PM on August 29, 2005 and corresponded well (2.33% error) to the data from the NWS Forecast Office.

Table 6.2 summarizes some of the important wind loading conditions that occurred during data collection on the test structure. All the load conditions will be analyzed in this section of the report.

Table 6.2. Selected wind loading conditions based on the field data

Load Case Number	Characteristic During Data Collection	Wind Speed (mph)	Time *	Date	Total Weight (lbs)
5	Peak wind speed	56.2	1:14:6.43 PM	August 29, 2005	13,298
6	Highest pressures	43.87	1:57:0.24 PM	August 29, 2005	12,495
7	Highest load[1]	36.87	2:19:36.24 PM	August 29, 2005	14,358
8	Lightest load[2]	24.27	3:25:17.09 PM	August 29, 2005	11,886
3 (previous)	Lowest wind speed	0.13	8:38:1.23 PM	August 28, 2005	13,087
9	Average over time interval around highest pressures[3]	43.87	±1 minutes from 1:57:0.24 PM	August 29, 2005	12,495

[1] wind effect causing highest summation of load cell during field test duration

[2] wind effect causing lightest summation of load cells during field test duration

[3] mean time in interval corresponding to the highest pressures recorded as the median value

* Standard time shown above was converted from hundredths of seconds since midnight in the data set. (e.g., 7,560,016 hsec converts to 9:00:16 PM)

6.2.1 Field Data

As previously mentioned, the effect of the Hurricane Katrina winds on the test structure was monitored using 68 load cells underneath the wood rafters/trusses and the 76 pressure cells on the hip roof sheathing (see Figure 3.8).

Figures 6.12 and 6.13 show examples of data collected for a load cell (i.e., *N01*) and a pressure cell (i.e., *S15P*), respectively, during the 13th hour of Hurricane Katrina. As clearly seen in the figures for the short duration, both the load cell and pressure cell data fluctuated greatly throughout the duration of the hurricane. Also, note that the field data for Hurricane Katrina was measured in hundredths of seconds since midnight, which was later converted to an adjusted military time. For example, adjusted military time of 1380.25 converts to 1:48:15 PM. The only difference in the adjusted military time from military time is that the minutes and seconds end in increments of 100, not 60.

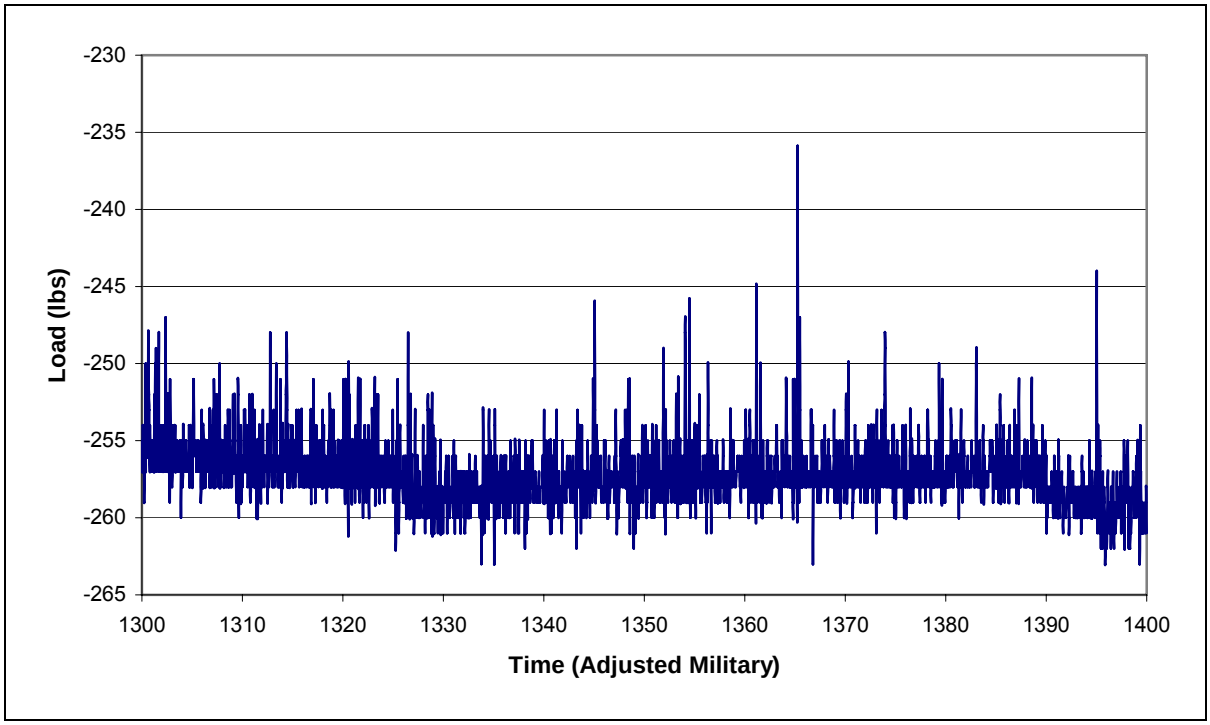

Figure 6.12. Loads recorded for adjusted military time duration from 1:00 PM – 2:00 PM August 29, 2005, for load cell *N01*

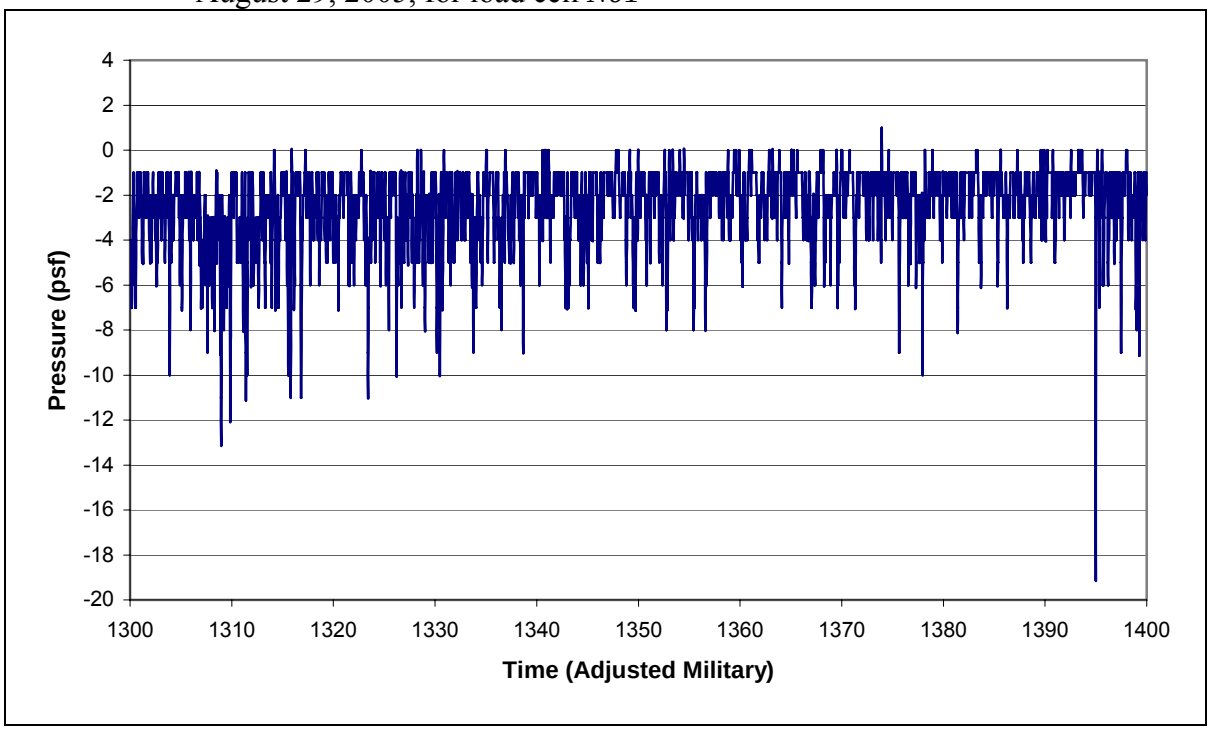

Figure 6.13. Pressures recorded for adjusted military time duration from 1:00 PM – 2:00 PM August 29, 2005, for pressure cell *S15P*

As seen for load cell *N01* in Figure 6.12, each load cell supporting the roof of the test structure recorded negative reactions throughout the duration of the data collection. (For the installation details and locations of the load cells, refer to Section 3.3). This is because each load cell was zeroed before installation and subjected to compression force or a negative number due to gravity load of the roof. Consequently, when the roof system experienced suction, the load cell expanded to become less negative, or more positive. Conversely, when the roof system experienced pressure, the load cell compressed to become more negative, or less positive. As seen in Figure 6.13, the pressures measured in this particular location were generally negative with rare occurrences of positive values. Negative pressures indicated suctions and positive pressures indicated pressures onto the test roof. Also, it is noted that the pressure cells were measured within an accuracy of ±1 psf.

For a wider array of the field data, both the load cell *N01* and pressure cell *S15P* were plotted for the entire duration of the field data collection. In addition to depicting the variations in reactions for the load cells and pressures for the pressure cells, Figures 6.14 to 6.21 identify some of the load cases included in Table 6.2. Load cell *N01* did not experience the most fluctuating reactions, but was located at a corner of the hip roof and showed considerable variations in the reaction force. Also, pressure cell *S15P* did record the maximum suction on the test roof, which reached a value of -19 psf, and was chose to be plotted for this reason.

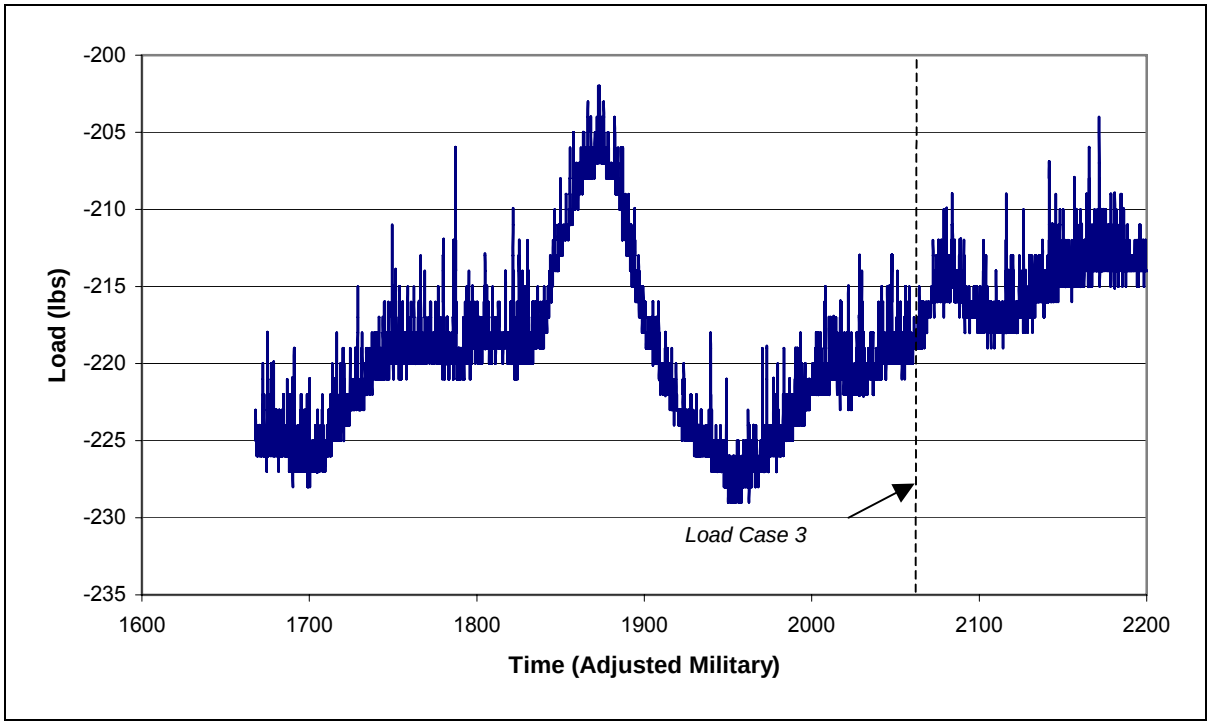

Figure 6.14. Loads recorded for adjusted military time duration from 4:00 PM – 10:00 PM August 28, 2005, for load cell *N01*

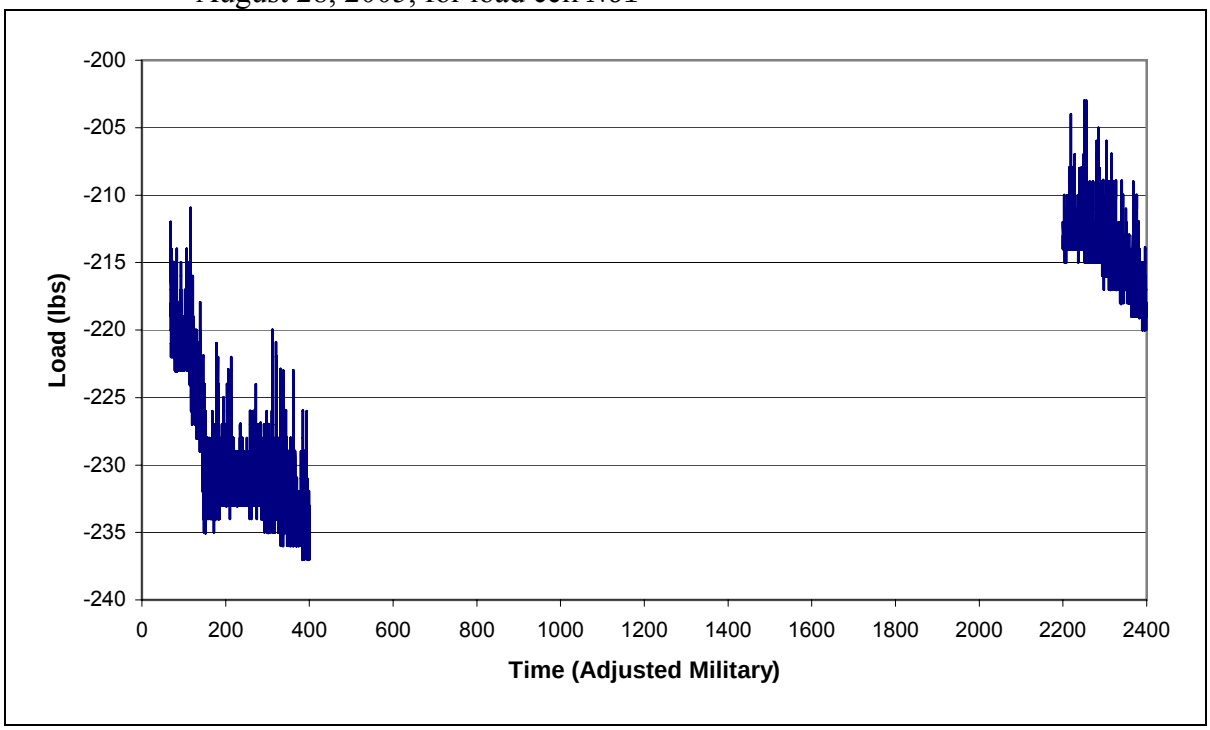

Figure 6.15. Loads recorded for adjusted military time duration from 10:00 PM August 28, 2005 – 4:00 AM August 29, 2005, for load cell *N01*

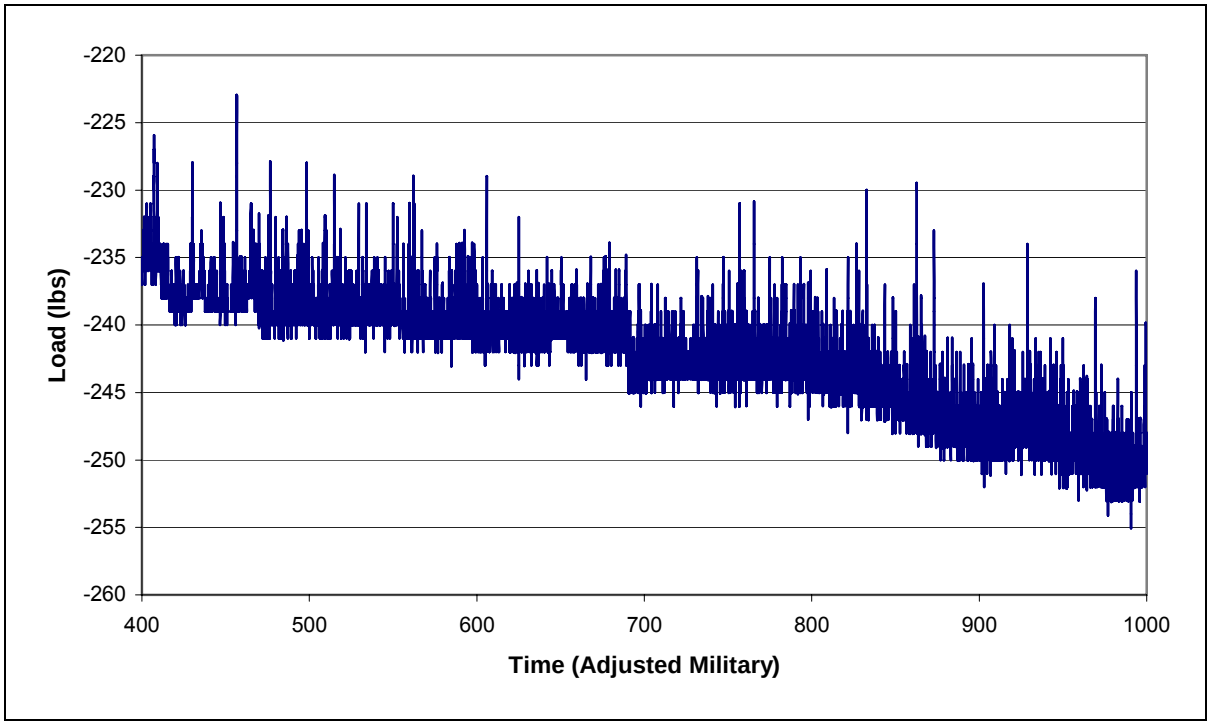

Figure 6.16. Loads recorded for adjusted military time duration from 4:00 AM – 10:00 AM August 29, 2005, for load cell *N01*

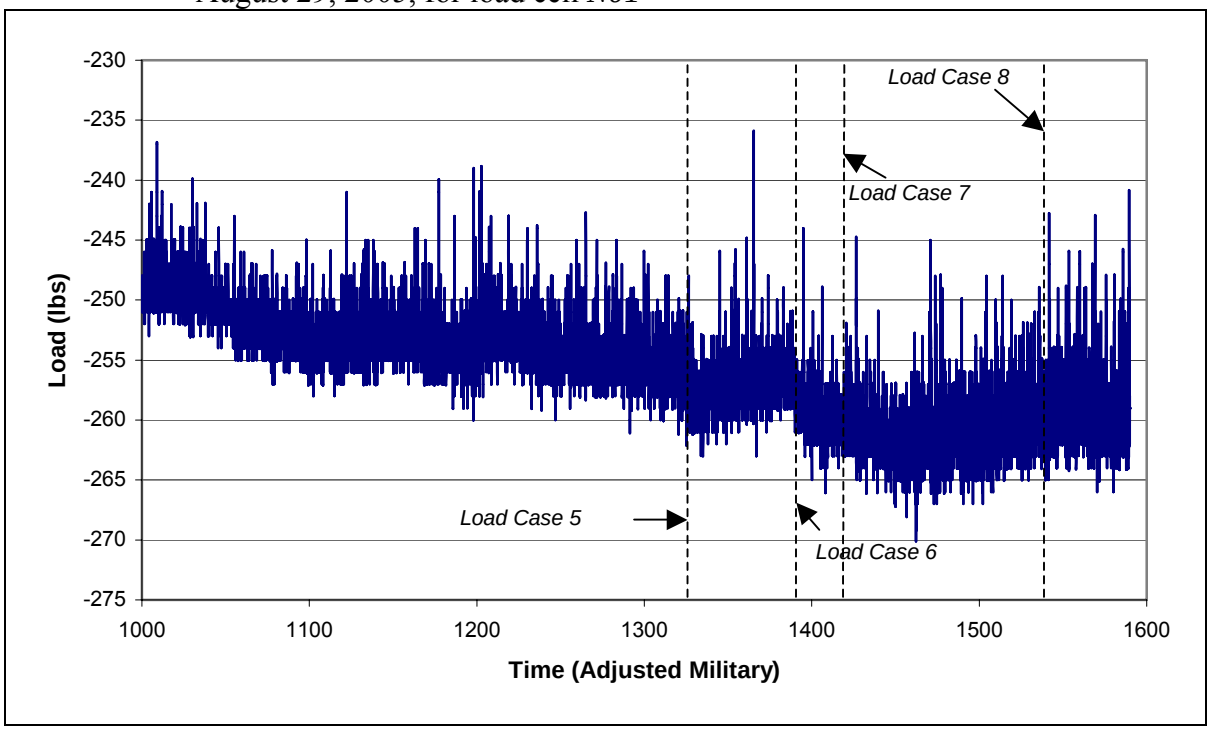

Figure 6.17. Loads recorded for adjusted military time duration from 10:00 AM – 4:00 PM August 29, 2005, for load cell *N01*

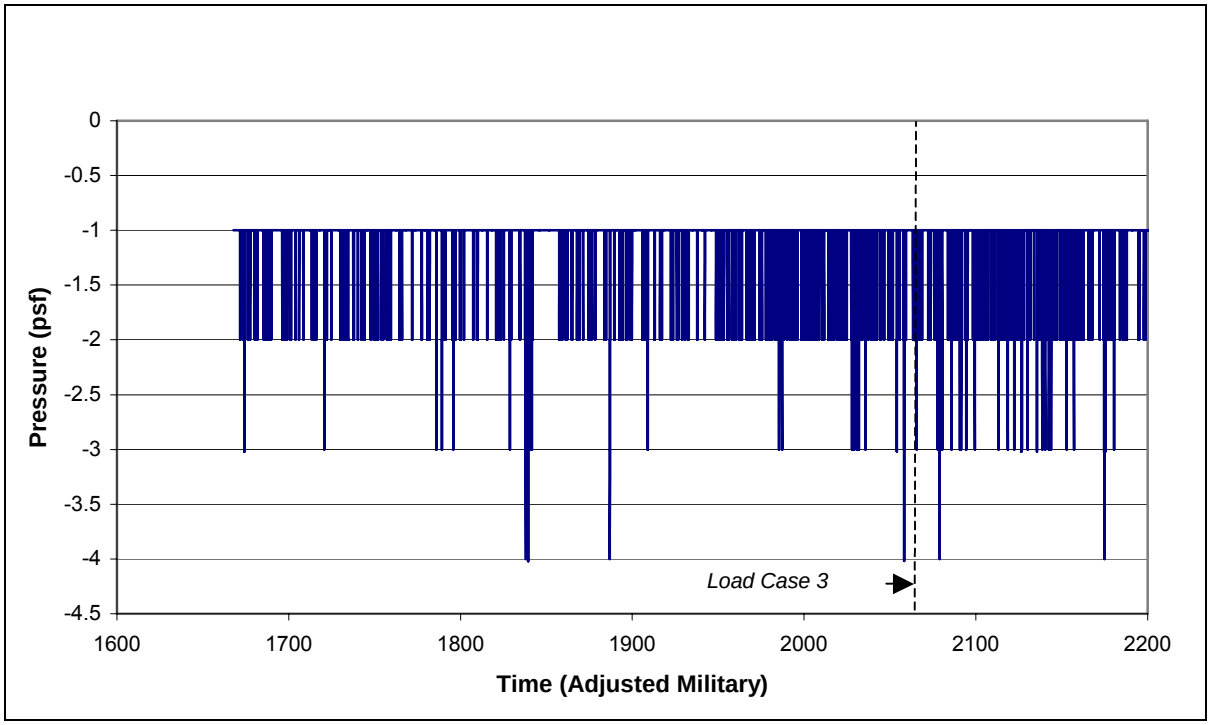

Figure 6.18. Pressures recorded for adjusted military time duration from 4:00 PM – 10:00 PM August 28, 2005, for pressure cell *S15P*

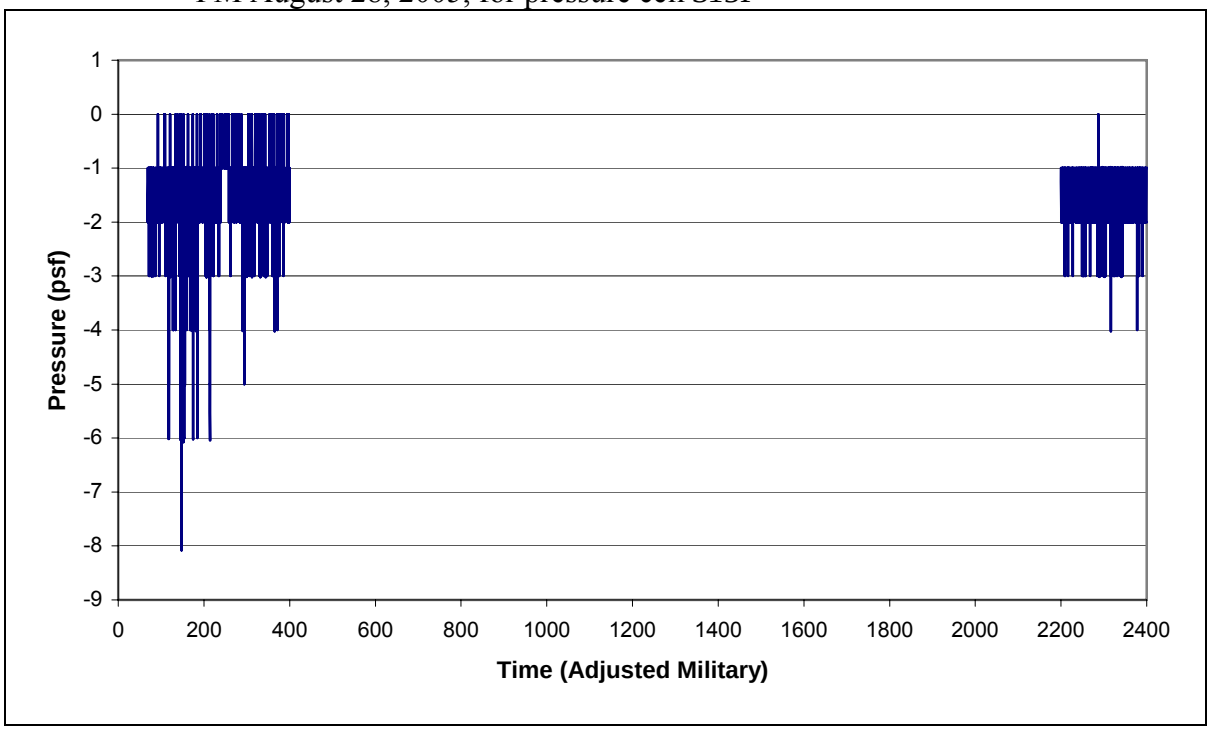

Figure 6.19. Pressures recorded for adjusted military time duration from 10:00 PM August 28, 2005 – 4:00 AM August 29, 2005, for pressure cell *S15P*

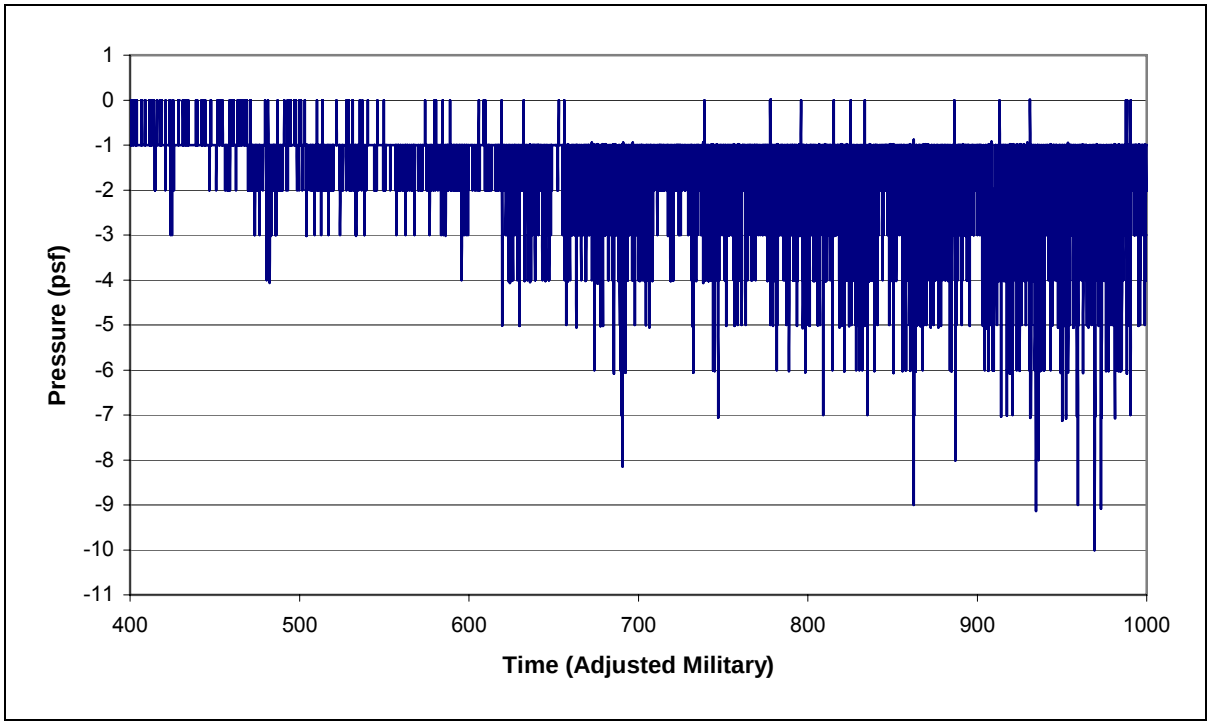

Figure 6.20. Pressures recorded for adjusted military time duration from 4:00 AM – 10:00 AM August 29, 2005, for pressure cell *S15P*

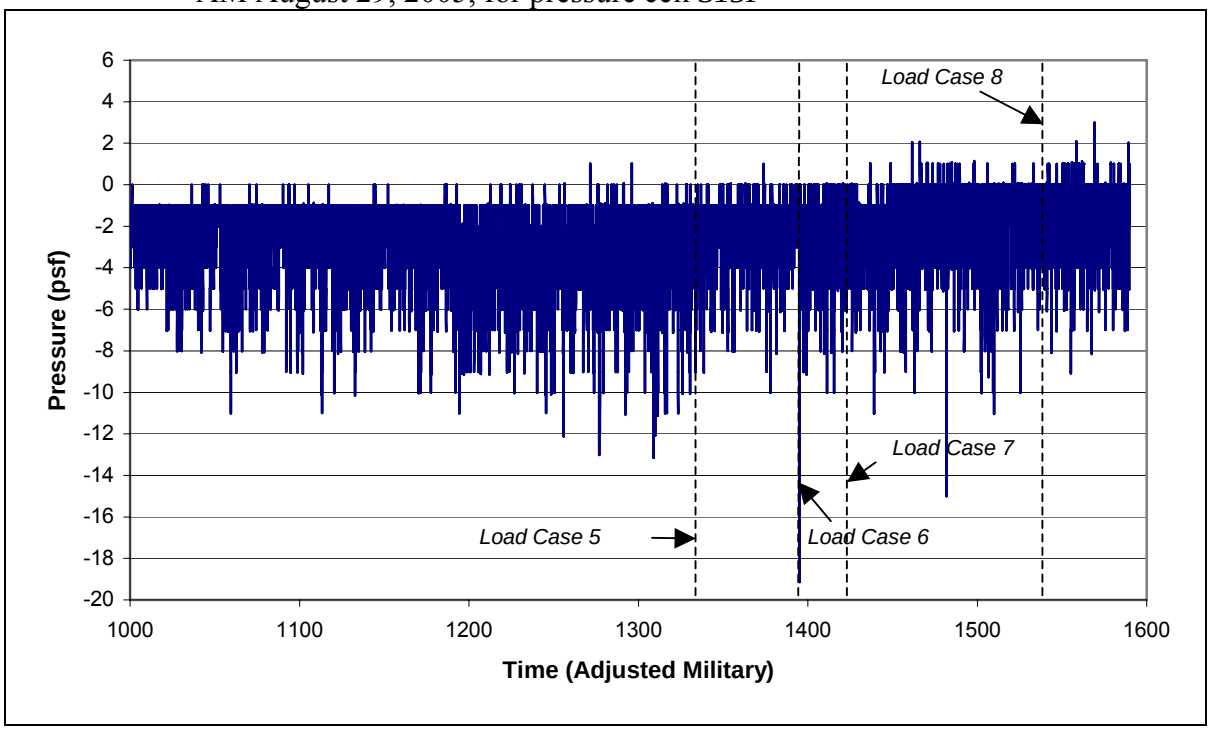

Figure 6.21. Pressures recorded for adjusted military time duration from 10:00 AM – 4:00 PM August 29, 2005, for pressure cell *S15P*

As shown in Figures 6.14 through 6.21, data collection was performed every second from 4:41:43 PM on August 28th, 2005 to 3:53:57 PM on August 29th, 2005. It is noted that there is no continuation line seen in Figures 6.15 and 6.19, which would reflect when the day switched from August 28, 2005 to August 29, 2005.

Furthermore, the peak wind speed did not produce the peak wind pressures observed on the roof of the test structure, which occurred at 1:57:0.24 PM on August 29, 2005, at a wind speed of 43.87 mph. The peak wind speed of 56.2 mph occurred 42 minutes and 53.81 seconds prior to recording the peak wind pressures. This could have been due to the continuous changes in wind speeds and direction and duration of attack on the test structure (see Section 6.1). Also, note that the sum of the load cell reactions did not occur at the same time as the pressure cells peaked. The test structure recorded the highest load of 14,358 lbs at 36.87 mph at 2:19:36.24 PM on August 29, 2005, and the lightest load of 11,886 lbs was at 24.27 mph at 3:25:17.09 PM on August 29, 2005. These variations corresponded respectively to 9.7% and –9.2% differences with respect to the gravity load of the roof obtained at the lowest wind speed at 8:38:1.23 PM on August 28, 2005, and a total fluctuation of 2,472 due to wind load effect on the roof of the test structure. Based on these observations, it is also clear that the maximum wind pressures and the time of the maximum wind effects did not occur simultaneously, and that the maximum wind effects occurred at a lower wind speed. This discrepancy could have been due to many reasons, including those mentioned in Section 6.1 for the staggered field data in the gravity analysis, duration of the wind loads, dynamic effects, change in wind load distribution, vortex shedding, and influence of precipitation.

Figures 6.22 through 6.25 show all the load cell reactions for Load Cases 4, 5, 6, 7, 8 and 9. Note that the load cell reactions were changed to positive reactions to simplify the discussion in this section, even though the actual recorded values were negative as shown in Figure 6.12. The negative reactions signified that the load cells of the test structure recorded an initial zero value before placement, and compression due to gravity loads.

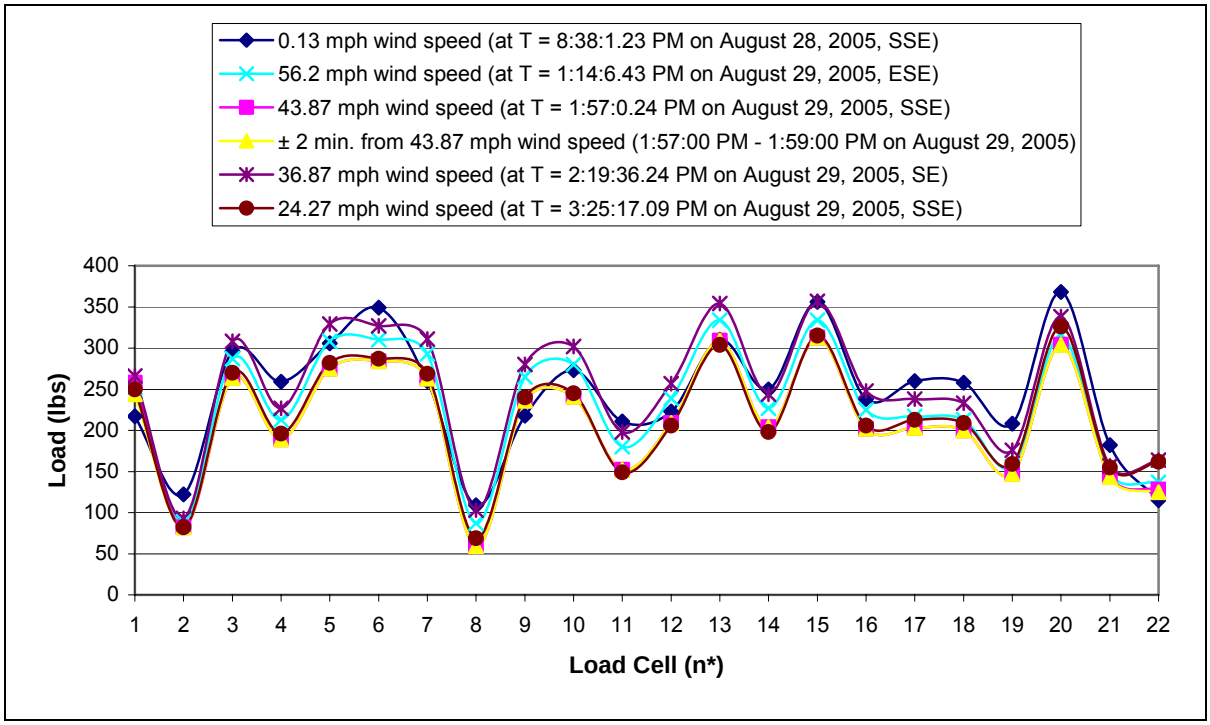

Figure 6.22. Data from load cells located on top of the north wall for Load Cases 3, 5, 6, 7, 8, and 9

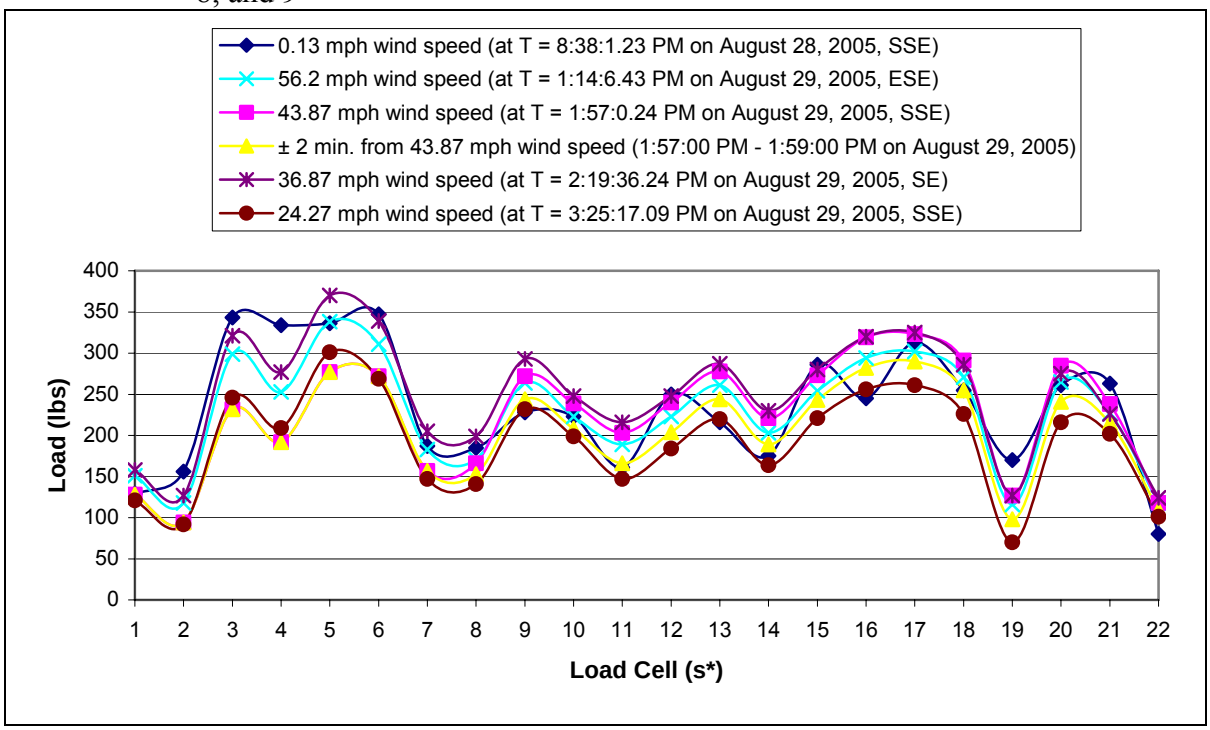

Figure 6.23. Data from load cells located on top of the south wall for Load Cases 3, 5, 6, 7, 8, and 9

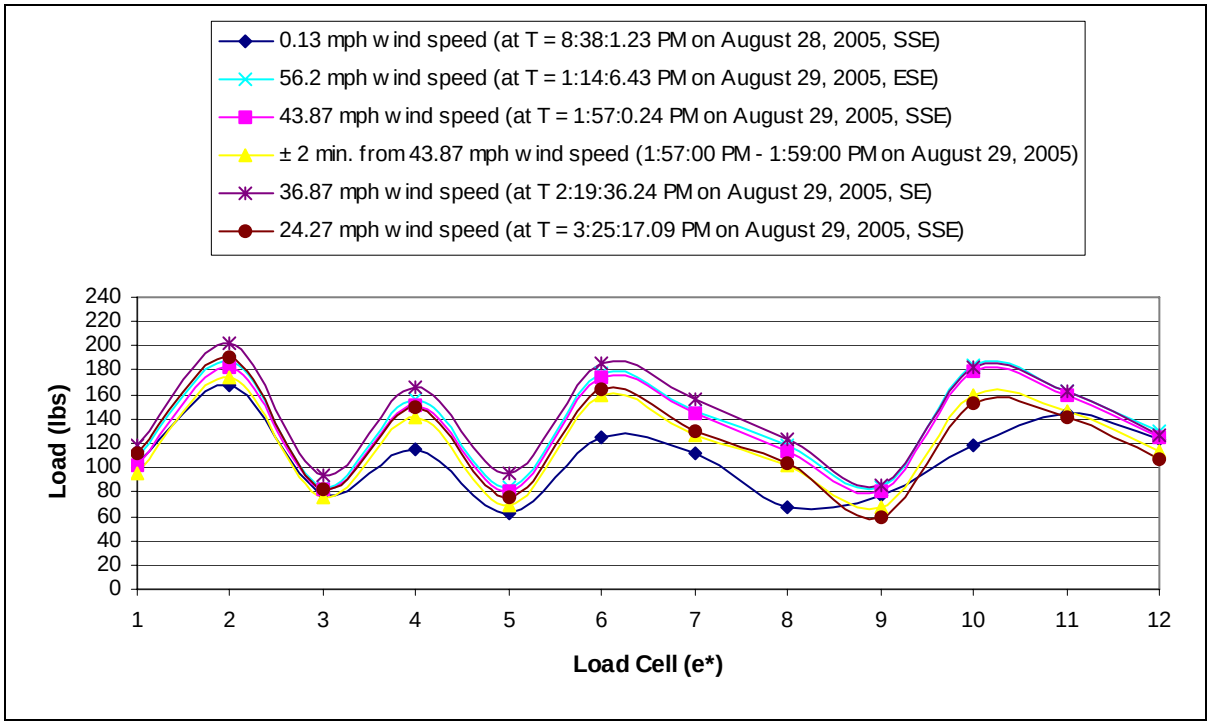

Figure 6.24. Data from load cells located on top of the east wall for Load Cases 3, 5, 6, 7, 8, and 9

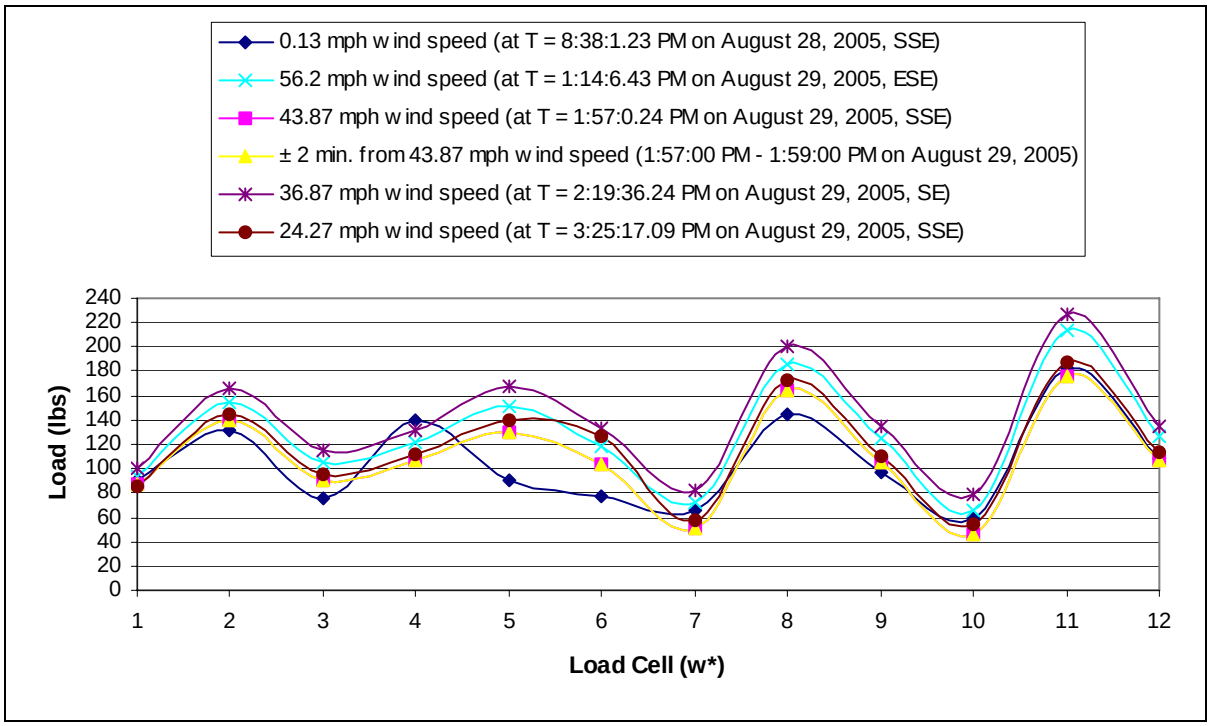

Figure 6.25. Data from load cells located on top of the west wall for Load Cases 3, 5, 6, 7, 8, and 9

Under the lowest wind speed of 0.13 mph, the load cells were expected to record downward reaction loads, which were assumed to represent the dead weight of the roof structure (see Section 6.1). This is due to insignificant wind pressures associated with the low wind speed. If wind loads induced suction on the entire roof, the load cells would experience less downward reaction forces. This was validated when the load cell data associated with the lowest wind speed were compared to those recorded at the highest recorded wind pressures as well as the peak wind speed. The results from Figures 6.22 to 6.25 don't validate this conclusion. For example, load cells *N01* and *N07* violated this conclusion, as load cells *N02* through *N06* caused this conclusion to be true. The reason for the discrepancy was due to the fluctuation on the load cells. However, when the highest load recorded and the lightest loads recorded were compared for the wind effect on the test structure, all of the load cells fit the noted trend. Therefore, the wind effect of the field data was best illustrated when using the highest load recorded and the lightest load recorded. Figures 6.26 through 6.29 show the wind effect of only the highest and lightest load recorded.

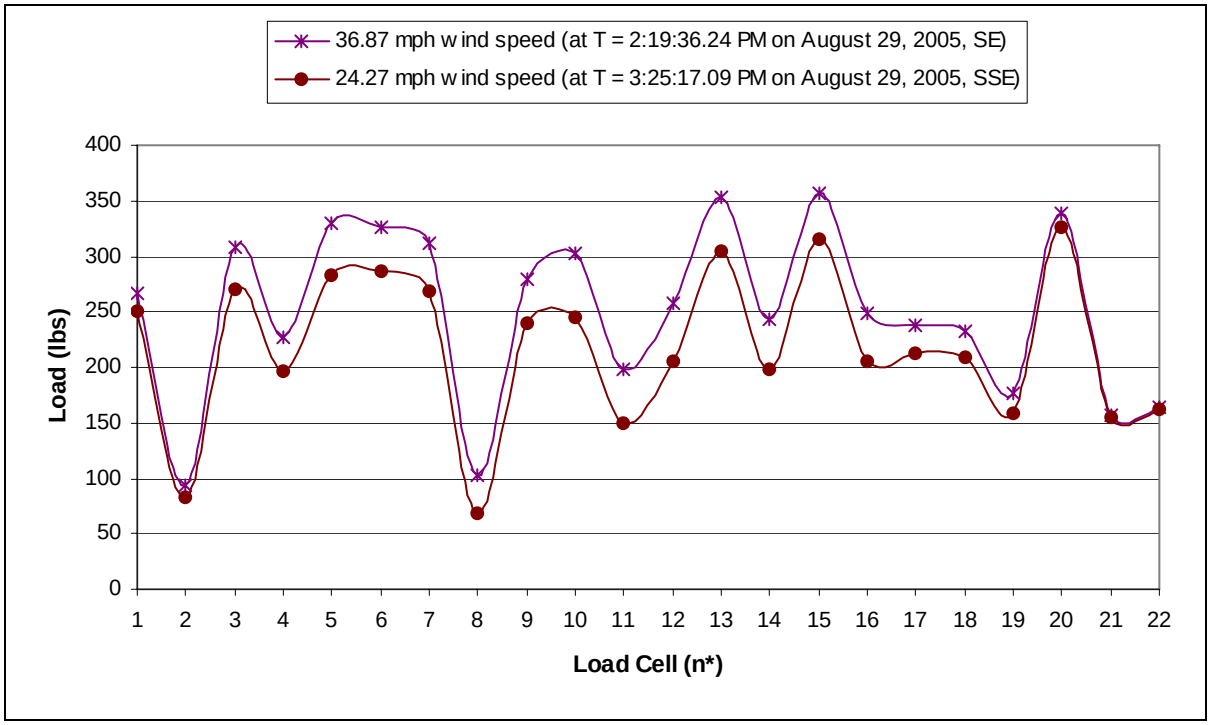

Figure 6.26. Data from load cells located on top of the north wall for maximum wind effects using Load Cases 7 and 8

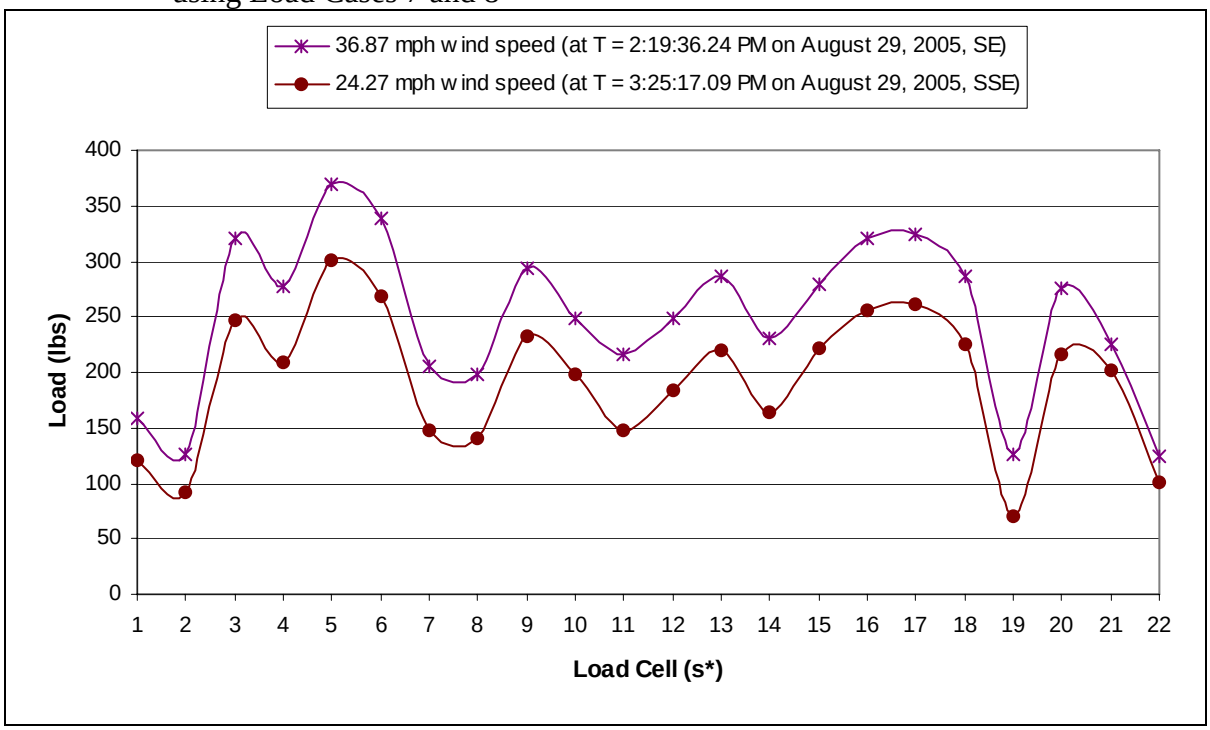

Figure 6.27. Data from load cells located on top of the south wall for maximum wind effects using Load Cases 7 and 8

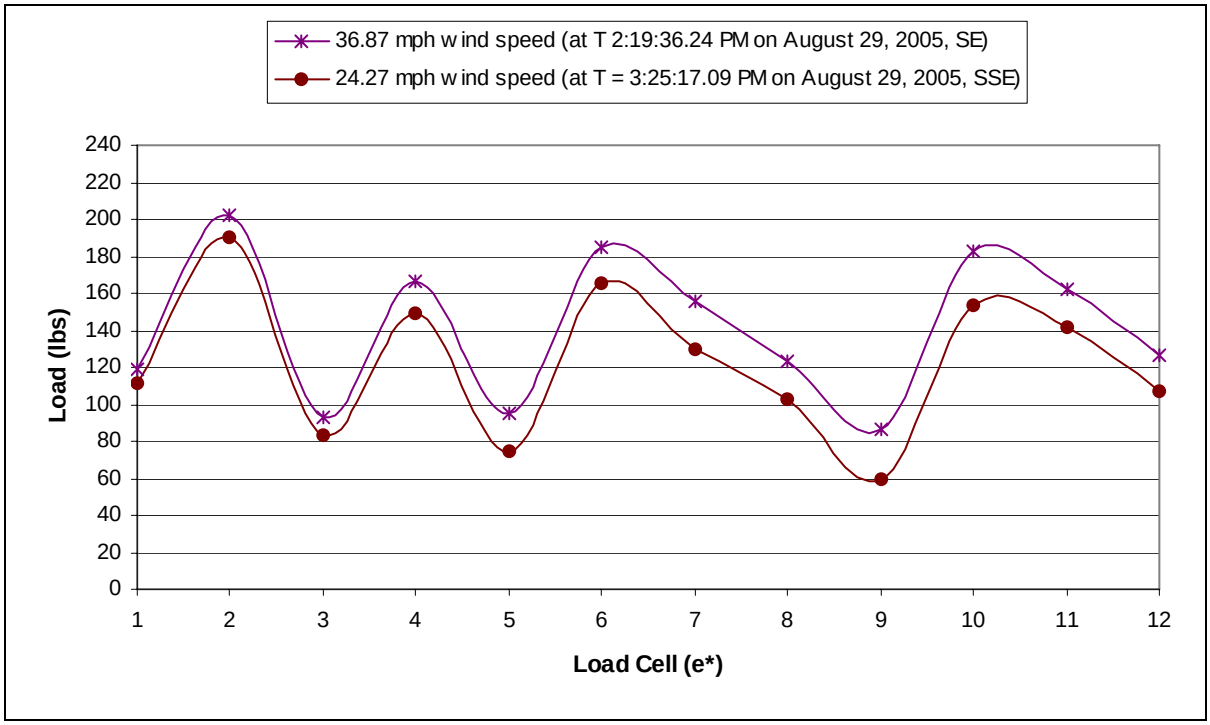

Figure 6.28. Data from load cells located on top of the east wall for maximum wind effects using Load Cases 7 and 8

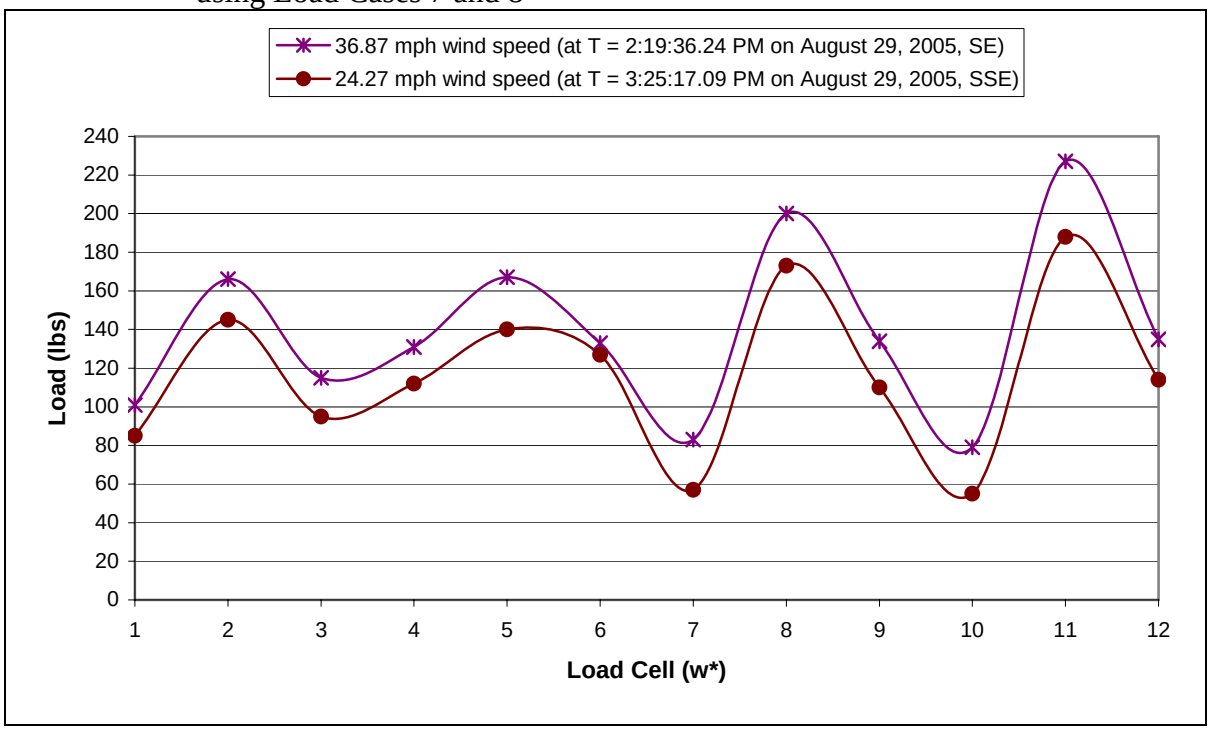

Figure 6.29. Data from load cells located on top of the west wall for maximum wind effects using Load Cases 7 and 8

In addition the demonstration of wind effects, the load cell reactions shown in Figures 6.26 to 6.29 are used to compare with results obtained from the finite element analyses that are reported in the subsequent sections. It is worthy to note that more in-depth statistical analyses of the collected field data and incorporation of dynamic effects could have been more appropriate, but they are beyond the scope of the work chosen for the study presented in this report. Other improvements that could be considered would be to the model itself by more accurately capturing the behavior of connections between different elements of the roof structure.

6.2.2 Finite Element Analysis

The roof of the test structure was analyzed using the ANSYS finite element program representing the effects of Hurricane Katrina wind at three different conditions: 1) wind effect due to the peak wind speed of 56.2 mph (Load Case 5), 2) wind effect due to the highest wind pressures recorded at 43.87 mph (Load Case 6), and 3) wind effect representing maximum suction developed over the entire roof during a 2-minute interval from the time that recorded the highest pressures with a wind speed of 43.87 mph (Load Case 9). The third wind effect extrapolated the field data to find the minimum reactions and the maximum suctions on the test roof during the 2-minute interval for a worst case scenario. In contrast to the third wind effect, which represents an envelope of the maximum suction over a time interval, the first two wind effects are evaluated for given instants in time. Over the chosen time interval, the third wind effect was chosen as a worst case scenario by considering only the maximum suctions experienced at each gauge location on the test roof, resulting in no

pressure acting on the roof. The suctions were considered rather than pressures to examine if the maximum effects were more comparable over the interval, rather than the time instants.

For all three cases, the effects due to wind pressure alone on the roof of the test structure were considered by subtracting the effects of gravity loads. In the finite element analysis this was achieved by only applying the wind loads. For the field data, the corresponding information was established by subtracting gravity effects reported in Figures 6.1 – 6.4 (Load Case 3) from the total reactions measured by the load cells. In this respect, there were two further cases considered. Case I refers to the wind load effect after the gravity load corresponding to Load Case 3 subtracted. Case II corresponds to the maximum possible effects on load cells, which was found by subtracting Load Case 3 from Load Case 8. Although the load cell data for the case occurred at a different time, this approach was to compare the reactions from the FE model with the maximum wind effect that occurred during Hurricane Katrina.

To represent the wind pressure on the finite element model of the roof of the test structure, the pressures found in the field at the locations of the pressure cells were interpolated to find the pressures at the nodes of the finite element model. Although the wind speeds needed to be adjusted from 25 ft of the anemometer height to the mean roof height of 12.5 ft (see Section 4.3.1), the data from the pressure cells did not need to be adjusted because they were measured along the roof surfaces. The wind pressures were interpolated as all the wind pressures across the whole test roof were known at several discrete locations (see Figure 3.8). This, in turn, produced the equivalent static wind pressures at the time the wind pressures were taken. This wind effect was measured to find how closely the load cell reactions for the field data and FE model correspond.

6.2.2.1 Analysis at a Wind Speed of 56.2 mph

The wind pressures measured in psf at the 56.2 mph wind speed (Load Case 5) are shown in Figure 6.30. The circled numbers represent suction on the test roof, while a number with a square around it correspond to a pressure into the test roof. Figures 6.36 and 6.42 are similar to Figure 6.30 for other wind conditions. In Figure 6.30, it is seen that only the southeast side of the test structure was under pressure at the peak wind speed. Therefore, the southeast side of the test structure should theoretically produce more compressive forces in the load cells around this location.

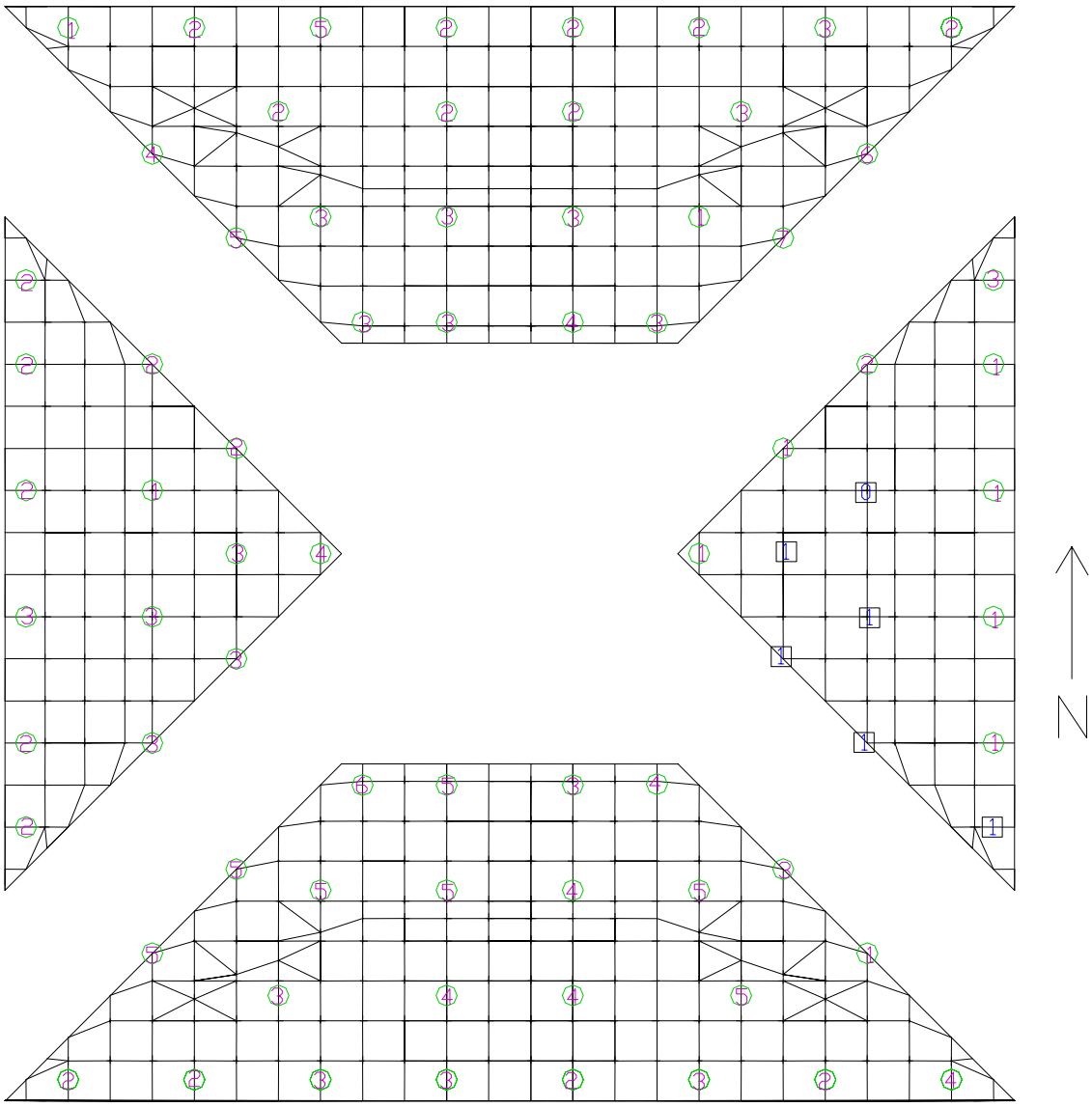

Figure 6.30. Wind pressures in psf at 56.2 mph on the roof of the test structure

Using the recorded wind pressures and suctions at the discrete locations of the pressure cells as shown in Figure 6.30, the wind pressures were linearly interpolated to give an equivalent wind pressure or suction for each hip roof sheathing element of the FE model. It is noted that the pressures at the nodes were averaged to find an equivalent hip roof sheathing pressure for sheathing elements. Figure 6.31 depicts the representation of the

interpolated wind pressures and suctions on the hip roof sheathing as modeled in the finite element analysis. Figure 6.37 and 6.43 are similar to Figure 6.31 for other wind load directions.

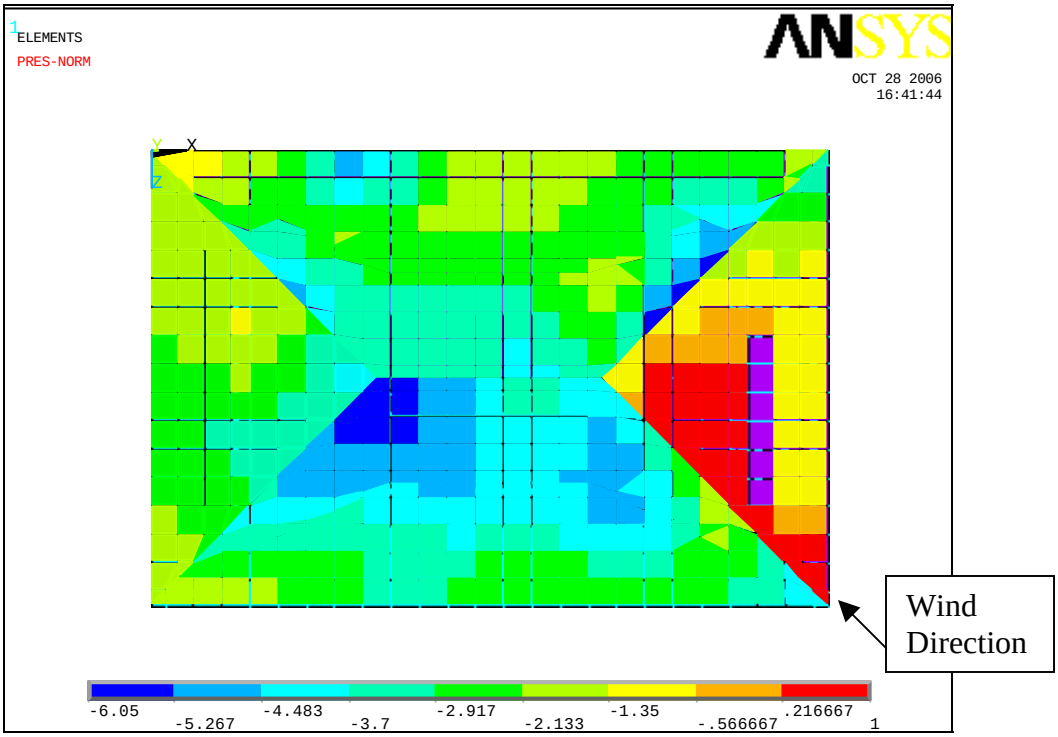

Figure 6.31. Wind pressures (positive values) or suctions (negative values) in psf represented in the FE model at 56.2 mph

After eliminating the influence of gravity loads, the finite element model of the roof system was analyzed only for the wind pressures shown in Figure 6.31. Figures 6.32 to 6.35 show the comparisons between the measured and analytical results of the reaction loads at the load cell locations for both Case I and Case II. In these figures, a negative load cell reaction indicates that the load cell was subjected to tension, which may be a direct effect of suction applied to the test roof. Conversely, a positive load cell reaction represents the load cell in compression, which could be likely due to a direct effect of pressure is applied to the

roof. Figures 6.38 to 6.41 and Figure 6.44 to 6.47 are similar to Figures 6.32 to 6.35 for comparing the reactions of the collected field data and the FE model.

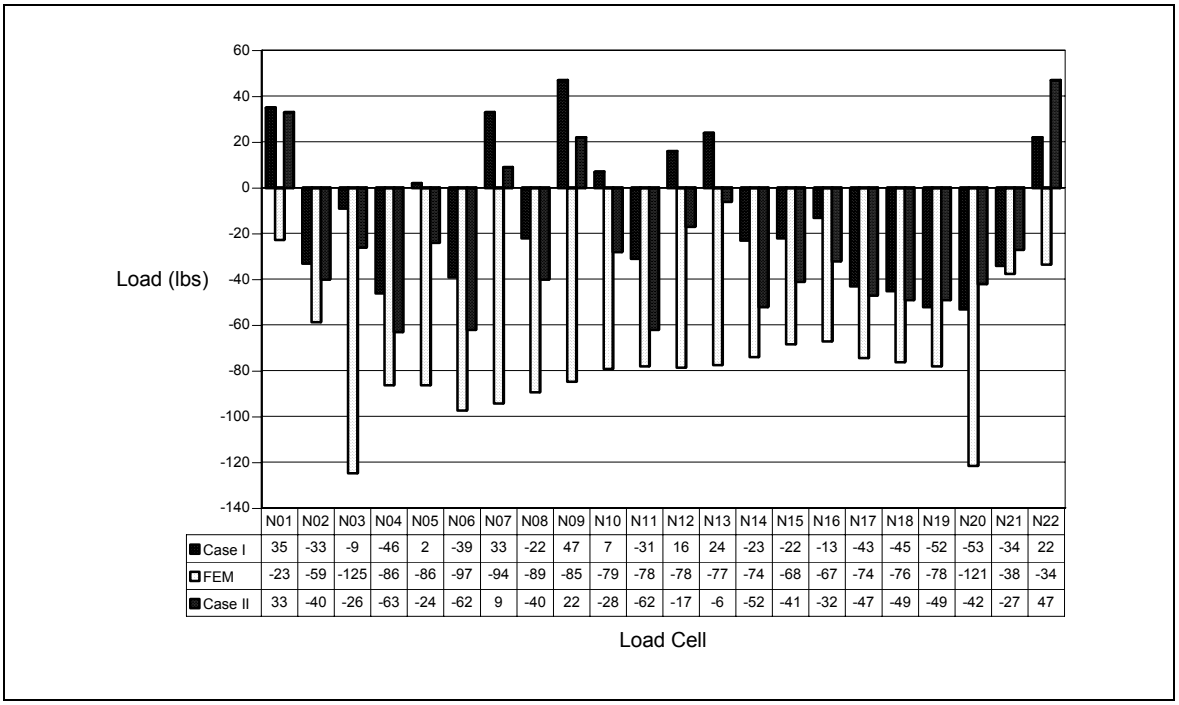

	N01	N02	N03	N04	N05	N06	N07	N08	N09	N10	N11	N12	N13	N14	N15	N16	N17	N18	N19	N20	N21	N22
Case I	35	-33	-9	-46	2	-39	33	-22	47	7	-31	16	24	-23	-22	-13	-43	-45	-52	-53	-34	22
FEM	-23	-59	-125	-86	-86	-97	-94	-89	-85	-79	-78	-78	-77	-74	-68	-67	-74	-76	-78	-121	-38	-34
Case II	33	-40	-26	-63	-24	-62	9	-40	22	-28	-62	-17	-6	-52	-41	-32	-47	-49	-49	-42	-27	47

Figure 6.32. Comparison of wind load reactions recorded by the load cells along the north wall with those computed using the wind pressures/suction from the FE model at a wind speed of 56.2 mph

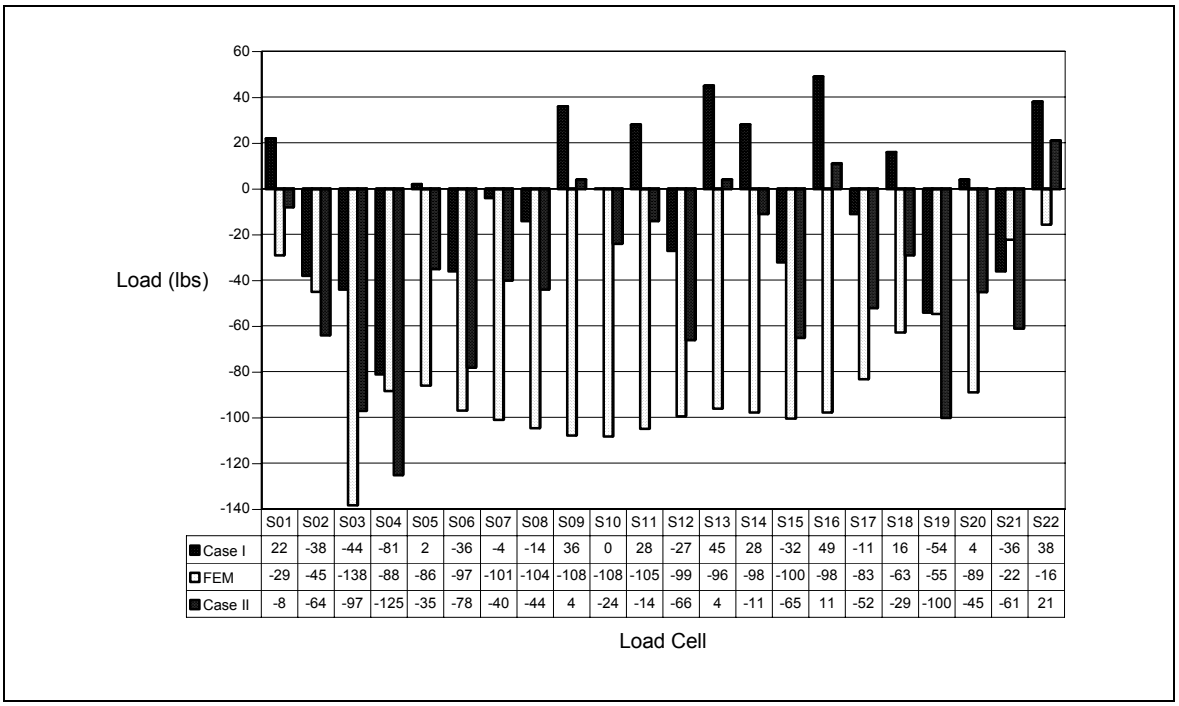

	S01	S02	S03	S04	S05	S06	S07	S08	S09	S10	S11	S12	S13	S14	S15	S16	S17	S18	S19	S20	S21	S22
Case I	22	-38	-44	-81	2	-36	-4	-14	36	0	28	-27	45	28	-32	49	-11	16	-54	4	-36	38
FEM	-29	-45	-138	-88	-86	-97	-101	-104	-108	-108	-105	-99	-96	-98	-100	-98	-83	-63	-55	-89	-22	-16
Case II	-8	-64	-97	-125	-35	-78	-40	-44	4	-24	-14	-66	4	-11	-65	11	-52	-29	-100	-45	-61	21

Figure 6.33. Comparison of wind load reactions recorded by the load cells along the south wall with those computed using the wind pressures/suction from the FE model at a wind speed of 56.2 mph

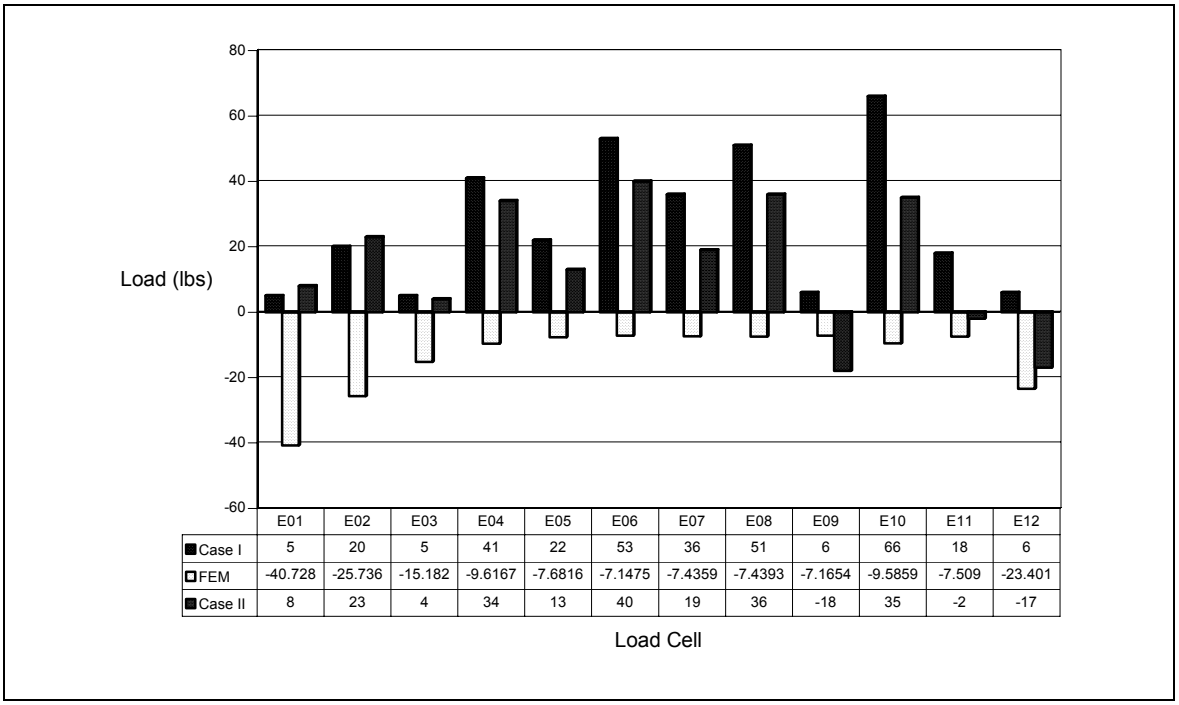

	E01	E02	E03	E04	E05	E06	E07	E08	E09	E10	E11	E12
Case I	5	20	5	41	22	53	36	51	6	66	18	6
FEM	-40.728	-25.736	-15.182	-9.6167	-7.6816	-7.1475	-7.4359	-7.4393	-7.1654	-9.5859	-7.509	-23.401
Case II	8	23	4	34	13	40	19	36	-18	35	-2	-17

Figure 6.34. Comparison of wind load reactions recorded by the load cells along the east wall with those computed using the wind pressures/suction from the FE model at a wind speed of 56.2 mph

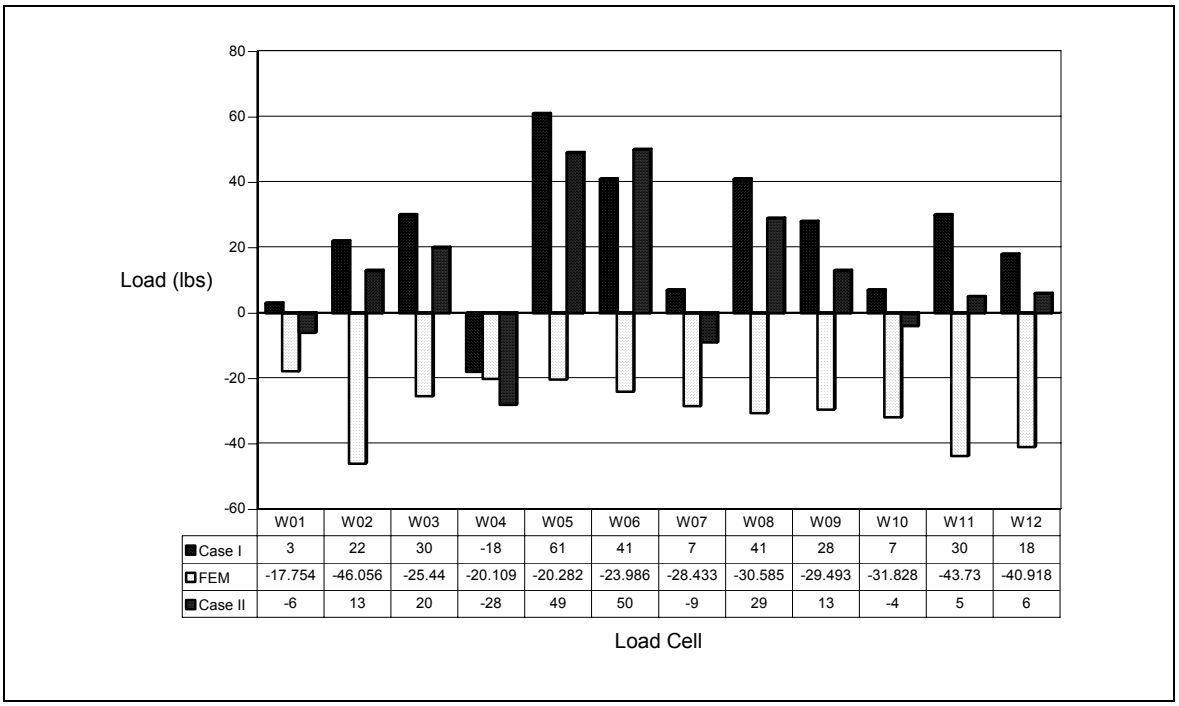

	W01	W02	W03	W04	W05	W06	W07	W08	W09	W10	W11	W12
Case I	3	22	30	-18	61	41	7	41	28	7	30	18
FEM	-17.754	-46.056	-25.44	-20.109	-20.282	-23.986	-28.433	-30.585	-29.493	-31.828	-43.73	-40.918
Case II	-6	13	20	-28	49	50	-9	29	13	-4	5	6

Figure 6.35. Comparison of wind load reactions recorded by the load cells along the west wall with those computed using the wind pressures/suction from the FE model at a wind speed of 56.2 mph

Figures 6.32 to 6.35 indicated that the only region where a less compressive reaction should have occurred was near the southeast wall, where there was pressure into the test structure. Both Case I and Case II of the field data did not capture this trend. The FE model showed this trend to be true to the estimated evaluation only along the east wall. The total wind effect for Case I showed a total wind loading of 211 lbs. This positive number indicated that there was some pressure built up on the test structure and weight was added to the test structure, which may have been due to precipitation during the hurricane event. This, however, was not reflected by the measurements of the pressure cells, as these pressure cells measured mostly suctions, which should have generally shown a consequent decrease in load cell reactions. The FE model showed this theoretical estimate to be true. The total wind loading for Case II was –1,201 lbs, which was the worst case scenario for wind loading. Although the wind effect was closer in comparison for Case II to the FE model's total wind loading of –4,041 lbs, there was an extreme amount of error between these data sets.

For further comparison of this static wind pressure along with the two other static wind pressures modeled and assumed, please turn to section 6.2.2.4.

6.2.2.2 Analysis under the Recorded Highest Wind Pressures

The wind pressures measured in psf at the highest wind pressures (Load Case 6) are shown in Figure 6.36. In Figure 6.36, it is seen that only the southeast side of the test structure was under pressure at Load Case 6. Therefore, the southeast side of the test structure should theoretically produce more compressive forces in the load cells around this location. The interpolation techniques were implemented as discussed in Section 6.2.2.1.

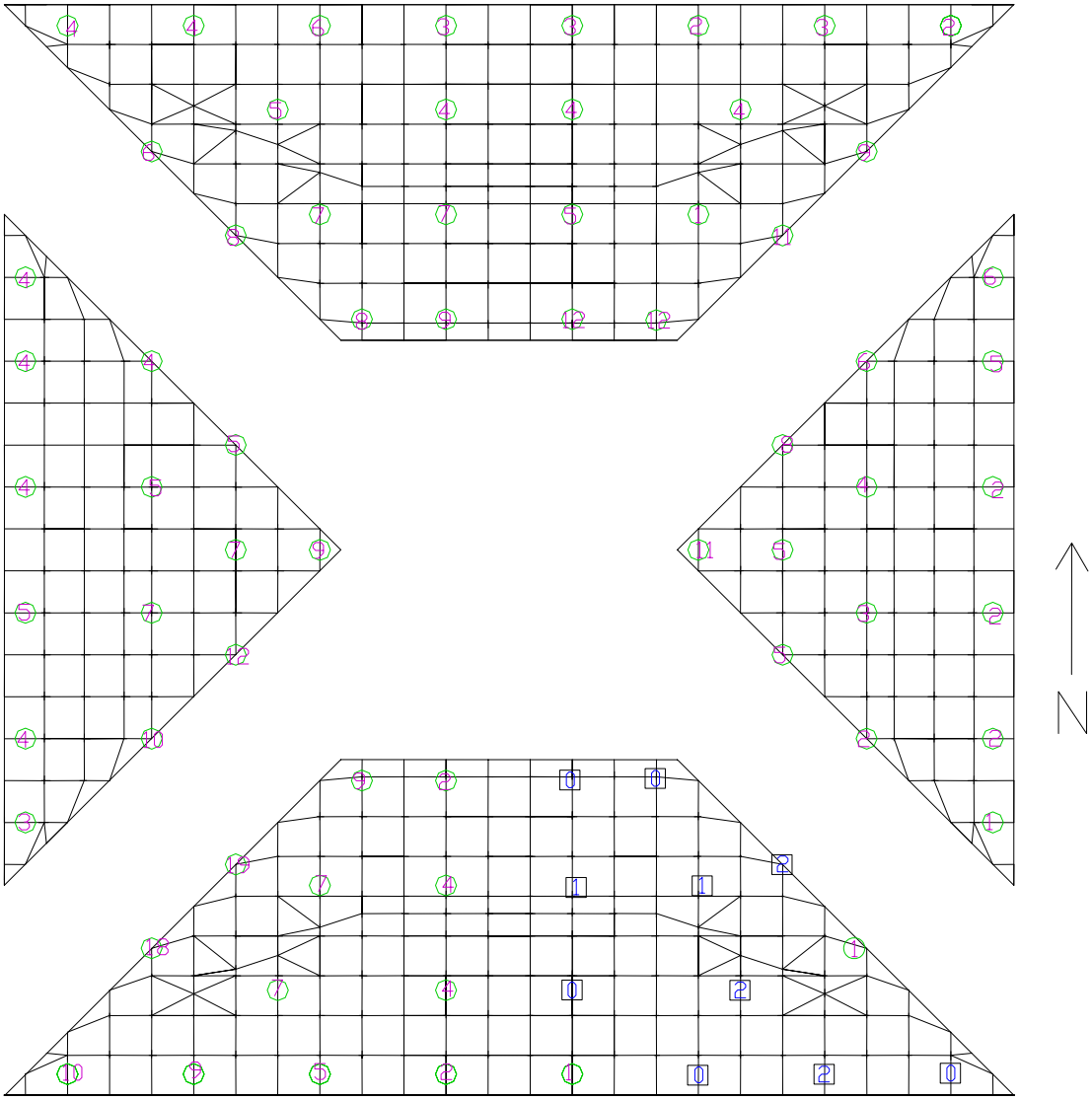

Figure 6.36. Wind pressures in psf at 43.87 mph on the roof of the test structure

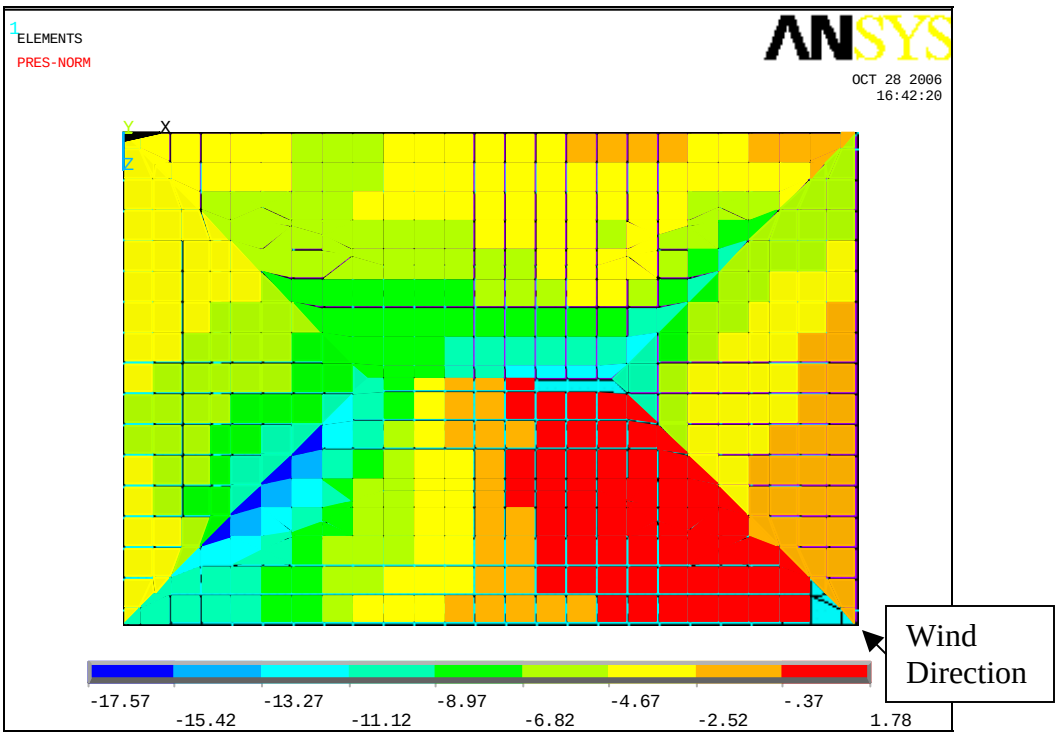

Figure 6.37. Wind pressures (positive values) or suctions (negative values) in psf represented in the FE model at 43.87 mph

The tested structure was analyzed considering only the wind pressures shown in Figure 6.37. Figures 6.38 to 6.41 show the measured and the analytical results of the reaction loads at the load cell locations for both Case I and Case II.

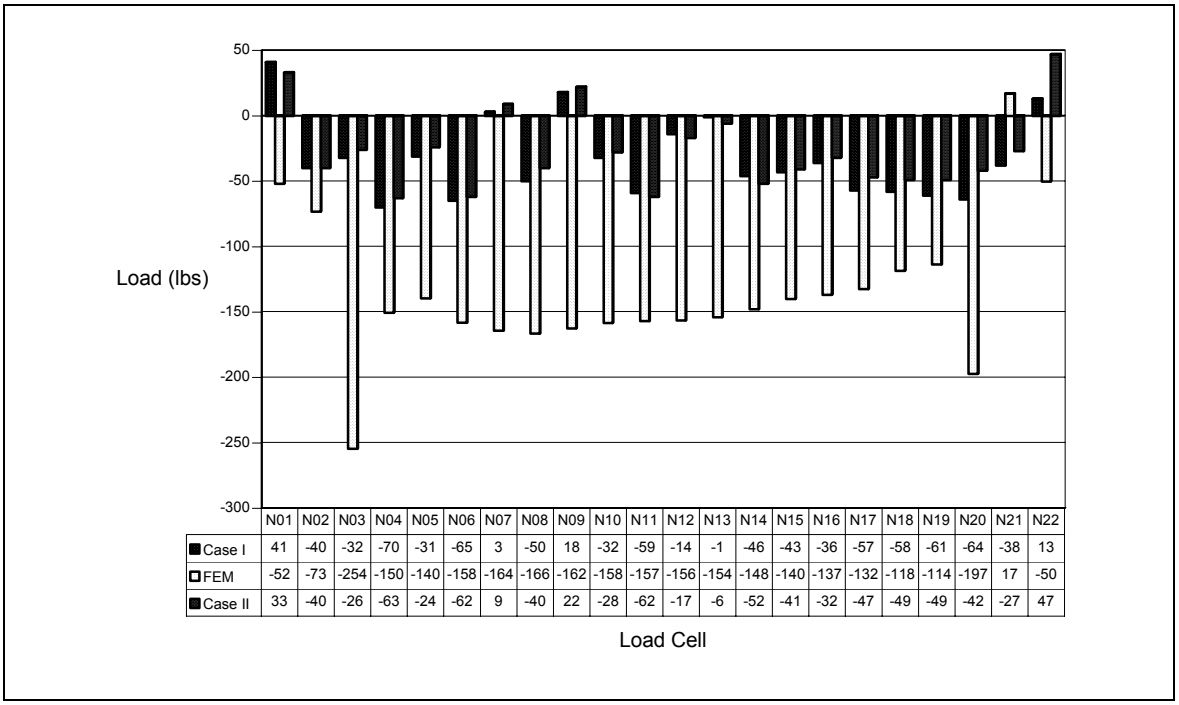

	N01	N02	N03	N04	N05	N06	N07	N08	N09	N10	N11	N12	N13	N14	N15	N16	N17	N18	N19	N20	N21	N22
Case I	41	-40	-32	-70	-31	-65	3	-50	18	-32	-59	-14	-1	-46	-43	-36	-57	-58	-61	-64	-38	13
FEM	-52	-73	-254	-150	-140	-158	-164	-166	-162	-158	-157	-156	-154	-148	-140	-137	-132	-118	-114	-197	17	-50
Case II	33	-40	-26	-63	-24	-62	9	-40	22	-28	-62	-17	-6	-52	-41	-32	-47	-49	-49	-42	-27	47

Figure 6.38. Comparison of wind load reactions recorded by the load cells along the north wall with those computed using the wind pressures/suctions from the FE model at a wind speed of 43.87 mph

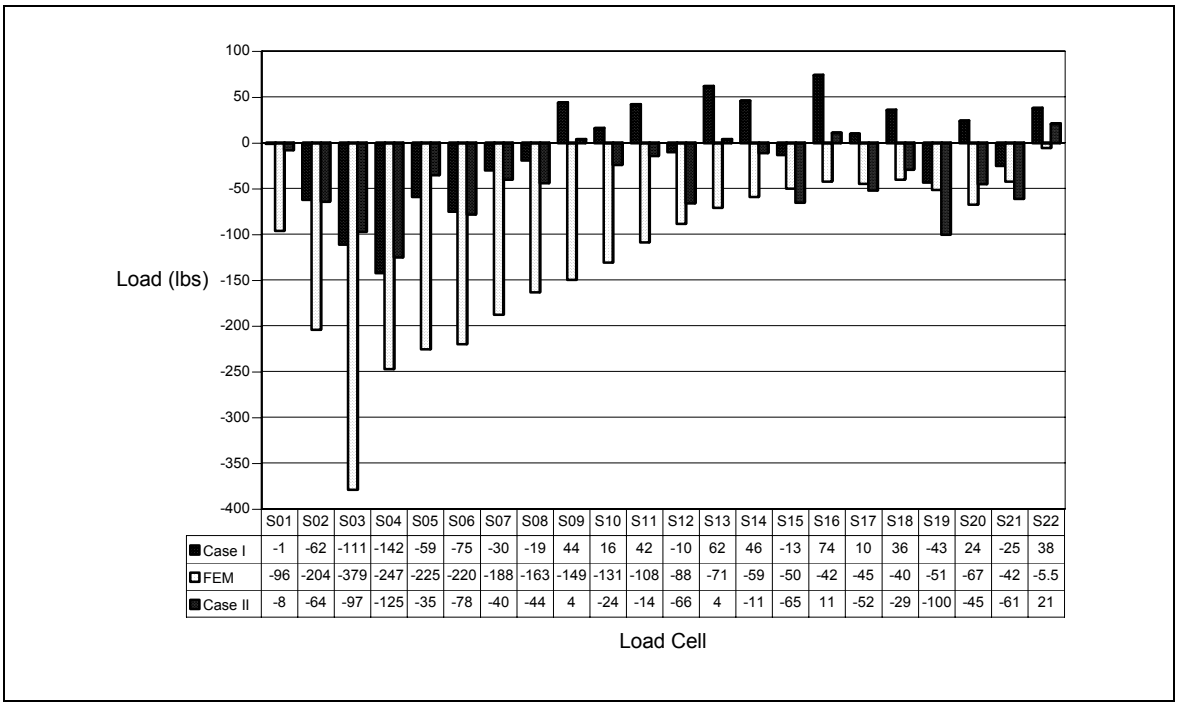

	S01	S02	S03	S04	S05	S06	S07	S08	S09	S10	S11	S12	S13	S14	S15	S16	S17	S18	S19	S20	S21	S22
Case I	-1	-62	-111	-142	-59	-75	-30	-19	44	16	42	-10	62	46	-13	74	10	36	-43	24	-25	38
FEM	-96	-204	-379	-247	-225	-220	-188	-163	-149	-131	-108	-88	-71	-59	-50	-42	-45	-40	-51	-67	-42	-5.5
Case II	-8	-64	-97	-125	-35	-78	-40	-44	4	-24	-14	-66	4	-11	-65	11	-52	-29	-100	-45	-61	21

Figure 6.39. Comparison of wind load reactions recorded by the load cells along the south wall with those computed using the wind pressures/suctions from the FE model at a wind speed of 43.87 mph

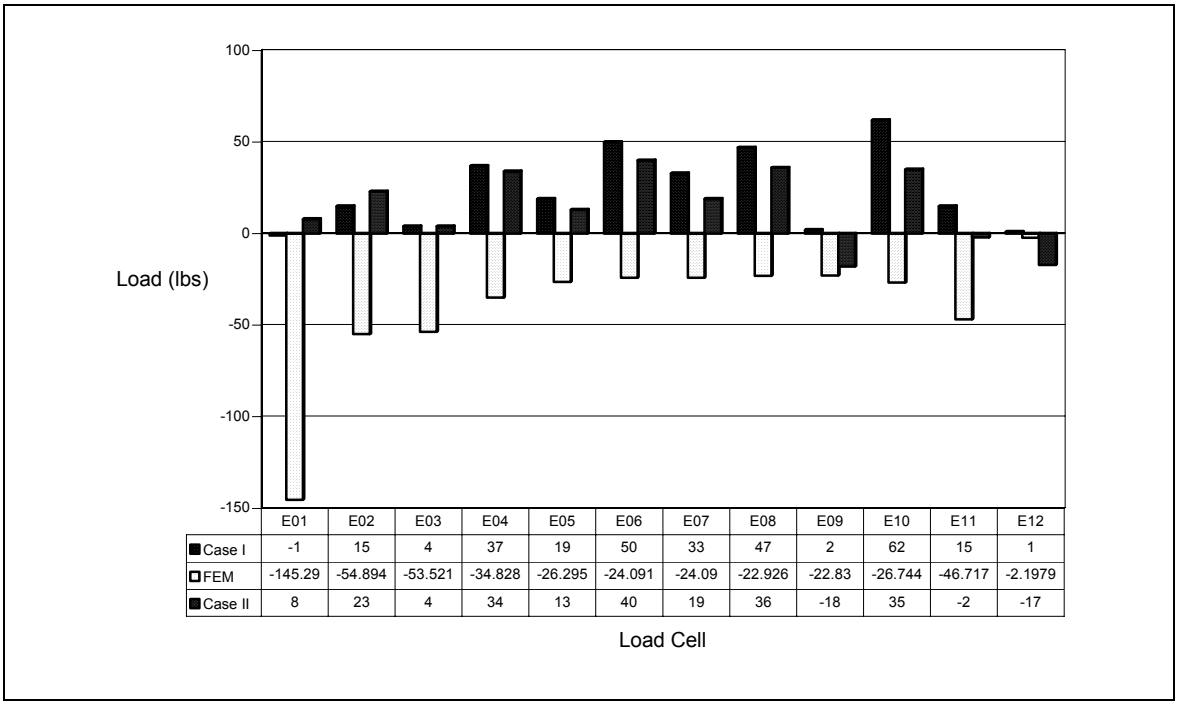

	E01	E02	E03	E04	E05	E06	E07	E08	E09	E10	E11	E12
Case I	-1	15	4	37	19	50	33	47	2	62	15	1
FEM	-145.29	-54.894	-53.521	-34.828	-26.295	-24.091	-24.09	-22.926	-22.83	-26.744	-46.717	-2.1979
Case II	8	23	4	34	13	40	19	36	-18	35	-2	-17

Figure 6.40. Comparison of wind load reactions recorded by the load cells along the east wall with those computed using the wind pressures/suctions from the FE model at a wind speed of 43.87 mph

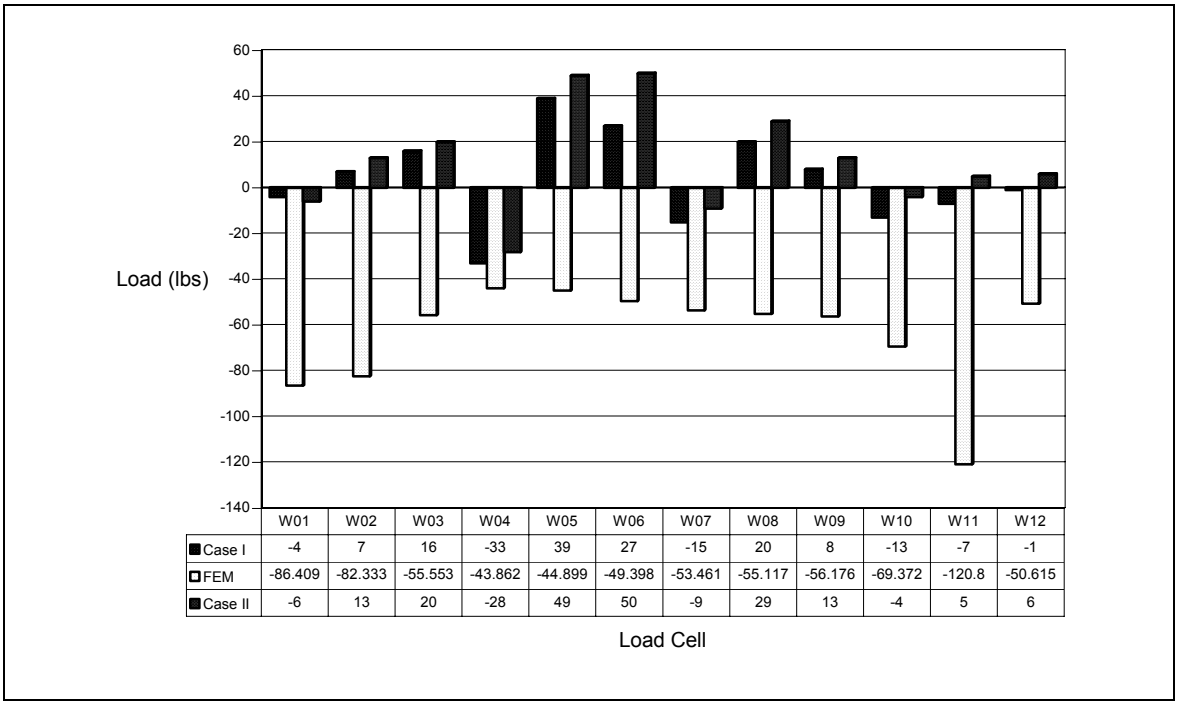

	W01	W02	W03	W04	W05	W06	W07	W08	W09	W10	W11	W12
Case I	-4	7	16	-33	39	27	-15	20	8	-13	-7	-1
FEM	-86.409	-82.333	-55.553	-43.862	-44.899	-49.398	-53.461	-55.117	-56.176	-69.372	-120.8	-50.615
Case II	-6	13	20	-28	49	50	-9	29	13	-4	5	6

Figure 6.41. Comparison of wind load reactions recorded by the load cells along the west wall with those computed using the wind pressures/suctions from the FE model at a wind speed of 43.87 mph

Figures 6.38 – 6.41 indicated that the only place a less compressive reaction should have occurred was near the southeast wall under the applied pressures. Both Case I and Case II of the field data did not capture this trend. However, the FE model showed this trend to be true. The total wind effect for Case I showed a value of –592 lbs. This negative number indicated that there was some suction built up by the test structure and weight was removed from the test structure, which was expected. The total wind loading for Case II was –1,201 lbs, which was the worst case scenario for wind loading. Although the wind effect was closer in comparison for Case II to the FE model's total wind loading of –6,888 lbs, there was an even more extreme amount of error between these data sets. In comparison to Section 6.2.2.1, this negative reaction should be higher than the previous analysis due to the higher suctions recorded from the test structure's pressure cells.

For further comparison of this static wind pressure along with the other two static wind pressures modeled and assumed, please refer to Section 6.2.2.4.

6.2.2.3 Analysis under Maximum Suction Recorded over a 2-Minutes Interval

The maximum suction induced by wind in psf over a ± 1-minute interval around Load Case 9 that corresponded to the time that induced the maximum suction on the roof are shown in Figure 6.42. As discussed in Section 6.2.2.1, the interpolation techniques were implemented to find the equivalent wind pressure acting on each sheathing element, which is shown in Figure 6.43. Consequently, the entire roof was subjected to much larger suction in this particular analysis than in the previous analyses. Therefore, this wind load case should theoretically cause the highest uplifting force to the roof of the test structure, resulting in

higher reduction to the compressive forces in the load cells, which were induced by the gravity load.

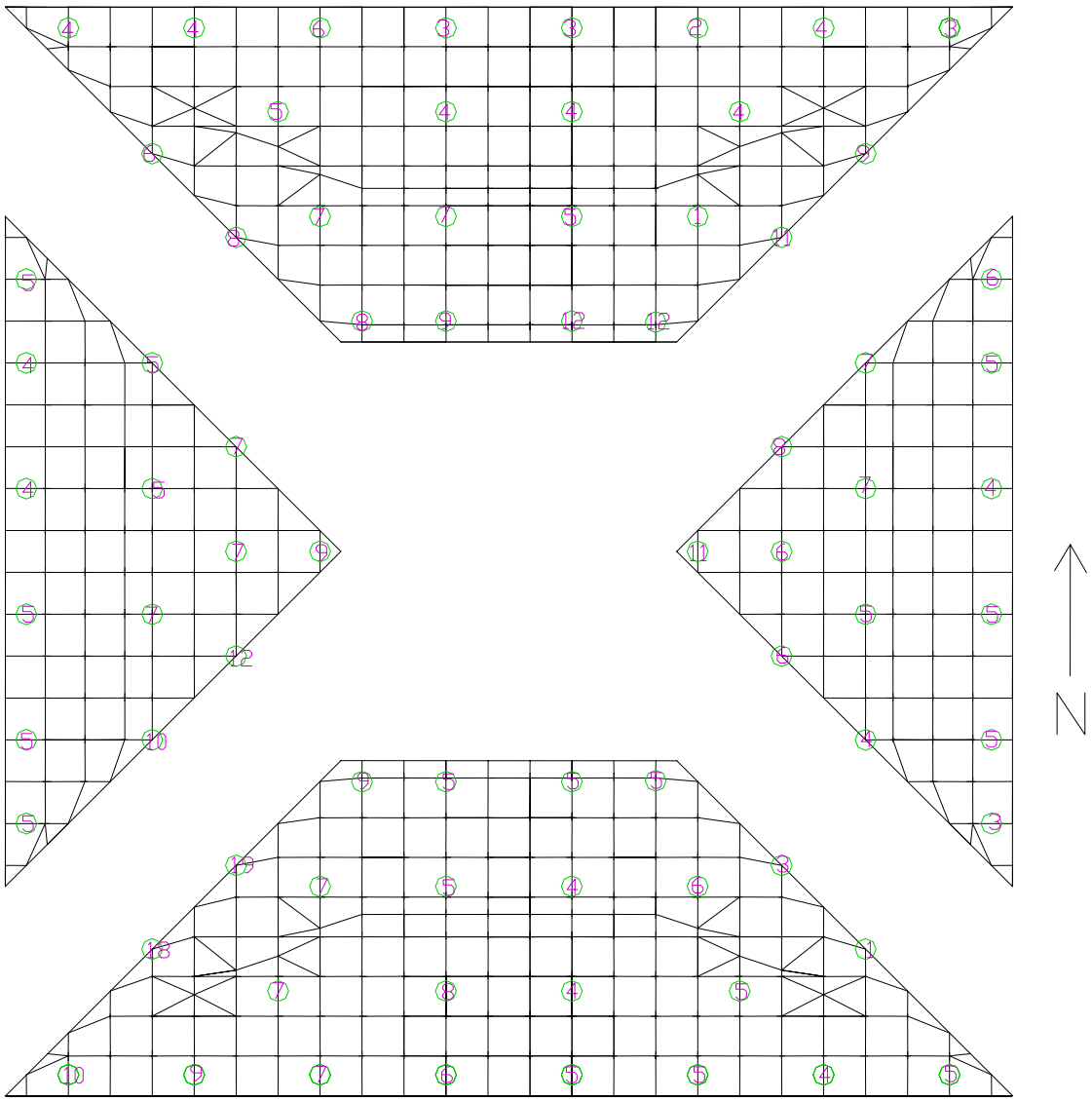

Figure 6.42. Wind pressures in psf at ± 1 minute from 43.87 mph on the roof of the test structure

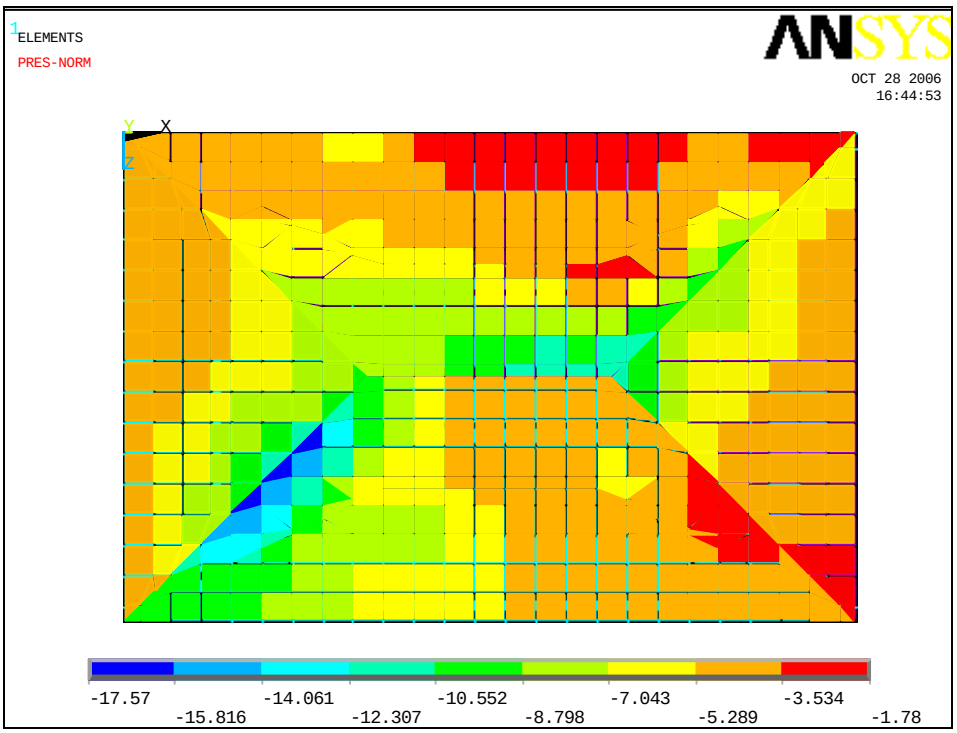

Figure 6.43. Wind pressures (positive values) or suctions (negative values) in psf represented in the FE model at ± 1 minute from 43.87 mph

Presented in Figures 6.44 to 6.47 are the results of the finite element analysis of the test roof subjected to the wind pressures shown in Figure 6.43. Again results from the two cases are compared to the finite element analysis results in all figures. Case I shows the measured load cell reaction recorded by individual load cell during the 2-minute interval to capture the maximum effect of suction imposed on the roof. Case II results corresponded once again to Load Case 8 minus Load Case 3 for a worst case scenario.

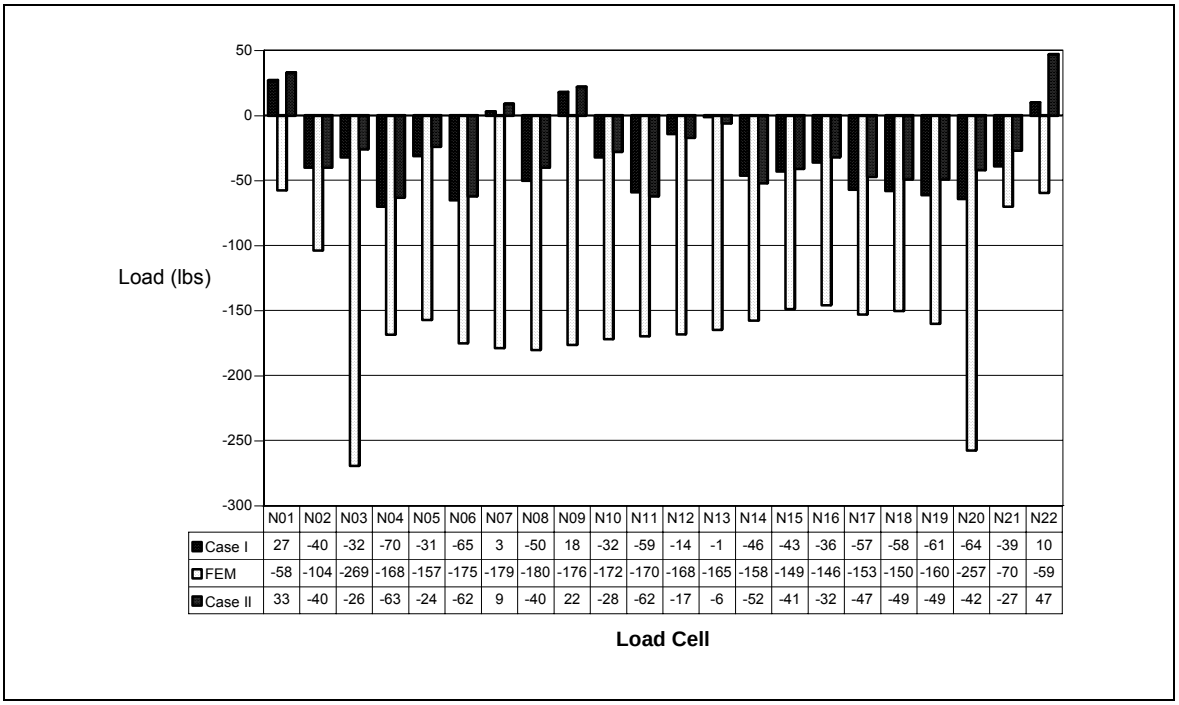

	N01	N02	N03	N04	N05	N06	N07	N08	N09	N10	N11	N12	N13	N14	N15	N16	N17	N18	N19	N20	N21	N22
Case I	27	-40	-32	-70	-31	-65	3	-50	18	-32	-59	-14	-1	-46	-43	-36	-57	-58	-61	-64	-39	10
FEM	-58	-104	-269	-168	-157	-175	-179	-180	-176	-172	-170	-168	-165	-158	-149	-146	-153	-150	-160	-257	-70	-59
Case II	33	-40	-26	-63	-24	-62	9	-40	22	-28	-62	-17	-6	-52	-41	-32	-47	-49	-49	-42	-27	47

Figure 6.44. Comparison of wind load reactions recorded by the load cells along the north wall with those computed using the wind pressures/suctions from the FE model at a wind speed of ± 1 minute from 43.87 mph

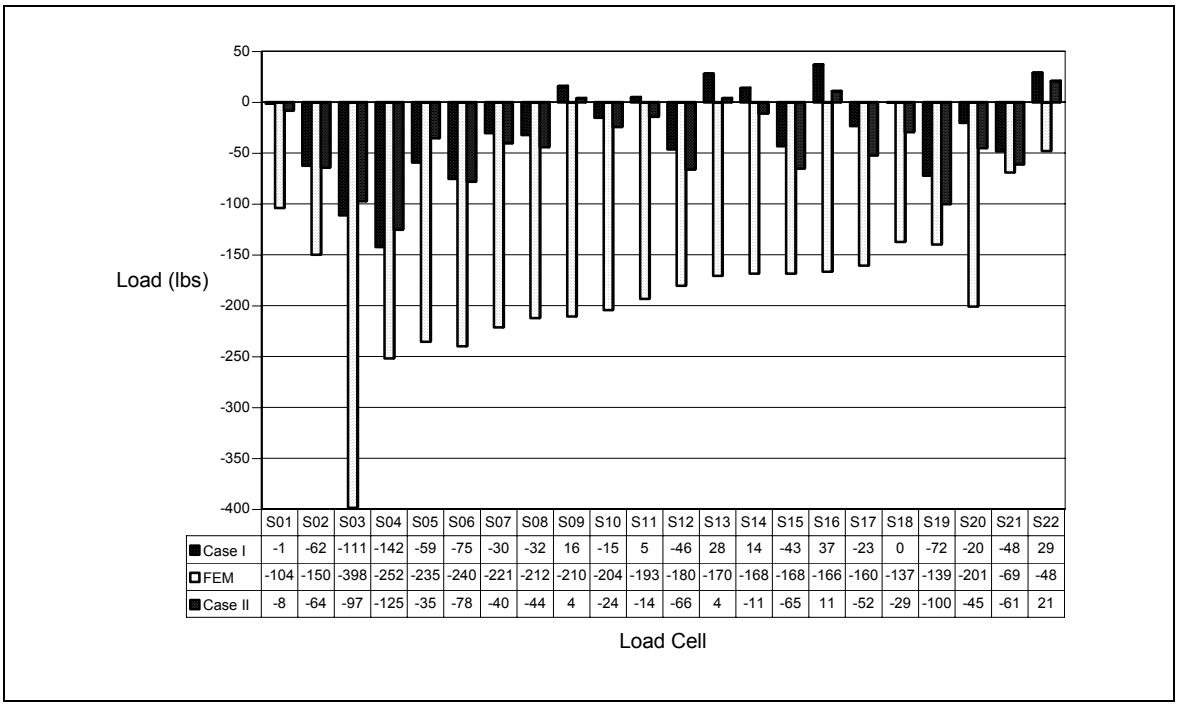

	S01	S02	S03	S04	S05	S06	S07	S08	S09	S10	S11	S12	S13	S14	S15	S16	S17	S18	S19	S20	S21	S22
Case I	-1	-62	-111	-142	-59	-75	-30	-32	16	-15	5	-46	28	14	-43	37	-23	0	-72	-20	-48	29
FEM	-104	-150	-398	-252	-235	-240	-221	-212	-210	-204	-193	-180	-170	-168	-168	-166	-160	-137	-139	-201	-69	-48
Case II	-8	-64	-97	-125	-35	-78	-40	-44	4	-24	-14	-66	4	-11	-65	11	-52	-29	-100	-45	-61	21

Figure 6.45. Comparison of wind load reactions recorded by the load cells along the south wall with those computed using the wind pressures/suctions from the FE model at a wind speed of ± 1 minute from 43.87 mph

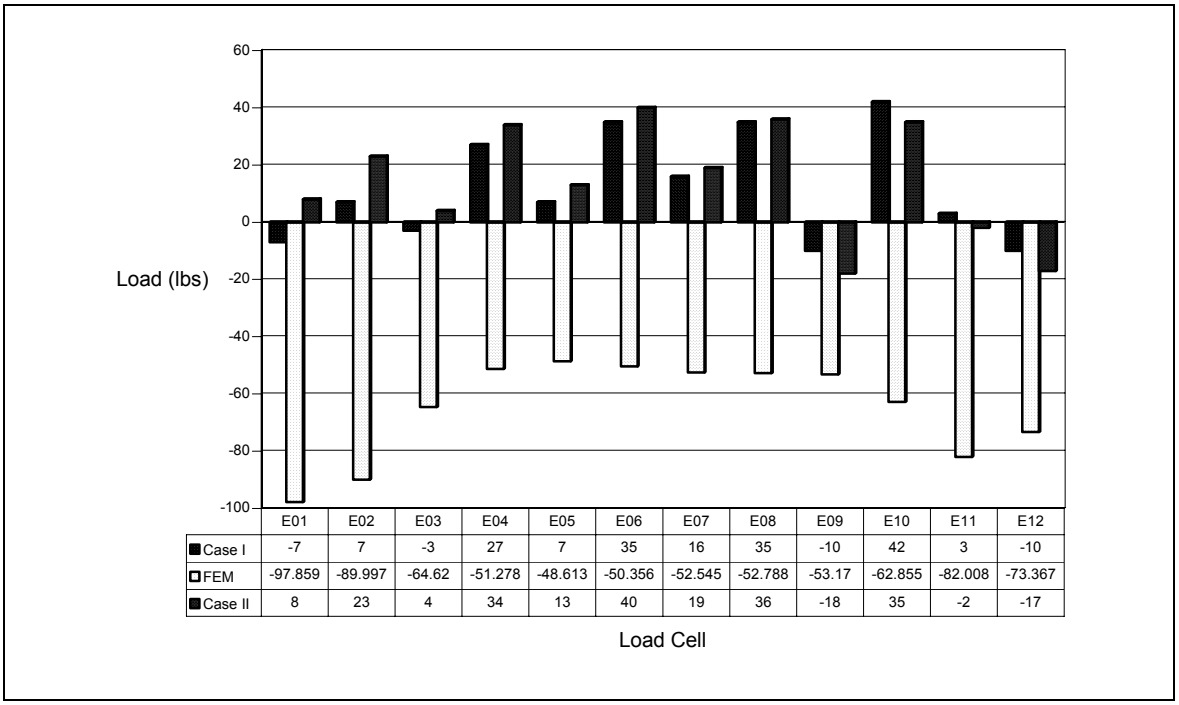

	E01	E02	E03	E04	E05	E06	E07	E08	E09	E10	E11	E12
Case I	-7	7	-3	27	7	35	16	35	-10	42	3	-10
FEM	-97.859	-89.997	-64.62	-51.278	-48.613	-50.356	-52.545	-52.788	-53.17	-62.855	-82.008	-73.367
Case II	8	23	4	34	13	40	19	36	-18	35	-2	-17

Figure 6.46. Comparison of wind load reactions recorded by the load cells along the east wall with those computed using the wind pressures/suctions from the FE model at a wind speed of ± 1 minute from 43.87 mph

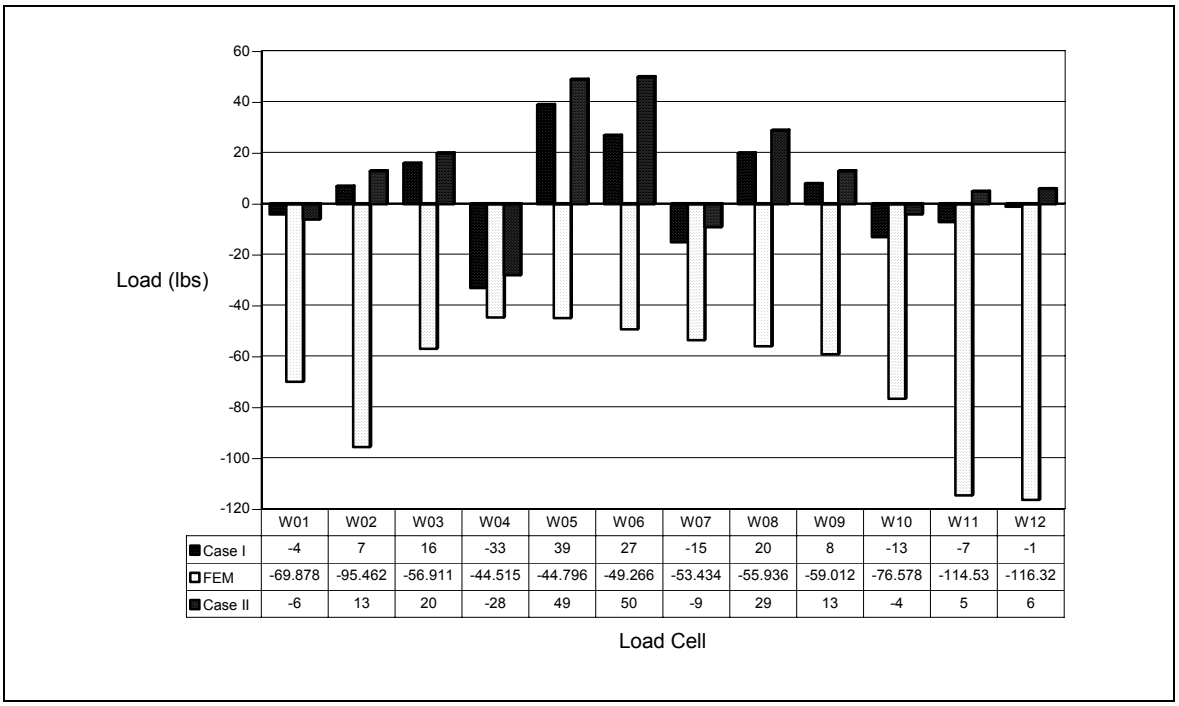

	W01	W02	W03	W04	W05	W06	W07	W08	W09	W10	W11	W12
Case I	-4	7	16	-33	39	27	-15	20	8	-13	-7	-1
FEM	-69.878	-95.462	-56.911	-44.515	-44.796	-49.266	-53.434	-55.936	-59.012	-76.578	-114.53	-116.32
Case II	-6	13	20	-28	49	50	-9	29	13	-4	5	6

Figure 6.47. Comparison of wind load reactions recorded by the load cells along the west wall with those computed using the wind pressures/suctions from the FE model at a wind speed of ± 1 minute from 43.87 mph

Figures 6.44 to 6.47 indicated that the only place a less compressive reaction should have occurred was near the northeast and southeast wall due to the lower suctions experienced at these locations. Both Case I and Case II of the field data did not capture this trend. However, the FE model showed this trend to be true. The total wind effect for Case I showed a value of –1,204 lbs. This negative number indicated that there was some suction built up by the test structure and weight was removed from the test structure, which was the expectation. The total wind loading for Case II was –1,201 lbs, which was the worst case scenario for wind loading. Both Case I and Case II are much closer in comparison, but are extremely poor in comparison to the FE model's total wind loading of –9,083 lbs. This negative reaction theoretically should be the highest of the previous analyses due to the higher suctions recorded from the test structure's pressure cells.

For further comparison of this load case with the results of the previous two static wind effects model, refer to Section 6.2.2.4.

6.2.2.4 Comparison of Results from Load Cases 5, 6, and 9

The total reactions of the test roof's field data and FE model are summarized for Load Cases 5, 6, and 9 in Table 6.3 below.

Table 6.3. Comparison of total measured reactions under the test roof due to wind loads for Load Cases 5, 6, and 9

Source	Total Measured Reactions by Load Cells (lbs)		
	Load Case 5	Load Case 6	Load Case 9
Case I and Case II (gravity loading)	13,087	13,087	13,087
Case I (gravity and wind loading)	13,298	12,495	11,883
Case II (gravity and wind loading)	11,886	11,886	11,886
Case I (wind loading)	211	-592	-1,204
Case II (wind loading)	-1,201	-1,201	-1,201
FEM (wind loading)	-4,041	-6,888	-9,083
Percent error FEM vs Case I (wind loading) (%)	105.22	91.41	86.74
Percent error FEM vs Case II (wind loading) (%)	70.28	82.56	86.78

A summary of the results from FE analyses are compared in Table 6.3, which generally shows poor correlations between the FE model results and the wind loading effect of the field data for the three load cases evaluated. The FE analysis results significantly over predict the wind loading effect in all cases. However, the decrease in total reaction due mainly to the suction caused by the wind effect is seen for both the FE model and the field data Case I. Case II showed a much closer prediction due to the worst case scenario of wind loading. The total weight of the test roof was not very conservative between the field data for Hurricane Katrina and the FE model. The larger FE model loads on the test structure could be attributed to almost every sheathing element being loaded normal to its surface, ignoring the influence of precipitation, and assumptions of boundary conditions used in the FE model formulation. Also, the possibility exists that the test structure may have undergone settlements at specific locations, due to quick spikes in pressures and suctions during the hurricane event.

6.3 Evaluation of Wind Load as per *ASCE 7-02 Standard*

The wind pressure distributions established for the roof of the test structure in Chapter 4 from *ASCE 7-02 Standard* is further examined in this section. In this process, two wind speeds are considered and the effects of gravity load are eliminated from both the field data and the FE analysis. First, the wind speeds of 120.34 mph (as established in Section 4.3.1), is of interest because this is the maximum wind speed that the test structure may experience with a 50-year or 100-year return period according the *ASCE 7-02 Standard.* Second, the wind speeds of 50.33 mph (as established in Section 4.3.1), which was the peak wind speed recorded near the test structure during Hurricane Katrina.

The direction of both the 120.34 mph and 50.33 mph wind speeds were taken as the east-southeastern direction, which was the observed direction of the peak wind speeds during Hurricane Katrina. The wind load effects stipulated from the *ASCE 7-02 Standard* were modeled as an equivalent static wind load pressure. This necessitated that the field data must be justified as to which wind speed and duration should be used for interpreting the wind load from the *ASCE 7-02 Standard*. It is worthy to note that when using the field data, the length of wind record, sampling error, averaging time, anemometer height, data quality, and terrain exposure of the anemometer should be taken into account whereas the *ASCE 7-02 Standard* uses only the basic wind speeds for the structure located in Pensacola, Florida.

According to article C6.5.4.2 of the *ASCE 7-02 Standard*, sampling errors can lead to large uncertainties in specification of the 50-year wind speed. These sampling errors are the errors associated with the limited size of the climatological data samples. As noted in the *ASCE 7-02 Standard*, it is possible to have a 20 mph error in wind speed at an individual station with a record length of 30 years. Also, the *ASCE 7-02 Standard* states that if the

meteorological data are used to justify a wind speed lower than 85 mph 50-year peak gust at a height of 33 ft, an analysis of sampling error is required to demonstrate that the wind record could not happen by chance. The wind record could be proven by showing that the difference between predicted wind speed and 85 mph contains 2 to 3 standard deviations of sampling error (*ASCE 7*, 2003). Other equivalent methods could be used for proving that the wind speed record could not happen by chance. The peak wind speed during Hurricane Katrina was verified by comparing it against those reported for the region. For example, the peak wind speed reported by the TV station WEAR in Pensacola, Florida, was determined to be 57.5 mph and was estimated to be a close comparison (2.33% error) to the peak wind speeds determined from the anemometer by the FPL researchers (see Section 3.5).

6.3.1 Wind Pressure Distribution as per *ASCE 7-02 Standard*

Both the wind pressure distributions for the MWFRS and C&C design were presented in Chapter 4 for Method 1 and 2 using the *ASCE 7-02 Standard*. Both wind pressure distributions are considerably different because one corresponds to an average wind pressure effects while the other represents the localized effects due to wind loads.

The MWFRS uses an average wind pressure distribution over the entire test structure (see Figures 4.3 through 4.10 for Method 2 at 50.33 mph wind speeds and Figure 4.11 for Method 1 at 120.34 mph). As Section 4.3.5.3 points out Method 1 at 50.33 mph wind speeds was not calculated because the design charts of the *ASCE 7-02 Standard* do not work for wind speeds below 85 mph. Also, Section 4.3.5.2 points out that to find the wind pressures at 120.34 mph for Load Cases 1 through 4, the wind pressures, torsional component, and overhang pressure need to be multiplied by 5.72. The MWFRS approach envelops the wind

pressures due to the internal pressures applied to the overall wind pressure design (as established in Section 4.3.5). This design load is what the test structure could see with a return period of 50 or 100 years (as established in Section 2.4). The C&C showed a higher wind pressure distribution for the hip roof due to the localized pressures that the test roof may see with a 50-year and 100-year return period (see Figures 4.18 through 4.21 for Method 2 and Figures 4.22 and 4.23 for Method 1). However, the test roof may not see these design wind pressures throughout the whole structure at one particular time or particular duration. The C&C design is very conservative in comparison to the MWFRS design. Tables 6.4 and 6.5 highlight this conservative difference of the MWFRS and C&C design for Method 1 and Method 2 design wind pressures and total loading at the peak Hurricane Katrina wind speed of 50.33 mph and the maximum expected wind speed for Pensacola, Florida, of 120.34 mph, respectively. The pressure distributions applied to the FE model as per the *ASCE 7-02 Standard* are provided in Appendix B. The additional load was taken from the FE model with the *ASCE 7-02 Standard* pressure distributions due to wind loading only.

Table 6.4. Comparison of MWFRS and C&C design wind pressure distributions for 50.33 mph wind speed on the hip roof using Method 1 and 2 of the *ASCE 7-02 Standard* without gravity loading

	MWFRS					C&C	
Applied	**Method 1**	**Method 2**				**Method 1**	**Method 2**
Pressure (psf)	**Case 1**	**Case 1**	**Case 2**	**Case 3**	**Case 4**		
Minimum	N/A	-3.41	-2.68	-1.80	-2.23	N/A	-7.94
Maximum	N/A	-0.27	-0.32	-0.39	-0.29	N/A	1.73
Added Weight* (lbs)							
Minimum		-3226	-2576	-2426	-2270		
Maximum		-1231	-1080	-927	-1147		

* Indicates the gain or reduction in equivalent weight of the roof due to wind effect

Table 6.5. Comparison of MWFRS and C&C design wind pressure distributions for 120.34 mph wind speed on the hip roof using Method 1 and 2 of the *ASCE 7-02 Standard* without gravity loading

	MWFRS					C&C	
Applied	Method 1	Method 2				Method 1	Method 2
Pressure (psf)	Case 1	Case 1	Case 2	Case 3	Case 4		
Minimum	-63.70	-19.49	-15.30	-10.28	-12.75	-30.30	-45.38
Maximum	-16.32	-1.55	-1.16	-2.21	-1.66	10.50	9.90
Added Weight* (lbs)							
Minimum	-37309	-18604	-14454	-14476	-12975		
Maximum		-6851	-5900	-5922	-6554		

* Indicates the gain or reduction in equivalent weight of the roof due to wind effect

As expected, Table 6.4 indicates that C&C design wind pressures are considerably higher than the MWFRS design wind pressures. The average of the minimum pressures for Method 2 MWFRS Load Cases was –2.53 psf, which was 3.14 times lower than the minimum Method 2 C&C design pressures. The average of the maximum pressures for Method 2 MWFRS Load Cases was –0.32 psf, which was 6.46 times lower than the maximum C&C design pressures. The average of the minimum added weight of the four Load Cases for Method 2 MWFRS was –2,624 lbs. The average of the maximum added weight of the four Load Cases for Method 2 was –1,096 lbs.

Similarly, Table 6.5 shows that C&C design wind pressures are considerably higher than the MWFRS design wind pressures. The average of the minimum pressures for Method 2 MWFRS Load Cases was –14.45 psf, which was 4.41 times lower than the minimum pressures of Method 1 MWFRS, 2.10 times lower than Method 1 of the minimum C&C design pressures, and 3.14 times lower than Method 2 of the minimum C&C design pressures. The average of the maximum pressures for Method 2 MWFRS Load Cases was –

1.65 psf, which was 10 times lower than the maximum pressures of Method 1 MWFRS, 7.38 times lower than maximum C&C design pressures, and 7.02 times lower than Method 2 of the maximum C&C design pressures. The average of the minimum added weight of the four Load Cases for Method 2 MWFRS was –15,127 lbs, which was 2.47 times lower than Method 1 MWFRS minimum added weight. The average of the maximum added weight of the four Load Cases for Method 2 was –6,307 lbs.

The wind pressure distributions applied to the FE model are provided in Appendix B. All the wind pressures were applied to the FE model in the direction normal to the surface of the sheathing elements. The torsional component, which is found from the forces calculated on the sheathing element, included in Load Cases 2 and 4 was also transferred to equivalent pressures normal to the sheathing elements of the hip roof in the following way:

- First, the torsional component was multiplied by the mean roof height of the test structure.
- Second, the overall torsion is dispersed to forces at the walls with eccentricity that is shown in Figure 6.48.

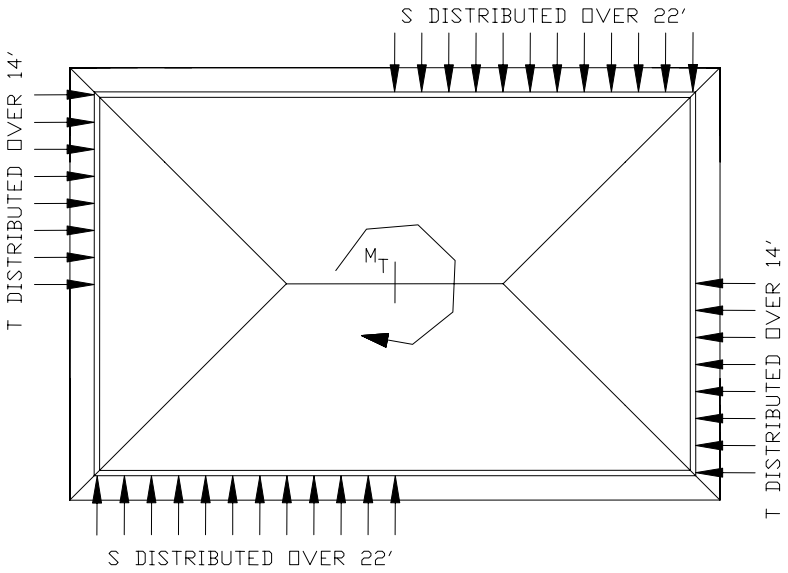

Figure 6.48. Equivalent forces to simulate the effects of torsion on the FE model

- Thirdly, the force components are found such that the force times the eccentricity about the center of the test structure is equal. Hence, the force components were found by Eq. 6.2 below:

$$M_T = 22xS + 14xT \tag{6.2}$$

$$S = \frac{14}{22}xT \tag{6.3}$$

- Lastly, the T and S forces were distributed along half the length of the wall. Figure 6.48 shows the hip roof surface that each distributed force will act was half of each hip roof surface to provide torsion on the test structure.

The strategy described above for applying the torsion to the finite element model of the roof was to avoid applying a concentrated moment as it can cause large localized deformations in the test structure. Refer to Appendix B for all the pressure distributions as applied in the FE model.

6.3.2 Comparison of Method 2 MWFRS Design Pressures against Field Data

The Method 2 MWFRS design pressures are directly compared to the field data from Hurricane Katrina in this section. Using the peak wind speed of 50.33 mph (as established in Section 4.3.1) established for Hurricane Katrina in the field for both cases, it is of interest to compare the code based values with the field data. Theoretically these loads should be close to one another if the field conditions match with those assumed in the *Standard*. Since the MWFRS is an average envelope of the design pressures, the field data must be averaged as well. Therefore, time intervals of 10 minutes and 2 hours were used to average the field data. The gravity load was eliminated from the FE analysis by simply turning off the gravity effect. The gravity load of the field data was subtracted out using Case I from Section 6.2.2. Case I in Table 6.3, which used Load Case 3, was used for the gravity load to subtract. Figures 6.49 through 6.52 compare the field data of the load cells for the four walls with the FE results obtained using the *ASCE 7-02 Standard* Method 2 MWFRS design wind pressures at 50.33 mph wind speeds.

In all cases, negative reactions indicate a loss of weight of the test roof due mostly to suctions induced by the wind. Conversely, positive reactions indicate a gain in weight due to pressure attacking the test roof. Also included in the figures are the minimum and maximum reactions taken from the FE model, which were established by finding all the reactions at the

load cells for each load case pressure distribution as per the *ASCE 7-02 Standard*. The average reactions were similarly determined. Since all four load cases used by Method 2 MWFRS design wind pressures had two FE plots (see Appendix B) for each load case due to the internal pressure enveloping the wind pressures, it was seen that a better comparison to the field data would be to look at each individual load cell for the wind effect, instead of each load case individually.

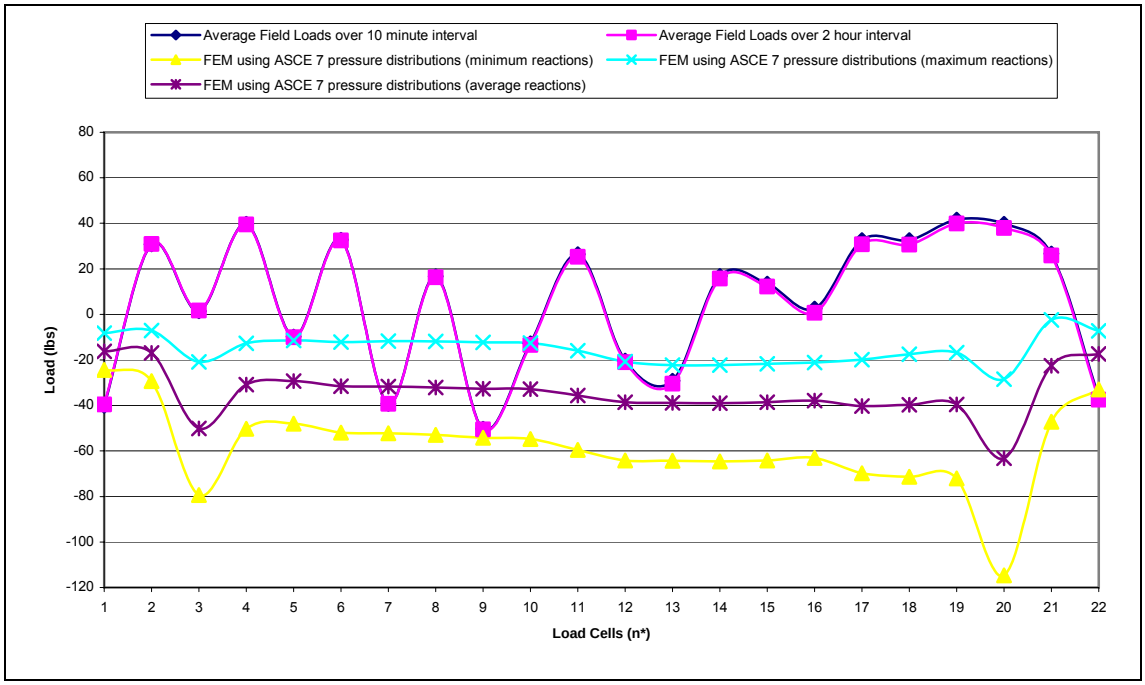

Figure 6.49. Load cell reactions from the north wall obtained for wind loads using peak wind speed of 50.33 mph during Hurricane Katrina and comparison with FE analysis results obtained using the *ASCE 7-02 Standard* MWFRS pressure distributions for Method 2

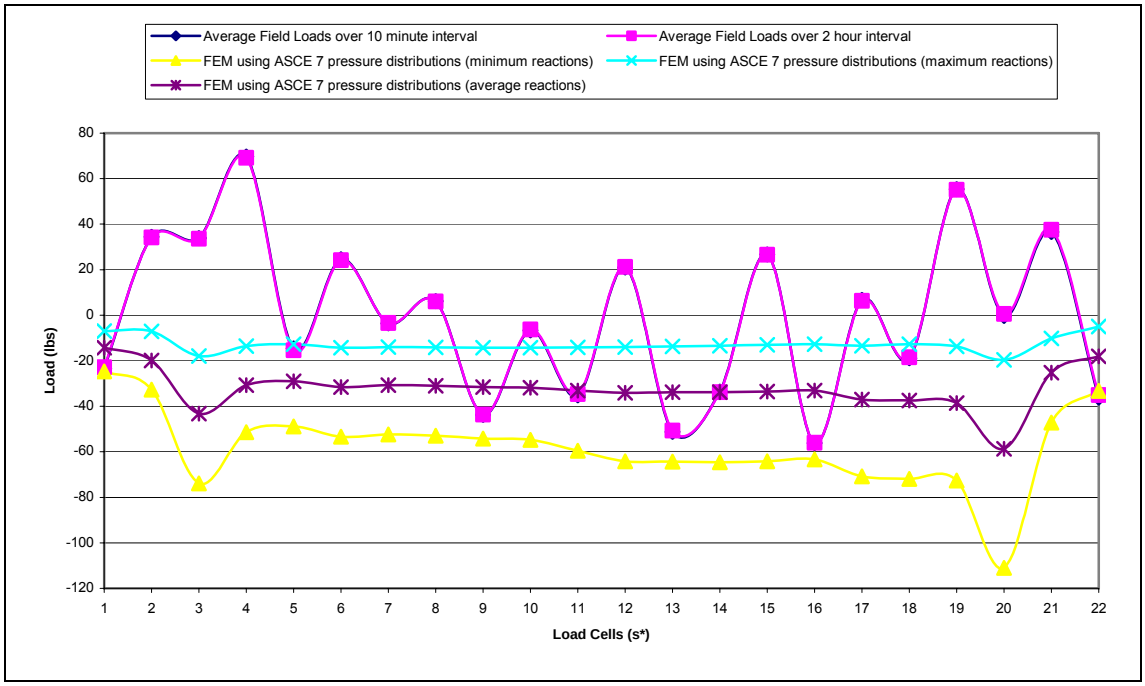

Figure 6.50. Load cell reactions from the south wall obtained for wind loads using peak wind speed of 50.33 mph during Hurricane Katrina and comparison with FE analysis results obtained using the *ASCE 7-02 Standard* MWFRS pressure distributions for Method 2

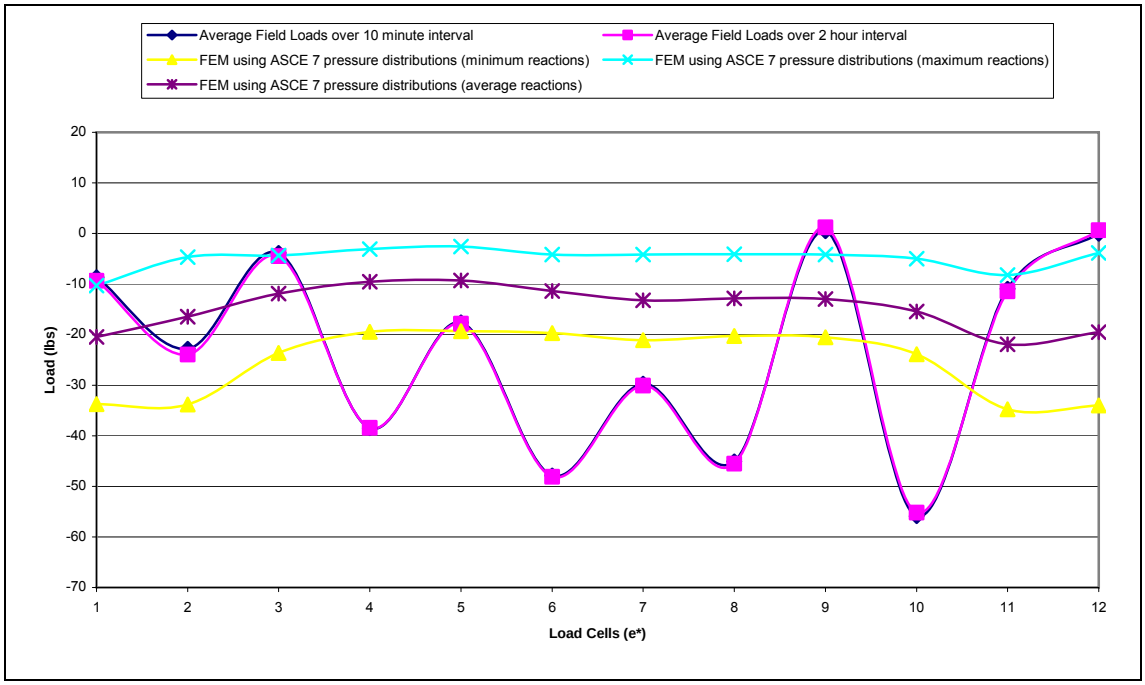

Figure 6.51. Load cell reactions from the east wall obtained for wind loads using peak wind speed of 50.33 mph during Hurricane Katrina and comparison with FE analysis results obtained using the *ASCE 7-02 Standard* MWFRS pressure distributions for Method 2

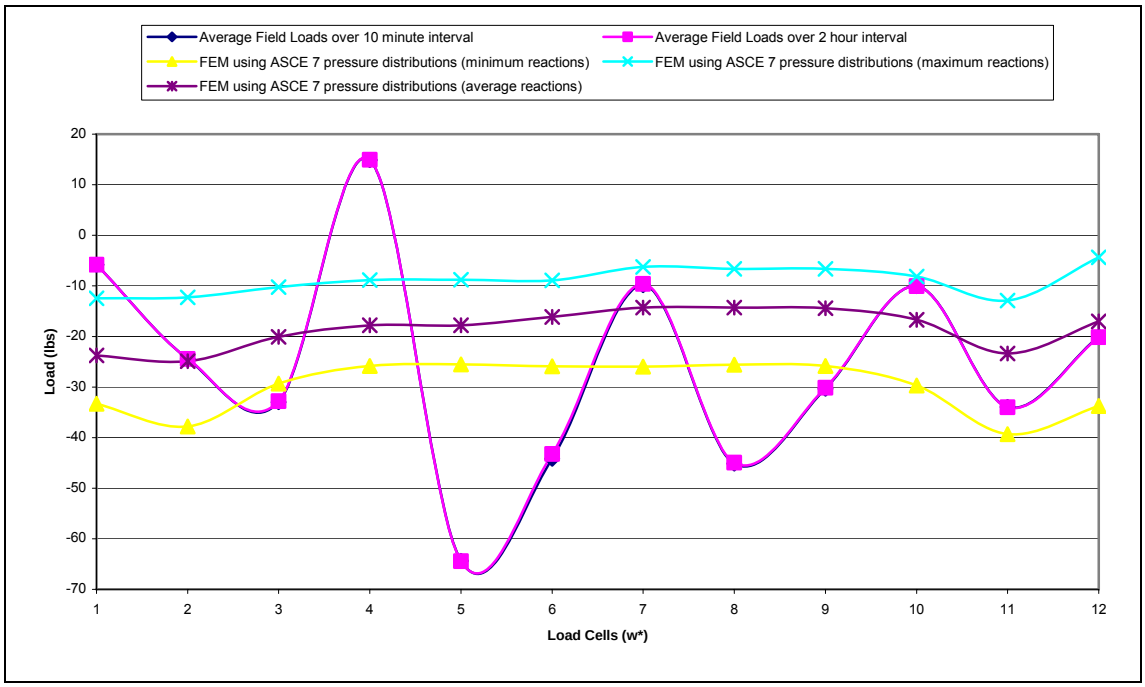

Figure 6.52. Load cell reactions from the west wall obtained for wind loads using peak wind speed of 50.33 mph during Hurricane Katrina and comparison with FE analysis results obtained using the *ASCE 7-02 Standard* MWFRS pressure distributions for Method 2

Figures 6.49 to 6.52 indicate that at the peak wind speed of 50.33 mph the averaged field data for both time intervals was nearly identical. This averaging of the field data was also looked at for 3 minutes, 5 minutes, 30 minutes, and 1 hour. This analysis showed little difference and was not included in the discussion. The reason why there was little difference in the averaged field data was that the average wind speeds were nearly identical to 25.9 mph because of the fluctuation that happened during each time interval. Obtaining the reactions for the FE model's applied pressure distributions from the *ASCE 7-02 Standard* Method 2 MWFRS design wind pressures yielded a good spread of reactions for the minimum, maximum, and average reactions for all four walls.

Figures 6.49 to 6.52 also showed that the averaged field data for all the walls fluctuated greatly between adjacent load cells. The reason for the fluctuating load cell reactions may have been the assumed gravity loading subtracted out of the field data and the reasons concluded in the gravity analysis (see Section 6.1). There can be no comment on the conservative nature of the *ASCE 7-02 Standard* to the field data because the results do not show a satisfactory comparison to analyze. Had the field data lie between the bounds of the *ASCE 7-02 Standard* pressure distributions utilized for Method 2 MWFRS design wind pressure or made a more linear variation between the field data load cells, this conservative or nonconservative nature could have been addressed.

6.3.3 MWFRS Design Pressures as per Method 2

The comparison of Method 2 MWFRS design pressures at 50.33 mph (as established in Section 4.3.1) are compared to Method 2 MWFRS design pressures at 120.34 mph (as established in Section 4.3.1) in this section to show the expected change in loads at the

highest possible wind speed. Theoretically the loads caused by the higher wind speeds should cause higher reactions at the loads cells because the pressure is increased on the test roof at a higher wind speed. Since the MWFRS is an average envelope of the design pressures, the load cells (support reactions) in the FE model were analyzed on an individual basis, instead of each load case. The gravity load was taken out of the FE analysis by simply turning off the acceleration of gravity. Figures 6.53 through 6.56 show all four walls of the load cells used for comparison of the *ASCE 7-02 Standard* Method 2 MWFRS design wind pressures at 50.33 mph and 120.34 mph wind speeds. Refer to Appendix B to see the FE model's applied wind pressure, as per the *ASCE 7-02 Standard*.

Negative reactions indicated a loss of weight on the test structure due mostly to suctions on the test roof. Positive reactions indicated a gain in weight on the test structure due to pressure attacking the test roof. The minimum and maximum reactions taken from the FE model were found by finding all the reactions at the load cells for each Load Case pressure distribution as per the *ASCE 7-02 Standard* and then the minimum and maximum reactions at each individual load cell were compared. The average reactions were similarly determined. Since all four load cases used by Method 2 MWFRS design wind pressures had two FE plots (see Appendix B) for each load case due to the internal pressure enveloping the wind pressures, it was seen that a better comparison to the field data would be to look at each individual load cell for the wind effect, instead of each load case individually.

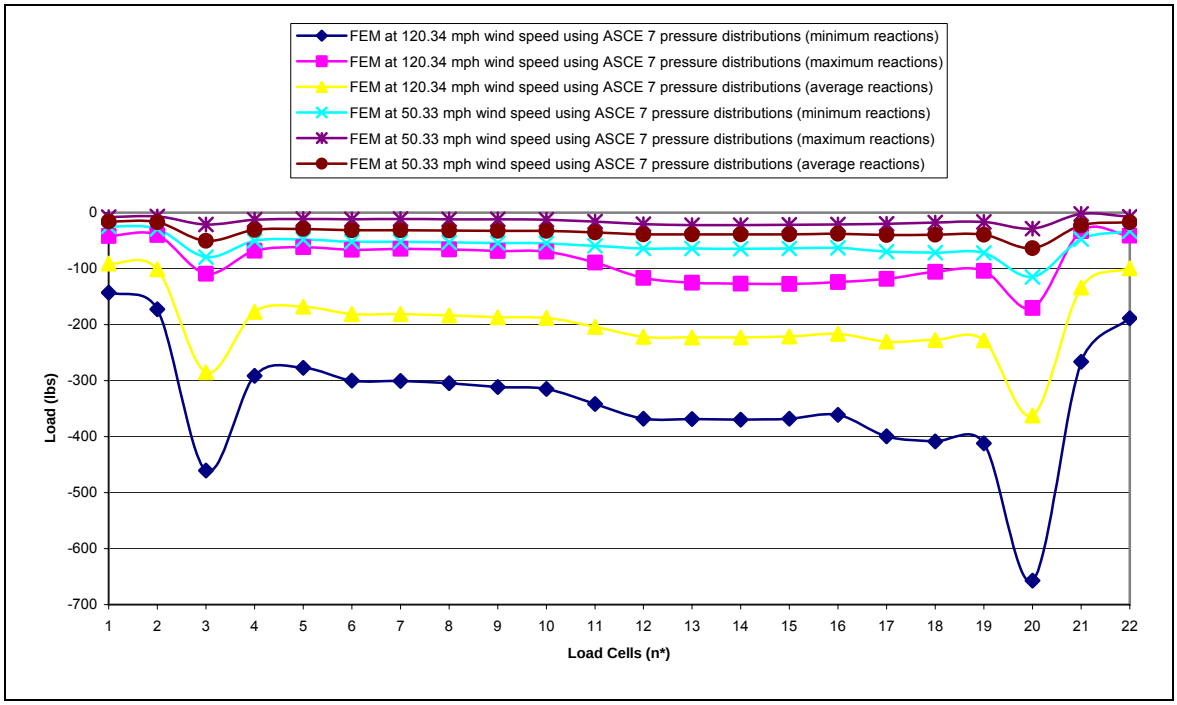

Figure 6.53. FE analysis results obtained from north wall load cell reactions obtained for wind loads using *ASCE 7-02 Standard* MWFRS Method 2 pressure distributions at both 50.33 mph and 120.34 mph wind speeds

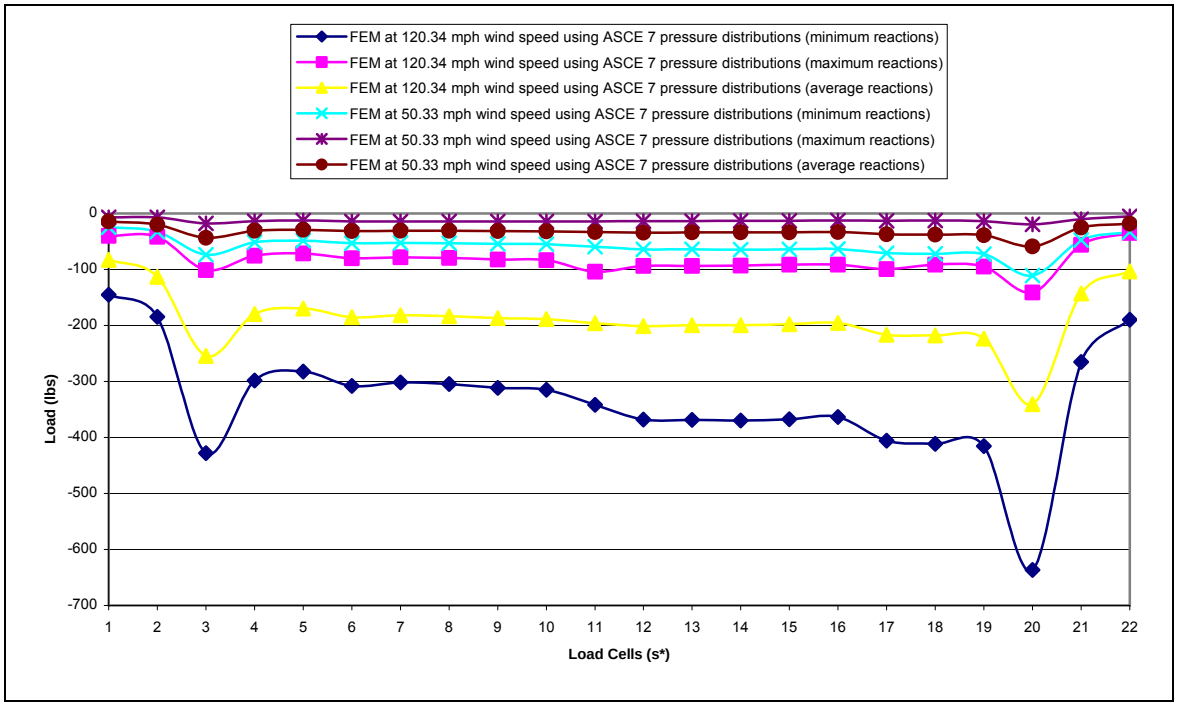

Figure 6.54. FE analysis results obtained from south wall load cell reactions obtained for wind loads using *ASCE 7-02 Standard* MWFRS Method 2 pressure distributions at both 50.33 mph and 120.34 mph wind speeds

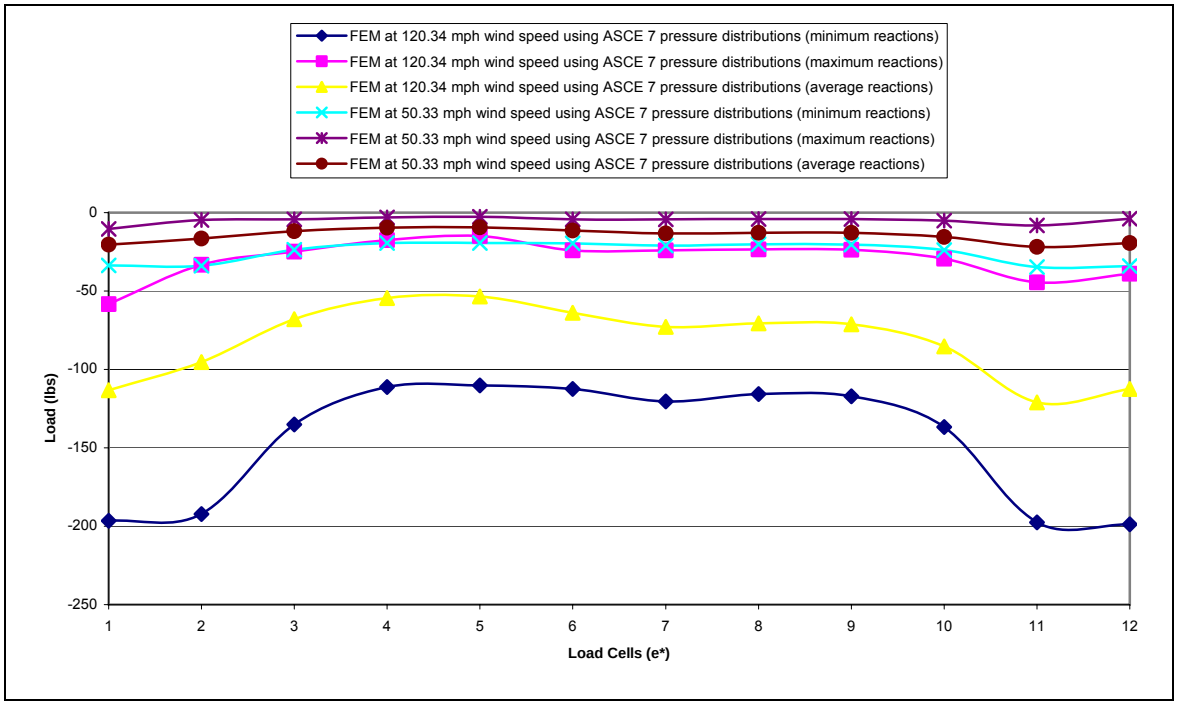

Figure 6.55. FE analysis results obtained from east wall load cell reactions obtained for wind loads using *ASCE 7-02 Standard* MWFRS Method 2 pressure distributions at both 50.33 mph and 120.34 mph wind speeds

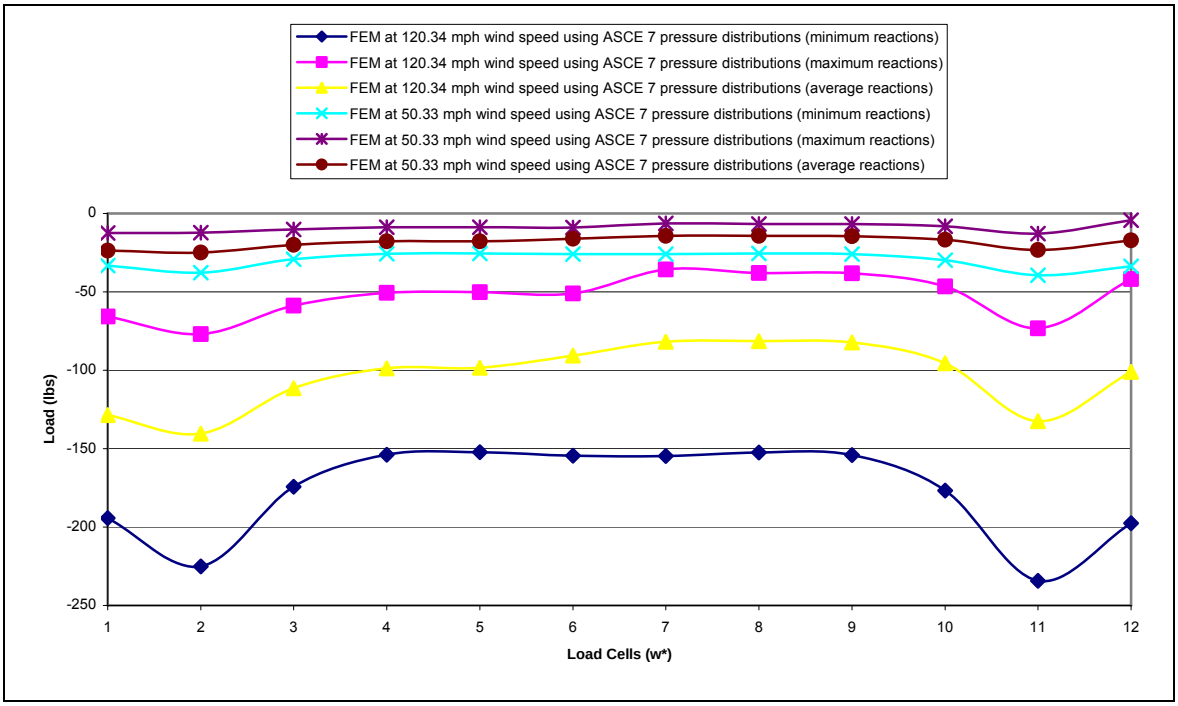

Figure 6.56. FE analysis results obtained from west wall load cell reactions obtained for wind loads using *ASCE 7-02 Standard* MWFRS Method 2 pressure distributions at both 50.33 mph and 120.34 mph wind speeds

Figures 6.53 to 6.56 show that the minimum reactions found at 50.33 mph wind speeds are generally close to the maximum reactions at 120.34 mph. Also, the spread in distribution of the reactions along each wall is almost uniform and symmetric about the structure. The minimum reactions at 50.33 mph wind speeds are roughly 5.78 times lower than the minimum reactions at 120.34 mph wind speeds and roughly 1.45 times lower than the maximum reactions found at 120.34 mph wind speeds. The maximum reactions at 50.33 mph wind speeds are roughly 6.16 times lower than the maximum reactions at 120.34 mph wind speeds. The average reactions at 50.33 mph wind speeds are roughly 5.74 times lower from the average reactions at 120.34 mph wind speeds. Obtaining the reactions for the FE model's applied pressure distributions from the *ASCE 7-02 Standard* Method 2 MWFRS design wind pressures yielded a good spread of reactions for the minimum, maximum, and average reactions for all four walls. It is noted that the test roof indicated the potential to uplift when the pressure distributions from the *ASCE 7-02 Standard* Method 2 MWFRS design wind pressures under the minimum reactions at 120.34 mph.

6.3.4 Comparison of C&C Wind Pressures to Field Data

Lastly, a comparison of the design wind pressures of the C&C design is compared to the pressure cell data obtained from the field for Hurricane Katrina. Table 6.6 shows the field data obtained from Hurricane Katrina at all hours to find the minimum pressure, maximum pressure, and where each minimum and maximum pressure occurred. In this table, a negative pressure indicates a suction and a positive pressure indicates a pressure into the test structure.

Table 6.6. Hurricane Katrina pressures from field data in units of psf

		Hurricane Katrina Field Data			
Time	Date	Min. (psf)	Min. pressure locations	Max. (psf)	Max. pressure location
4:00 - 5:00 PM	August 28, 2005	-5	n03p, n15p	0	n01p, n06p, n08p, n10p, n14p, s01p, s07p, s23p, w10p, e02p, e03p, e04p, e06p, e07p, e08p, e09p, e11p
5:00 - 6:00 PM	August 28, 2005	-5	n03p, n15p	1	e02p, e06p
6:00 - 7:00 PM	August 28, 2005	-5	n03p, n15p	1	e02p
7:00 - 8:00 PM	August 28, 2005	-5	n03p, n15p	1	e02p, e06p
8:00 - 9:00 PM	August 28, 2005	-6	n15p, n20p	1	e02p, e03p, e06p
9:00 - 10:00 PM	August 28, 2005	-6	n15p	1	e02p, e03p, e06p
10:00 - 11:00 PM	August 28, 2005	-7	n15p	2	e02p
11:00 PM - 12:00 AM	August 28, 2005	-6	n15p	2	e02p
12:00 - 1:00 AM	August 29, 2005	-6	n15p	2	e02p
1:00 - 2:00 AM	August 29, 2005	-9	e14p	3	e04p, e09p
2:00 - 3:00 AM	August 29, 2005	-8	n15p	2	e06p
3:00 - 4:00 AM	August 29, 2005	-7	n15p	2	e02p
4:00 - 5:00 AM	August 29, 2005	-7	n15p	2	e02p
5:00 - 6:00 AM	August 29, 2005	-6	n03p, n15p	2	s04p, e02p
6:00 - 7:00 AM	August 29, 2005	-8	s15p	2	e06p, e09p, e12p
7:00 - 8:00 AM	August 29, 2005	-8	s09p	2	e02p, e03p, e06p, e08p, e09p, e11p, e12p
8:00 - 9:00 AM	August 29, 2005	-10	s09p	3	e09p
9:00 - 10:00 AM	August 29, 2005	-10	s09p, s15p	3	s04p, e03p, e06p, e08p
10:00 - 11:00 AM	August 29, 2005	-12	s09p	3	e06p
11:00 AM - 12:00 PM	August 29, 2005	-11	s09p, s15p	3	e02p, e09p, e12p
12:00 - 1:00 PM	August 29, 2005	-13	s09p, s15p	4	e06p
1:00 - 2:00 PM	August 29, 2005	-19	s15p	3	s04p, s23p, e06p, e09p, e13p
2:00 - 3:00 PM	August 29, 2005	-16	s09p	4	s05p, s09p, s11p, s17p, s18p, s20p, s23p
3:00 - 4:00 PM	August 29, 2005	-14	n20p, w11p	5	s18p, s23p

Table 6.6 suggests that the minimum pressure was a suction of –19 psf while a maximum pressure of up to 5 psf was developed on the test roof. Also, the pressure data summarized in this table indicate that Hurricane Katrina produced the maximum wind effects toward the end of the data collection period by recording the highest and lowest pressures. It should be noted that the reason the instrumentation was stopped after 4:00 PM on August 29, 2005 was due to loss of power (FPL, 2006). Therefore, the remaining discussion will focus on the period within which the data was collected.

As previously mentioned in Section 3.5, the peak wind speed was from the east-southeastern direction. Theoretically the east and southeast corners of the test structure should see the most wind pressures into the test structure and suctions at the leeward or far northwest corner of the structure. Table 6.6 shows that the maximum pressure into the test structure occurred mostly along the east wall and the minimum pressure was along the north wall. This is in good agreement with the predominant direction identified for wind attack in that large pressures experienced on the windward walls and large suctions experienced on the leeward walls. However, this was not in good agreement with the *ASCE 7-02 Standard* because most of the wind pressure distributions showed suctions at the wind speeds analyzed from the east-southeastern direction (see Appendix B). Reasons for this discrepancy could have been due to the change in wind direction when the maximum and minimum pressures occurred on the test roof.

The minimum and maximum pressures were only compared for the C&C design wind pressures and the field data shown in Table 6.6. As Table 6.4 showed, the C&C design maximum pressure was 1.73 psf and the minimum pressure was –7.94 psf. Therefore, since the maximum pressure was 2.89 times higher in the field than the C&C and the minimum

suction was 2.39 times higher in the field, the *ASCE 7-02 Standard's* C&C design wind pressure distribution was not very conservative.

CHAPTER 7. SUMMARY, CONCLUSIONS, AND RECOMMENDATIONS FOR FUTURE RESEARCH

7.1 Conclusions

This chapter summarizes the findings of the study presented in this report and recommend opportunities for future research.

7.1.1 Analysis of the Tested Structure Under Gravity Load

Section 6.1 addressed the gravity analysis of the FE model produced for the test roof. The purpose of this analysis was to examine how well the gravity analysis results obtained from the FE model compared to the comparable field data.

The FE results were first compared with data corresponding to four low wind speeds measured both before and after the peak wind speed during Hurricane Katrina occurred. The load cells were compared using Load Cases 1, 2, 3, and 4 to the FE results as shown in Figures 6.1 – 6.4. The field data showed a close comparison between one another compared to the reactions obtained from the FE results. It should be noted that the load cells located at the identical location did not give an identical reading. This indicated that there were some discrepancies between the load cells measured in the field.

When the load cells from identical locations were averaged using the lowest wind speed of 0.13 mph (Load Case 3) and compared with the FE results, the results were much closer as shown in Figures 6.5 – 6.8. This showed a much closer comparison to the FE results and improved the comparison between the data sets. A few load cells, however,

showed a ±10% error along the north and south walls. These errors may have been attributed to the variations due to the realistic support conditions at these particular locations of discrepancy.

The following conclusions were drawn from this part of the study:

- Since the field data from Hurricane Katrina was not tested under calm wind conditions prior to a hurricane event, it was determined that taking a periodic gravity load measurement during wet and dry seasons would alleviate this problem. Also, the FPL group did find initial load cell reactions when the load cells were first instrumented to the test roof. However, this load of 16,149 lbs was 23.4% larger than the gravity load chosen of 13,087 lbs.
- Since the gravity load analysis was done at low wind speeds, it was assumed that the wind loads were found by subtracting out the gravity load of 13,087 lbs established at a wind speed of 0.13 mph. This consequently indicated when there was a suction or pressure imposed on the test roof. Although the pressure cells on the test roof could verify this, the pressure experienced on a residential roof can be subjected to localized behavior. It is recommended that by instrumenting the test roof more heavily, it may be directly determined if the test roof was experiencing a suction or pressure during a hurricane event.
- Finally, to determine if the FE model was modeled correctly in Chapter 5, a field test could be carried out with static point loads applied. By testing the roof at the specified load cells, the discrepancies seen in Figures 6.5 – 6.8 and the hip rafter (Figure 3.4), the load sharing evaluation and modeling approach in the FE model could be better verified. Also, by recalibrating the load and pressure cells in the test

roof, the reliability of the field data could be verified. This recalibration could be done by carefully removing a particular load cell or pressure cell out of the test roof and recalibrating it before placing it back in the test roof.

7.1.2 Analysis of the Tested Structure Under Wind Loads

Section 6.2 addressed the wind effect for three different static wind speeds. The purpose of this section was to address how well the static normal wind pressures recorded in the field compared to the linearly interpolated field pressures applied to the FE model for calculating the load cell reactions.

Two static times and one time interval were chosen for this wind effect analysis. The loading cases were as follows: 1) wind effect due to the peak wind speed of 56.2 mph (Load Case 5), 2) wind effect due to the highest pressures recorded at 43.87 mph (Load Case 6), and 3) wind effect due to a 2-minute interval around the time that recorded the highest pressures and a wind speed of 43.87 mph (Load Case 9). The three static wind speeds chosen evaluated the design pressures recorded on the test roof at the aforementioned wind speeds and linearly interpolated the recorded pressures at the discrete locations (see Figure 3.8) to apply the appropriate design pressures to the sheathing elements of the FE model. The gravity loading was subtracted from the field data using two different Cases. Case I was for the lowest wind speed (Load Case 3) and Case II was the worst case scenario (Load Case 8 minus Load Case 3). The gravity load effects were also removed from the FE model. Figures 6.32 – 6.35, 6.38 – 6.41, and 6.44 – 6.47 show the resulting reactions measured from the three applied static normal pressures for both Case I and Case II of the field data and the FE model. Table 6.3 shows the overall comparison of the three wind loads applied.

From Table 6.3 and aforementioned figures, the tabulated results generally showed poor correlation between the FE model results and the wind loading effect of the field data. However, the increase of loading due to the wind effect for both the FE model and the field data were evident. Case II showed a much closer prediction to the FE model's reactions measured due to the worst case scenario chosen for the wind load. The total weight on the test roof was not very conservative between the field data obtained for Hurricane Katrina and the FE model. Discrepancies between the data sets could have been attributed to almost every sheathing element of the FE model being loaded normal to its surface, ignoring the influence of precipitation, and modeling of boundary conditions used in the FE model. Also, the possibility exists that the test structure may have undergone settlement at specific locations, due to quick spikes in pressures and suctions during the hurricane event.

The following suggestions were drawn from this part of the study:

- Since the wind applied to the test roof was applied normal to the test roof in psf due to the discrete pressure cell locations, the need exists to determine if there are any other vertical or horizontal wind loads acting on the test structure as well. Analysis of this issue may correct the large discrepancy between the FE model and the field data.
- As was discussed previously in Section 7.1.1, a static loading analysis would be pertinent to see if the load-sharing used in the roof system is not modeled correctly in the FE model.
- More pressure ports in the roof system could be utilized to obtain a better distribution of wind load.

7.1.3 Evaluation of Wind Load as per *ASCE 7-02 Standard*

Section 6.3 addressed the wind effect as per the *ASCE 7-02 Standard* (see Chapter 4) for both the main wind force-resistance system (MWFRS) and the components and cladding (C&C). The purpose of this section was to investigate the conservative nature of the *Standard* when used for wind design in the hurricane prone region of Pensacola, Florida. This section of the report showed how well both the MWFRS and C&C wind design methodologies compared, and examined the field data to the pressure distributions of the MWFRS at the peak wind speed of Hurricane Katrina.

As Section 6.3.1 showed, the design pressures obtained for the MWFRS and the C&C differed significantly. This was anticipated due to the fact that the C&C values represent localized pressure expected at any particular region and time and the MWFRS shows an averaged pressure over the entire structure applied for a given time. Since the pressures specified in the *ASCE 7-02 Standard* for the MWFRS were applied to the FE model, the wind loading effect was quantified in terms of equivalent weight of the roof system could be found for the wind loading effect.

As Section 6.3.2 showed, the design pressures for the MWFRS were compared to the field data for the peak wind speed of 50.33 mph (as established in Section 4.3.1) during Hurricane Katrina. The results indicated that the field data did not vary much over a 10-minute averaging time or a 2-hour averaging time. The field data showed large fluctuations in the reactions recorded between adjacent load cells over the time interval. The reason for the fluctuating load cell reactions may have been the assumed gravity loading subtracted out of the field data and the reasons concluded in the gravity analysis (see Section 6.1). There can be no comment made on the conservative nature of the *ASCE 7-02 Standard* to the field

data because the results did not show a satisfactory comparison to analyze. Had the field data lie between the bounds of the *ASCE 7-02 Standard* pressure distributions utilized for Method 2 MWFRS design wind pressure or made a more linear variation between the field data load cells, this conservative or nonconservative nature could have been addressed.

As Section 6.3.3 showed, the design pressures for the MWFRS at both 50.33 mph and 120.34 mph wind speeds were applied to the FE model for comparison with load cell reactions. Although the trend lines were followed for the general shape of the reactions measured, the window from the minimum reactions measured to the maximum reactions measured increased significantly. This indicated that as the wind speeds increased, the window of reactions measured increased significantly.

As Section 6.3.4 showed, the design pressures for the C&C and the field data were compared. The maximum and minimum values measured in the field showed a much larger values than the C&C pressures established from the *ASCE 7-02 Standard*. This indicated that the C&C approach was not conservative when compared to the field data from Hurricane Katrina.

The following suggestions were drawn from this part of the study:

- The *ASCE 7-02 Standard* showed much variation in design pressures for the MWFRS and C&C approaches. This was due to the localized effect estimated to occur during the C&C approach and the average wind loading estimated to occur during the MWFRS approach.
- The *ASCE 7-02 Standard* could not be addressed for its conservative nature when comparing the MWFRS applied pressures to the FE model to the field data at the

peak wind speed for Hurricane Katrina due to the variations in load cell data obtained from the field.

- As the wind speeds increased and subsequently the pressures imposed on the FE model of the roof increased, the window of the minimum and maximum reactions increased as well.
- Finally, when comparing the C&C approach to the field data, the field data recorded significantly higher reactions than the C&C approach for the peak wind speed of Hurricane Katrina. The C&C estimated in the *ASCE 7-02 Standard* was not conservative when compared to field data for a hurricane event at similar wind speeds. The maximum pressure was 2.89 times higher in the field than the C&C pressures and the minimum suction was 2.39 times higher in the field than the C&C pressures.

7.2 Future Research

The purpose of this section is to address the possible areas of future research that may be utilized in this subject matter at a later time. Various areas of future research will be addressed in subsequent order of the chapters in this report. For a more detailed discussion of this section the reader is referred to the appropriate chapters as will be mentioned below.

7.2.1 Chapter 2: Literature Review

A FE approach to modeling the entire light frame building (LFB) was provided in this chapter. Modeling the entire structure was important because much of the response and performance of a light-frame building (LFB) is dictated by the structure's diaphragms and

intercomponent connections (Collins et al. 2005). Therefore, the connections utilized in the construction of the LFB must be well defined in a finite element model. Also, proper estimates of the material properties used in the LFB to ensure a more accurate FE model of the test roof. Kasal et al. (1994) analyzed the most detailed FE model for a LFB, which was tested by Phillips (1990).

Another area of interest when modeling a roof system is to incorporate some of the finite element modeling assumptions that were used by Zhong et al. (1998) such as joint eccentricities and partial composite action. If the test structure was tested in the field under static point loads, the results could be obtained for more accurate representation of the load-sharing effects and more accurately model the connections used in construction of the rafters and trusses. Also, with the field test the researchers could utilize the data to incorporate spring elements at the connections of the rafters and trusses.

7.2.2 Chapter 3: Details of the Test Structure and Instrumentation Scheme

A full 24-hour duration of Hurricane Katrina field data was provided by the FPL group. This data could be further evaluated to find several different comparisons for statistical purposes of correlations between other Hurricanes in the area including, historical wind speeds for the area, dynamic analysis evaluation given the wind speeds direction and magnitude from Hurricane Katrina, and load cell and pressure cell data found from other Hurricanes collected on the test structure. These are only a few of the possible areas of future research for the instrumentation of the test structure and statistical analysis.

7.2.3 Chapter 4: Distribution of Wind Pressure on the Roof in Accordance with the *ASCE 7-02 Standard*

This chapter provided the minimum design wind loads for the whole structure as well as the components and cladding, which analyzed the studs in the walls and the rafters and trusses in the hip roof, using the *ASCE 7-02 Standard*. Since the peak wind speeds of Hurricane Katrina were from the east-southeastern direction, the analysis of the results dealt with winds from the east and southeast. Given that the test structure was located in Pensacola, Florida, for a basic wind speed of 120.34 mph (as established in Section 4.3.1), the test structure could be analyzed from winds from all eight quadrants. Also, a site visit could analyze the site conditions around the structure, which could have influenced the topography used in the *ASCE 7-02 Standard*. A load test on the structure could investigate the assumption that this was mostly a rigid structure. Although this is a low-rise structure with symmetry about the ridge, a wind tunnel test could be used for comparing the results to the Method 1 and 2 wind design of the *Standard*.

APPENDIX A. WOOD RAFTERS AND TRUSSES USED IN CONSTRUCTION OF THE TEST STRUCTURE

A1

TOP CHORD 2x4 SP #2
BOT CHORD 2x4 SP #2
WEBS 2x4 SP #3: W1, W11 2x6 SP #2

110 MPH WIND, 15.00 FT MEAN HGT, SBC, ENCLOSED BLDG, LOCATED ANYWHERE IN ROOF,
WIND TC DL = 5.0 PSF, WIND BC DL = 5.0 PSF.
DEFLECTION MEETS L/240.00 LIVE AND L/180.00 TOTAL LOAD.

NAILING SCHEDULE: (12d_box_nails)
TOP CHORD: 1 ROW @ 12" o.c.
BOT CHORD: 1 ROW @ 12" o.c.
WEBS : 1 ROW @ 4" o.c.
USE EQUAL SPACING BETWEEN ROWS AND STAGGER NAILS
IN EACH ROW TO AVOID SPLITTING.

#1 HIP SUPPORTS 7-0-0 JACKS TO BC.

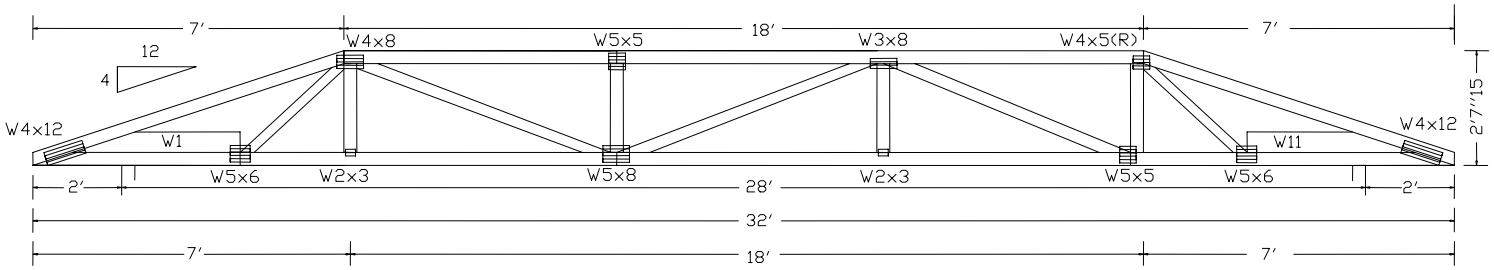

QTY = 2 PLIES = 2 TOTAL = 4

TC LL	30.0 PSF
TC DL	7.0 PSF
BC DL	10.0 PSF
BC LL	0.0 PSF
TOT.LD.	47.0 PSF
DUR.FAC.	1.33

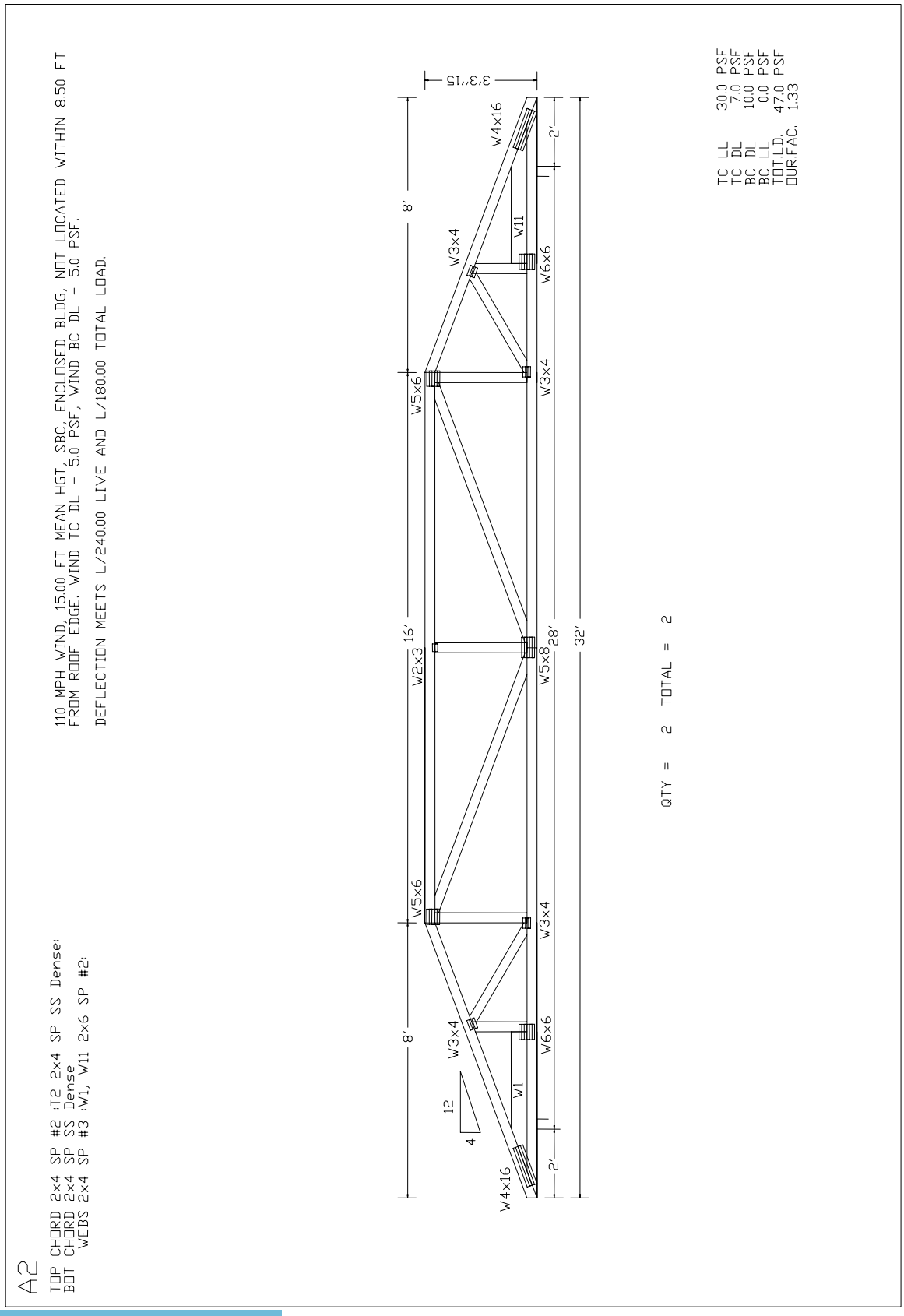

A3

TOP CHORD 2x4 SP #2
BOT CHORD 2x4 SP 2700f-2.2E
WEBS 2x4 SP #3 :W1, W11 2x6 SP #2:

110 MPH WIND, 15.00 FT MEAN HGT, SBC, ENCLOSED BLDG, NOT LOCATED WITHIN 8.50 FT FROM ROOF EDGE. WIND TC DL - 5.0 PSF, WIND BC DL - 5.0 PSF.

DEFLECTION MEETS L/240.00 LIVE AND L/180.00 TOTAL LOAD.

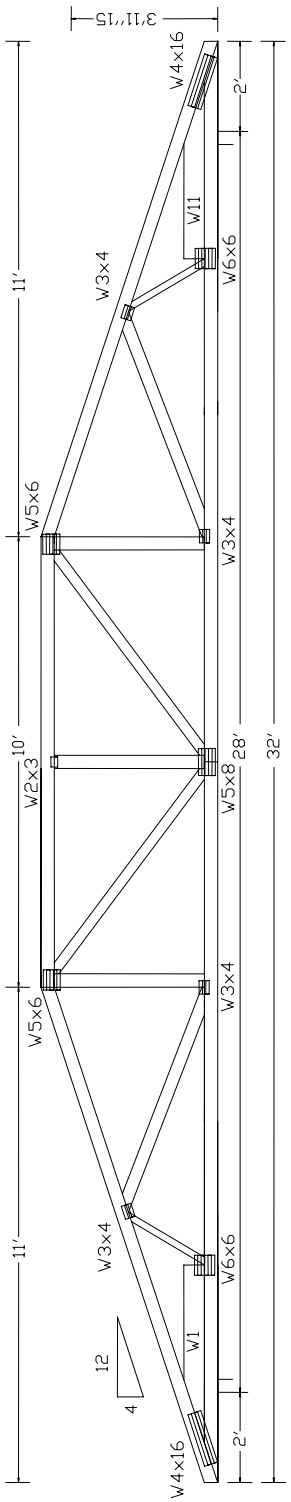

QTY = 2 TOTAL = 2

TC LL	30.0 PSF
TC DL	7.0 PSF
BC DL	10.0 PSF
BC LL	0.0 PSF
TOT.L.D.	47.0 PSF
DUR.FAC.	1.33

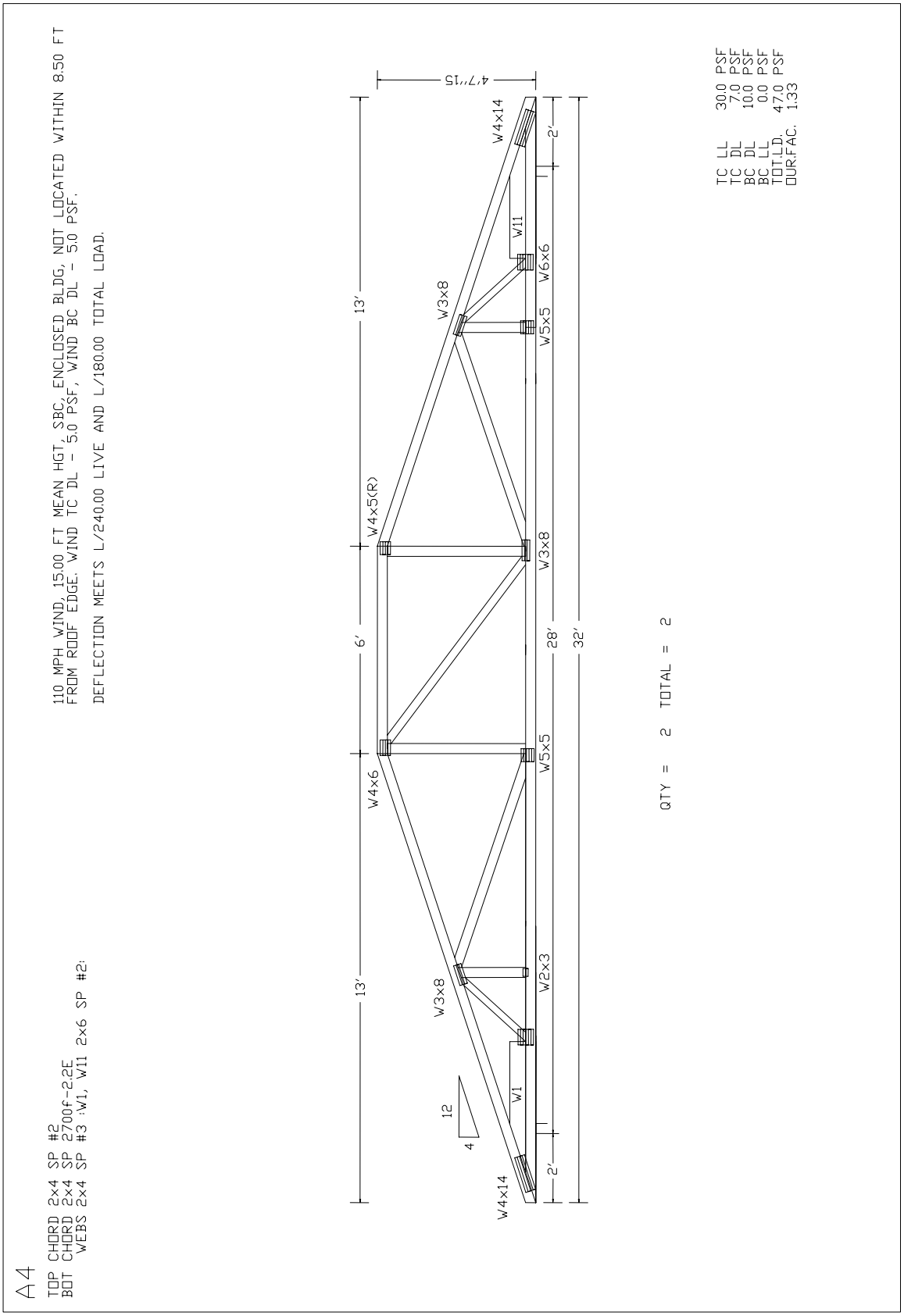

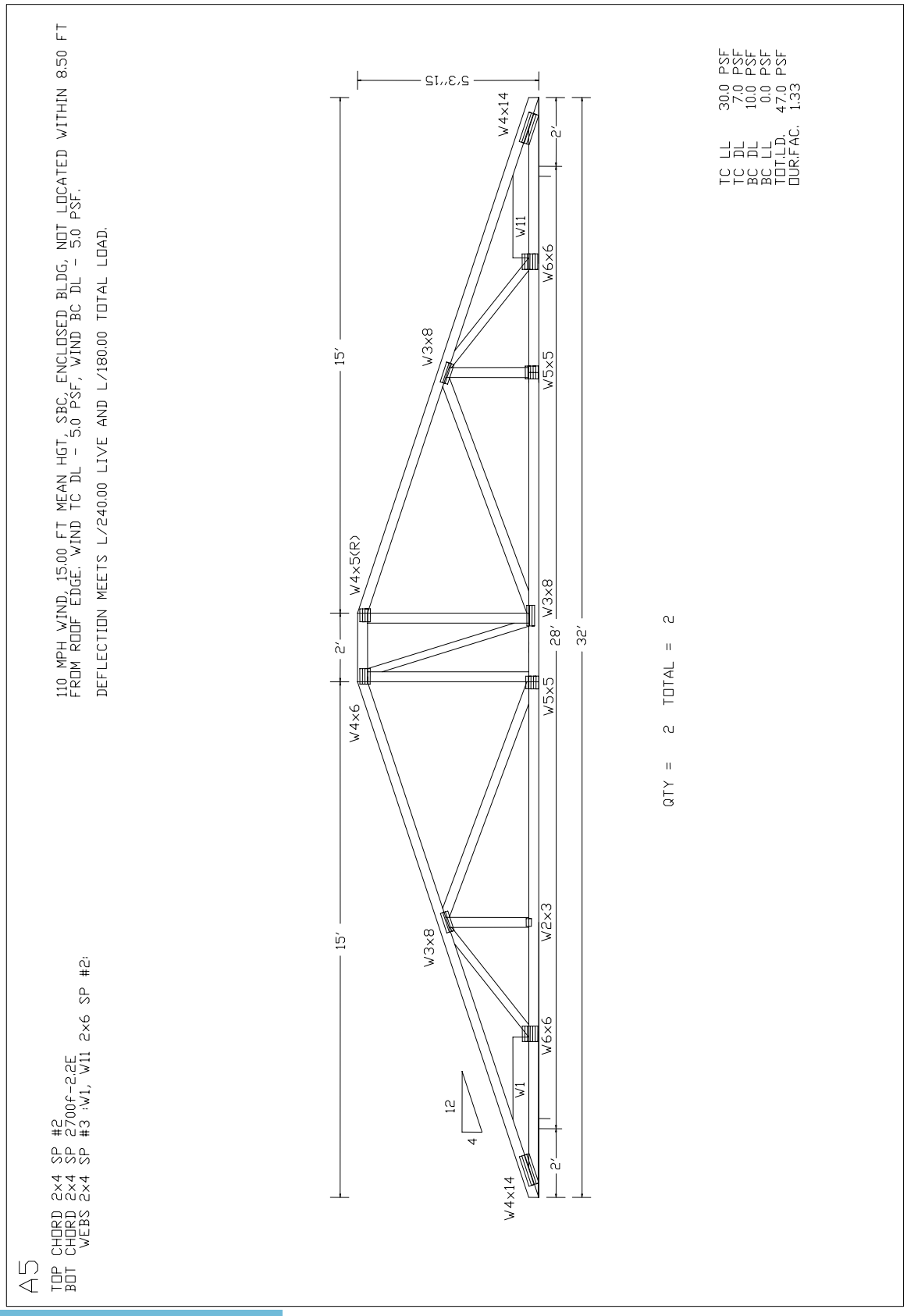

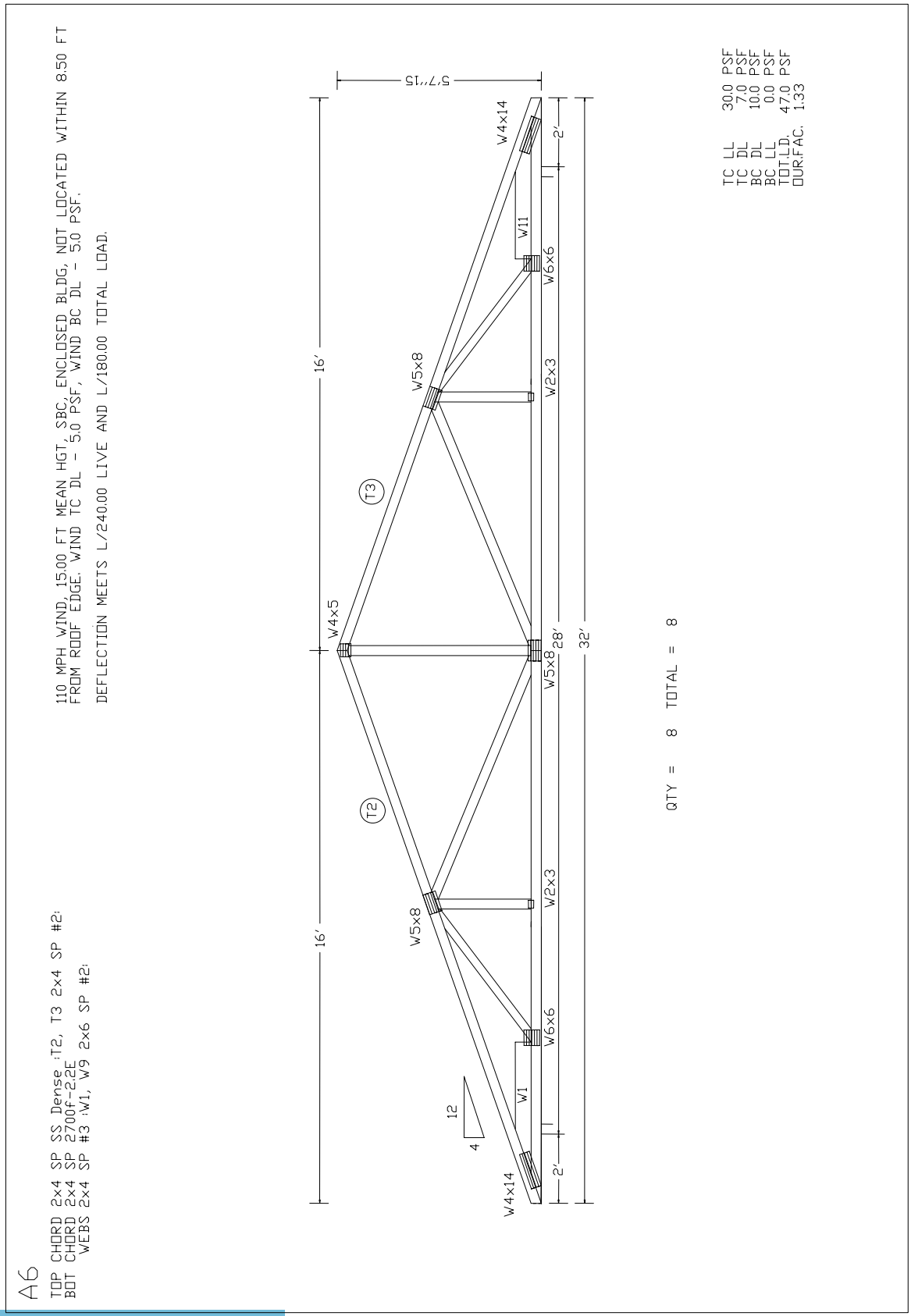

HJ10

TOP CHORD 2x4 SP #2
BOT CHORD 2x4 SP #2
WEBS 2x6 SP #2 :W2 2x4 SP #3:

110 MPH WIND, 15.00 FT MEAN HGT, SBC, ENCLOSED BLDG, NOT LOCATED WITHIN 4.50 FT FROM ROOF EDGE. WIND TC DL = 5.0 PSF, WIND BC DL = 5.0 PSF.

DEFLECTION MEETS L/240.00 LIVE AND L/180.00 TOTAL LOAD.

TC LL	30.0 PSF
TC DL	7.0 PSF
BC DL	10.0 PSF
BC LL	0.0 PSF
TOT.LD.	47.0 PSF
DUR.FAC.	1.33

QTY = 4 TOTAL = 4

CJ5

TOP CHORD 2x4 SP #2
BOT CHORD 2x4 SP #2
WEBS 2x6 SP #2

110 MPH WIND, 15.00 FT MEAN HGT, SBC, ENCLOSED BLDG, NOT LOCATED WITHIN 4.50 FT FROM ROOF EDGE. WIND TC DL = 5.0 PSF, WIND BC DL = 5.0 PSF.

IN LIEU OF STRUCTURAL PANELS OR RIGID CEILING USE PURLINS TO BRACE TC @ 24.00" OC, BC @ 120.00" OC.

DEFLECTION MEETS L/240.00 LIVE AND L/180.00 TOTAL LOAD.

QTY = 8 TOTAL = 8

TC LL	30.0 PSF
TC DL	7.0 PSF
BC DL	10.0 PSF
BC LL	0.0 PSF
TOT.LD.	47.0 PSF
DUR.FAC.	1.33

CJ3

TOP CHORD 2x4 SP #2
BOT CHORD 2x4 SP #2
WEBS 2x6 SP #2

110 MPH WIND, 15.00 FT MEAN HGT, SBC, ENCLOSED BLDG, LOCATED ANYWHERE IN ROOF, WIND TC DL = 5.0 PSF, WIND BC DL = 5.0 PSF.

IN LIEU OF STRUCTURAL PANELS OR RIGID CEILING USE PURLINS TO BRACE TC @ 24.00'' OC, BC @ 120.00'' OC.

DEFLECTION MEETS L/240.00 LIVE AND L/180.00 TOTAL LOAD.

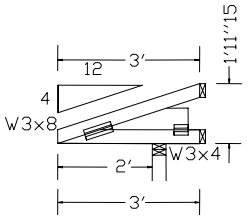

QTY = 8 TOTAL = 8

TC LL	30.0 PSF
TC DL	7.0 PSF
BC DL	10.0 PSF
BC LL	0.0 PSF
TOT.LD.	47.0 PSF
OUR.FAC.	1.33

EJ7

TOP CHORD 2x4 SP #2
BOT CHORD 2x4 SP #2
WEBS 2x6 SP #2

110 MPH WIND, 15.00 FT MEAN HGT, SBC, ENCLOSED BLDG, LOCATED ANYWHERE IN ROOF,
WIND TC DL = 5.0 PSF, WIND BC DL = 5.0 PSF.

DEFLECTION MEETS L/240.00 LIVE AND L/180.00 TOTAL LOAD.

QTY = 20 TOTAL = 20

TC LL	30.0 PSF
TC DL	7.0 PSF
BC DL	10.0 PSF
BC LL	0.0 PSF
TOT.LD.	47.0 PSF
DUR.FAC.	1.33

APPENDIX B. FE MODEL PLOTS OF *ASCE 7-02 STANDARD* PRESSURE DISTRIBUTIONS

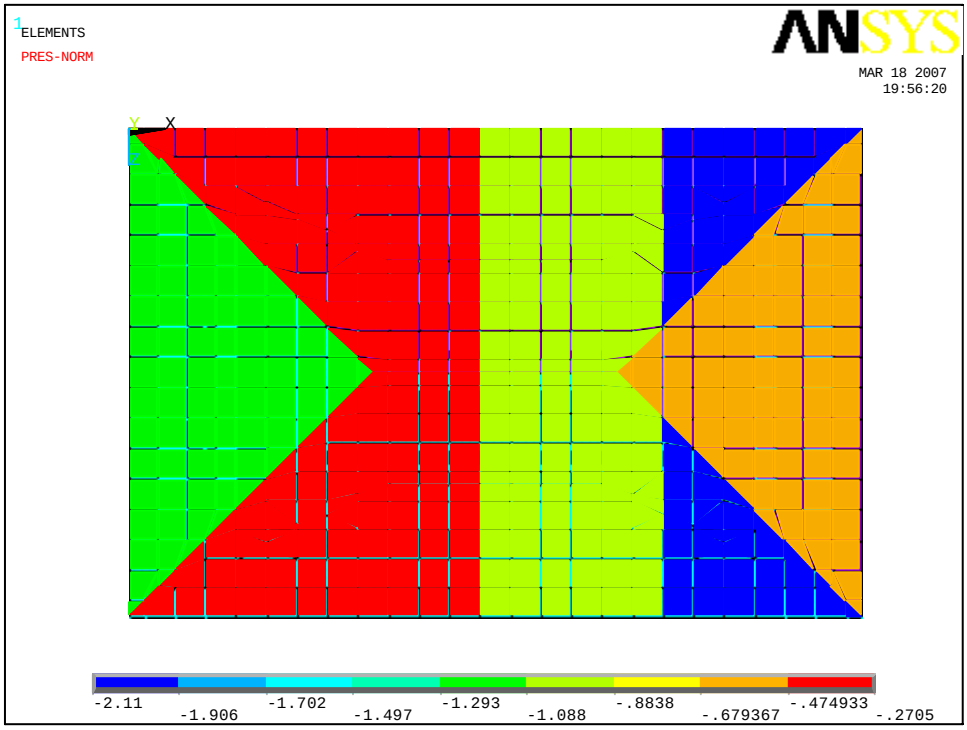

Figure B.1. Method 2: MWFRS Case 1 for wind direction east at 50.33 mph wind speed with internal pressure of 0.6494 psf

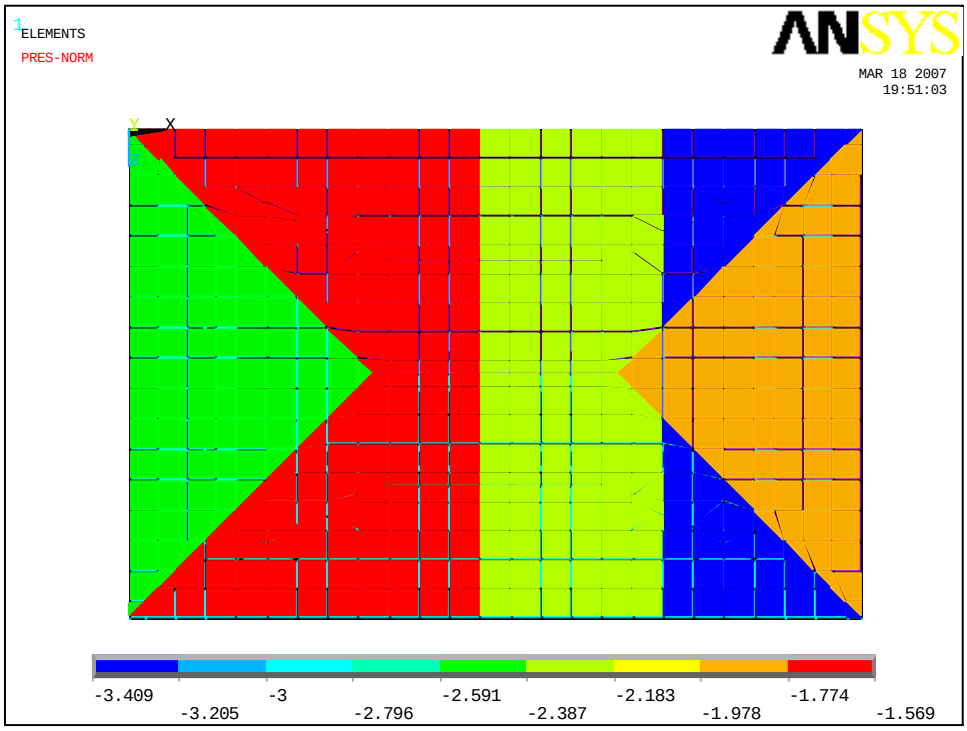

Figure B.2. Method 2: MWFRS Case 1 for wind direction east at 50.33 mph wind speed with internal suction of -0.6494 psf

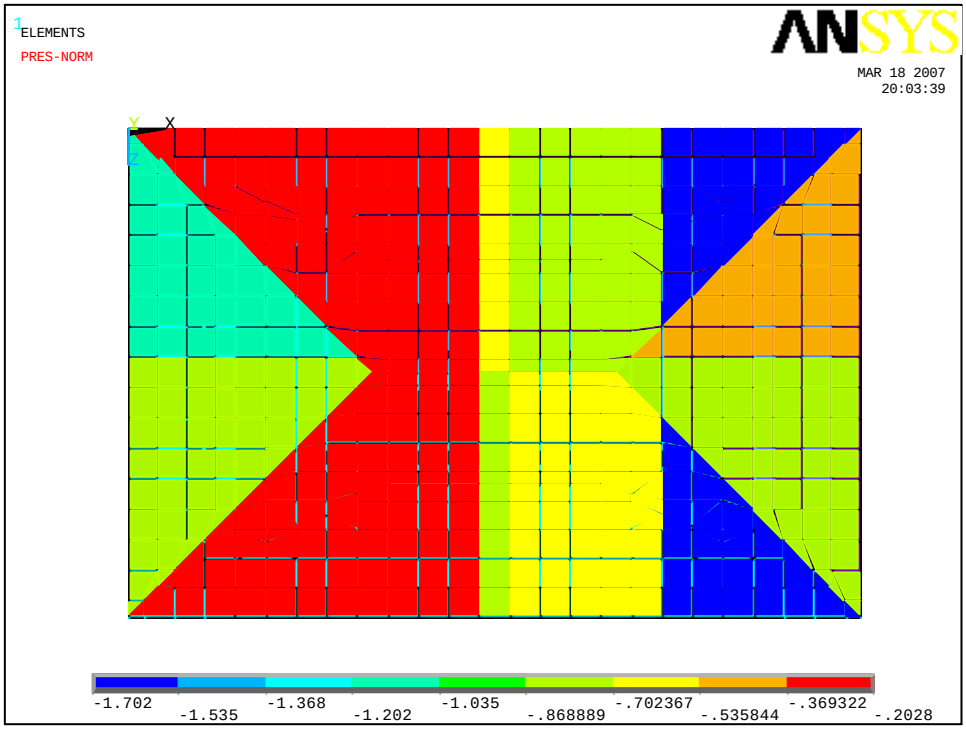

Figure B.3. Method 2: MWFRS Case 2 for wind direction east at 50.33 mph wind speed with internal pressure of 0.4871 psf

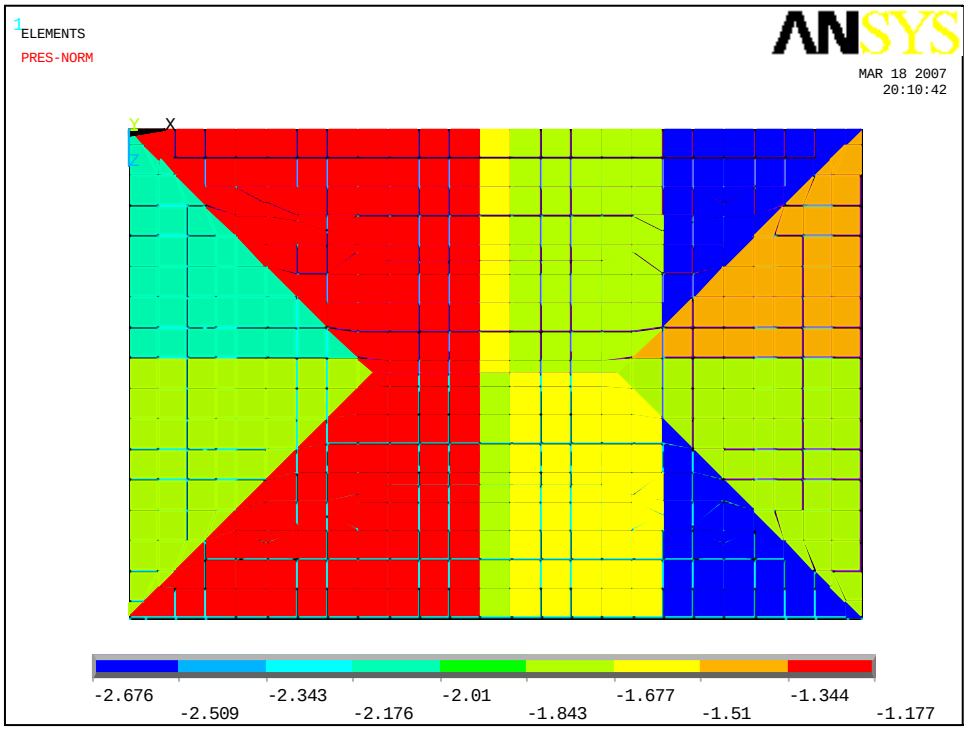

Figure B.4. Method 2: MWFRS Case 2 for wind direction east at 50.33 mph with internal suction of -0.4871 psf

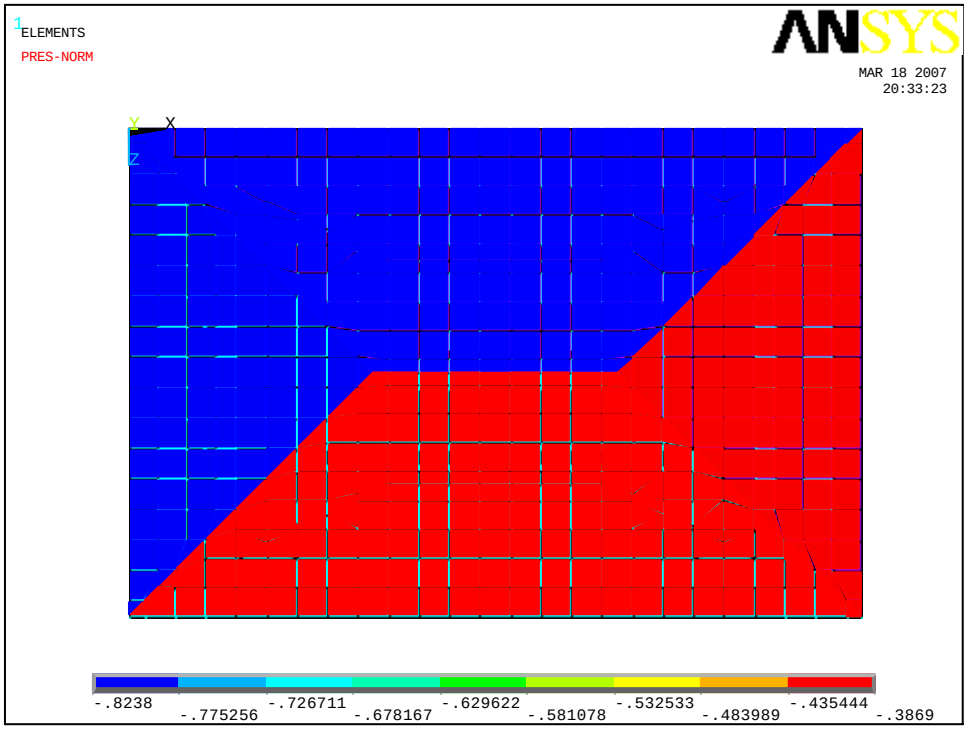

Figure B.5. Method 2: MWFRS Case 3 for wind direction southeast at 50.33 mph with internal pressure of 0.4871 psf

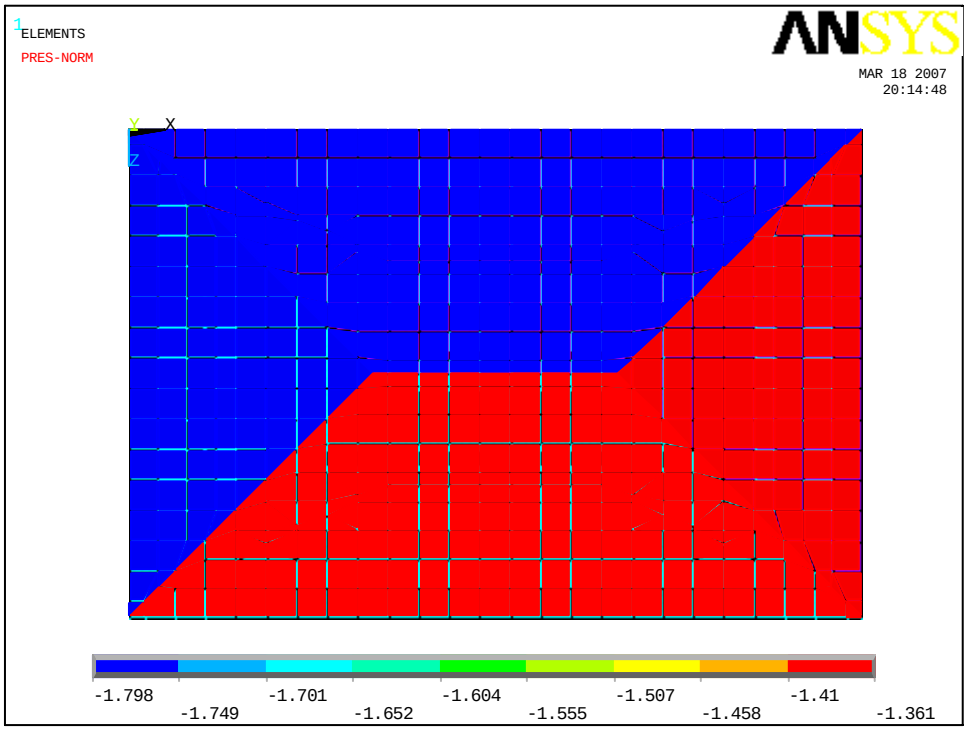

Figure B.6. Method 2: MWFRS Case 3 for wind direction southeast at 50.33 mph with internal suction of -0.4871 psf

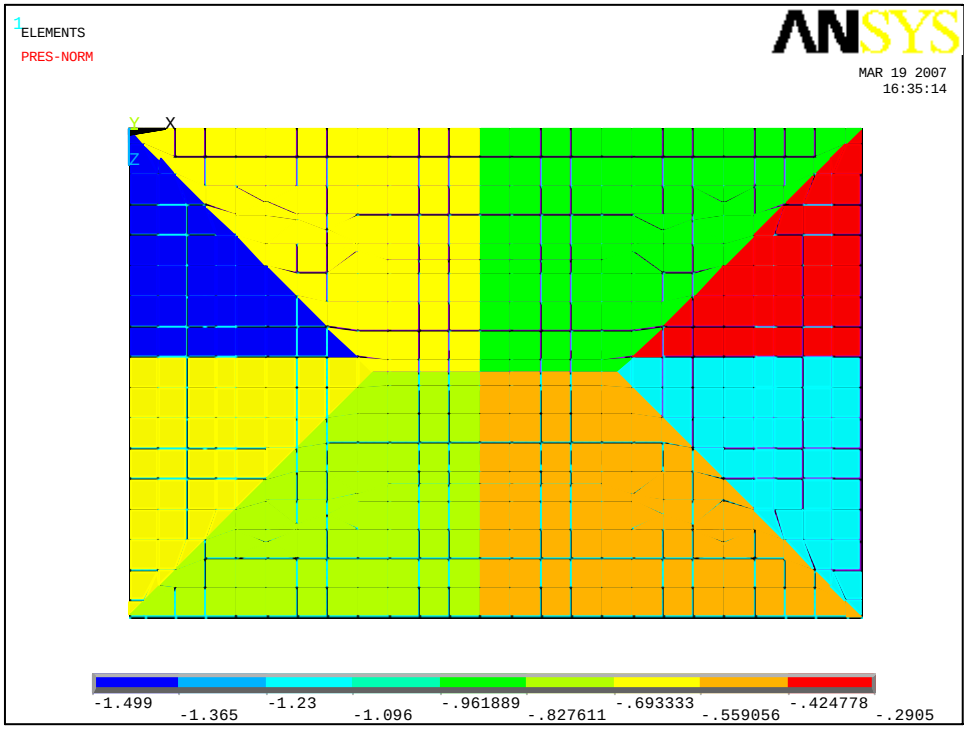

Figure B.7. Method 2: MWFRS Case 4 for wind direction southeast at 50.33 mph with internal pressure of 0.3656 psf

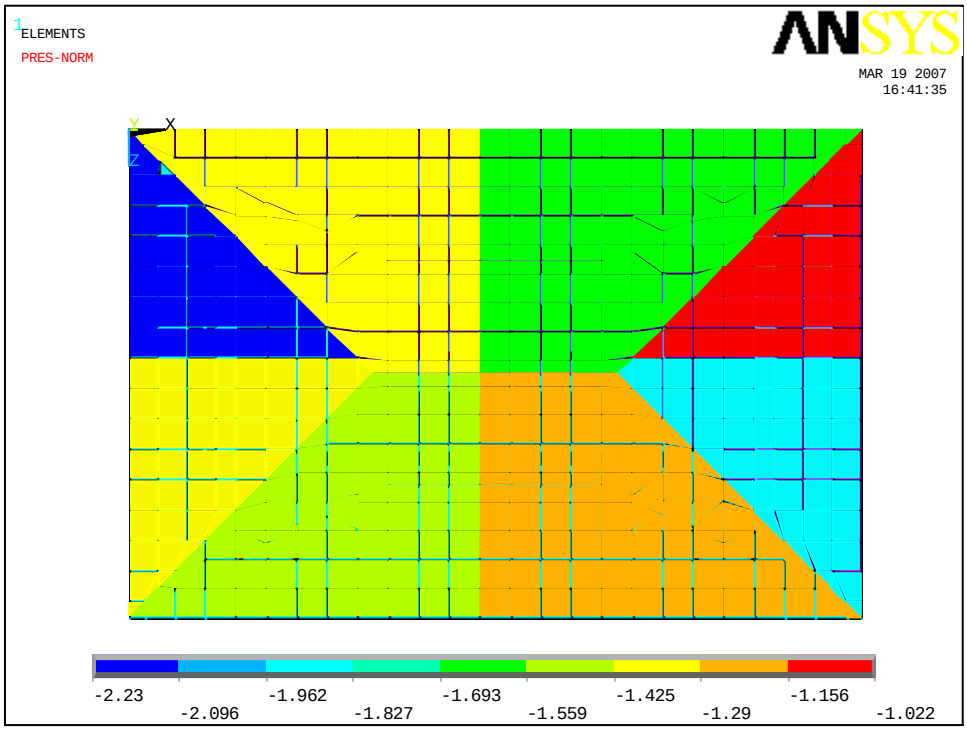

Figure B.8. Method 2: MWFRS Case 4 for wind direction southeast at 50.33 mph with internal suction of -0.3656 psf

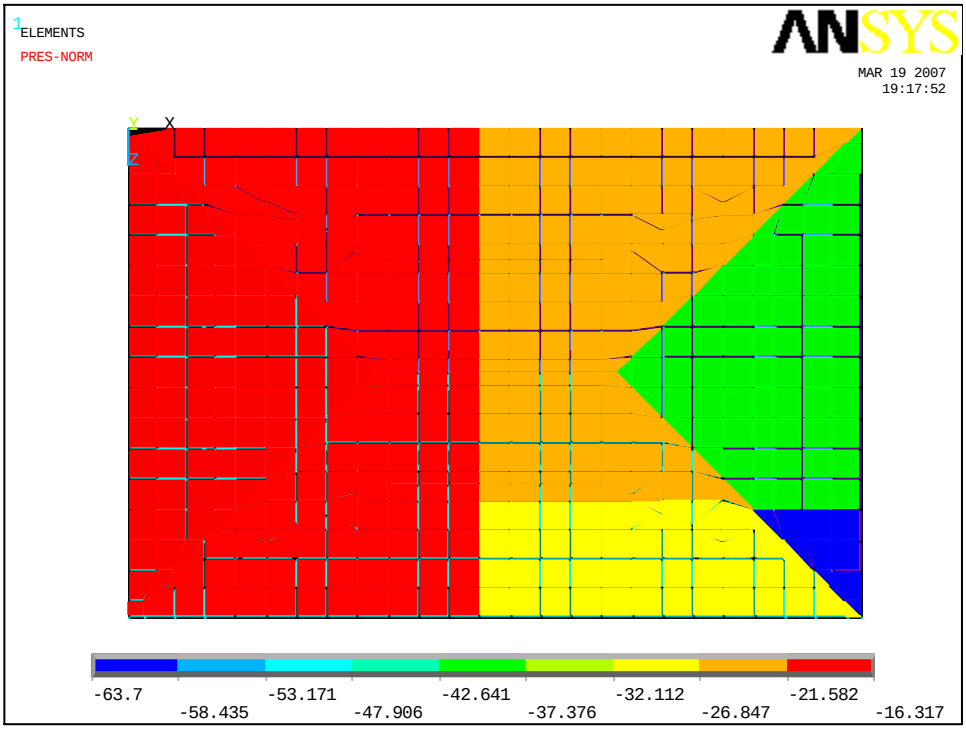

Figure B.9. Method 1: MWFRS Case 1 for wind direction east at 120.34 mph

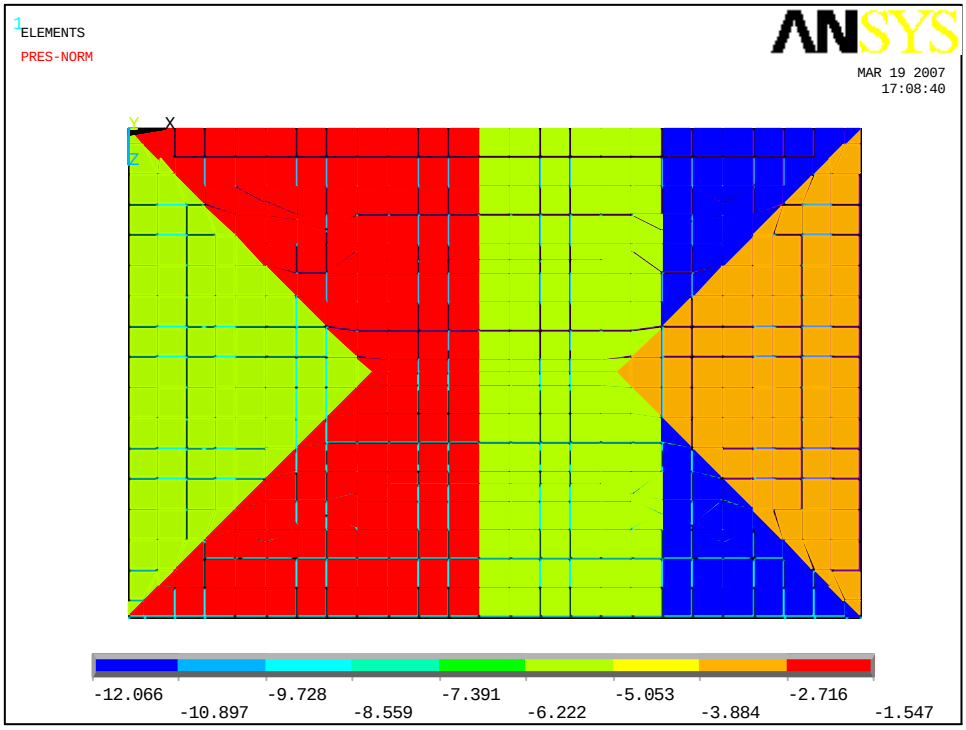

Figure B.10. Method 2: MWFRS Case 1 for wind direction east at 120.34 mph with internal pressure of 3.7125 psf

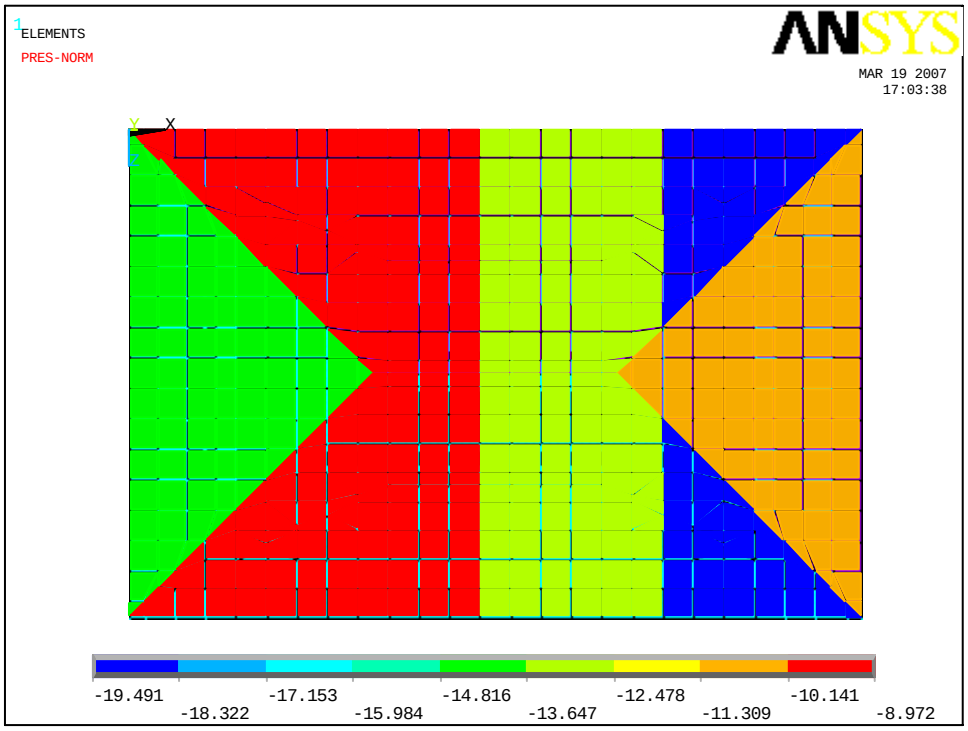

Figure B.11. Method 2: MWFRS Case 1 for wind direction east at 120.34 mph with internal suction of -3.7125 psf

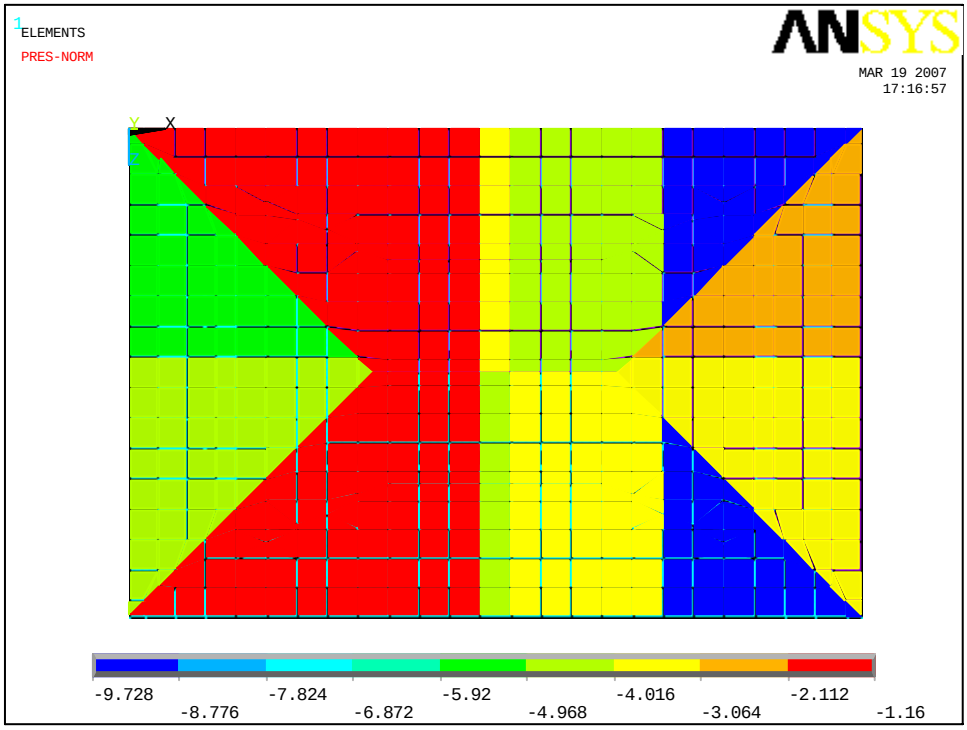

Figure B.12. Method 2: MWFRS Case 2 for wind direction east at 120.34 mph with internal pressure of 2.7844 psf

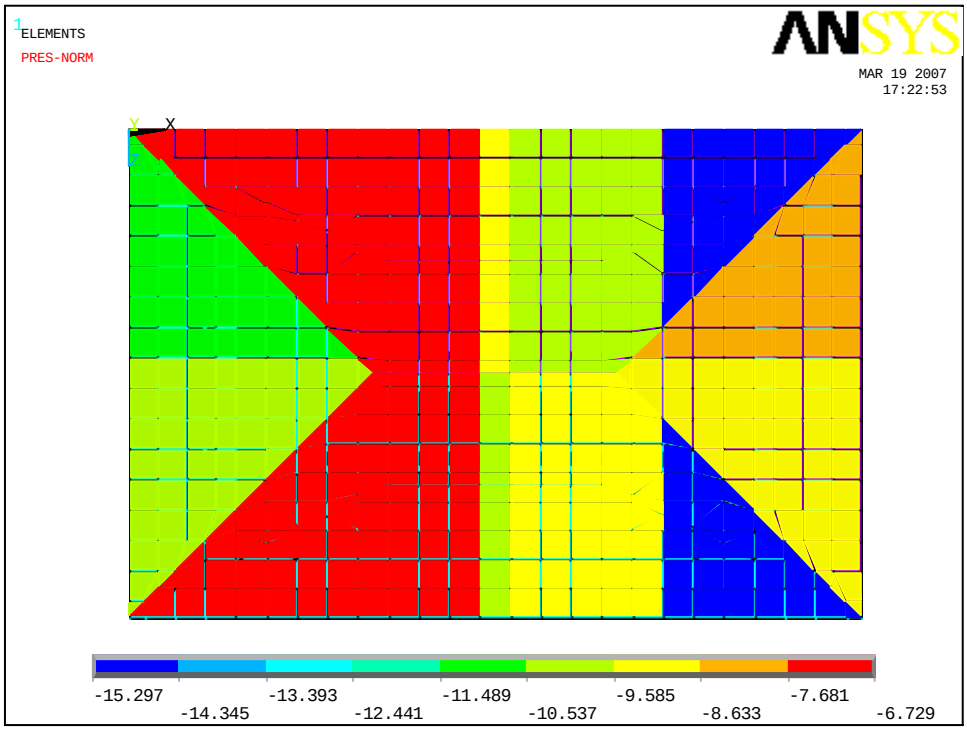

Figure B.13. Method 2: MWFRS Case 2 for wind direction east at 120.34 mph with internal suction of -2.7844 psf

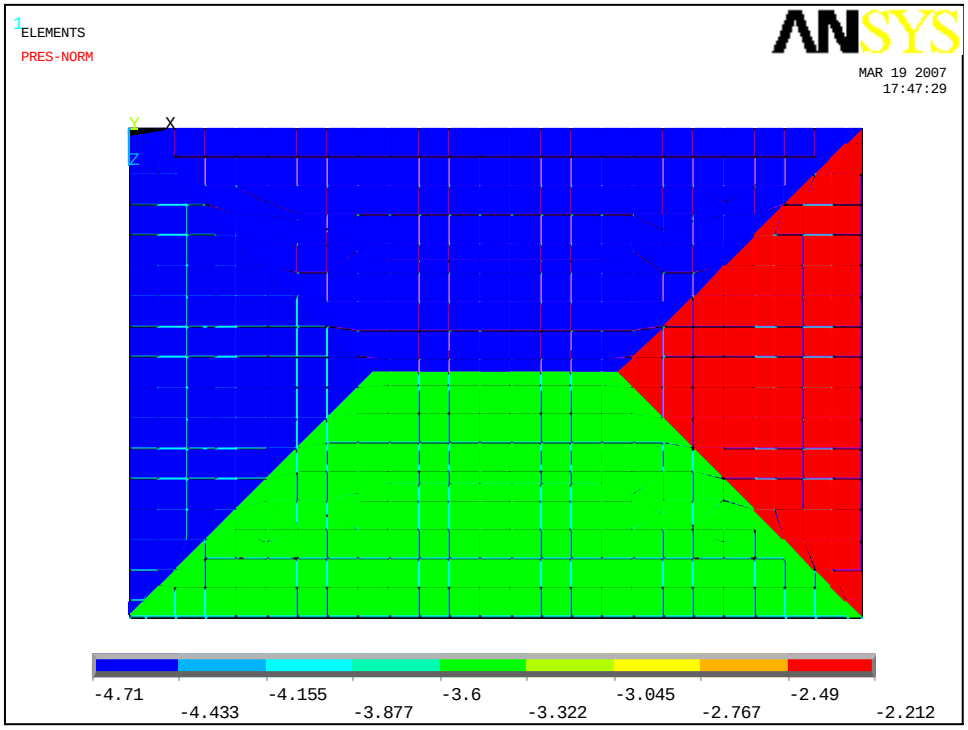

Figure B.14. Method 2: MWFRS Case 3 for wind direction southeast at 120.34 mph with internal pressure of 2.7844 psf

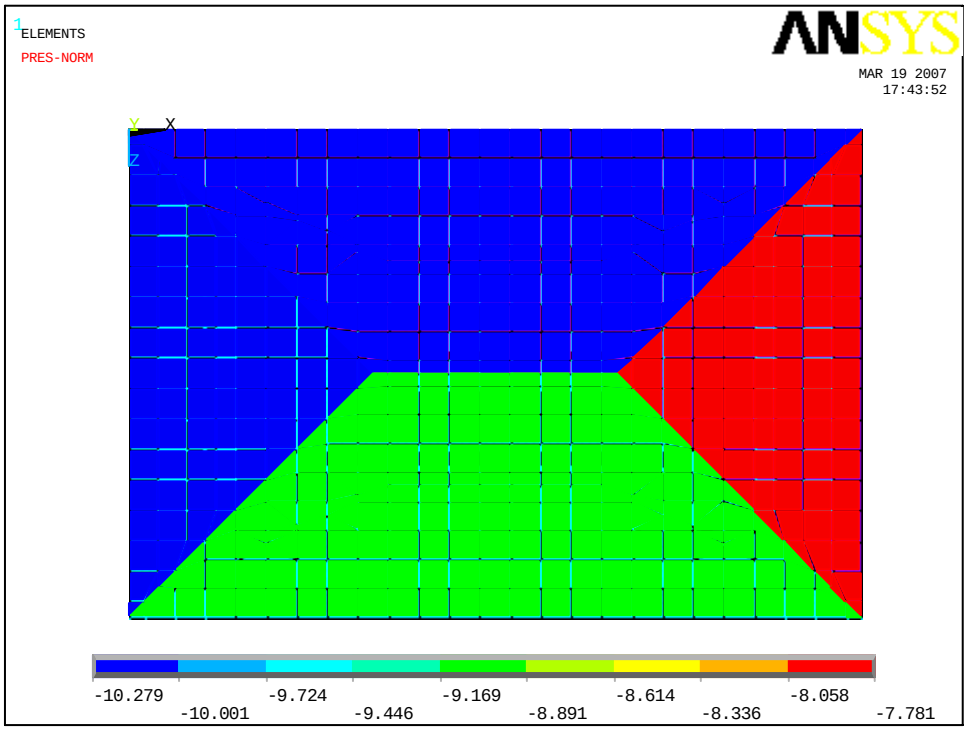

Figure B.15. Method 2: MWFRS Case 3 for wind direction southeast at 120.34 mph with internal suction of -2.7844 psf

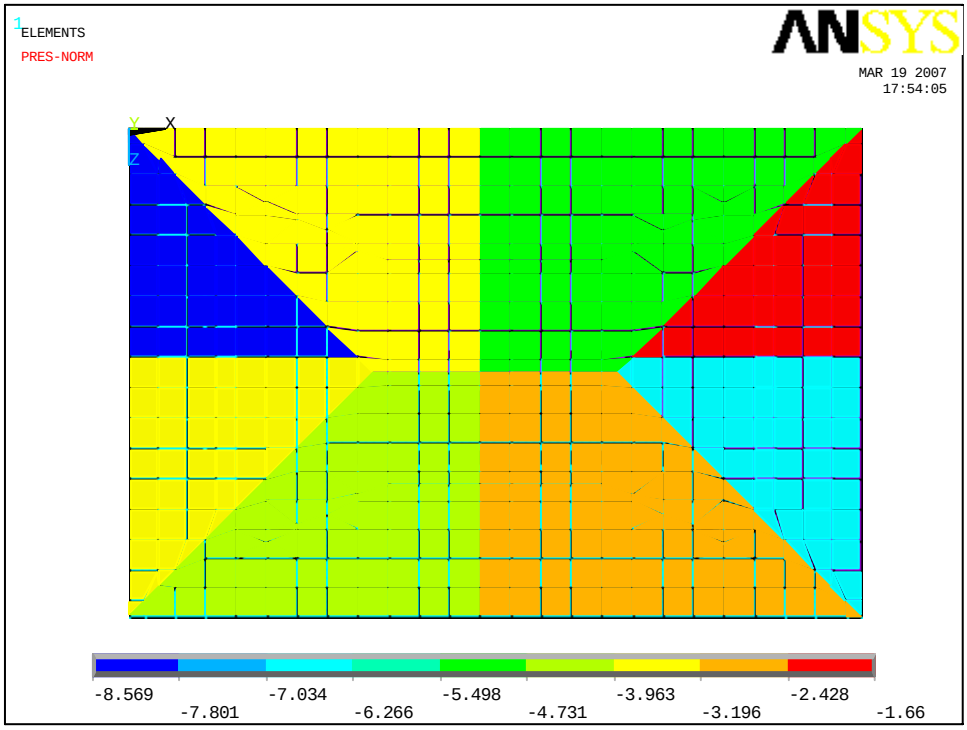

Figure B.16. Method 2: MWFRS Case 4 for wind direction southeast at 120.34 mph with internal pressure of 2.0901 psf

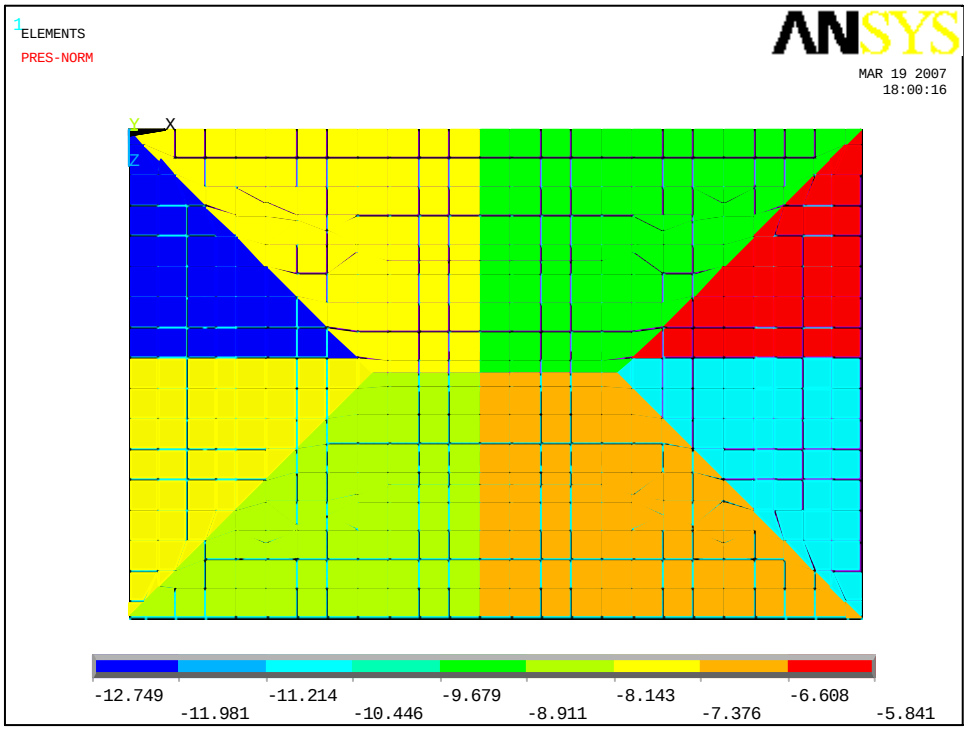

Figure B.17. Method 2: MWFRS Case 4 for wind direction southeast at 120.34 mph with internal suction of -2.0901 psf

REFERENCES CITED

1. American Wood Council. *National Design Specification Supplement.* Design Values for Wood Construction. (2001). p. 12,37,42.

2. ASCE. (1999). Minimum design loads for buildings and other structures. *ASCE 7-98,* Reston, Va.

3. ASCE. (2003). Minimum design loads for buildings and other structures. *ASCE 7-02,* Reston, Va.

4. ASCE newsletter. (2001). Department of Civil and Coastal Engineering. Website from, www.ce.ufl.edu/newsletters/Su01.pdf. Retrieved April 2006.

5. Ayscue, Jon K. (1996). "Hurricane Damage to Residential Structures: Risk and Mitigation." The John Hopkins University. Baltimore, Maryland. *Natural Hazards Research and Applications Information Center Institute of Behavior Science.* University of Colorado. Website from, http://www.colorado.edu/hazards/wp/wp94/wp94.html. Retrieved April 2006.

6. Bailey, Colin (2006). "Structural Analysis." Website from, http://www.mace.manchester.ac.uk/project/research/structures/strucfire/Design/performance/structureAnalyses/default.htm. Retrieved April 2006.

7. Castellon, M. (2005). "Storm – Making the World Safer from Hurricanes Sometimes Means Facing Them Head-On." *Vista.* 25-27. Website from, http://www.depts.ttu.edu/communications/downloads/Taken%20by%20Storm.pdf. Retrieved April 2006.

8. Collins, M., Kasal, B., Paevere, P., and Foliente, G. C. (2005). "Three-dimensional model of light frame wood buildings. I: Model Description." *J. Struct. Eng.*, 131(4), 676-683.

9. Collins, M., Kasal, B., Paevere, P., and Foliente, G. C. (2005). "Three-dimensional model of light frame wood buildings. II: Experimental Investigation and Validation of the Analytical Model." *J. Struct. Eng.*, 131(4), 684-692.

10. Cook, Richard L., Jr. 1991. "Lessons Learned by a Roof Consultant." In *Hurricane Hugo One Year Later*, Benjamin A. Sill and Peter R. Sparks, Editors. New York: American Society of Civil Engineers.

11. Cramer, S. M., and Wolfe, R. W. (1989). "Load-distribution model for light-frame wood roof assemblies." *J. Struct. Engrg.,* ASCE, 115(10), 2602-2617.

12. Cramer, S., Shrestha, D., and Mtenga, P. (1993). "Computation of member forces in metal plate connected wood trusses." *Structural Engineering Review* 5(3), 209-218.

13. FEMA. Hazards – "Saffir/Simpson Hurricane Scale." National Hurricane Center. Website from, http://www.fema.gov/hazards/hurricanes/saffir.shtm. Retrieved April 2006.

14. Flager County's Official Source for Emergency Information. "Protecting Your Home – Hurricane Clips & Straps." Website from, http://www.flagleremergency.com/er/homeprotection_straps.asp. Retrieved April 2006.

15. FPL Group, Madison, Wisconsin. Field data collection for Hurricane Katrina and various correspondences through interviews and email. Obtained 2006.

16. FPL Group, Madison, Wisconsin. Powerpoint for Test Structure and Hurricane Ivan Data Analysis. Obtained 2006.

17. FPL News Release. "Hurricanes and Homes." Website from, http://www.fpl.fs.fed.us/pressroom/newsreleases/nr-2001jul02-hurricane-house.html. Retrieved April 2006.

18. Georgiou, P.N. (1985). "Design wind speeds in tropical cyclone regions." Ph.D. Thesis, University of Western Ontario, London, Ontario, Canada.

19. Gerhards, C. (1983). "Effect of high-temperature drying on the bending strength of yellow-poplar 2 x 4's." *Forest Prod. J.* 33(2):61-67.

20. Gupta, R. (2005). "System behaviour of wood truss assemblies." *Prog. Struct. Engng. Mater.* 2005; 7, 183-193.

21. Hurricane Katrina Storm Path. Website from, http://en.wikipedia.org/wiki/Hurricane_Katrina. Retrieved April 2006.

22. Infoplease. "2005 Hurricane Season." Website from, http://www.infoplease.com/ipa/A0932571.html. Retrieved April 2006.

23. Insurance Information Institute. "Facts and Statistics: Catastrophes." Website from,http://www.iii.org/media/facts/statsbyissue/catastrophes/?table_sort_748341=6. Retrieved April 2006.

24. J.M. Harold Construction, Construction Documents for Wood Trusses and Rafters. Pensacola, Florida. Obtained 2006.

25. Jones, N., and Porterfield, M. (1999). "Hurricane House Braces for New Storm Season – Data from North Carolina Structure Could Help Future Homes Stand Up to High Winds." Website from, http://www.jhu.edu/news_info/news/home99/jul99/hurricane.html. Retrieved April 2006.

26. Kasal, B. (1992). "A nonlinear three-dimensional finite-element model of a light-frame wood structure." PhD thesis, Univ. of Oregon State, Corvallis, Oregon.

27. Kasal, B., Leichti, R., and Itani, R. (1994). "Nonlinear finite-element model of complete light-frame wood structures." *J. Struct. Eng.,* 120(1), 100-119.

28. Kasal, B., Collins, M., Paevere, P., Foliente, G. (2004). "Design models of light frame wood buildings under lateral load." *J. Struct. Eng.*, 130(8), 1263-1271.

29. Kuenzi, E. W., and Wilkinson, T. L. (1971). Composite beams—effect of adhensive or fastener rigidity. *Res. Paper FPL-152,* U.S. Department of Agriculture, Forest Products Laboratory, Madison, Wis.

30. Mtenga, P., Cramer S., Peyrot, A., and Wolfe, R. (1995). "System factors for light-frame wood truss assemblies." *J. Struct. Eng.,* 121(2), 290-300.

31. National Hurricane Preparedness. National Hurricane Center. "Hurricane Basics." Website from, http://www.nhc.noaa.gov/HAW2/english/basics.shtml. Retrieved April 2006.

32. National Weather Service Forecast Office – Mobile/Pensacola. "Extremely Powerful Hurricane Katrina leaves a Historic Mark on the Northern Gulf Coast – A Killer Hurricane Our Country Will Never Forget." Website from, http://www.srh.noaa.gov/mob/0805Katrina/. Retrieved April 2006.

33. Paevere, P. J., Foliente, G. C., and Kasal, B. (2003). "Load-sharing and re-distribution in a one-story wood frame building." *J. Struct. Eng.*,129(9), 1275-1284.

34. Pamphlet for Distance Learning Programs From ASCE: Structural Engineering and Management Topics. 2006.

35. Percival, D. and Comus, Q. (1980). "Load distribution in a full-scale nailed-glued hip-roof system." *Forest Products Journal* (FPS). 30(11), 17-21.

36. Pinelli, P.J., Simiu, E., Gurley, K., Subramanian, C., Zhang, L., Cope, A., Filliben, J., Hamid, S., (2004). "Hurricane damage prediction model for residential structures." *J. Struct. Eng.*, 130(11), 1685-1691.

37. Phillips, T. L. (1990). "Load-sharing characteristics of three-dimensional wood diaphragms." MS thesis, Washington State Univ., Pullman, Wash.

38. Simiu, E.,and Scanlan, R. *Wind Effects on Structures-Fundamental and Applications to Design*. 3rd ed. New York: John, Wiley & Sons, Inc., 1996.

39. Stahl, D., Cramer S., Wolfe R., (1996). "Behavior of metal-plate-connected trusses with squared-end webs." Wood Engineering Journal. Pp. 78-84.

40. Swanson Analysis Systems, Inc. (2000). *ANSYS Theory Manual* (www.ansys.com), Houston, Pa.

41. Swanson Analysis Systems, Inc. (2006). *ANSYS 9.0 Theory Manual* (www.ansys.com), Houston, Pa.

42. Vickery, P.J. and Twisdale, L.A. (1995). "Prediction of hurricane wind speeds in the United States." *J. Struct. Engrg.* ASCE, 121(11), 1691-1699.

43. Waltz, N. (2002). "Truss joist investigation into hip roof system behavior." Biographies and Abstracts, Forest Products Society 56th Annual Meeting, Madison, WI, USA.

44. Wolfe, R. W., and McCarthy, M. (1989). "Structural performance of light-frame roof assemblies—I. Truss assemblies designed for high variability and wood failure." *Res. Paper FPL-RP-492*, U.S. Department of Agriculture, Forest Products Laboratory, Madison, Wis.

45. Wolfe, R. W., and LaBissoniere, T. (1991). "Structural performance of light-frame roof assemblies – II. Conventional truss assemblies." *Res. Paper FPL-RP-499,*U.S. Department of Agriculture, Forest Products Laboratory, Madison, Wis.

46. Zhong Li, Gupta, R., Miller, T. (1998). "Practical approach to modeling of wood truss roof assemblies." *Practice Periodical on Strucural Design and Construction*, 119-124.

ACKNOWLEDGEMENTS

I personally wish to thank my co-major professors Dr. Fouad Fanous and Dr. Sivalingam Sritharan in the Civil Engineering department for their expert advise and help they have given me throughout this research investigation. They made sure this report would be well written and coached me through any questions I had during this whole research investigation. They were also great professors during my graduate school experience.

I would like to thank the FPL group from Madison, Wisconsin for sharing their research data with Iowa State University and myself. Without their input this finite element (FE) model would not have had any comparisons to verify the FE model. Actually other comparisons could have been made, but nothing cool like Hurricane Katrina attacking a residential house. Also, Dr. Terry Wipf needs to be thanked for speaking with the FPL group to attain their data and for ensuring them that Iowa State University would produce the best results compared to other well-suited universities.

I would like to thank my committee members Dr. Partha Sarkar in the Aerospace Engineering department and Dr. Terry Wipf in the Civil Engineering department for being on my committee. They were both great professors during my graduate school experience.

Finally, I would like to thank my family for standing behind my decision upon entering graduate school. I am the first Civil Engineer (Structural Emphasis) in the family. I would also like to thank my wife Jennifer for the patience she has shown during my graduate schooling. It helped that Jenny was in graduate school at the same time because many hours were shared together at Town Engineering in Ames, Iowa. Thanks for all the love and support.